1996

Investigations into single-slug dense-phase pneumatic conveying

Gang Xie
University of Wollongong

INVESTIGATIONS INTO SINGLE-SLUG DENSE-PHASE PNEUMATIC CONVEYING

A thesis submitted in fulfilment of the requirements

for the award of the degree of

MASTER OF ENGINEERING(HONOURS)

from

UNIVERSITY OF WOLLONGONG

by

Gang Xie

B. E. (SJU), M. E. (WTU)

Department of Mechanical Engineering

Jan. 1996

ACKNOWLEDGMENTS

This paper is to memorise my late grandfather, W. Xie, who had supplied all costs for the study.

I would like to thank my supervisor, Dr. Peter W. Wypych, Associate professor in the Department of Mechanical Engineering at the University of Wollongong, for his supervision, encouragement and constructive suggestions during the period of my study. I am indebted to Dr R. Pan, the staff of Key Centre for Bulk Solids and Particulate Technologies, for his valuable assistance in the development of the theory.

My thanks are extended to the technical staff in Bulk Solids Handling Laboratory with whose help the experiments were conducted. Particularly, I would like to express my gratitude to Mr. D. Cook, Mr. I. Frew, Mr. Peter May and Mrs. W. Halford.

Special acknowledgment is made to my dear wife Yanqiong Huangfu and my parents for their unfailing help and encouragement.

SUMMARY

It is recognised that pneumatic conveying has some advantages over other mechanical conveying methods and has been successfully employed for many years in the chemical, food and process industries for the transport of powder and granular materials. Traditionally, the solids are transported in the form of dilute-phase, which may cause high energy consumption, high pipe attrition and high particle degradation. Hence, a more recently developed method of conveying, called dense-phase (non-suspension flow), is receiving increased interest and attention.

It has been widely accepted that dense-phase pneumatic conveying has many advantages over that of dilute-phase, for example, lower pipe erosion and particle degradation. However, its design is almost empirical. Since it is expensive and time consuming to obtain the design data on a large-scale test rig, the application and potential of this new mode of conveying have been hampered. It is evident that the most critical design factor is pressure drop. Investigators have invested a lot of time and effort in developing several theories to predict these parameters, but somehow their wide usage is limited (eg, different materials, pipelines).

After reviewing existing theories in detail, the author has found a serious error in a popular model for the prediction of pressure drop in single-slug dense-phase pneumatic flow. The purpose of this study is to analyse the mechanism of slug flow and develop a new method for determining pressure drop accurately, so that commercially used dense-phase pneumatic conveying systems can be designed by theory.

The present study lays the foundation for modern dense-phase pneumatic conveying design. Subsequent investigators and prospective users of the system will benefit from this work mainly in three aspects: (1) a better knowledge about the conveying mechanism; (2) a more accurate estimation of the operating factors; (3) a design based more on theory than empiricism.

TABLE OF CONTENTS

LIST OF FIGURES

LIST OF TABLES

NOMENCLATURE

a Ergun Constant

A Cross-sectional area of pipe (m^2)

A_{st} Cross-sectional area of stationary layer in pipe (m^2)

b Ergun Constant

C Volumetric solids fraction

C_w Particle-wall cohesion (Pa)

D Pipe diameter (m)

d_p Effective diameter of particles (m)

F_r Froude number of bulk material

G Fluid mass flow rate (kgs^{-1})

g Acceleration due to gravity (ms^{-2})

k Constant

K_w Stress transmission coefficient

L_{AB}, L_{BC}, L_{CD}, L_{DE} Distance between two near pressure meters (m)

L_p Horizontal length of pipe (m)

L_{pm} Distance between two pressure meter (m)

L_s Slug length (m)

m_s Particle mass flow rate (kgs^{-1})

m_f Air mass flow rate (kgs^{-1})

p_0 Atmospheric air pressure (Pa)

p Interstitial air pressure (Pa)

R Pipe radius (m)

T Friction force per unit slug length (Nm^{-1})

T_w Total friction force (Nm^{-1})

T_{sw} Friction force due to bulk material weight (N)

T_{rw} Friction force due to σ_x (N)

t_c Cycle time (s)

t_{pm} Signal appearance time between two neighbour pressure meters (s)

$V_{a\min}$ Minimum air velocity (ms^{-1})

V_b Blow tank volume (m^3)

V_m Mean fluid velocity (ms^{-1})

V_s Particle velocity (ms^{-1})

V_p Slug velocity (ms^{-1})

V_{AB}, V_{BC}, V_{CD}, V_{DE} Average slug velocity at different pipe segments (ms^{-1})

ΔV Coordinate

W_b Weight of material loaded in blow tank (kg)

W_d Weight of material conveyed into discharge tank (kg)

x Coordinate

α Ratio of the cross-sectional area of stationary layer to the pipe cross sectional area

α_b Ratio of the cross-sectional area of stationary layer behind slug to the pipe cross-sectional area

α_f Ratio of the cross-sectional area of stationary layer in front of slug to the pipe cross-sectional area

Δp Maximum pressure drop (Pa)

ε Voidage

η Dynamic viscosity of fluid $Pa \cdot s$

ρ_0 Atmospheric air density (kgm^{-3})

ρ_f Density of air behind slug (kgm^{-3})

ρ_b Bulk density (kgm^{-3})

ρ_e Submerged effective density (bulk density minus fluid density) (kgm^{-3})

$\rho_{b\text{-}st}$ Bulk density of slug stationary layer (kgm^{-3})

ρ_s Particle density (kgm^{-3})

σ_b Intergranular normal stress at back face of moving slug (Pa)

σ_f Intergranular normal stress at front face of moving slug (Pa)

σ_w Total radial stress (Pa)

σ_{sw} Radial stress due to particle mass (Pa)

σ_{rw} Radial stress due to σ_x (Pa)

σ_x Intergranular normal stress along the pipe axis (Pa)

$\overline{\sigma_x}$ Average axial stress (Pa)

$d\sigma_x$ Coordinate

σ_z Coordinate

$\overline{\tau}$ Shear stress between particles and internal wall (Pa)

τ_w Total shear stress between particles and internal wall (Pa)

τ_{rw} Shear stress between particles and internal wall caused by σ_{rw} (Pa)

τ_{sw} Shear stress between particles and internal wall caused by σ_{sw} (Pa)

ϕ Internal friction angle (°)

ϕ_w Wall friction angle (°)

ϕ_i Coordinate

μ_w Wall friction coefficient

ω Coordinate

γ_b Bulk specific weight with respect to water at 4^0C

μ Dynamic viscosity of fluid $Pa \cdot s$

CHAPTER 1

INTRODUCTION

1. INTRODUCTION

It is recognised that pneumatic conveying has some advantages over other mechanical conveying models and has been successfully employed for many years in the chemical, food and processing industries for the transport of powder and granular materials. Traditionally, the solids are transported in the form of dilute-phase, but because of high pipe wear and high particle degradation, a newly developed conveying form called single-slug dense-phase is receiving increased attention.

The flow patterns observed in a horizontal pipe as air velocity is progressively reduced are:

(1) Fully suspended flow

Fully suspended flow is conventional lean-phase conveying as shown in Fig. 1(a). All the particles are airborne and form a fairly uniform suspension with some particles being supported by turbulent eddies and other bouncing from top to bottom of the pipe.

(2) Stratified flow

Stratified flow (see Fig. 1(b)) is very similar to fully suspended flow in that the majority of particles are airborne. However, there is a concentration gradient over the pipe cross-section, with most of the particles travelling in the lower portion of the pipe. Some particles are conveyed by bouncing and rolling along the bottom of the pipe.

(3) Dune conveying

The solids form two layers (see Fig. 1(c)), the top layer consists of virtually particle-free gas and the lower layer consists of slowly moving particles, at a packing density approaching their bulk density, with faster-moving ripples or dunes travelling along the

top of this solids layer. This regime is generally considered to be an unstable mode of flow representing the transition from dilute to dense phase flow.

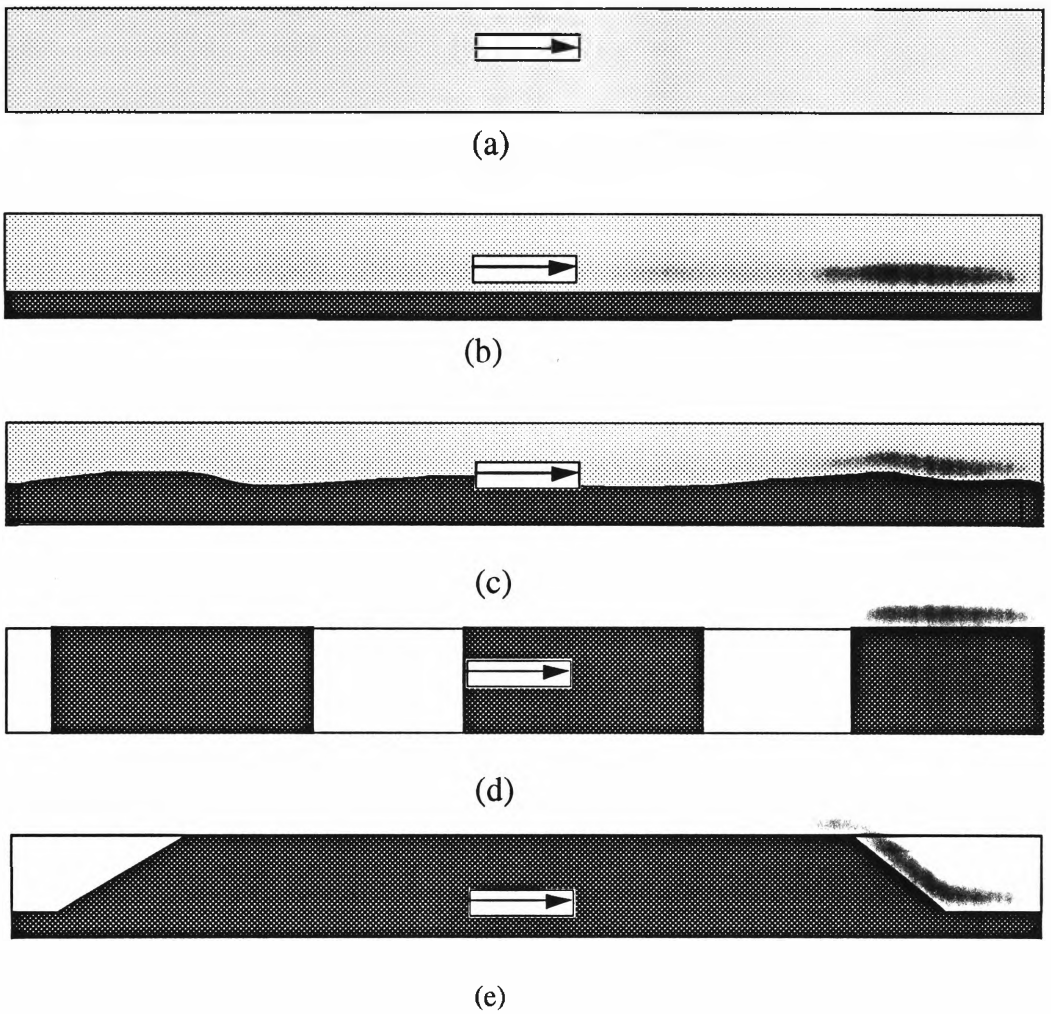

Fig. 1.1 Schematic flow patterns of pneumatic conveying in horizontal pipe

(4) Slug/plug conveying.

Slug/plug conveying (see Fig. 1(d) or Fig. 1(e)) is the flow regime used in commercial dense-phase systems. It should be noted that the flow patterns shown in Fig. 1(d) and Fig. 1(e) are two typical slug/plug flows. The essential feature of slug/plug flow is that, particles build up and fill the entire pipe cross-section. Generally, for cohesionless materials, the "packed material" sweeps up the stationary particles in front and simultaneously leaves behind a stationary layer; for cohesive materials, the "packed

material" leaves nothing behind while travelling forward, and is called the plug flow. It should be noted that many materials (eg blue metal, crushed coal) cannot be conveyed in this manner and traditionally dilute-phase has been the only option. However, by limiting the amount of material along the pipeline, such materials still can be conveyed in dense-phase (ie in the form of single-slug per cycle). This thesis mainly concentrates on this type of flow.

Owing to its low velocity and high pressure drop, the slug system features the following advantages and disadvantages over the dilute-phase system:

(1) Low particle degradation;
(2) low pipe attrition;
(3) Only a small filter is required;
(4) It is possible to transport a given mass of solids with a less amount of gas, which is important when expensive gases are required if the conveying gas is other than air, eg. nitrogen to convey explosive powders;
(5) Does not provide continuous conveying;
(6) Its design is almost empirical.

Since it is expensive and time consuming to obtain the design data on a large-scale test rig, the application and potential of this new mode of conveying have been hampered. It is evident that the most critical design factor is pressure drop. Investigators have invested a lot of time and effort in developing several theories, but somehow their wide usage has been limited (eg, different materials, pipelines).

Perhaps, the most influential researcher in this area has been Konrad, his article published in 1980 [19] has been quoted by numerous successors [1, 7, 11, 15, 21, 23-26, 28, 34,

37], and its basic idea is accepted widely. In fact, the Konrad theory has dominated slug research for over 15 years. Afterwards, several articles about the pressure drop in slug flow were published; in 1987 Zheng Luqing et al [37] presented their research on cement, raw mix, and pulverised coal ash; in 1988 Aziz and Klinzing [1] published their investigation on cohesive coal; in 1994 Dhedapkar et al [7] described a method for slug system design; for several products, Wypych, Pan and Mi have researched slug flow vigorously in recent years, and good progress has been achieved [23-28, 35, 36].

However, there is, as yet, no universally accepted set of formulae for slug systems; its design is almost empirical. Generally, manufacturers will design a system to convey a granular material only after actual tests in a pilot plant, followed by scale-up and the judicious application of their knowledge from previous installations. The reasons are summarised as following:

(1) The properties of the proposed materials vary dramatically, each material can be conveyed by a broad range of air mass flow rates at various pressure drops. The pressure drops are themselves a function of the amount of material mass loaded in the blow tank, as well as its density, shape, and physical characteristics, as well as of pipe diameter and direction of flow -- horizontal or vertical. Thus, it is rather difficult to visualise the various mechanisms of flow.

(2) The pipes engaged in previous investigations are usually small and short. Also the previous researchers consider slug flow similar to gas/liquid flow [17,18]. However, bulk materials are neither gas nor liquid, nor solid, but they do have some physical characteristics of gas, liquid or solid.

Konrad [16] highlights his slug theory by reviewing his previous theoretical work seriously. However, for the novice, the Konrad pressure drop theory appears too complex to be of practical use. Furthermore, the mechanism of slug flow has not yet been well understood, even whether the stress state in the slug is active or passive is a controversial problem. Also, the diverse versions of pressure drop models only tend to exacerbate exisiting confusion [1, 4, 7, 11, 19, 21, 23, 28, 37].

After reviewing existing theory in detail, the author has found serious errors in the prediction of pressure drop in dense-phase pneumatic flow. The purpose of this study is to analyse the mechanism of slug flow in more detail, find a new way to determine the pressure drop mathematically with good accuracy, and hence design mainly by theory full-scale dense-phase pneumatic conveying systems. The study is focused on seven aspects:

(1) The force analyses of a slug slice including the effect of voidage;
(2) The distribution of the stress transmission coefficient;
(3) Deriving a formula to correlate the particle velocity and the slug velocity;
(4) Investigation into the stationary layer caused by a moving slug;
(5) Presenting the pressure drop expression;
(6) Find the relationship between slug velocity and air flow;
(7) Conducting experiments on large-scale test rigs.

The present study lays the foundation for modern dense-phase pneumatic conveying design, and subsequent investigators and prospective users of the system will benefit from this work mainly in three areas:

(1) A better knowledge about the conveying mechanism;

(2) A more accurate estimation for the operating factors;

(3) A design based more on theory than empiricism.

Finally, conclusions of this paper and suggestions for future research are presented.

CHAPTER 2

LITERATURE REVIEW

2. LITERATURE REVIEW

Dense-phase pneumatic conveying has been in use for decades, but there still exists a lot of confusion, with the main problems listed below:

(1) The definition of dense-phase conveying is still a matter of some debate;
(2) Dense-phase systems have been successfully employed by a number of commercial firms, but the basic physics have not been fully understood
(3) The concept of saltation in horizontal flow and choking in vertical flow create unstable regimes, and again the physics are not fully known;
(4) Conflicting test results cause numerous controversies and there is a lack of a coherent theory to explain the discrepancies.

In the past decades, many articles about slug flow have been published. Konrad [16] reviewed the previous literature (published before 1986) about slug flow critically and carefully. Hence, the extensive theoretical and experimental investigations into slug flow undertaken since 1980 are considered below.

2.1 Suitability of Bulk Material

Experience has demonstrated that the criteria for dense-phase suitability are more strict than for dilute-phase.

Geldart [9] first classified bulk materials into four groups according to their mean particle size and density difference for the purpose of predicting fluidisation behaviour.

Dixon [5] suggested that some materials have a natural tendency to slug in dense phase conveying systems whereas others tend towards dune-flow. Based on Geldart's classification of fluidisation, Dixon generated the slugging diagram for assessing the suitability of a material to be conveyed in dense-phase, see Fig. 2.1. A brief description of Dixon's diagram for each of the four "slugging" categories is listed below;

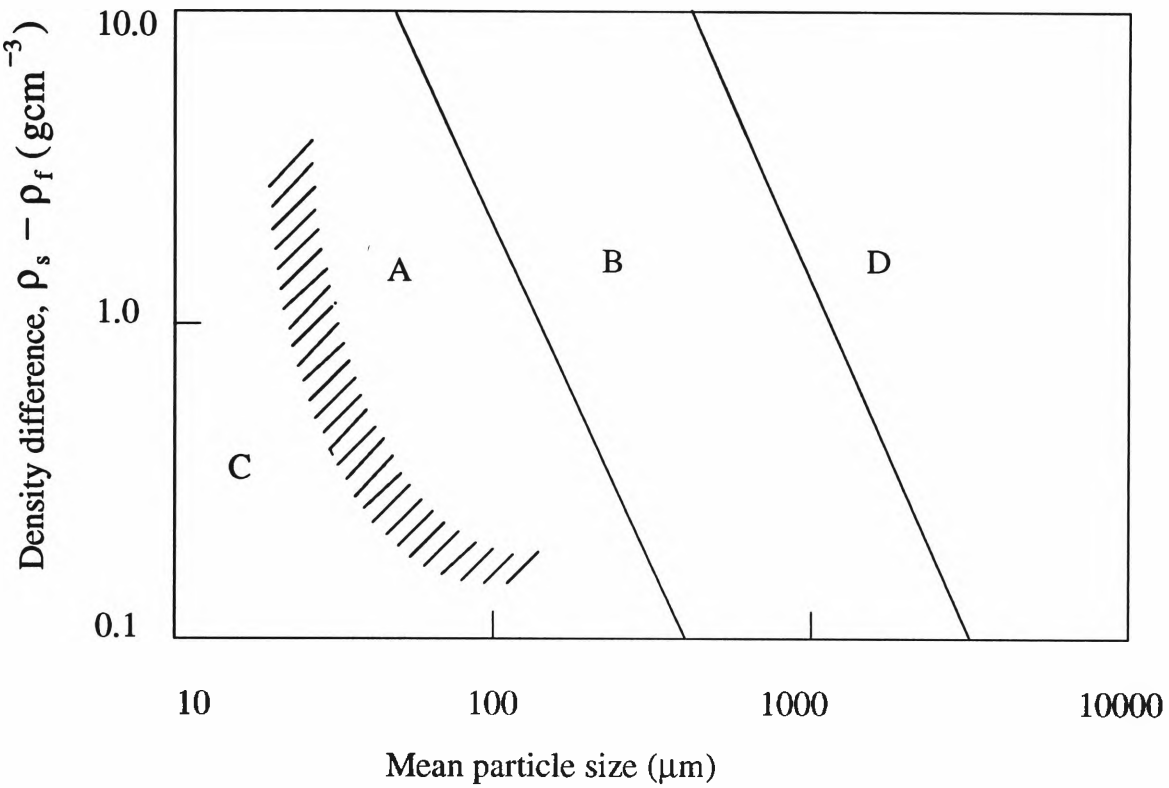

Fig. 2.1 Dixon [5] slugging diagram for a 100mm diameter pipe

(1) **Group A** Powders are the best candidates for dense-phase conveying and can achieve high solids/gas loadings. They do not display natural slugging ability, but can be made to slug by techniques developed by vendors of dense-phase pneumatic handling equipment.

(2) **Group B** powders can be troublesome (eg. severe pipe vibrations) if high solids/gas ratios are contemplated.

(3) **Group C** products arguably are the worst candidates for dense-phase conveying. This can be attributed to their poor fluidisation characteristics.

(4) **Group D** materials are also good candidates for dense-phase conveying. Although they have relatively low solids/gas ratios (ie. compared with Group A powders), they probably can be conveyed at higher loadings than Group B materials.

To date, Dixon's slugging diagram [5] has been used most commonly for assessing the suitability of a material to be conveyed in dense-phase. However, Dixon's work is still imprecise as the behaviour of solids are extremely complex, other factors such as particle size distribution and the ratio of pipeline diameter to average particle diameter may affect the suitability also.

Jones et al [13] studied the potential of a product to be conveyed in dense-phase and pointed out that the two properties which are identified as most useful for determining conveyability are the permeability of a product to air and the ability of a product to retain air.

Mainwaring and Reed [22] firstly presented a diagram for the potential of dense-phase conveying according to the permeability of a material, and found that materials exhibiting high values of permeability factor generally can be conveyed in the plug mode of dense-phase conveying, while the other materials are conveyed either in dense-phase moving bed type flow or dilute-phase.

2.2 Force Analyses in a Slug Slice

It should be noted that Janssen's paper of 1895 is the foundation for the theory of pressures in grain silos, Roberts [31] introduces Janssen's theory in order to celebrate the 100th anniversary of the epic paper " Versuche über Getreidedruck in Silozellen" (On the Measurement of Pressures in Grain Silos). Janssen's theory has been applied to solve silo

bin pressure problems. However, the forces on a slug are more complex than that in silos and bins.

Based on the method of Janssen (1895) [31] and the work of Hancock and Nedderman [10], Konrad et al [19] considered that in any cross sectional area both voidage and particles take up the entire cross-sectional area of pipe. They derived an equilibrium equation and obtained a solution; Konrad et al [19] also considered an analogy between slug pneumatic conveying and two-phase gas/liquid flow and perhaps are the first ones to give an expression to calculate stationary layer. However, Konrad's expression for pressure drop is too complex, and it is evident that in any cross-sectional area the area occupied by particles is $(1-\varepsilon)A$, not A. Apparently, the slug force analyses of Konrad et al [19] is not perfect. However, Konrad's theory actually has been accepted widely [1, 11, 21, 23-26, 28, 30, 34, 37]. All existing versions of slug theory are based on it, because they are derived as follows although few differences exist among them.

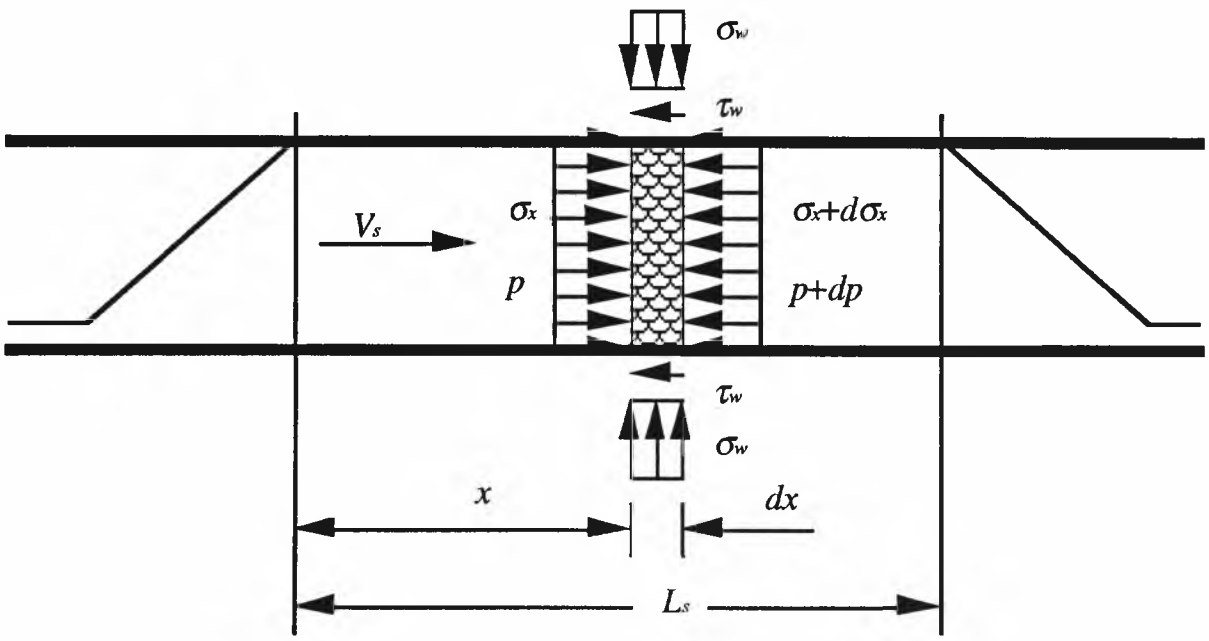

Fig.2.2 Forces acting on elemental slice of a moving slug

A brief description of previous slug force analyses and equilibrium is presented below:

See Fig. 2.2, force balance equation is;

$$(p+dp)\cdot A+(\sigma_x+d\sigma_x)\cdot A-p\cdot A-\sigma_x\cdot A+\mathrm{T}\cdot dx=0 \tag{2.1}$$

Rearranging Equation (2.1);

$$\frac{dp}{dx}+\frac{d\sigma_x}{dx}+\frac{\mathrm{T}}{A}=0 \tag{2.2}$$

based on the difference for force analyses, $\frac{\mathrm{T}}{A}$ has three forms.

Without considering porosity, all previous slug investigators extend their research based on the solution to Equation (2.2). For cohensionless materials, the solution is;

$$\frac{\Delta p}{L_s}=\frac{4\mu_w K_w}{D}\sigma_f+\omega\rho_b g\mu_w \tag{2.3}$$

where ω is a constant related to the friction caused by slug weight. The following different approaches have been used to estimate ω.

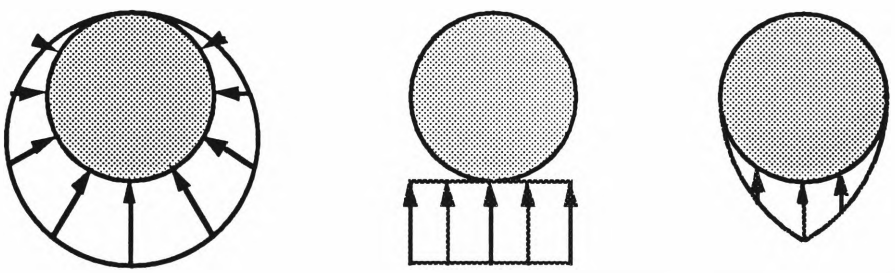

(a) Hydrostatic model (b) Block model (c) Lower half pressure model

Fig. 2.3 The different analyses of the wall stress caused by particle weight

(1) Many investigators [1, 19, 21, 23-26, 28, 30, 34, 37] consider that the normal stress at the pipe wall, caused by the slug weight only, is due to "hydrostatic pressure" as shown in Fig 2.3(a), under this situation $\omega=2$.

(2) See Fig. 2.3(b), some researchers [28] believe that the friction caused by the slug weight is equal to that of a rigid block of the same weight contacting to the pipe wall, it is derived that $\omega = 1$.

(3) Zheng et al [37] considered the stress acting in the lower half of the pipe only, see Fig 2.3(c), $\omega = \frac{8}{3\pi}$.

Without considering that bulk materials can move from place to place under certain conditions, the force analysis of Fig. 2.3(b) is questionable. The force analysis in Fig. 2.3(c) is inaccurate because it fails to calculate the stress in the upper half of the pipe and the calculation of the stress in the lower half is unreasonable. If the upper half of the pipe was removed, surely, without the restriction of the pipe wall the particles in the upper half part would flow outwards. Also bulk materials cannot be considered as solid blocks. Compared to the force analyses in Fig. 2.3(b) and Fig. 2.3(c), the force analysis in Fig. 2.3(a) is more reasonable.

2.3 Stress Transmission Coefficient

There are many conflicting theories for this subject, for novices the subject is very confusing.

There are two kinds of stress state, namely active and passive which come from retaining wall theory. Many slug investigators quote these terms, but none of them provide explanation. The following is a brief description for the definitions: [38]

(1) **Active stress:** A retaining wall is required mainly to resist the lateral pressure exerted by the retained materials. If a retaining wall with a backfill consisting of cohesionless material as shown in Fig. 2.4(a) is moved away from the backfill slightly, the soil would also tend to move with the wall. The frictional forces would become fully mobilised along the failure surface which is approximately a plane surface at an angle of $(45^{\circ} + \phi/2)$ with the horizontal (see Fig. 2.4(a), $\angle ABC = 45^{\circ} + \phi/2$). The force that is causing failure is a minimum and is termed as active earth pressure or commonly called active stress.

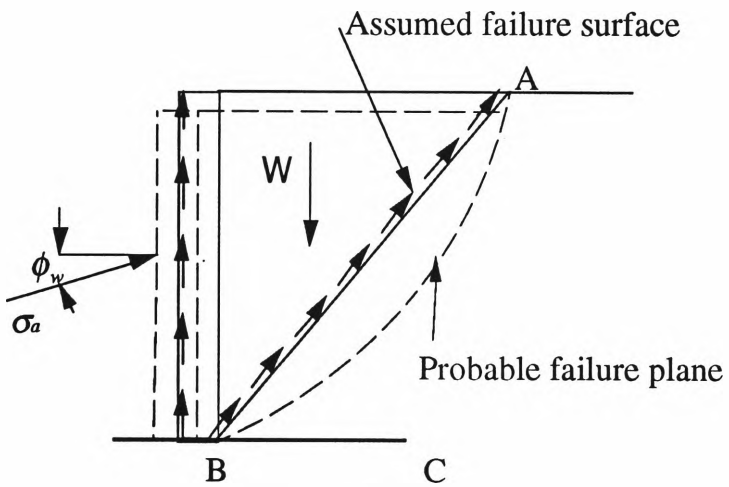

(a) Active earth pressure σ_a

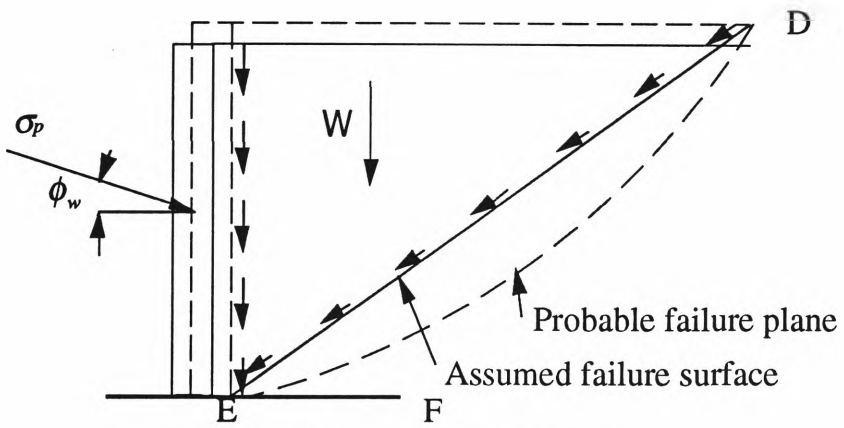

(b) Passive earth pressure σ_p

Fig. 2.4 Definition for stress state

(2) Passive stress: If the wall is moved into the backfill as in Fig. 2.4(b), the failure surface is again approximately a plane surface at an angle of $(45^{\circ} - \phi/2)$ with the horizontal (see Fig. 2.4(b), $\angle DEF = 45^{\circ} - \phi/2$). The displacement of the wall against the soil should be sufficient to overcome frictional resistance along the failure surface and to lift the weight of the wedge upward along the failure surface. The pressure in this case is maximum and is termed as passive earth pressure, or commonly called passive stress.

Konrad writes [19] "since granular materials are frictional, it is rarely possible to predict the stress distribution unambiguously. Normally it is only possible to predict the range within which the stresses must lie, the two extremes being known as the active and passive solutions". According to powder mechanics, a slug slice can keep balance with wide range of stress transmission coefficient.

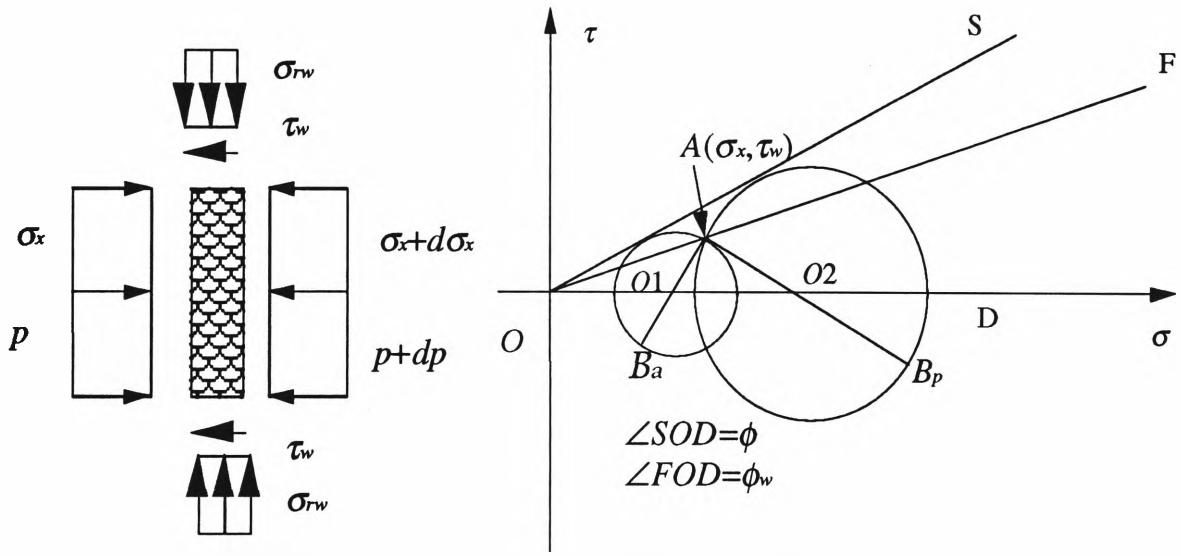

(a) A slug alice (b) Mohr circle

Fig. 2.5 Mohr circle diagram for an element of cohensionless material

The forces acting on the slug element in Fig. 2.2 are shown in Fig. 2.5(a). The corresponding Mohr circle for a cohesionless material is shown in Fig. 2.5(b).

Based on Konrad' s article [19], if point $A(\sigma_x, \tau_w)$ in Fig. 2.5(b) is known, then, the stress condition B_p is for the passive case and B_a for active case. The actual value of radial stresses is situated between B_a and B_p. Konrad declared that the radial stress σ_r is a passive stress of σ_x, the expression is

$$K_w = \frac{\sigma_{rw}}{\sigma_x} = \frac{1+\sin\phi\cos(\omega+\phi_w)}{1-\sin\phi\cos(\omega+\phi_w)} \tag{2.4}$$

where $\sin\omega = \frac{\sin\phi_w}{\sin\phi}$ for cohesionless materials.

If the stress is active, then the stress transmission coefficient can be calculated as;

$$K_w = \frac{\sigma_{rw}}{\sigma_x} = \frac{1-\sin\phi\cos(\omega-\phi_w)}{1+\sin\phi\cos(\omega-\phi_w)} \tag{2.5}$$

where $\sin\omega = \frac{\sin\phi_w}{\sin\phi}$ for cohesionless materials.

Based on the above, $K_w \geq 1$ for passive state, and $K_w \leq 1$ for active state. Konrad et al [19] only give the range of stress transmission coefficient.

Equation (2.4) is accepted widely [1, 21, 28, 30, 37]. Mi and Wypych [23-26] modified Equation (2.4), and considered an intermediary angle ϕ_i which is greater than ϕ_w and less than ϕ (that is, $\phi_w \leq \phi_i \leq \phi$, replacing ϕ in Equation (2.4)/Equation (2.5) with ϕ_i for the calculation of K_w). Based on the experiments of four bulk materials, Mi and Wypych [23] found that the stress state is active and give an empirical formula for ϕ_i;

$$\phi_i = \frac{4}{3}\phi_w\gamma_b^{1/3} \tag{2.6}$$

Legel and Schwedes [21] considered that K_w approximately equal to the ratio of horizontal to vertical stress for the calculation of stresses in silos and hoppers, $K_w \approx 1 - \sin\phi$ and is adopted from soil mechanics.

Konrad' s analyses for the force balance in an element of bulk material is valuable, however, his Mohr circle presentation is only valid for the element on the boundary of the slug and the pipe. Ref. [19, 28] considered the stress state as passive, and analyses the variation range of ϕ_i. The empirical formula for ϕ_i recommended by Mi and Wypych [23, 26] may be useful for slug research, but its validity needs to be examined by further experiments. The consideration of Legel and Schwedes [21] is simple, but further experiments are needed.

A widely accepted formula for stress transmission coefficient has not been available. In fact, the calculation of stress transmission coefficient has troubled slug investigators for many years.

2.4 Stationary Layer

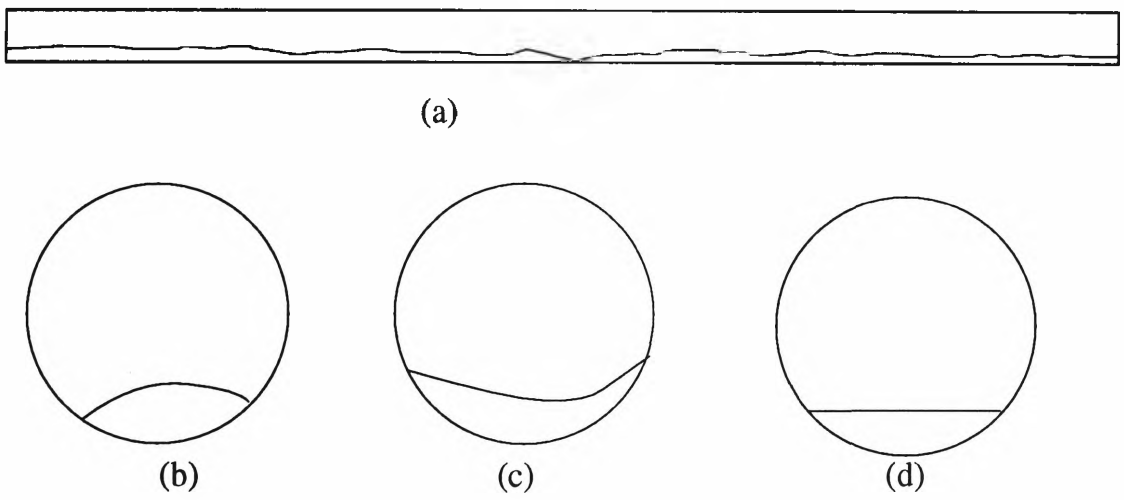

Fig. 2.6 The profiles of particles left behind a moving slug

A typical stationary layer left behind a moving slug is shown in Fig. 2.6

The slug sweeps up the stationary layer in front of it and simultaneously deposits a stationary layer. Konrad et al[18, 19] considered that an analogy between dense-phase pneumatic conveying and two-phase gas/liquid flow and adopted an expression to calculate α;

$$\alpha = \frac{1}{1 + \frac{V_s}{0.542\sqrt{gD}}} \tag{2.7}$$

Konrad and Davidson [18] carried out tests to verify Equation (2.7) and state "the motion of each gas slug relative to the particle plug ahead of it appears to be the same as for a gas bubble moving through an invisid liquid in a horizontal tube". Mi and Wypych [23, 26] also performed experiments and found that the agreement was quite good.

Both Konrad et al [19] and Mi et al [23, 26] adopted the method of photographs to estimate the value of α. All slug researchers have observed that the fluctuation of slug velocity is considerable, This means that the thickness of the stationary layer behind a moving slug is not always the same, see Fig. 2.6(a), and in any cross-sectional area, the profiles of particles left behind are different from one to another, see Fig. 2.6(b) and Fig. 2.6(c). An ideal profile is shown in Fig. 2.6(d). Thus, the accuracy of such a measurement method is doubtful. It is believed that the photographic method may overestimate stationary layer, thus, the validity of Equation (2.7) should be examined by further tests.

2.5 Relationship between Slug Velocity (V_p) and Particle Velocity (V_s)

Considering the similarity between slug movement and liquid flow, Konrad et al [19] found

$$V_s = (1-\alpha)V_p \tag{2.8}$$

If the bulk density of the stationary layer is not equal to that of the slug, another investigator [21] determined

$$V_s = (1-\alpha\cdot\frac{\rho_{b\cdot st}}{\rho_b})V_p \tag{2.9}$$

which results from a mass flow balance at the slug.

2.6 Estimation of the Stress (σ_f) in front of Slug

Considering velocity with respect to the front face of the moving slug, Konrad et al [19] derived the stress (σ_f) by a momentum balance;

$$A\sigma_f = \rho_b A(V_p - V_s)[V_p - (V_p - V_s)]$$

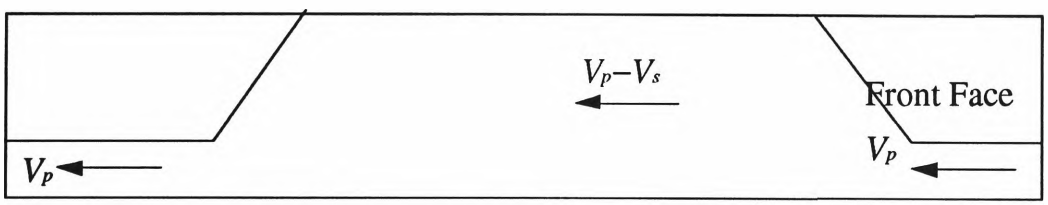

Fig. 2.7 The slug movement analysis of Konrad

so that

$$\sigma_f = \rho_b(V_p - V_s)V_s \tag{2.10}$$

Another Konrad expression [19, 28] for σ_f is

$$\sigma_f = \frac{\alpha \rho_b V_s^2}{1-\alpha} \tag{2.11}$$

The stress (σ_f) expression of Mi and Wypych [23] is based on momentum theory and is different from that of Konrad [19];

$$\sigma_f = \frac{A_{st}}{A} \rho_b V_s^2 = \alpha \rho_b V_s^2 \tag{2.12}$$

It should be noted that slug velocity (V_p) is not equal to particle velocity (V_s). Due to the slug "picking up" the stationary layer, the slug velocity is greater than that of the particles contained in the slug.

Now the stress (σ_f) is the stress between particles and along the axial direction. Since in any cross-sectional area A, particles occupy the area of $(1-\varepsilon)A$. A in the momentum balance and Equation (2.12) should be replaced by $(1-\varepsilon)A$. Former investigators [1, 7, 11, 15, 21, 23-26, 28, 30, 34, 37] have overlooked this voidage affect.

2.7 Pressure Drop and Slug Length

The pressure drop across a slug can vary between a linear and an exponential function. If the material particles are not packed enough to significantly affect the permeability of the slug, the pressure drop is proportional to the slug length; if the material particles interact in such a way as to reduce the permeability significantly, the pressure drop increases exponentially with slug length [6].

Present slug investigators, such as Konrad et al [19], Gu and Klinzing [28], Borzone and Klinzing [4], Mi et al [23] and Pan et al [28], have demonstrated experimentally a linear pressure drop with slug length.

2.8 Air Leakage through Slug

Both Konrad et al [19] and Pan et al [28] adopted the Ergun [8] Equation to estimate pressure drop and air supply. This empirical equation was developed by Ergun to estimate the pressure drop through packed columns. The media was an incompressible fluid and the factors considered to influence the pressure drop were;

(1) Rate of fluid flow;
(2) Viscosity and density of the fluid;
(3) Closeness and orientation of packing;
(4) Size, shape, and surface of the particles.

Ergun [8] based pressure drop on simultaneous kinetic and viscous energy losses:

$$\frac{\Delta p}{L} = a\mu V_m + bGV_m \tag{2.13}$$

or

$$\frac{\Delta p}{L} g = 150\frac{(1-\varepsilon)^2}{\varepsilon^3 d_p^2}\cdot \mu V_m + 1.75\frac{1-\varepsilon}{\varepsilon^3 d_p}\cdot GV_m \tag{2.14}$$

where G is the mass flow rate of the fluid and V_m is the superficial fluid/gas velocity measured at average pressure.

It is evident from Equation (2.14) that pressure drop strongly depends on the effective diameter of particles (d_p), which sometimes is difficult to measure and represent the complete bulk solid; Tsuji et al [33] commented that the pressure across a moving slug was less than that across a packed bed of the same particles. Hence, the Ergun Equation did not appear suitable for slug investigation.

Mi and Wypych [23] considered the slug and the particles moving at the same velocity (V_s), they used an empirical formula to correlate superficial air velocity with slug velocity, however, the empirical expression also is a function of (d_p).

$$V_s = k(V_a - V_{a\min}) \tag{2.15}$$

where $V_{a\min}$ is the minimum air velocity and k is the slope of the line of best fit, Mi and Wypych [23] found that

$$V_{a\min} = \frac{\rho_s g \tan\phi_w \varepsilon^3 d_p^2}{180(1-\varepsilon)\eta} \tag{2.16}$$

$$k = 105\frac{\varepsilon d_p}{D} \cdot (\frac{\tan\phi_w}{\tan\phi})^{1/3} \tag{2.17}$$

Both Equation (2.16) and Equation (2.17) contain d_p, thus, the application of Equation (2.15) is not convenient for products with a wide range of particle size.

In order to avoid the measurement of d_p, Konrad et al [19] obtained the values of a and b in Equation (2.13) by experiment, but Konrad et al [19] did not explain the procedure. Pan [27] introduced his own method to measure the Ergun Constants of a and b.

2.9 Brief Descriptions of Recent Slug Investigation

Konrad is one of the most important slug investigators and published a well organised article [16] in 1986, in which he reviewed the approaches in slug research before 1984. Brief descriptions of the slug investigations between 1984 and 1995 are provided below.

Generally, there are two factors that mostly concern slug users and investigators, one is pressure drop (Δp), the other is slug velocity (V_p). In order to predict their values, two equations are needed. Konrad et al [19] and Pan and Wypych [28] use Equation (2.3) and Equation (2.14) in their articles, one is based on powder mechanics analysis, the other on the Ergun Equation. Mi and Wypych [23] developed an empirical formula (that is Equation (2.15)) to correlate slug velocity (V_p) with superficial air velocity (V_a), not the Ergun Equation (2.14).

Mi and Wypych [23] found that the pressure drop across the length (L_p) of horizontal pipe is

$$\Delta p = (1 + 1.084 K_w Fr^{0.5} + 0.542 Fr^{-0.5}) \frac{2 g \mu_w m_s L_p}{A V_s} \tag{2.18}$$

where $Fr = \frac{V_s^2}{gD}$, and m_s is bulk material flow rate.

Legel and Schwedes [21] presented a semi-empirical formula to predict the pressure drop in horizontal slug flow. Unfortunately, there is an error in their data measuring system, they measured the friction by load cell, as shown in Fig. 2.8(a). Their test system, in fact, is equivalent to a mass-spring system, as shown in Fig. 2.8(b), in which the recorded data

is not usually equal to the exciting force. Thus, the validity of the semi-empirical formula is doubtful.

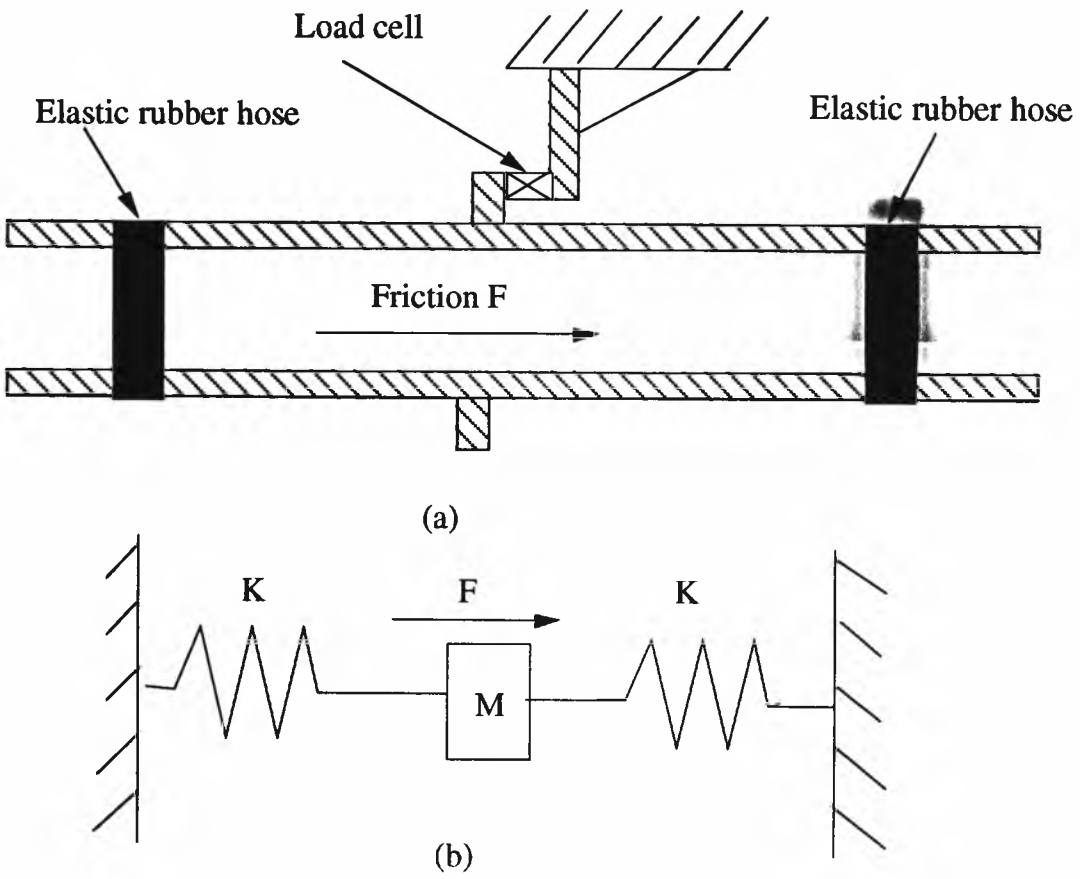

Fig 2.8 Schematic drawing of measuring pipe

Aziz and Klinzing [1] conducted an experimental study of coal as a plug at low air velocity in a horizontal pipe and a 45^0 inclined pipe. They concluded that the pressure drop varied linearly with the plug length and was essentially independent of the air velocity. Aziz and Klinzing [1] analysed the force balance of a plug element in a 45^0 inclined pipe, see Fig. 2.9:

$$\frac{dp}{dx}+\frac{d\sigma_x}{dx}+\frac{4\tau_w}{D}+\rho_b g\sin\alpha=0 \tag{2.19}$$

They calculated τ_w by Equation (2.20).

$$\tau_w = C_w + \sigma_w \tan \phi_w \tag{2.20}$$

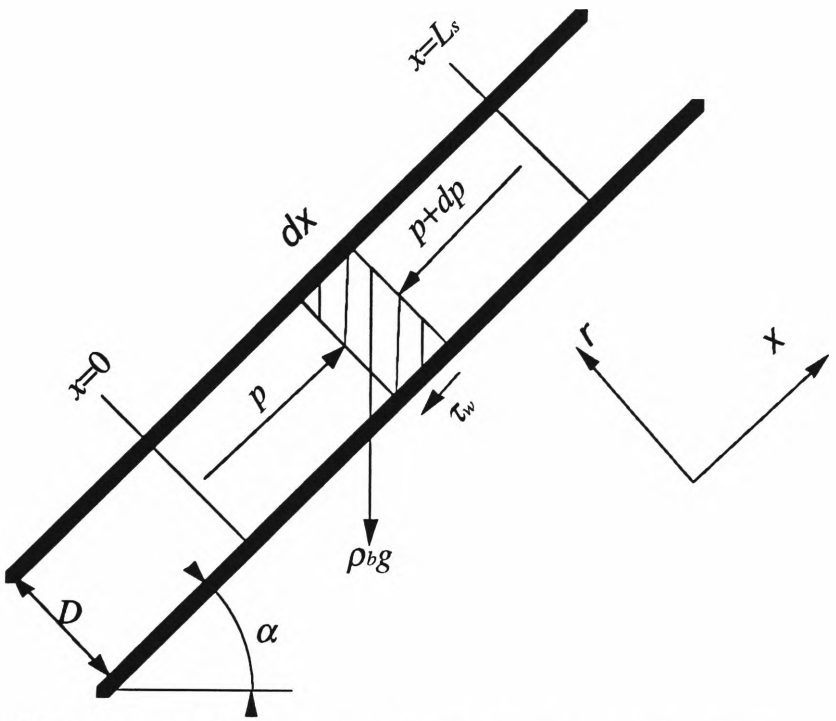

Fig. 2.9 The force balance on a plug of cohesive powder in an inclined pipeline

They derived Equation (2.21) and Equation (2.22) by manipulation of the Mohr's Circle diagram:

for passive failure:

$$\tau_w = C_w + K_w \sigma_w \tan \phi_w + R\rho_b g \tan \phi_w + (K_w + 1)C \cos \phi \tan \phi_w \cos(\omega + \phi_w) \tag{2.21}$$

where K_w and ω is the same as that in Equation (2.4)

and for active failure:

$$\tau_w = C_w + K_w \sigma_w \tan \phi_w + R\rho_b g \tan \phi_w - (K_w + 1)C \cos \phi \tan \phi_w \cos(\omega - \phi_w) \tag{2.22}$$

where K_w and ω are the same as that in Equation (2.5)

Aziz and Klinzing considered that $Rg\rho_b \tan\phi_w$ in Equation (2.21) or Equation (2.22) is to account for the normal stress at the wall due to the effect of gravity. It should be noted that $Rg\rho_b \tan\phi_w$ is only valid for $\alpha = 0$, thus, for inclined pipe, the stress caused by particle weight is $(Rg\rho_b \tan\phi_w)\cos\alpha$, not $Rg\rho_b \tan\phi_w$. Aziz and Klinzing's analysis is questionable, and hence, their theoretical expression of pressure drop gradient is not correct. However, their experimental work is valuable.

Gu and Klinzing [11] have investigated vertical plug flow of cohesive coal in 2- and 4-inch pipes, they found that the plug velocities appeared to be a weak function of the plug length but were largely controlled by the air velocity, and as plug length increased, the plug velocity decreased a little at a fixed air flow rate. This means that air leakage varied inversely with the plug length, or in other words, the air leakage can be negligible if the slug is long enough. However, as other investigators, Gu and Klinzing [11] failed to consider voidage in the analyses of force balance equation.

Dhodapkar, Plasynski and Klinzing [7] addressed the plug system, They analysed the overall pulse-piston system, and then introduced the design procedure, the system capacity under a given diameter is discussed also. However, the calculation of many factors such as the pressure drop, slug velocity, and air leakage is controversial, thus, further research is needed.

Tsuji and Morikawa [32] are possibly one of the first researchers to have investigated the plug flow of coarse particles in a horizontal pipe with a sub-pipe for secondary air injection. Their investigation includes particle flow pattern, the behaviour of particles left

behind a moving plug, and pressure drop. This work is valuable in understanding slug conveying.

Wilson [34] derived the balance differential equation for a moving slug (see Equation (2.23)), he gave an expression for σ_w (see Equation (2.24));

$$\frac{dp}{dx}+\frac{d\sigma}{dx}=\frac{\bar{\tau}}{D} \tag{2.23}$$

$$\sigma_w = K_w\sigma_x - \rho_e g c z \tag{2.24}$$

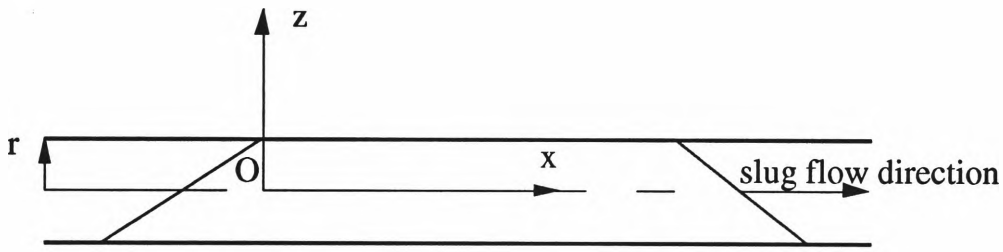

Fig. 2.10 Coordinate system for slug flow

ρ_e is the submerged effective density (density of solids minus density of fluid) c is volumetric solids fraction (volume of solids/total volume). Wilson considered that the top-to-bottom variation of c is negligible, but c, together with K_w will vary in the x direction only, see Fig. 2.10, Wilson chose the origin position where $\sigma_w = 0$ and $z = R$. It is evident that Wilson's balance equation (2.23) conflicts with that of Konrad et al [19] and his origin position does not exist at all. According to Mi and Wypych's [23] experimental investigation, the intergranular stress in a moving slug is very small, and c can be actually treated as a constant.

Rao et al [30] predicted the shape of the gas-particle interface between two particle plugs conveyed pneumatically through a horizontal pipeline, As their research is based on Konrad's theory which is controversial, the result is unreliable.

Grindle [39] described a commercially used slug system with the capacity of 2-30t/h for a wide range of stoneground wholemeal flours.

Jiang Hong et al [40] derive a model for stratified flow, the assumptions for modelling stratified flow are

(1) In dilute suspension, particle-particle interaction is negligible and all particles move at the same average velocity in the flow direction;

(2) In a dense sliding bed, gas and solid have the same velocity and voidage in a sliding bed is approximately equal to that of a loosely packed bed;

(3) Solids are spherical particles with the same size, the gaseous phase is incompressible and the conveying process is isothermal;

(4) The surface of the sliding bed is flat.

Wypych [35, 36, 41] is one of the modern slug activists, he has been engaged in dense-phase pneumatic conveying research for many years. He has published numerous papers about the slug system test rig, design consideration, the classification of granular materials, and the slug theory investigation. Wypych and Hauser [41] proposed basic principles for the design of low-velocity pneumatic conveying systems after summarising the progress in research and technology. They indicated that the design considerations must include the following three aspects:

(1) Selecting a most suitable pattern of conveying for the given material by analysing the material characteristics and using the existing methods of material/conveying phase classification;

(2) Selecting the most suitable conveying system to confirm flow pattern and avoid pipeline blockages;

(3) Establishing reliable and economical operating conditions according to conveying characteristics.

Wypych and Hauser [41] further recommended the method for the selection of flow pattern.

There is very little data available about energy consumption. Mi and Wypych [23] considered that the required power for slug system is

$$N = \Delta p \cdot A \cdot V_a = (1 + 1.084 K_w Fr^{0.5} + 0.542 Fr^{-0.5}) \frac{2 g \mu_w m_s L_p}{V_s} V_a \qquad (2.25)$$

where $Fr = \frac{V_s^2}{gD}$, m_s is bulk material flow rate, and V_a is superficial air velocity.

Based on Equation (2.25), Mi and Wypych [23] calculated the 'economical superficial air velocity, mass flow rate and the maximum pressure drop'.

2.10 Summary of Investigations into Dense-Phase Pneumatic Conveying

(1) Despite many years of research, the theories for dense-phase pneumatic conveying are still primitive;

(2) Generally, the derivation of a theory is only based on limited materials, and all existing theories ignore the aerodynamic drag on individual particles and the pressure drop caused by air only;

(3) There are over a dozen theories for dense-phase pneumatic conveying, but none of them is universally accepted, conflicting theories often cause confusion;

(4) Its basic mechanism has not been fully understood yet, empirical formulae are widely employed for the calculation of some factors;

(5) Owing to the complex mechanism of conveying, large scale test rigs are needed for its investigation.

CHAPTER 3

THEORY

3 THEORY

3.1. Introduction

Dense phase pneumatic conveying is receiving increased attention because of low pipe erosion and low material degradation. The pressure drop has been the subject of a number of theoretical analyses and experimental investigations[1, 4, 6, 7, 11, 12, 14-21, 23-30, 32-37].

The aim of this chapter is to develop a model for single-slug flow, the model should be capable of predicting pressure drop and slug velocity which are essential for slug system design.

According to experimental observation, of an ideal bulk material in normal slug flow, four characteristics exist:

(1) Mixture of air and particles is isotropic

Although particle size and shape are quite different within the mixture, most of the particles are in contact with each other and it is reasonable to assume the particle collection as an isotropic material.

(2) All particles in the pipe are mixed fully with air, but maintain contact with their nearest neighbours.

Particle velocity is much lower than its saltation velocity (ie. for dilute-phase). Hence, particles build up and fill up the pipe during conveying, see Fig. 3.1.

(3) The mixture is relatively incompressible.

The flowing mixture is composed of air and solids. The air is compressible, but the solids are in a loose-packed condition and hence relatively incompressible (ie. for granular products such as grain and plastic pellets).

(4) There is very little movement between particles in the steady-state area of a moving slug

A moving slug can be divided into two main areas (see Fig. 3.1): particles in the steady-state area travel in the same direction and at the same velocity although some slip may occur between particles, their relative positions do not change; in the transient area, the particles move in different directions and at different velocities. Generally, transient areas only take a small portion.

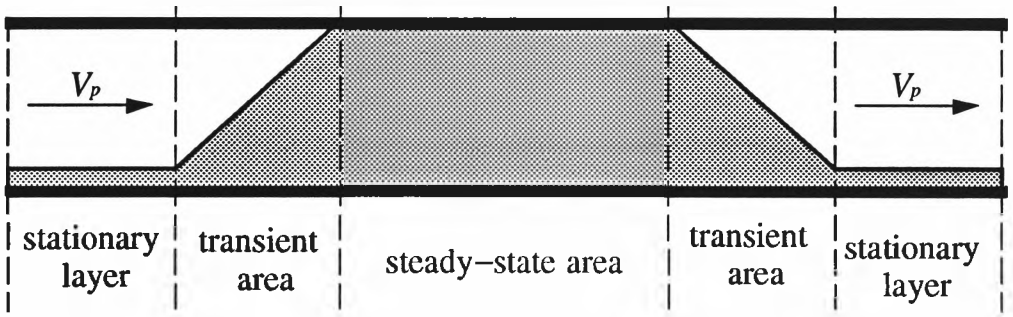

Fig. 3.1 Various areas of moving slug

3.2. Force and Stress Analyses

3.2.1 Force Analyses

In an elemental slice of material in the steady-state area (see Fig. 3.2.), p and dp denote interstitial air pressure within the moving slug and its increment. σ_x denotes the cross-sectional intergranular normal stress along the pipe axis and $d\sigma_x$ denotes its increment.

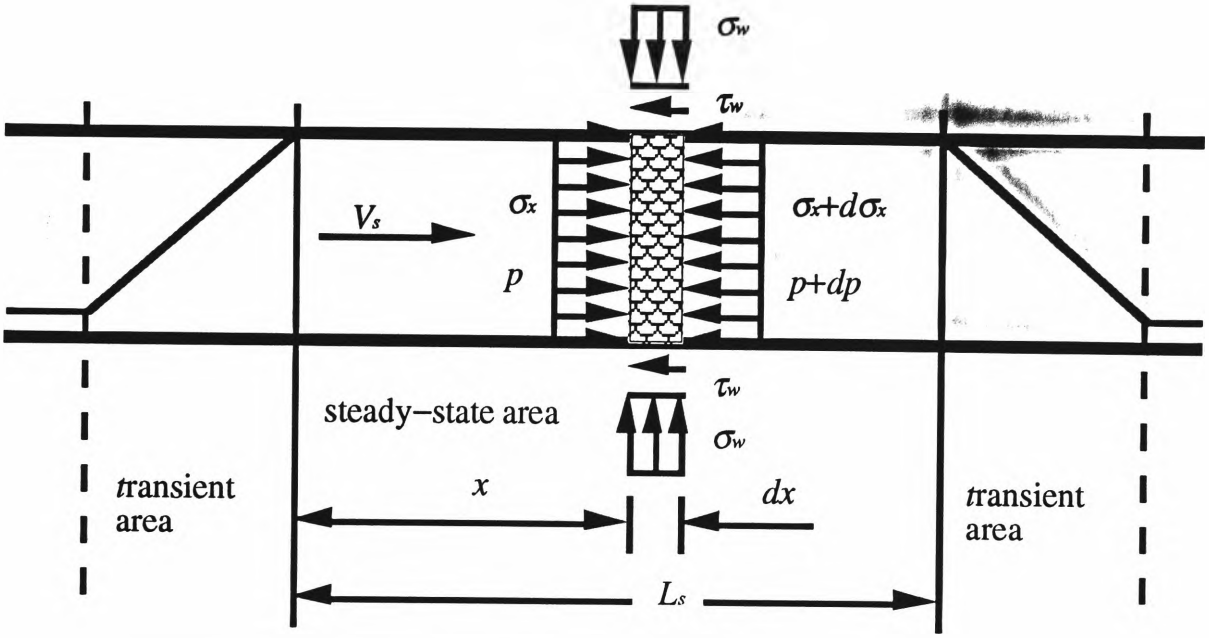

Fig. 3.2 Forces acting on elemental slice in steady-state area of a moving slug

Statistically, in any cross-sectional area of a slug, the area occupied by particles is $(1-\varepsilon)A$, not A, thus, σ_x and $\sigma_x + d\sigma_x$ act on area $(1-\varepsilon)A$, not on A. Slug flow is more or less similar to the movement of a capsule, in that both are activated by pressure drop. For a capsule, the effective pushing area is the actual cross-sectional area of capsule, not pipe cross-sectional area. For the same reason, the effective area of a slug is the area occupied by particles, not entire pipe cross-sectional area, that is $(1-\varepsilon)A$, not A.

What has been described above is quite different to the theory of Konrad et al [19], who considered p, $p+dp$, σ_x and $\sigma_x + d\sigma_x$ all acting on the entire pipe cross-sectional area A. The Konrad theory and its derived results or other similar analyses have been accepted widely [1, 7, 11, 21, 23-26, 28, 30, 34, 37].

Janssen, a German Engineer, published the celebrated paper "Versuche über Getreidedruck in Silozellen" (On the Measurement of Pressure in Grain Silos) in 1895. Janssen's research laid the foundation for our understanding of the behaviour of particulate solids under silo storage conditions. Roberts [31] published a review marking the 100 year anniversary of Janssen's epic paper. Based on this paper [31], the present author found that the stresses Janssen considered 100 years ago are the average stresses (ie. due to gravity and forces between particles and the silo wall). However, in slug flow the interaction forces occur between particles, interstitial air and the pipe wall. It is the intergranular normal stress along the pipe axis (σ_x), not the average axial stress ($\overline{\sigma_x}$) that is of interest here. The intergranular normal stress along the pipe axis is defined as $\sigma_x = \frac{F}{(1-\varepsilon)A}$, while the average axial stress as $\overline{\sigma_x} = \frac{F}{A}$, where F is the total intergranular force acting along the axial direction.

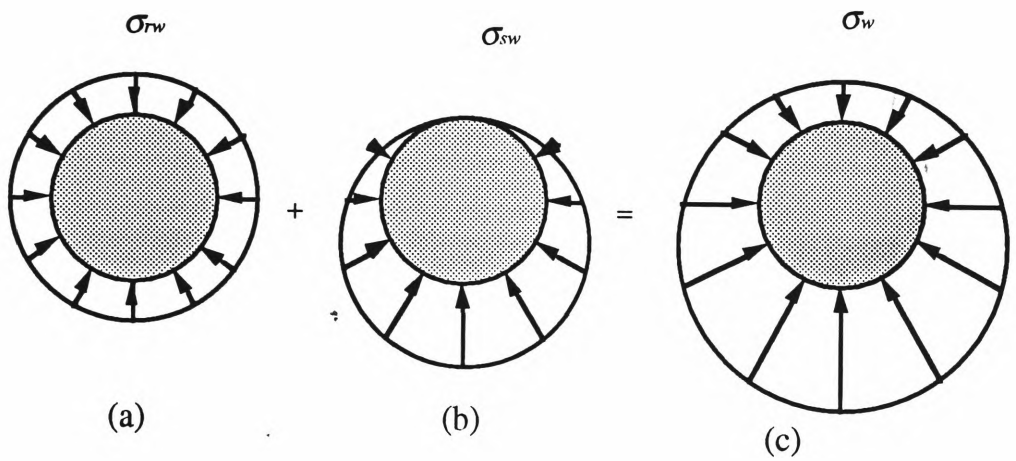

Fig. 3.3 Stress analyses
(a) Normal wall stress due to intergranular normal stress
(b) Normal wall stress due to bulk material weight
(c) Total normal wall stress

Konrad et al [19] have not applied Janssen's theory [31] correctly. In fact, all the latest versions of slug theory are based on Konrad's investigation [19] or have overlooked voidage (ε) [1, 7, 11, 21, 23-26, 28, 30, 34, 37].

Now σ_w is the total normal stress acting on the pipe internal surface, and is equal to the sum of σ_{sw} and σ_{rw} as shown in Fig. 3.3. T_{sw} and T_{rw} denote the friction force caused by σ_{sw} and σ_{rw} respectively, and T_w is equal to the sum of T_{sw} and T_{rw}.

σ_{sw} is caused by the material weight, see Fig. 3.4, and is the normal stress at the wall due to "hydrostatic pressure", $\sigma_{sw} = (1+\cos\theta)\rho_b g R$ [19]. The friction force (T_{sw}) acting on the slice is caused by σ_{sw}, and is equal to:

$$T_{sw} = \int_0^{2\pi} \tau_{sw} dA = \int_0^{2\pi} (\mu_w \sigma_{sw})(R dx d\theta) = 2\pi \mu_w \rho_b g R^2 dx \qquad (3.1)$$

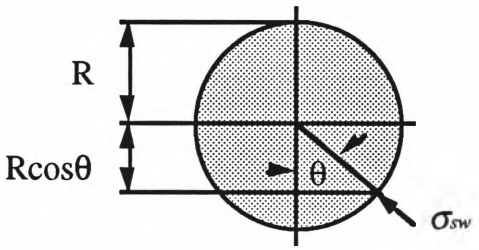

Fig. 3.4 Cross section of slug

Since σ_{sw} is considered as "hydrostatic pressure", the area (dA), contact area between "hydrostatic body" and wall, should be $Rdxd\theta$.

Without a pipe, the slug would spray outward. Apparently, σ_{rw} is perpendicular to σ_x and is caused by σ_x. We take the ratio of σ_{rw} to σ_x as stress transmission coefficient (K_w). According to powder mechanics, σ_{rw} and σ_x can keep balance at wide distribution of stress transmission coefficient (K_w) (namely from active stress state to passive stress state). The relationship of σ_{rw} and σ_x has troubled slug investigators for many years, even whether the stress state in slug is active or passive is a controversial problem. Konrad et al [19] considered that the stress state is passive, and this idea was widely accepted by other slug investigators [1, 4, 7, 11, 14, 15, 21, 23-27, 28-30, 34-37].

However, recently Mi and Wypych [23] investigated multi-slug flow and found that the stress state is active. Because of the inconvenience in the determination of stress transmission coefficient (K_w), some investigators [23] prefer to empirical formulae. Based on many experiments, the present author recommends the following empirical formula (refer to Appendix A).

$$K_w = \frac{1}{1+\sin\phi} \tag{3.2}$$

Friction force (T_{rw}) of the slice is caused by σ_{rw} :

$$T_{rw} = \int_0^{2\pi} \tau_{rw} dA = \int_0^{2\pi} (\mu_w \sigma_{rw})[(1-\varepsilon) R dx d\theta]$$

$$= \int_0^{2\pi} (\mu_w K_w \sigma_x)[(1-\varepsilon) R dx d\theta]$$

$$= (1-\varepsilon)(2\pi R \mu_w K_w \sigma_x) dx \tag{3.3}$$

Note, since interstitial air pressure and particle stress are treated separately, the area (dA) of particles in contact with pipe wall should be $(1-\varepsilon)Rdxd\theta$, not $Rdxd\theta$ as appeared in Equation (3.1).

T_w is the slice's total friction force on the pipe wall.

$$T_w = T_{sw} + T_{rw}$$

Substituting T_{sw} and T_{rw} in Equation (3.1) and (3.3) respectively into above Equation;

$$T_w = 2\pi R\mu_w[\rho_b gR + (1-\varepsilon)K_w\sigma_x]dx$$

Letting

$$T = 2\pi R\mu_w[\rho_b gR + (1-\varepsilon)K_w\sigma_x] \tag{3.4}$$

(T can be considered as friction force per unit slug length)

then:

$$T_w = Tdx \tag{3.5}$$

3.2.2 Equilibrium Equation and its Solution

The axial forces acting on particles of a slug cross-sectional area (see Fig. 3.2) can be summarised as follows:

Table 3.1: Axial forces acting on material of a slug slice

Force	Format
intergranular normal force	$\sigma_x(1-\varepsilon)A$
intergranular normal force	$(\sigma_x + d\sigma_x)(1-\varepsilon)A$
force caused by interstitial air pressure	$p(1-\varepsilon)A$
force caused by interstitial air pressure	$(p+dp)(1-\varepsilon)A$
total friction force	$2\pi R\mu_w[(1-\varepsilon)K_w\sigma_x + \rho_b gR]dx$

Assuming the slice obeys the Coulomb failure criterion and particle cohesion is negligible, and according to equilibrium, the following differential equation can be derived:

$$\frac{dp}{dx}+\frac{d\sigma_x}{dx}+\frac{T}{(1-\varepsilon)A}=0 \tag{3.6}$$

If σ_x and p are functions of x only, and the pressure gradient is constant [19, 23, 28], then $\frac{dp}{dx}=-\frac{\Delta p}{L_s}$. The solution to Equation (3.6) is:

$$\sigma_x = C\exp(-\frac{4\mu_w K_w}{D}x)+(\frac{\Delta p}{L_s}-\frac{2\rho_b g\mu_w}{1-\varepsilon})\frac{D}{4\mu_w K_w} \tag{3.7}$$

where C is an integration constant.

If $\sigma_x = \sigma_b$ at x=0 and $\sigma_x = \sigma_f$ at x= L_s (3.8)

then from Equation (3.7):

$$\sigma_x = \frac{\sigma_b-\sigma_f}{1-\exp(-\frac{4\mu_w K_w}{D}L_s)}\exp(-\frac{4\mu_w K_w}{D}x)+(\frac{\Delta p}{L_s}-\frac{2\rho_b g\mu_w}{1-\varepsilon})\frac{D}{4\mu_w K_w} \tag{3.9}$$

and

$$\sigma_f = \frac{\sigma_b-\sigma_f}{1-\exp(-\frac{4\mu_w K_w}{D}L_s)}\exp(-\frac{4\mu_w K_w}{D}L_s)+(\frac{\Delta p}{L_s}-\frac{2\rho_b g\mu_w}{1-\varepsilon})\frac{D}{4\mu_w K_w} \tag{3.10}$$

Generally, slug length (L_s) is much longer than pipe diameter (D), thus, $\frac{4\mu_w K_w}{D}\cdot L_s >> 1$ [19, 23, 28], and for steady state slug conveying, $\sigma_b \approx \sigma_f$, so that

$$\sigma_f = (\frac{\Delta p}{L_s}-\frac{2\rho_b g\mu_w}{1-\varepsilon})\frac{D}{4\mu_w K_w} \tag{3.11}$$

Rearranging Equation (3.11):

$$\frac{\Delta p}{L_s} = \frac{4\mu_w K_w}{D}\sigma_f + \frac{2\rho_b g \mu_w}{1-\varepsilon} \tag{3.12}$$

3.2.3 Stress in Front of Slug

As the material in the stationary layer "hits" the advancing slug and joins the slug movement, its velocity changes from 0 to V_s. According to the momentum theory, the system gains a momentum of $(\alpha_f V_s \Delta t A \rho_b)V_s$ in a period of Δt and the slug is subjected to a force F:

$$F = (\alpha_f V_s \Delta t A \rho_b)V_s / \Delta t$$

The area occupied by particles in the cross-section is $(1-\varepsilon)A$, not A. Hence:

$$\sigma_f = \frac{F}{(1-\varepsilon)A} = \frac{\alpha_f \rho_b V_s^2}{1-\varepsilon} \tag{3.13}$$

A similar analysis gives the result for σ_b

$$\sigma_b = \frac{\alpha_b \rho_b V_s^2}{1-\varepsilon} \tag{3.14}$$

For steady slug conveying, $\alpha_f \approx \alpha_b = \alpha$.

3.2.4 Relationship between Slug Velocity (V_p) and Particle Velocity (V_s)

At a certain moment, the front face of a slug is ACB (see Fig. 3.5) and particle velocity is V_s. After time Δt, the particles in ACB move to $A_1C_1B_1$, During this time, the slug "picks up" stationary layer BB_1 ($BB_1 = \Delta tV_s$) which ends up in position A_1C_1FE. Because the volume of CBB_1C_1 is equal to that of A_1C_1FE:

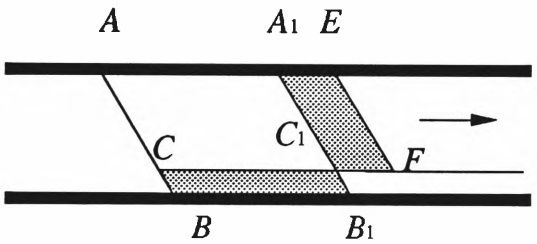

Fig. 3.5 Slug movement

$$\alpha \cdot \Delta tV_s = (1-\alpha) \cdot \Delta V \Delta t$$

$$\Delta V = \frac{\alpha}{1-\alpha} \cdot V_s \tag{3.15}$$

Obviously, the front face velocity or slug velocity (V_p) is larger than the particle velocity (V_s), so that:

$$V_p = V_s + \Delta V = \frac{V_s}{1-\alpha} \tag{3.16}$$

The same result can be derived by applying momentum theory to the back face of the slug.

3.2.5 Length of Slug

For $\alpha_f \approx \alpha_b = \alpha$, the length of slug is

$$L_s = \frac{W_b}{\rho_b(A - A_{st})} = \frac{W_b}{\rho_b A(1-\alpha)} \tag{3.17}$$

The slug sweeps up the stationary layer in front of it and simultaneously deposits a stationary layer behind. The length of the moving slug varies during steady-state operation. If $\alpha_f > \alpha_b$, the length of moving slug will become longer and, if $\alpha_f < \alpha_b$, then the length will become shorter. Since the thickness of a slug trace is influenced by the particle properties and operating factors, it is impossible to repeat an experiment/operation exactly. That is, the thickness of the stationary layer in front and behind a slug is not exactly the same. Fortunately , $\alpha_f \approx \alpha_b$, thus, the variation of L_s is limited.

3.2.6 Stationary Layer behind Moving Slug

Konrad et al [19] considered an analogy between dense-phase pneumatic conveying and two-phase gas/liquid flow and adapted an equation to calculate α. However, slug flow is different from gas/liquid flow mainly in two areas: the internal friction angle ϕ of a bulk solid is greater than that of a fluid (for a fluid, ϕ=0) and there is interlocking/slipping between particles within a moving slug; there is air flow through the slug (although air leakage is very little). The data in Table 3.2 and Table 3.3 show that Konrad et al [19] overestimates the stationary layer behind a moving slug.

Based on the investigation of Konrad et al [18, 19] and considerable mathematical work (eg curve fitting), the author found the following empirical formula to represent well the experimental values of α (see Tables 3.2 and 3.3):

$$\alpha = \frac{1}{1+0.6\frac{\exp(\phi)V_s}{\sqrt{D}}} \tag{3.18}$$

where $\phi(rad)$ is the material's internal friction angle.

Compared to the Konrad equation [19]:

$$\alpha_K = \frac{1}{1+\frac{V_s}{0.542\sqrt{gD}}} = \frac{1}{1+0.59\frac{V_s}{\sqrt{D}}} \tag{3.19}$$

If $\phi = 0$, then equation (3.18) and equation (3.19) would be almost the same.

In Table 3.2, α_k is consistently greater than the tested value (α_t) of stationary layer, often giving nearly two times the measured value. The reason may be that the interlocking between particles results fewer particles left. The more the material internal friction (ϕ) is, the heavier the interlocking will be, resulting in the fewer particles left. Thus, the author considers that α varies inversely with ϕ. Refer to Appendix B for detailed explanation of Table 3.2.

Table 3.2: Comparison of α for PP pellets

($\phi = 27.2^{\circ}$, α_t – test results, α – based on Equation (3.18), α_k – based on Equation (3.19)

Exp. No.	$D(m)$	$V_s(ms^{-1})$	α_t	α	α_K
220-2	0.0525	1.363	0.16	0.15	0.22

220-3	0.0525	1.300	0.13	0.15	0.23
230-3	0.0525	1.733	0.12	0.12	0.18
230-4	0.0525	1.704	0.12	0.12	0.18
230-5	0.0525	1.676	0.15	0.12	0.19
230-6	0.0525	1.664	0.13	0.12	0.19
230-7	0.0525	1.545	0.13	0.13	0.20
230-8	0.0525	1.668	0.15	0.12	0.19

Also, as shown in Table 3.3, Equation (3.18) has been found to predict well the values of α_t determined by Pan and Wypych[28].

Table 3.3: Comparison of α for silica flux

($\phi = 42.4^{\circ}$, α_t – test results, α – based on Equation (3.18), α_k – based on Equation (3.19))

No.	$D(m)$	$V_s(ms^{-1})$	α_t	α	α_K
1	0.105	3.509	0.10	0.07	0.14
2	0.105	2.295	0.11	0.10	0.19
3	0.105	2.084	0.11	0.11	0.21
4	0.105	1.783	0.11	0.13	0.24

(Note: the data in Table 3.3 are based on tests conducted by Pan and Wypych [28])

3.2.7 Pressure Drop in Horizontal Pipe

Substituting Equation (3.13) and (3.17) into Equation (3.12):

$$\Delta p = \frac{1}{1-\varepsilon}\left(\frac{4K_w\mu_w}{D}\alpha\rho_b V_s^2 + 2\rho_b g\mu_w\right)L_s \qquad (3.20)$$

It should be stressed that ρ_b for the calculation of L_s (see Equation (3.17)) and Δp (see Equation (3.20)) is assumed to be equal to the loose-poured bulk density.

If the whole slug is take as an element, Equation (3.20) can be derived by another method.

Since $\alpha_f \approx \alpha_b$ for steady state slug conveying, according to Equation (3.7), σ_x is a constant along the slug, $\sigma_x = \sigma_f \approx \sigma_b$ (see Fig. 3.6(b)). The slug is subjected to five forces (see Fig. 3.6(c)), its balance equation can be written as

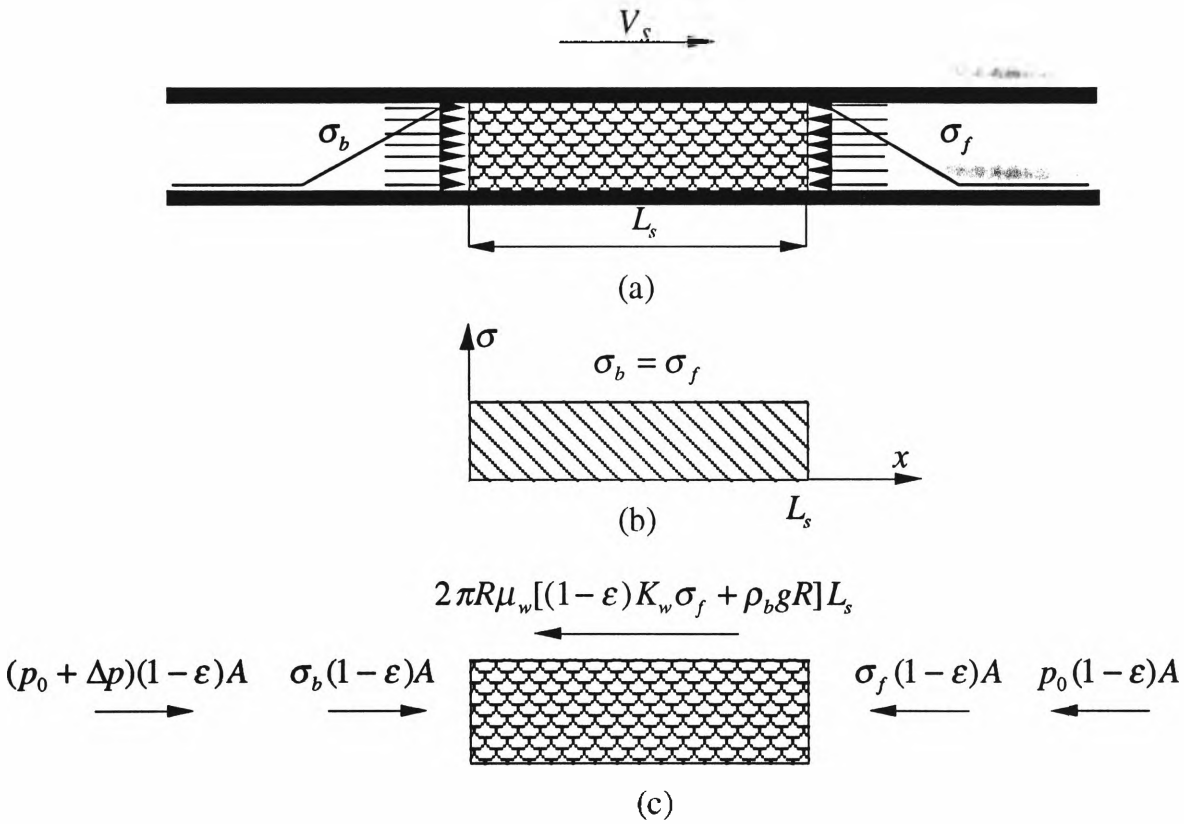

Fig. 3.6 Force analyses on single-slug

$$(p_o + \Delta p)(1-\varepsilon)A + \sigma_b(1-\varepsilon)A - \sigma_f(1-\varepsilon)A - p_o(1-\varepsilon)A$$

$$= 2\pi R\mu_w[(1-\varepsilon)K_w\sigma_f + \rho_b gR]L_s \qquad (3.21)$$

Considering that $D=2R$, $A=\pi R^2$, $\sigma_f = \frac{\alpha_f \rho_b V_s^2}{1-\varepsilon}$ (see Equation (3.13)), and $\sigma_b = \sigma_f = \sigma$, the derived equation for Δp is found to be exactly the same as Equation (3.20).

3.2.8 Relationship between Air Flow-Rate (m_f) and Slug Velocity (V_p)

Some investigators [19, 28, 32] adopted the Ergun [8] Equation to estimate air pressure drop in a slug system. The Ergun Equation strongly depends on effective diameter of particles (d_p), which in many cases is difficult/sometimes impossible to measure; others [23] use an empirical formula to correlate superficial air velocity with slug velocity, however, their empirical equation also is a function of d_p. Keeping in mind that in order to correlate air flow-rate (m_f) and slug velocity (V_p), d_p should be avoided in any equation(s).

Considering that the highly packed particles "block" the whole cross-sectional area of pipe and the slug is long enough (generally from several metres to over ten metres) to limit air percolation effectively, the particles travel more than likely as an extruded stream of material, rather than an air-conveyed stream. Thus, it is assumed that the air flow loss through the slug is so small that it can be neglected. Conversely, all the air is stored behind the slug (that is, in blow tank and pipe behind moving slug).

If cycle time is t_c, then the air supply will be equal to $m_f t_c$ and the air stored in blow tank will be equal to $(V_b + (L_p - L_s)A)\rho_f$, thus

$$m_f t_c = (V_b + (L_p - L_s)A)\rho_f \tag{3.22}$$

Note: experimental data from large scale test rigs have indicated that as the slug comes out of the blow tank, it gradually moves faster and faster. However, the maximum pressure drop generally occurs after a short while when all material is extruded from the blow tank. It is considered that the slug has a uniform velocity within a short distance after it leaves the blow tank. Therefore:

$$t_c \approx \frac{L_p}{V_p} \tag{3.23}$$

The density of air in blow tank and pipe can be calculated as:

$$\rho_f = \frac{p_o + \Delta p}{p_o}\rho_o \tag{3.24}$$

Substituting Equation (3.23) and (3.24) into Equation (3.22):

$$m_f = (V_b + (L_p - L_s)A)\cdot\frac{1}{t_c}\cdot\frac{p_o + \Delta p}{p_o}\rho_o \tag{3.25}$$

or

$$m_f = (V_b + (L_p - L_s)A)\cdot\frac{V_p}{L_p}\cdot\frac{p_o + \Delta p}{p_o}\rho_o \tag{3.26}$$

In order to verify Equation (3.25) or (3.26), tests have been conducted on a small-scale test slug rig, the tested material was PP pellets, a good permeable bulk solid. Detailed description about the test rig and data processing are presented in appendix B. The results are shown in Table 3.4.

Table 3.4: Comparison of air mass flow rates

($V_b = 0.113m^3$, $L_p = 21.3m$, $D = 0.0525m$, $p_o = 101kPa$, $\rho_O = 1.2kgm^{-3}$, m_{ft} –measured air mass flow-rate, m_f –predicted air mass flow-rate based on Equation (3.25))

Exp. No.	$\Delta p(kPa)$	$t_c(s)$	$L_s(m)$	$m_{ft}(kgs^{-1})$	$m_f(kgs^{-1})$
220-2	23	14.0	2.931	0.014	0.016
220-3	33.5	14.0	3.081	0.014	0.017
230-3	29	12.5	3.146	0.014	0.019
230-4	23	11	1.955	0.015	0.021
230-5	22	11	2.208	0.015	0.021
230-6	23	11	2.044	0.015	0.021
230-7	24.5	12	2.018	0.015	0.019
230-8	22	11	2.038	0.015	0.021
260-2	48	9.0	3.612	0.025	0.027
260-3	38	7.0	3.658	0.025	0.036
260-4	41	8.5	3.717	0.025	0.030
260-5	46	8.0	3.670	0.025	0.033
260-6	37	8.0	3.708	0.025	0.031
260-8	62	10.5	5.634	0.024	0.027
260-9	50	9.5	5.455	0.024	0.028

Equation (3.25) generally overestimates the values of air mass flow-rate. The main reason is that maximum pressure drop (Δp), not average pressure drop, was used in Equation (3.25). The tested slug length varied from about $2m$ to $5.5m$. Obviously, the longer the slug is, the less the air "leakage" will be.

CHAPTER 4

TEST FACILITY AND PROCEDURES

4. TEST FACILITY AND PROCEDURES

4.1 Test Facility

The single-slug test rigs used in this thesis are depicted in Fig. 4.1(a) and (b). The test rigs allow products, air flow-rates and slug velocities to be of similar scale to industrial applications, and the test rigs consist primarily of a blow tank, pipeline, a discharge tank, pressure meters and a data recorder.

The effective volume of the blow tank is $0.113m^3$, see Fig. 4.2, granular materials are poured in by opening material inlet valve. Top air is used for extruding particles out of the blow tank in the form of single-slug. In order to clean the pipeline after the completion of tests, boost air is employed. Pipeline is the combination of mild steel pipes fitted with flanges. Total pipeline length of one rig is $158m$, of which $4.6m$ is vertical height, and another rig has a total length of $101m$, of which $4.3m$ is vertical height. There are three horizontal bends in both of the rigs. In order to measure pressure drops and slug velocities along the pipeline, five pressure meters are installed, the distances between two neighbouring pressure meters are shown in Fig. 4.1.

Air pressures are measured with pressure meters, see Fig. 4.1. Refer to Fig. 4.3 for an exploded view of a typical pipeline air pressure meter tapping location. The pressure meter is connected to the pipe socket by a quick connector. The air pressure and air mass flow-rate are measured directly by the data logging system, while slug velocities are obtained indirectly by analysing pressure-time diagrams. The material weight poured into blow tank and conveyed to discharge tank is measured manually with an electrical scale.

D=0.069m, V_b=0.113cubic metre, Bend Radius=1.0m, A, B, C, D, E-Pressure Meter

L_{AB}=16.55m, L_{BC}=58.75m, L_{CD}=28.84m, L_{DE}=30.0m, Total Pipe Length=158m

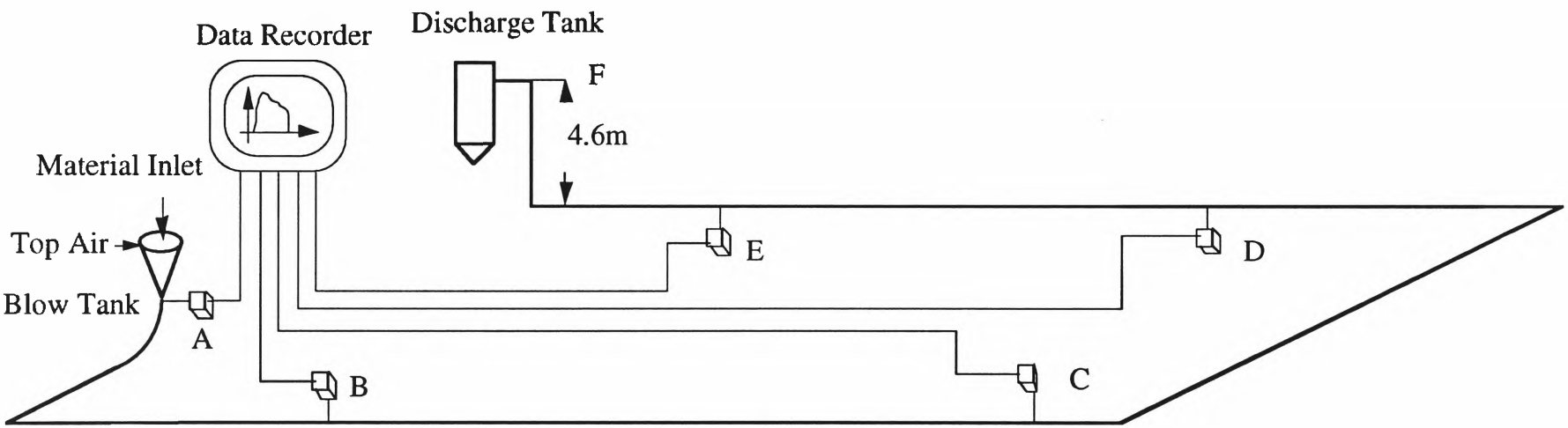

Fig. 4.1(a) Schematic layout of test rig

D=0.105m, V_b=0.113cubic metrer, Bend Radius=1.25m, A, B, C, D, E-Pressure Meter

L_{AB}=26.14m, L_{BC}=20.00m, L_{CD}=12.02m, L_{DE}=20.0m, Total Pipe Length=101m

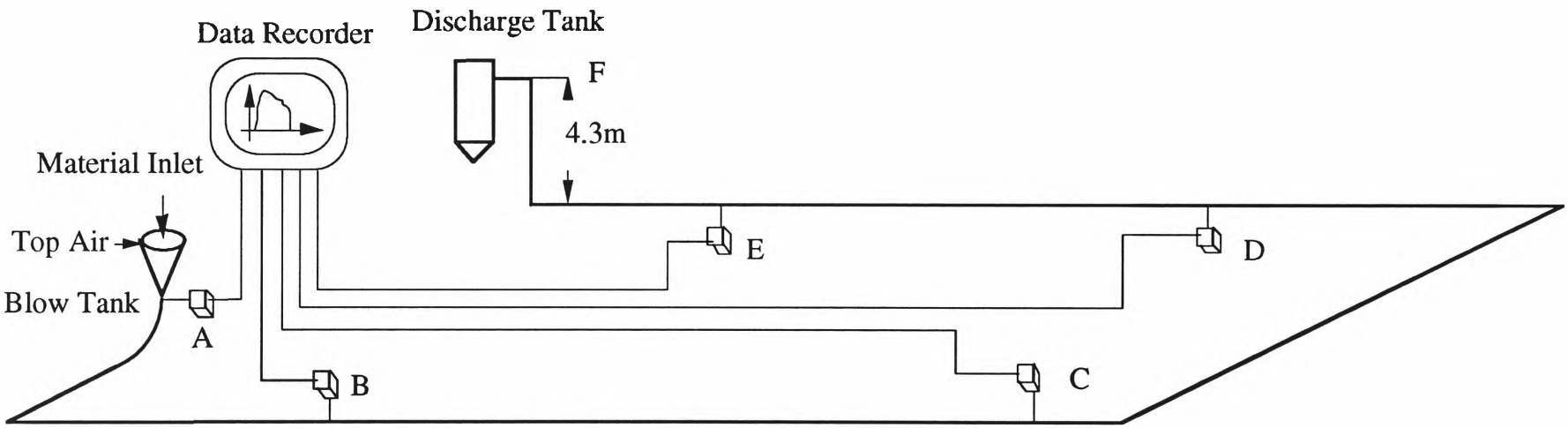

Fig. 4.1(b) Schematic layout of test rig

After all pressure meters are calibrated, they are connected to the pipeline and the relevant data acquisition system.

The air supply system in Bulk Solids Handling Laboratory ensures sufficient, clean and dry air at a maximum pressure of $800kPag$. During a conveying trial, the supplied air mass flow-rate is constant irrespective of downstream air pressure fluctuations. The air mass flow-rate is measured during the test and adjusted before the next when needed.

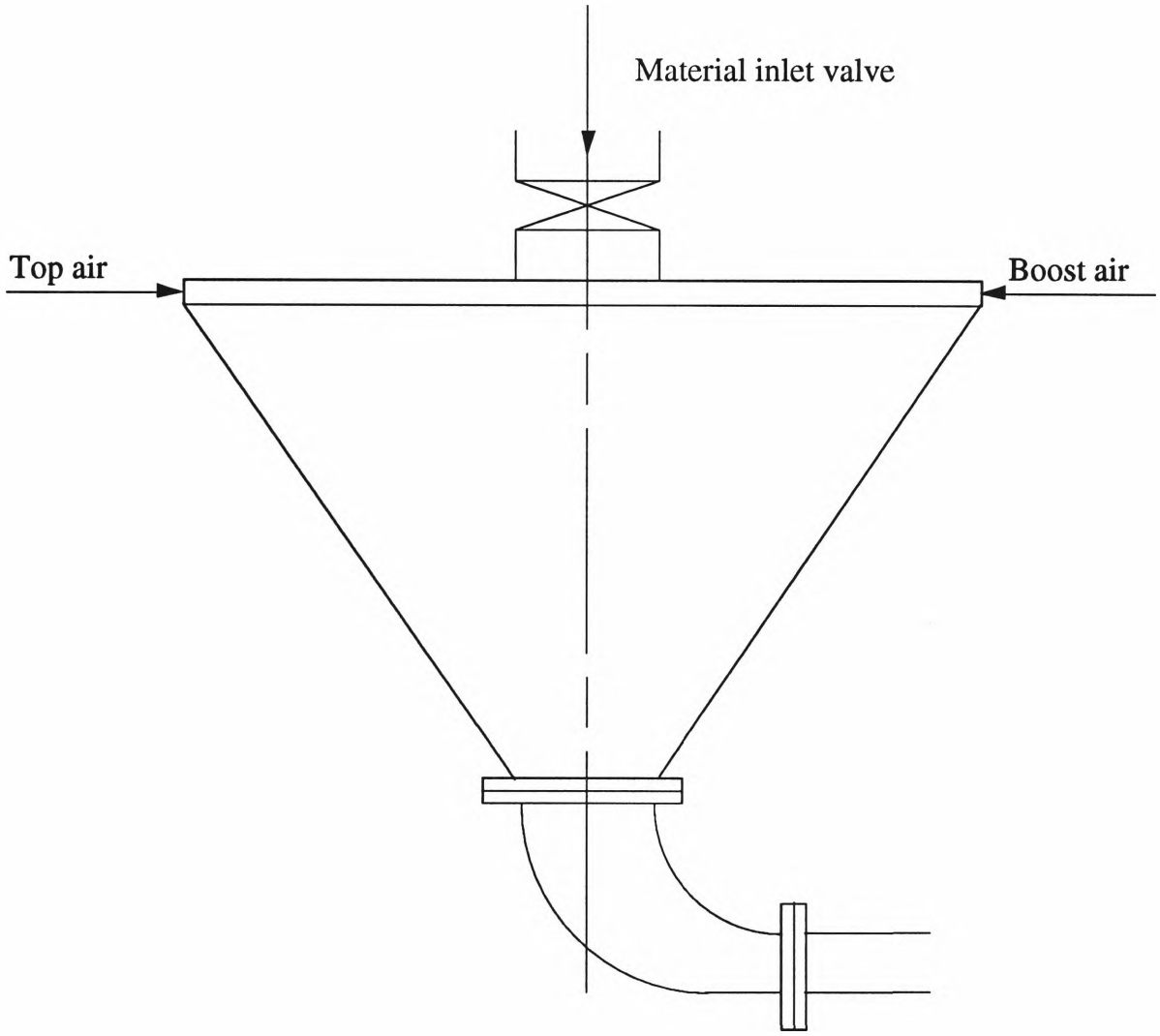

Fig. 4.2 Configuration of blow tank

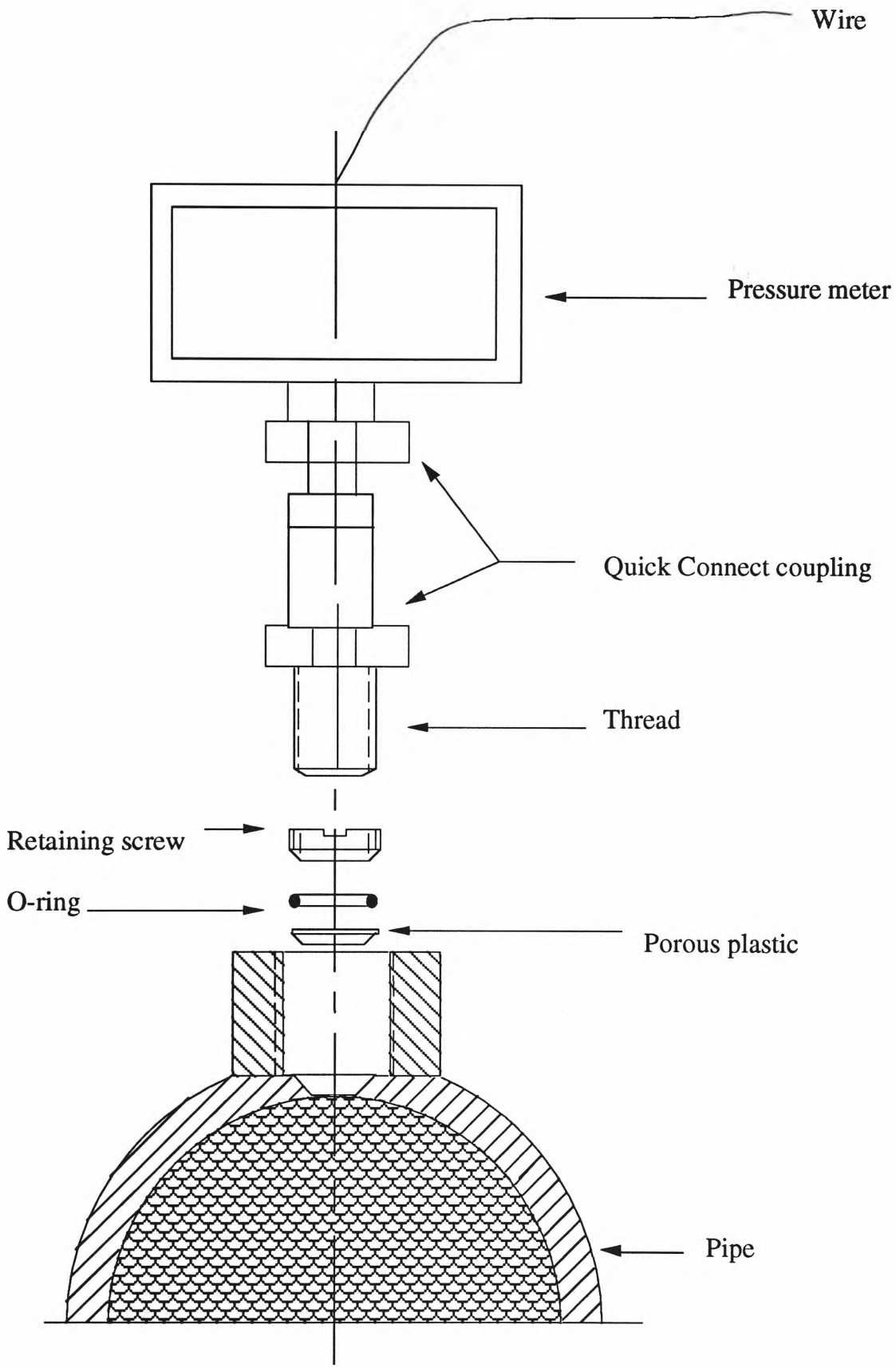

Fig. 4.3 Exploded view of a typical pressure meter tapping location

4.2 Test Materials

Pneumatic conveying performance can vary considerably for different bulk materials. Some materials can be conveyed over a wide range of flow conditions, from dilute-phase to slug flow. while other materials are restricted to dilute-phase. It is believed that the conveyability of bulk materials is dependent on their physical properties. Thus, in order to ensure satisfactory performances, the properties of the materials should be assessed.

There are several terms to describe the properties of a product, the properties possibly affecting the performance are particle size and the size distribution, particle density, bulk density, internal friction angle and wall friction angle.

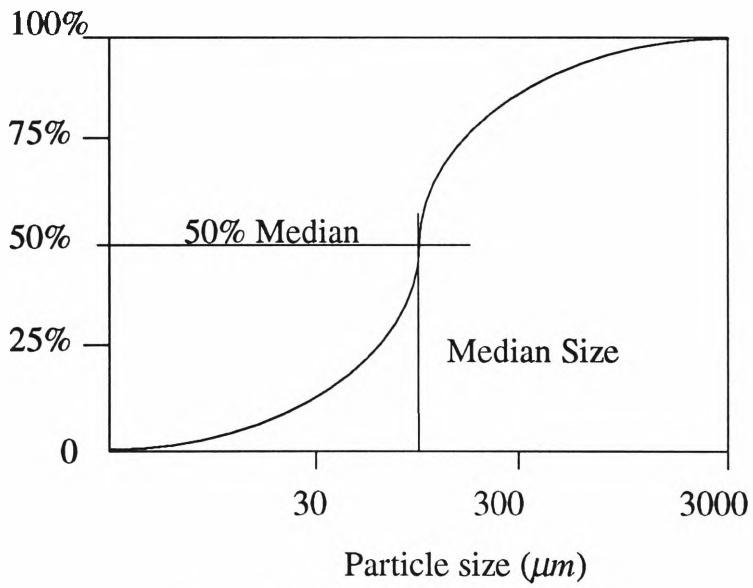

Fig. 4.4 Particle size distribution

The shapes of products vary significantly, it is difficult and sometimes impossible to measure particle size especially when the particles have irregular shape. Ergun [8] used a term called effective diameter of particles. However, Ergun's method is time consuming and inaccurate. The mostly used approach is to plot the data graphically, as shown in Fig.

4.4, which gives an appreciation of the range of particle size. In this paper, all products are almost monosize and particle diameter is much less than that of the pipeline.

Particle density and bulk density are important properties and can be easily measured in a bulk material laboratory (eg, using a pycnometer and a measuring cylinder respectively).

Since particle density is not equal to bulk density, this means that there is voidage between particles, the average percentage occupied by voidage can be calculated;

$$\varepsilon = 1 - \frac{\rho_b}{\rho_s} \tag{4.1}$$

There exists friction between particles and friction between pipe wall and particles, the value of particle internal friction angle represents quantitatively the friction between particles, while that of wall friction angle the friction between pipe wall and particles, both of them can be measured by standardised experimental procedures.

Only limited materials can be conveyed pneumatically in dense-phase, and some only by the help of special apparatus (eg. by pass, air knife, etc). Dixon [5] recognised that the fluidisation properties of a product have significant influences on its dense-phase conveyability, he classified materials into four groups and generated a diagram as shown in Fig. 2.1. Four granular materials, good candidates for natural slugging dense-phase pneumatic conveying, are selected for single-slug tests. each material has nearly monosized particle size and similar particle shape. Refer to Table 4.1 for a summary of the physical properties and relevant coefficients of the tested materials.

Table 4.1: Physical properties and relevant coefficients of tested materials

(polypropylene pellets=PP pellets, polyethylene pellets=PE pellets)

granular materials	surface shape	$\rho_b(kgm^{-3})$	$\rho_s(kgm^{-3})$
PP pellets	sphere	526.0	895.0
wheat	oval	811.5	1449.0
PE pellets	cylinder	494.0	865.0
blue metal	irregular	1210.0	2992.0

$\phi(°)$	$\phi_w(°)$	$\varepsilon = 1-\frac{\rho_b}{\rho_s}$	$\mu_w = \tan(\phi_w)$	$K_w = \frac{1}{1+\sin\phi}$
27.2	14.2	0.412	0.253	0.686
43.7	16.0	0.440	0.287	0.591
44.7	15.2	0.429	0.271	0.587
42.0	17.5	0.596	0.315	0.599

Note: ρ_s was determined by using a gas pycnometer and ρ_b a measuring cylinder.

4.3 Test Procedures

The operating procedure of the commercial single slug system is :

(1) Open material inlet valve and pour material (mass (W_b)) into blow tank, then close the valve;

(2) Open top air inlet valve (air mass flow-rate is m_f);

(3) Turn off air inlet valve after single-slug has been conveyed to discharge tank;

(4) Repeat above procedure.

In order to get nearly continuous conveying, two blow tanks are employed by some users.

The test procedure adopted for this research work is:

(1) Set top air mass flow-rate;

(2) Weigh the material loaded into blow tank and pour the material into the blow tank;

(3) Switch on data recorder, and then open top air inlet valve;

(4) After the conveying cycle, turn off top air inlet valve and weigh the material in discharge tank;

(5) Repeat step (2) to (4) at least 5 times (until the mass of material loaded into blow tank approximately equals mass of conveyed materials);

(6) Clean pipe.

m_f should be selected carefully to ensure good slug movement. If m_f is too high, the slug will be forced through the pipeline at high pressure, thus increasing particle degradation, If m_f is too low, then the slug will not move. Predicting the boundaries of slug flow is not an objective of this thesis. Following is the procedure for predicting pressure drop and slug velocity for a given m_f:

(1) Determine bulk material physical properties (such as ρ_b, ρ_s, ϕ, ϕ_w)by experiment, and calculate relevant coefficients, such as ε, μ_W and K_W;

(2) Determine test system factors, such as L_p, D, V_b, W_b, m_f;

(3) Assume initial particle velocity (V_s);

(4) Calculate V_p by Equation (16), L_s by Equation (17) and α by Equation (18);

(5) Estimate Δp by Equation (20);

(6) Estimate m_f by Equation (25);

(7) Compare the predicted m_f in step (6) with the m_f in step (2);

(8) Repeat from step (3) to (7) until convergence is obtained.

4.4 Slug Velocity and Pressure Drop

Slug velocity can be obtained by dividing the distance between two pressure meters with the time difference of the signal occurrence, see Fig. 4.5.

$$V_p = \frac{L_{pm}}{t_{pm}} \tag{4.3}$$

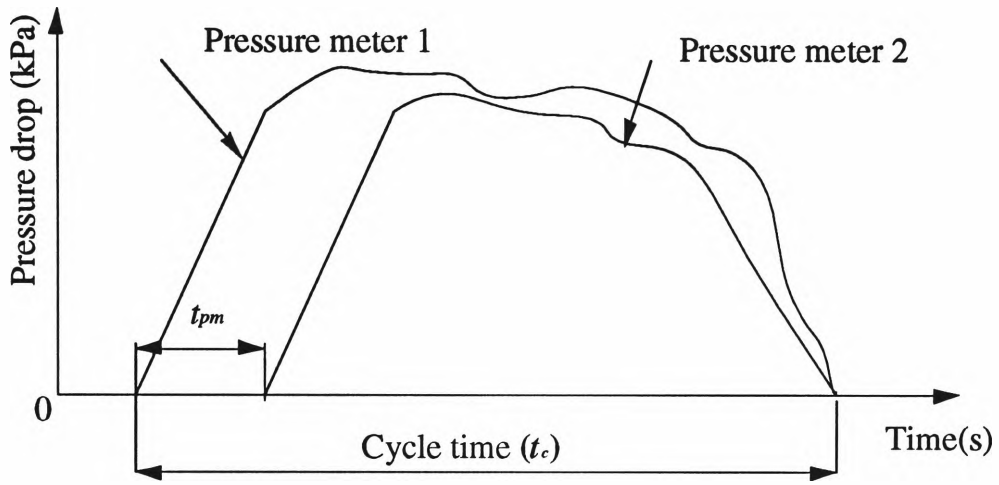

Fig. 4.5 The analysis of pressure drop diagram

It should be noted that the conveying mechanism is extremely complex by examining the relationship between pressure drop and slug velocity, see Fig. 4.6.

Pressure drop is proportional to friction force, or pressure drop fluctuates according to the change of friction force. Since the conveying medium is air, a compressible gas, and the recorded diagram of pressure drop is not a horizontal line (see Fig. 4.6(a)), slug velocity varies inversely with pressure drop. Generally, air mass flow-rate is a constant, if pressure drop becomes less (eg. from AA to BB), the pressurised air (see Fig. 4.6(b)) will expand, thus, slug velocity will increase. If pressure drop increases (eg. from BB to CC), the pressurised air will compress, thus, slug velocity will reduce. For example, if volume (V_b) of blow tank is $0.113m^3$, distance between slug and blow tank is $50m$ and diameter of pipeline is $0.105m$, the volume of pressurised air is;

$$0.113 + 50 * (\frac{0.105}{2})^2 * \pi = 0.546m^3$$

If the pressure in the blow tank reduces from $200kPa$ to $120kPa$ within 3 seconds, thus, we can estimate the distance of slug movement based on air expansion;

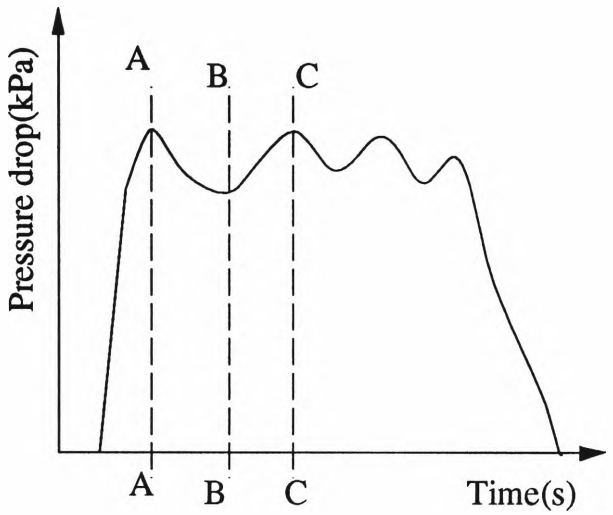

(a) Pressure drop vs time diagram

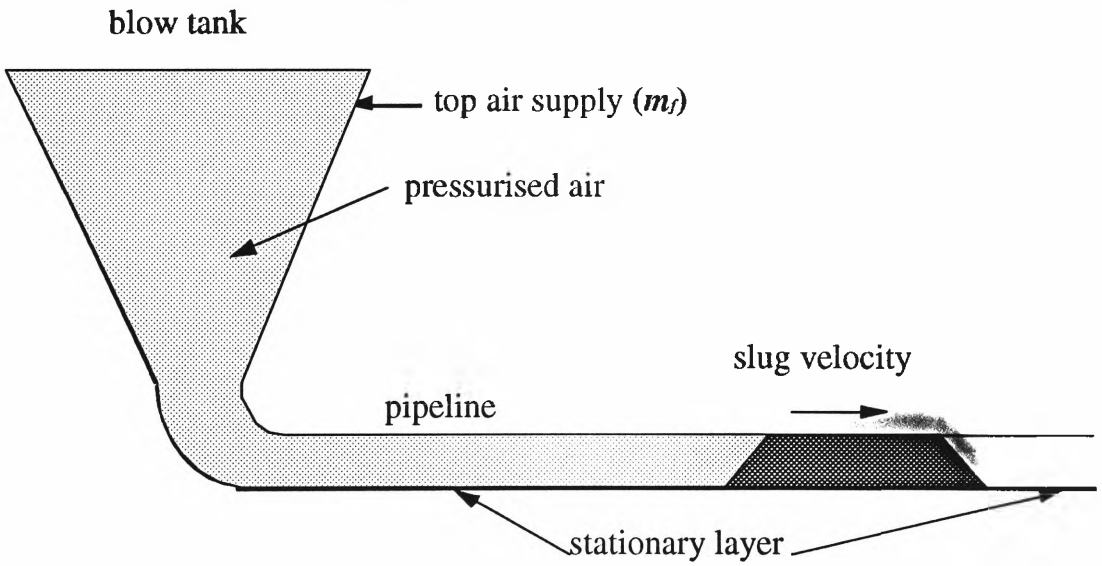

(b) Single-slug system

Fig. 4.6 Relationship analyses of slug velocity and pressure drop

$$(0.546 * \frac{200+101}{120+101} - 0.546) * \frac{1}{(\frac{0.105}{2})^2 \pi} = 22.8m$$

From this analysis, the increase in slug velocity is $7.6ms^{-1}$.

4.5 Single-Slug Behaviour

Shortly after a product is poured into blow tank (see Fig. 4.7(a)), the material inlet valve will be closed. The bulk material is pushed out of blow tank by air from top air supply valve, theoretically, all particles in blow tank form single-slug, however, as the slug moves ahead, it may become several short slugs. The reasons may be

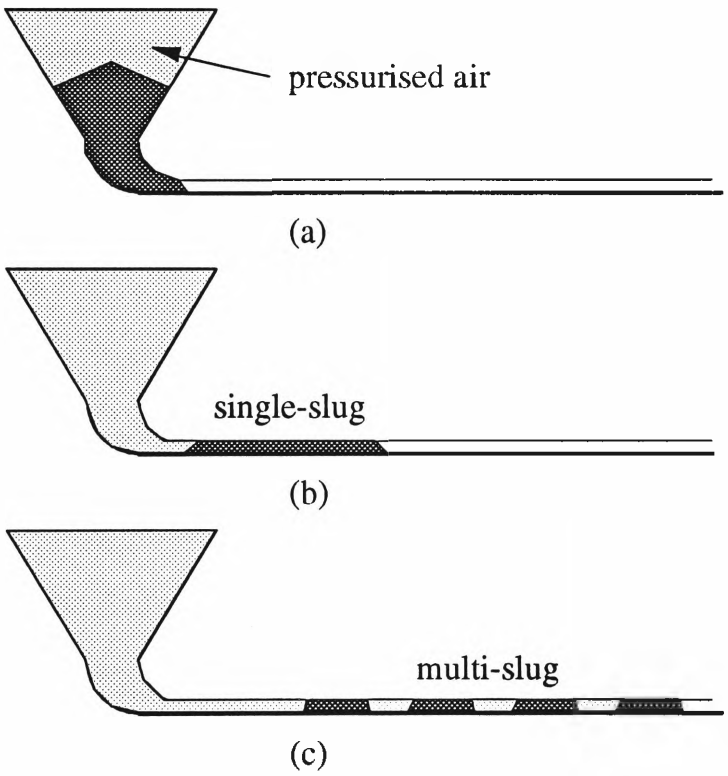

Fig. 4.7 Single-slug movement

(1) Resistance along the slug is not uniform, some parts, such as flanges or rusty pipe, have variable friction force;

(2) Generally, particles are cohensionless, they can bear pressure force only;

(3) There is air leakage through the slug, if a crevice has appeared, air may store in it and the gap become larger and larger, thus, a single-slug breaks down into multi-slug;

(4) The material may display natural slugging ability and have a "preference" to break up into several slugs.

The slug separation procedure can be detected by two methods:

(1) Install a sight glass towards the end of the conveying system, multi-slug may be watched directly;

(2) Install several pressure meters along pipeline, and analyse pressure drop vs time diagrams. See Fig. 4.8

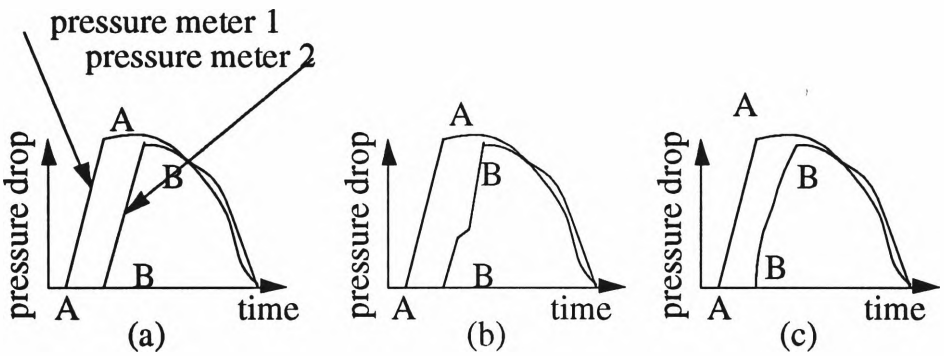

Fig. 4.8 Slug flow pattern analyses

Generally, when single-slug moves through a pressure meter, the recording diagram is a straight line (such as line A-A in Fig. 4.8 and B-B in Fig. 4.8(a)), if a pressure meter has a recording diagram as shown in Fig. 4.8(b) or Fig. 4.8(c) in which line B-B is not straight, then the single-slug would have broken into several segments.

4.6 Test Data and Discussion

Several experiments are conducted on the test rigs shown in Fig. 4.1(a) and 4.1(b), large scale plots are presented from Appendix C to J for the purpose of measuring t_{pm}, Δp and m_f with higher accuracy. See Fig. 4.5, t_{pm} is the time required for slug to travel from pressure meter A to B.

Table 4.2: Single-slug test for PP pellets

($m_f = 0.060 kgs^{-1}$, $D = 0.069m$, predicted pressure drop $\Delta P = 114.1 kPa$, predicted slug velocity $V_p = 2.80 ms^{-1}$)

Exp. No.	$W_b(kg)$	$W_d(kg)$	Exp. $\Delta P(kPa)$	Exp. $V_p(ms^{-1})$
1	20.0	6.0	100	2.76
2	20.0	22.5	120	2.76
3	20.0	23.0	110	2.76
4	20.0	20.5	111	2.76
5	20.0	20.0	112	2.76
6	20.0	19.5	110	2.76

Table 4.3: Single-slug test for PP pellets

($m_f = 0.062 kgs^{-1}$, $D = 0.069m$, predicted pressure drop $\Delta P = 115.2 kPa$, predicted slug velocity $V_p = 2.90 ms^{-1}$)

Exp. No.	$W_b(kg)$	$W_d(kg)$	Exp. $\Delta P(kPa)$	Exp. $V_p(ms^{-1})$
1	20.0	9.5	110	2.76
2	20.0	12.5	125	2.76
3	20.0	27.5	120	2.76
4	20.0	22.5	122	2.76
5	20.0	21.5	115	3.31
6	20.0	20.5	100	3.31
7	20.0	21.5	115	2.76
8	20.0	19.0	113	2.76

Table 4.4: Single-slug test for wheat

($m_f = 0.066 kgs^{-1}$, $D = 0.069m$, predicted pressure drop $\Delta P = 156.4 kPa$, predicted slug velocity $V_p = 2.60 ms^{-1}$)

Exp. No.	$W_b(kg)$	$W_d(kg)$	Exp. $\Delta P(kPa)$	Exp. $V_p(ms^{-1})$
1	30.0	24.0	160	2.54
2	30.0	26.0	155	2.76
3	30.0	33.0	172	2.54
4	30.0	27.0	160	2.36
5	30.0	32.0	162	2.54
6	30.0	31.5	155	2.76

Table 4.5: Single-slug test for wheat

($m_f = 0.049 kgs^{-1}$, $D = 0.069m$, predicted pressure drop $\Delta P = 142.2 kPa$, predicted slug velocity $V_p = 2.03 ms^{-1}$)

Exp. No.	$W_b(kg)$	$W_d(kg)$	Exp. $\Delta P(kPa)$	Exp. $V_p(ms^{-1})$
1	25.0	6.0	108	2.36
2	25.0	22.0	110	2.76
3	25.0	22.0	120	2.36
4	25.0	25.5	120	2.36
5	25.0	28.5	110	2.36
6	25.0	26.5	110	2.36

Table 4.6: Single-slug test for PE pellets

($m_f = 0.057 kgs^{-1}$, $D = 0.069m$, predicted pressure drop $\Delta P = 93.5kPa$ predicted slug velocity $V_p = 2.97ms^{-1}$)

Exp. No.	$W_b(kg)$	$W_d(kg)$	Exp. $\Delta P(kPa)$	Exp. $V_p(ms^{-1})$
1	18.5	15.0	108	3.31
2	18.5	18.0	108	3.01
3	18.5	18.0	115	3.01
4	18.5	19.0	112	3.01
5	18.5	18.0	110	3.01
6	18.5	18.5	121	3.01

Table 4.7: Single-slug test for PE pellets

($m_f = 0.047 kgs^{-1}$, $D = 0.069m$, predicted pressure drop $\Delta P = 87.1kPa$, predicted slug velocity $V_p = 2.53ms^{-1}$)

Exp. No.	$W_b(kg)$	$W_d(kg)$	Exp. $\Delta P(kPa)$	Exp. $V_p(ms^{-1})$
1	18.5	9.0	86	2.76
2	18.5	22.5	103	2.76
3	18.5	20.0	105	2.76
4	18.5	16.0	95	3.01
5	18.5	18.5	102	2.76
6	18.5	18.0	90	2.76

According to the test results from Table 4.2 to Table 4.7, the predicted pressure drop and slug velocity are fairly consistent with the test results. Note, compared with Konrad [17], who admitted that his model "consistently underpredicted the experimental pressure drop, often giving only half the measured value", the results are considered quite good.

The derivation of the model was mainly based on the tests of PP pellets on the $0.0525m$ diameter pipe (see Table 3.2 and Table 3.4) although some data with silica flux on $0.105m$ diameter pipe were available (see Table 3.3). However, it has been proven above that the model can be scaled to $0.069m$ diameter pipe and to other granular materials, such as wheat and PE pellets.

Pipe blockage or slug deterioration will occur if lower or higher air mass flow-rate was used. Since the boundary of slug conveying is another subject, the premise of this paper is that particles are in slug movement.

Table 4.8 is based on the plots of Appendix E and shows average slug velocities for A-B (V_{AB}), for B-C (V_{BC}), for (V_{CD}), and for (V_{DE}). It is evident that $V_{AB} < V_{BC} < V_{CD} < V_{DE}$ and $V_{AB} << V_{DE}$ (although the tested material is wheat, the same phenomena can be observed from other granular materials such as PP pellets and PE pellets). The slug moves faster and faster, but the system pressure drop generally does not increase (see the plots from Appendix C to J). This is probably due to the fact that the kinetic coefficient of friction decreases with increasing slug velocity. Hence, the pressure drop depends more on the starting conditions (eg static coefficient of friction, initial velocity).

Table 4.8: Change of slug velocities ($D = 0.069m$, $m_f = 0.066kgs^{-1}$,wheat)

Exp. No.	$L_{AB} = 16.55m$ $V_{AB}(ms^{-1})$	$L_{BC} = 58.75m$ $V_{BC}(ms^{-1})$	$L_{CD} = 28.84m$ $V_{CD}(ms^{-1})$	$L_{DE} = 30.00m$ $V_{DE}(ms^{-1})$
1	2.54	5.88	8.24	10.0
2	2.76	6.53	7.21	10.0
3	2.54	5.34	9.61	10.0
4	2.36	5.34	9.61	15.0
5	2.54	5.34	7.21	10.0
6	2.76	4.90	7.21	10.0

According to the test data in Table 4.8, as the slug travels forward its velocity becomes larger and larger. Fig. 4.9 is based on the data of test No. 5 in Table 4.8. It is evident that the slug velocity (V_p) is function of pipe length (L_p) (eg the final slug velocity is about four times the initial one) and the predicted slug velocity (V_p) based on the model of this paper is the minimum (initial) slug velocity.

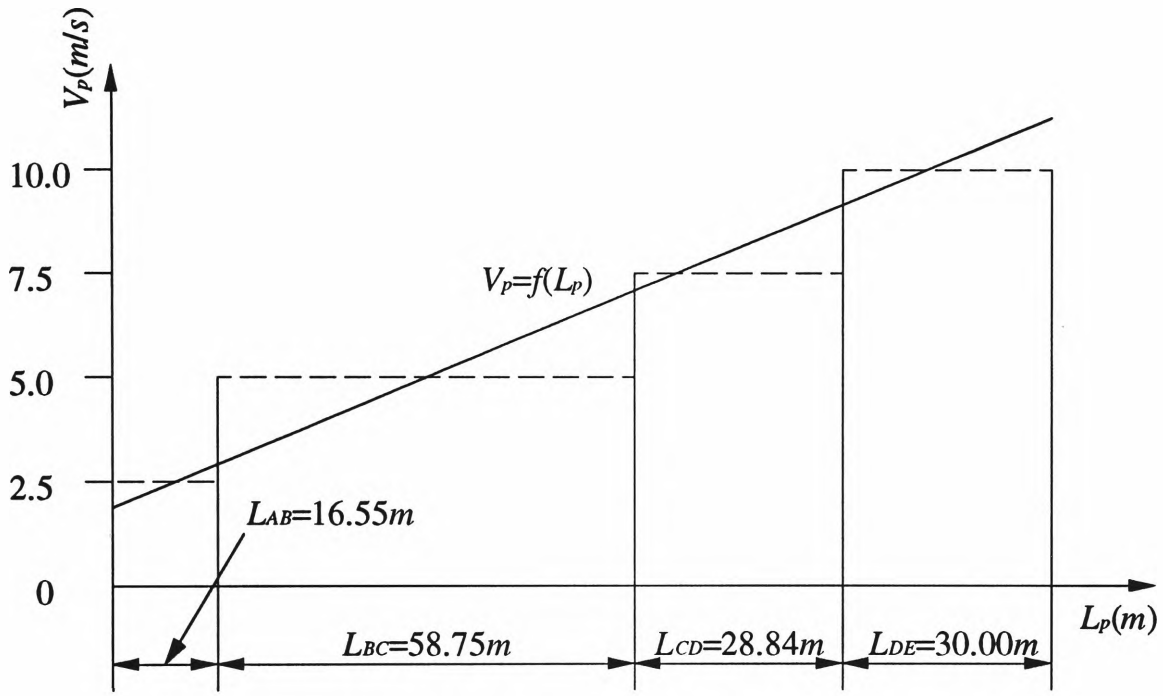

Fig. 4.9 Slug velocity analysis

Table 4.9 and Table 4.10 provide the test results obtained on blue metal for a pipe diameter of 0.105m (see Fig. 4.1(b)). It is found that the measured pressure drop has a wide distribution, and is reasonably close to the predicted pressure drop. However, the measured slug velocity is always greater than the predicted one. It should be noted that the distance (ie L_{AB}) between the blow tank and the first pressure meter for the test rig shown in Fig. 4.1(a) is 16.55m, whereas, L_{AB} for the test rig in Fig. 4.1(b) is 26.14m. The main reason that the measured slug velocity in Table 4.9 and Table 4.10 is greater than the predicted value is that the latter is based on a much longer section of pipe (and hence greater range of velocity).

Future work to address this issue and the increase of V_p along the pipeline is discussed in section 5.2.

Table 4.9: Single-slug test for blue metal

($m_f = 0.095 kgs^{-1}$, $D = 0.105m$, predicted pressure drop $\Delta P = 184.7 kPa$, predicted slug velocity $V_p = 2.30 ms^{-1}$)

Exp. No.	$W_b(kg)$	$W_d(kg)$	Exp. $\Delta P(kPa)$	Exp. $V_p(ms^{-1})$
1	60.0	2.0	110	4.51
2	60.0	70.0	120	4.36
3	60.0	57.5	125	7.92
4	60.0	60.0	90	7.06
5	60.0	59.0	85	8.71

Table 4.10: Single-slug test for blue metal

($m_f = 0.095 kgs^{-1}$, $D = 0.105m$, predicted pressure drop $\Delta P = 221.8 kPa$ predicted slug velocity $V_p = 2.00 ms^{-1}$)

Exp. No.	$W_b(kg)$	$W_d(kg)$	Exp. $\Delta P(kPa)$	Exp. $V_p(ms^{-1})$
1	75.0	17.0	85	6.54
2	75.0	77.0	135	4.36
3	75.0	73.0	180	6.54
4	75.0	69.5	195	6.54
5	75.0	73.5	155	5.23
6	75.0	87.5	215	5.23

The $D = 0.069m$ pipeline was scheduled as the main test rig. Due to the large particle size of the blue matel, the $D = 0.105m$ pipeline had to be employed.

CHAPTER 5

CONCLUSIONS AND FUTURE RESEARCH

5. CONCLUSIONS AND FUTURE RESEARCH

5.1. Conclusions

This thesis was aimed at developing a model for predicting the total horizontal pipeline pressure drop for single-slug pneumatic conveying. Theoretical analyses with experimental research were carried out for stationary layer and air leakage under single-slug condition. The formulae for the pressure drop in horizontal single-slug conveying are presented. In order to verify the validity of these formulae, considerable tests have been conducted, the following conclusions are based on the investigations and findings of this thesis.

5.1.1 Flow Pattern

(1) Particle velocity is much lower than its saltation velocity (ie. for dilute-phase). Hence, particles build up and fill up the pipe during conveying.

(2) When particles are pushed out of blow tank, they move in single-slug, if pipeline is long enough, the single-slug usually breaks into several segments.

5.1.2 Force Analyses in Slug

(1) In any cross-sectional area of a slug, particles only take part of the area, the remaining area is taken by voidage.

(2) Slug travelling is more similar to piston movement, rather than air conveyed material such as dilute-phase pneumatic conveying.

(3) Voidage should be taken into account for establishing the equilibrium equation. Pressure drop balances the friction forces due to material weight and the radial stress caused by the "impact" between stationary layer and slug flow.

5.1.3 Stationary Layer

(1) Slug sweeps up the stationary layer in front of it and simultaneously deposits a stationary layer behind. On average, the thickness of the stationary layer in front of and behind a slug is approximately the same.

(2) The thickness of stationary layer is influenced by the particle properties and operating factors, the author stresses that it varies inversely with bulk material internal friction.

(3) Experimentally, the thickness of stationary layer can be estimated by the consideration of material weight left in pipeline and pipeline diameter.

5.1.4 Transportation Media

(1) Air is the most commonly used gas for dense-phase pneumatic conveying. It moves the slug by the pressure differences between slug front and back.

(2) Generally, the pressure on the back of the slug is much higher than that on the front of the slug. Voidage in slug allows air to leak through, but air leakage only is a very small portion of the air "supplement", thus a high pressure drop can be maintained during slug conveying. Or in other words, if most of the air supplement percolated through slug, the pressure drop across the slug and system would be low.

(3) The air supplement is approximately equal to the air mass stored in blow tank and the pipeline behind the moving slug and is in the form of high pressure.

5.1.5 Slug Velocity

(1) Theoretically, slug velocity is not equal to particle velocity, the former is slightly greater than the latter.

(2) As the slug moves forward its velocity becomes larger and larger. However, pressure drop decreases, not increases as expected, the reasons may be the reduction of wall friction coefficient, the bulk material to be aerated and pressurised air expansion.

(3) Many factors such as material properties, air mass flow-rate, pipe diameter and the conveyed particle weight can influence slug velocity.

5.1.6 Pressure Drop

(1) Pressure drop is the combination of many factors such as particle properties, pipeline diameter, pipeline length, blow tank volume, material weight loaded in blow tank and so on.

(2) Some of the factors are difficult to determine, such as the estimation of wall friction angle and stress transmission coefficient, these factors may vary with slug movement. However, pressure drop is a strong function of these factors, increasing the difficulty to predict pressure drop accurately.

(3) The maximum pressure drop usually occurs at the moment that particles are pushed out of blow tank (ie due to overcoming maximum friction).

5.2 Suggestions for Further Research

5.2.1 Experiments

Although the model in this paper can be applied to commercial slug systems and the test rigs are almost the same size as that used in industry, further experiments still are recommended to examine the effect of different pipe diameters, pipe length, products, and air mass flow-rates.

5.2.2 Slug Velocity

Tests have shown that the slug moves faster and faster along pipeline, in order to limit slug velocity and save particle degradation and pipe attrition further, quantitative analysis is needed. Additional instrumentation and faster data logging facilities are needed for the test rig used in this project.

5.2.3 Pressure Drop in Vertical Pipe and Bends

This thesis focused on pressure drop in horizontal pipe, the length of vertical pipe and bends only take a small portion of the total pipe length in the test rigs, thus, the pressure drop caused by vertical pipe and bends is omitted. However, in some slug systems, the influence of vertical pipe and bends cannot be neglected. Hence, additional instrumentation should be installed to monitor the effects and obtain sufficient data for modelling purposes.

CHAPTER 6

REFERENCES

6. REFERENCES

[1] Aziz, Z. B., and Klinzing, G. E., Plug Flow Transport of Cohesive Coal: Horizontal and Inclined Flows, Powder Technology, Vol. 55, 1988, pp 97-105.

[2] Beck, C. M., Instrumentation and Control for Minimum Energy Consumption in Pneumatic Conveying, PhD Thesis, University of Bradford, UK, 1986.

[3] Bridle, I., Woodhead, S. R., Burnett, A. J. and Barnes, R. N., A Review of Techniques for the Investigation of Particle Degradation in Pneumatic Conveying Systems, 5th International Conference on Bulk Materials Storage, Handling and Transportation, Newcastle, 10-12 July 1995, pp 205-210.

[4] Borzone, L. A. and Klinzing, G. E., Dense-Phase Transport: Vertical Plug Flow, Powder Technology, Vol. 53, 1987, pp 273-283.

[5] Dixon, G., How do Different Powders Behave, Bulk Storage Movement Control, May/June, 1979, pp 81-88.

[6] Dickson, A. J., Skews, B. W. and Marcus, R. D., Plug Phase Conveying, Pneumotransport 4, Fourth International Conference on the Pneumatic Transport of Solids in Pipes, Jun. 26-28, 1978, California, USA, D 6-73.

[7] Dhodapkar, V. S., Plasgnski, S. I. and Klinzing, G. E., Plug Flow Movement of Solids, Powder Technology, Vol. 81 1994 pp 3-7.

[8] Ergun, S., Fluid Flow through Packed Columns, Chemical Engineering Progress, Vol. 48, 1952, pp 89-94.

[9] Geldart, D., Types of Gas Fluidisation, Powder Technology, Vol. 7, 1973, pp 285-292.

[10] Hancock, A. W. and Nedderman, R. M., Prediction of Stresses on Vertical Bunker Walls, Trans. Instn Chem. Engrs, Vol. 52, 1974 pp 170-179.

[11] Hong, Gu and Klinzing, G. E., Vertical Plug Flow of Cohesive Coal in 2- and 4-Inch Pipes, Powder Technology, Vol. 57, 1989, pp 59-67.

[12] Jones, M. J., The Influences of Bulk Particulate Properties on Pneumatic Conveying Performances, PhD thesis, School of Engineering, Thames Polytechnic, UK, 1988.

[13] Jones, M. G., Mills, D. and Mason, J. S., Pneumatic Conveying of High Bulk Density Products, Pneumatech 2, International Conference on Pneumatic Conveying Technology, Sep. 4-6, 1984, Canterbury, UK, pp 19-39.

[14] Klinzing, N. D, Rohatgi, N. D., Zaltash, A. and Myler, C. A., Pneumatic Transport - a Review, Powder Technology, Vol. 51, 1987, pp 135-149.

[15] Klintworth, J. and Marcus, R. D., A Review of Low-Velocity Pneumatic Conveying Systems, Bulk Solids Handling, Vol. 5, No. 4, 1985, pp 747-753.

[16] Konrad, K., Dense-Phase Pneumatic Conveying: A Review, Powder Technology, Vol. 49, 1986, pp 1-35.

[17] Konrad, K., Dense-Phase Pneumatic Conveying Through Long Pipelines: Effect of Significantly Compressible Air Flow on Pressure Drop, Powder Technology, Vol. 48, 1986, pp 193-203.

[18] Konrad, K. and Davison, J. F., The Gas-Liquid Analogy in Horizontal Dense-Phase Pneumatic Conveying, Powder Technology, Vol. 39, 1984, pp 191-198.

[19] Konrad, K., Harrison, D., Nedderman, R. M. and Davidson, J. F., Prediction of the pressure drop for horizontal dense phase pneumatic conveying of particles, Pneumotransport 5, Int. Conf. on Pneumatic Transport of Solids in Pipes, London, U.K, April 16-18, 1980, pp 225-244.

[20] Kraus, M. N., Pneumatic Conveying of Bulk Materials, McGraw-Hill Publications Co., New York, 1980.

[21] Legel, D. and Schwedes, J., Investigation of Pneumatic Conveying of Plug of Cohesionless Bulk Solids in Horizontal Pipe, Bulk Solids Handling, Vol. 4, 1984, pp 399-405.

[22] Mainwaring, N. J. and Reed, A. R., An Appraisal of Dixon's Slugging Diagram for Assessing the Dense Phase Conveying Potential of Bulk Solid Materials, Pneumatech 4, Fourth International Conference on Pneumatic Conveying Technology, Mar. 1987, pp 221-234.

[23] Mi, B. and Wypych, P. W., Pressure Drop Prediction in Low-Velocity Pneumatic Conveying, Powder Technology, Vol. 81, 1994, pp 125-137.

[24] Mi, B. and Wypych, P. W., Particle Slug Velocity in Horizontal Slug-Flow Pneumatic Conveying, Powder Handling & Processing, Vol. 5, 1993, pp 227-233.

[25] Mi, B., Wypych, P. W., and Pan R., Low-Velocity Pneumatic Conveying of Fine Powders, 5th International Conference on Bulk Materials Storage, Handling and Transportation, Newcastle, 10-12 July 1995, pp 185-189.

[26] Mi, B., Low-Velocity Pneumatic Transportation of Bulk Solids, PhD Dissertation, The University of Wollongong, Australia, 1994.

[27] Pan, R., Minimum Superficial Air Velocity in Low-Velocity Slug-Flow Pneumatic Conveying of Bulk Solid Materials, 5th International Conference on Bulk Materials Storage, Handling and Transportation. Newcastle, 10-12 July 1995, pp 239-242.

[28] Pan, R. and Wypych, P. W., Pressure Drop Prediction in Single-slug pneumatic Conveying, Powder Handling & Processing, Vol. 7, No. 1, 1995, pp 63-68.

[29] Ramakrishnan, T. and Roa, M. M., Energy Consumption in Dense Phase Pneumatic Conveying System: Experimental Studies, 5th International Conference on Bulk Materials Storage, Handling and Transportation. Newcastle, 10-12 July 1995, pp 243-247.

[30] Rao, M. M., Ramakrishnan, T. and David, P., Numerical Study of Plug-Type Pneumatic Conveying, Powder Handling & Processing, Vol. 3, No. 1, 1991, pp 57-60.

[31] Roberts, Alan W., 100 Years of Janssen, 5th International Conference on Bulk Materials Storage, Handling and Transportation, Newcastle, 10-12 July 1995, pp 1-19.

[32] Tsuji, Y. and Morikawa, Y., Plug Flow of Coarse Particles in a Horizontal Pipe, J. of Fluids Engineering, Vol. 104, 1982, pp 198-206.

[33] Tsuji, Yutaka, Recent Studies of Pneumatic Conveying in Japan, Bulk Solids Handling, Vol. 3, No. 3, 1983, pp 589-595.

[34] Wilson, K. C., Analysis of Slip of a Particulate Mass in a Horizontal Pipe, Bulk Solids Handling, Vol. 1, No. 2, 1981, pp 295-299.

[35] Wypych, P. W., Latest Developments in the Pneumatic Pipeline Transport of Bulk Solids, 5th International Conference on Bulk Materials Storage, Handling and Transportation. Newcastle, 10-12 July 1995, pp 47-56.

[36] Wypych, P. W. and Arnold, P. C., Plug-Phase pneumatic Transportation of Bulk Solids and the Importance of Blow Tank Air Injection, Powder Handling & Processing, Vol. 1, No. 3, 1989, pp 271-275.

[37] Zheng Luqing, Zhang Yaolin and Pan Xinzhang, Analysis of the Pressure Drop for Horizontal Plug Pneumatic Conveying of Particles, Bulk Solids Handling, Vol. 7, 1987, pp 859-864.

[38] Ramiah, B., K., Soil Mechanics and Foundation Engineering, A. A. Balkema/Rotterdam/1982

[39] Grindle, P., The Pneu-Phase Pneumatic Conveying System, Bulk Solids Handling, Vol. 8, No. 1 1988, pp 86.

[40] Jiang Hong, Yi-shen Snen and Shu-lin Liu, A Model for Gas-Solid Stratified Flow in Horizontal Dense-Phase Pneumatic Conveying, Powder Technology, Vol. 77, 1993, pp 107-114.

[41] Wypych, P. W. and Hauser, G., Design Considerations for Low-Velocity Conveying System and Pipelines, Pneumatech 4, Fourth International Conference on Pneumatic Conveying Technology, Jun. 26-28, 1990, Glasgow, Scotland.

[42] Craig, R. F., Soil Mechanics, Chapman & Hall, 1994

APPENDICES

Appendix A Stress Transmission Coefficient (K_w)

Konrad et al [19] gave the range of stress transmission coefficient, that is

$$\frac{1-\sin\phi\cos(\omega-\phi_w)}{1+\sin\phi\cos(\omega-\phi_w)} \le K_w \le \frac{1+\sin\phi\cos(\omega+\phi_w)}{1-\sin\phi\cos(\omega+\phi_w)} \tag{A.1}$$

where $\sin\omega = \frac{\sin\phi_w}{\sin\phi}$ for cohesionless materials.

Mi and Wypych [23] found that the stress state in a slug is active, thus $\sigma_{rw} \le \sigma_x$, and

$$K_w \le 1 \tag{A.2}$$

Combining equation (A.1) and (A.2):

$$\frac{1-\sin\phi\cos(\omega-\phi_w)}{1+\sin\phi\cos(\omega-\phi_w)} \le K_w \le 1 \tag{A.3}$$

By analysing the Mohr circle presented by Konrad et al [19], it can be seen that $cos(\omega-\phi_w) \approx 1$ is a reasonable approximation. Hence:

$$\frac{1-\sin\phi\cos(\omega-\phi_w)}{1+\sin\phi\cos(\omega-\phi_w)} \approx \frac{1-\sin\phi}{1+\sin\phi}. \tag{A.4}$$

Also, simplifying equation (A.3)

$$\frac{1-\sin\phi}{1+\sin\phi} \le K_w \le 1 \tag{A.5}$$

Due to the difficulty in finding K_w exactly, the author suggests a mean value of the stress transmission coefficient:

$$K_w = \frac{1}{2}\left(\frac{1-\sin\phi}{1+\sin\phi}+1\right) = \frac{1}{1+\sin\phi} \tag{A.6}$$

Appendix B Experimental Plots for Tables 3.2 and 3.3

In order to measure the stationary layer behind a moving slug and to find the relationship between air mass flow-rate and slug velocity, a small test rig (see Fig. B.1) was used. Pressure meter A is connected to channel 6, pressure meter B to channel 5 and pressure meter C to channel 7.

Detailed experimental results are provided in Table B.1 to Table B.4. W_b is the weight of material loaded into blow tank, W_d the weight of material conveyed into discharge tank. After finishing a set of tests, the author found some material (W_{bot}) left in the bottom of blow tank. Δp is tha maximum pressure drop while the slug is moving along the horizontal pipe segment (see Fig. B.2). The time for the slug to reach pressure meter C is t_c. V_p is the slug velocity and calculated by equation (B.1)

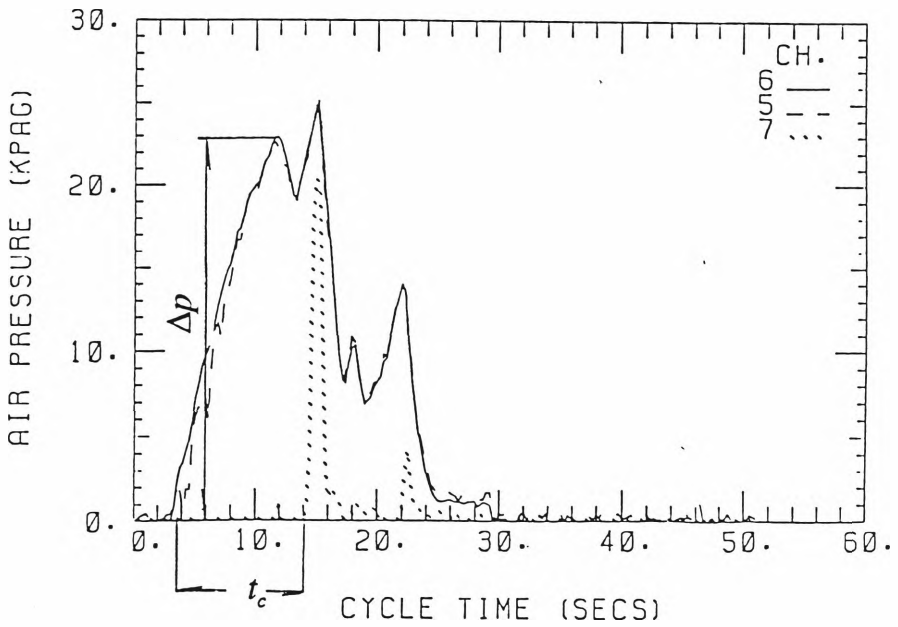

Fig. B.2 Measurement of Δp and t_c

$$V_p = \frac{L_{BC}}{t_c} \tag{B.1}$$

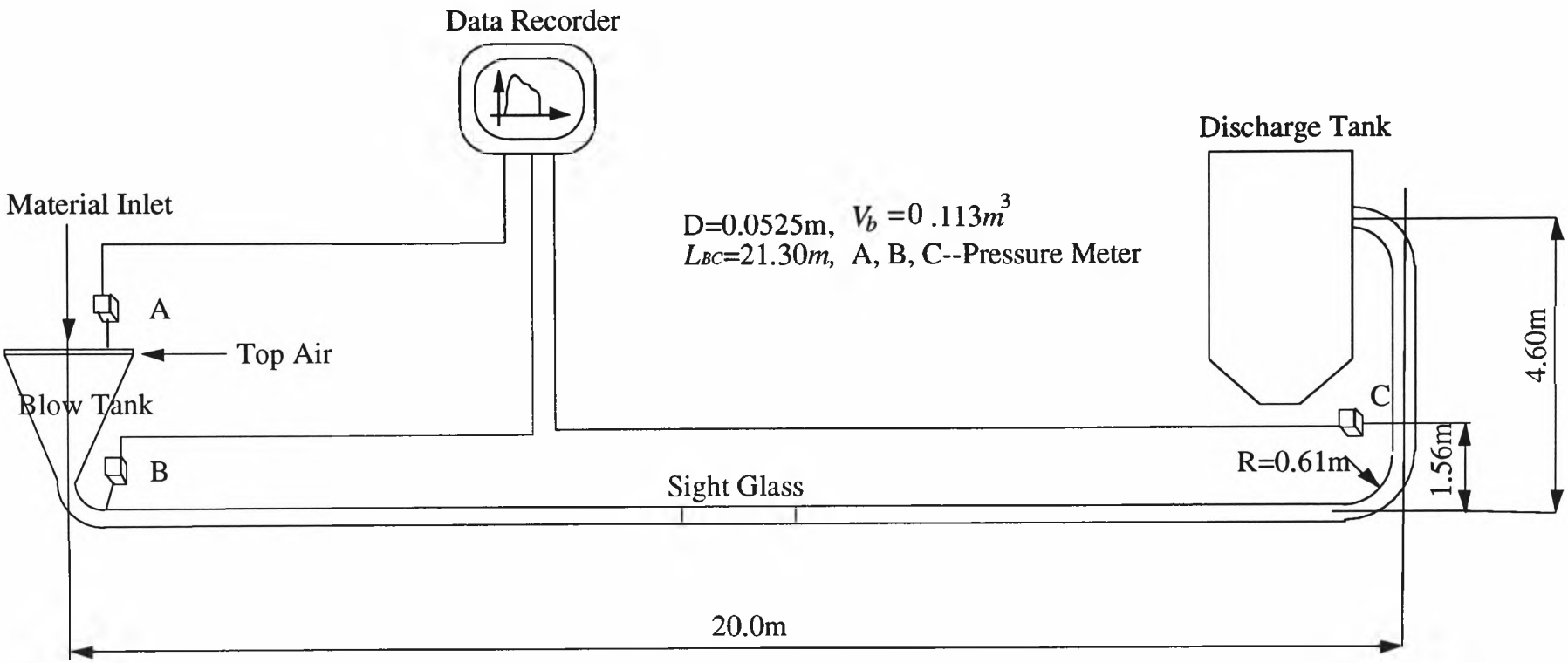

Fig. B.1 Schematic layout of test rig

Since the horizontal pipe length (L_{BC}=19.81m) is relatively short, the measured slug velocity is considered relatively stable.

α_f is the ratio of cross-sectional area of stationary layer in front of the slug to the pipe cross-sectional area, and α_b the ratio of the cross-sectional area of the stationary layer behind the slug to the pipe cross-sectional area. The value of α_b found in one experiment is equal to α_f in the following experiment.

$$\alpha_b = \frac{W_{left}}{\rho_b L_h [\pi(\frac{D}{2})^2]} \tag{B.2}$$

where W_{left} is the weight of material left in the horizontal pipe as a stationary layer, and can be easily calculated by analysing the relationship between W_b, W_d, and W_{bot}. L_h is the horizontal pipe length ($L_h = 20.0m$ in this test rig)

$\bar{\alpha}$ is the average of α_f and α_b:

$$\bar{\alpha} = \frac{1}{2}(\alpha_f + \alpha_b) \tag{B.3}$$

It is found that $\alpha_f \neq \alpha_b$,. This means that the rate of particles being picked up by the slug is different to rate of particles being left behind. Based on equation (3.16), particle velocity (V_s) is calculated by :

$$V_s = \frac{V_p}{2\left[\left(\frac{1}{1-\alpha_f}\right)+\left(\frac{1}{1-\alpha_b}\right)\right]} \tag{B.4}$$

L_s is slug length, and is calculated by:

$$L_s = \frac{W_b}{A\rho_b(1-\bar{\alpha})} \tag{B.5}$$

From Equation (3.26), the prediction of m_f requires the values of L_s and t_c, where t_c is cycle time and can be measured from experimental plots. As slug length varies along the pipeline, it is difficult to measure directly, and average slug length is calculated using Equation (B.5).

Table B.1 Experiment data and results ($m_{ft} = 0.014 kgs^{-1}$)

Exp. No.	$W_b(kg)$	$W_d(kg)$	$W_{bot}(kg)$	$\Delta p(kPa)$	$t_c(s)$
220-1	3.0	0.0	2.0	--	--
220-2	3.0	0.4	2.0	23	14.0
220-3	3.0	3.6	2.0	33.5	14.0

$V_p(ms^{-1})$	α_b	α_f	$\overline{\alpha}$	$V_s(ms^{-1})$	$L_s(m)$
--	0.0439	0	--	--	--
1.521	0.1581	0.0439	0.1010	1.363	2.931
1.521	0.1317	0.1581	0.1449	1.300	3.081

Table B.2 Experiment data and results ($m_{ft} = 0.015 kgs^{-1}$)

Exp. No.	$W_b(kg)$	$W_d(kg)$	$W_{bot}(kg)$	$\Delta p(kPa)$	$t_c(s)$
230-1	2.0	0.0	2.0	--	--
230-2	2.0	0.0	2.0	--	--
230-3	2.0	1.25	2.0	22	11.0
230-4	2.0	2.05	2.0	23	11.0
230-5	2.0	1.3	2.0	22	11.0
230-6	2.0	2.4	2.0	22	11.0
230-7	2.0	2.1	2.0	23	12.0
230-8	2.0	1.5	2.0	22	11.0

$V_p(ms^{-1})$	α_b	α_f	$\overline{\alpha}$	$V_s(ms^{-1})$	$L_s(m)$
--	--	--	--	--	--
--	0.0878	0	--	--	--
1.963	0.1208	0.0878	0.1043	1.733	1.961
1.936	0.1186	0.1208	0.1197	1.704	1.995
1.936	0.1493	0.1186	0.1340	1.676	2.028
1.936	0.1317	0.1493	0.1405	1.664	2.044
1.775	0.1273	0.1317	0.1295	1.545	2.018
1.936	0.1493	0.1273	0.1383	1.668	2.038

Table B.3 Experiment data and results ($m_{ft} = 0.025 kgs^{-1}$)

Exp. No.	$W_b(kg)$	$W_d(kg)$	$W_{bot}(kg)$	$\Delta p(kPa)$	$t_c(s)$
260-1	4.0	1.75	1.5	--	--
260-2	4.0	4.25	1.5	48	9.0
260-3	4.0	3.2	1.5	38	7.0
260-4	4.0	4.05	1.5	41	8.5
260-5	4.0	4.45	1.5	46	8.0
260-6	4.0	3.1	1.5	37	8.0

$V_p(ms^{-1})$	α_b	α_f	$\overline{\alpha}$	$V_s(ms^{-1})$	$L_s(m)$
--	0.0329	0	--	--	--
2.367	0.0220	0.0329	0.0275	2.302	3.612
3.043	0.0571	0.0220	0.0396	2.922	1.961
2.506	0.0577	0.0571	0.0549	2.362	1.995
2.663	0.0329	0.0527	0.0428	2.549	2.028

2.663	0.0724	0.0329	0.0527	2.523	2.044

Table B.4 Experiment data and results ($m_{ft} = 0.024 kgs^{-1}$)

Exp. No.	$W_b(kg)$	$W_d(kg)$	$W_{bot}(kg)$	$\Delta p(kPa)$	$t_c(s)$
260-7	6.0	2.3	1.0	--	--
260-8	6.0	7.45	1.0	62	10.5
260-9	6.0	5.95	1.0	50	9.5

$V_p(ms^{-1})$	α_b	α_f	$\overline{\alpha}$	$V_s(ms^{-1})$	$L_s(m)$
--	0.0966	0	--	--	--
2.029	0.0329	0.0966	0.0648	1.895	5.634
2.242	0.0351	0.0329	0.0340	2.166	5.455

The pressure drops in Tables B.3 and B.4 are higher than those in Tables B.1 and B.2. For the higher pressure, the pressurised air expands very quickly when the slug enters the discharge tank. This causes some of the stationary layer to be conveyed also into the discharge tank. Hence, α_f or α_b in Tables B.3 and B.4 are smaller than the value in Tables B.1 and B.2. For this reason, the data inTable 3.2 are based on Tables B.1 and B.2, where more accurate values of α_f and α_b were obtained.

As this thesis concentrates on the prediction of pressure drop (Δp) and slug velocity (V_p), the selection of m_f is considered the subject of future work.

EXPERIMENT NO. 220-1
TOTAL MASS OF AIR USED (KGS) =

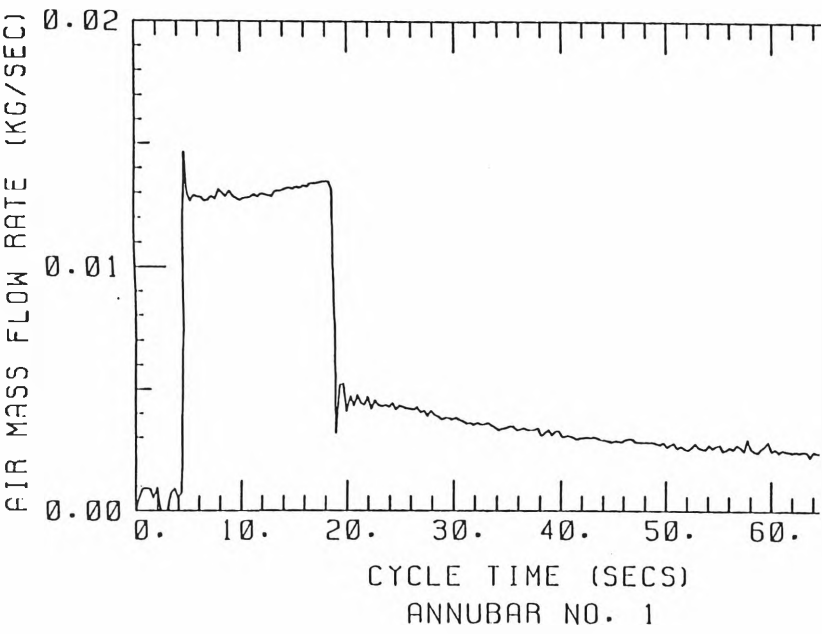

TEST DATE: 12\5\95
0.342

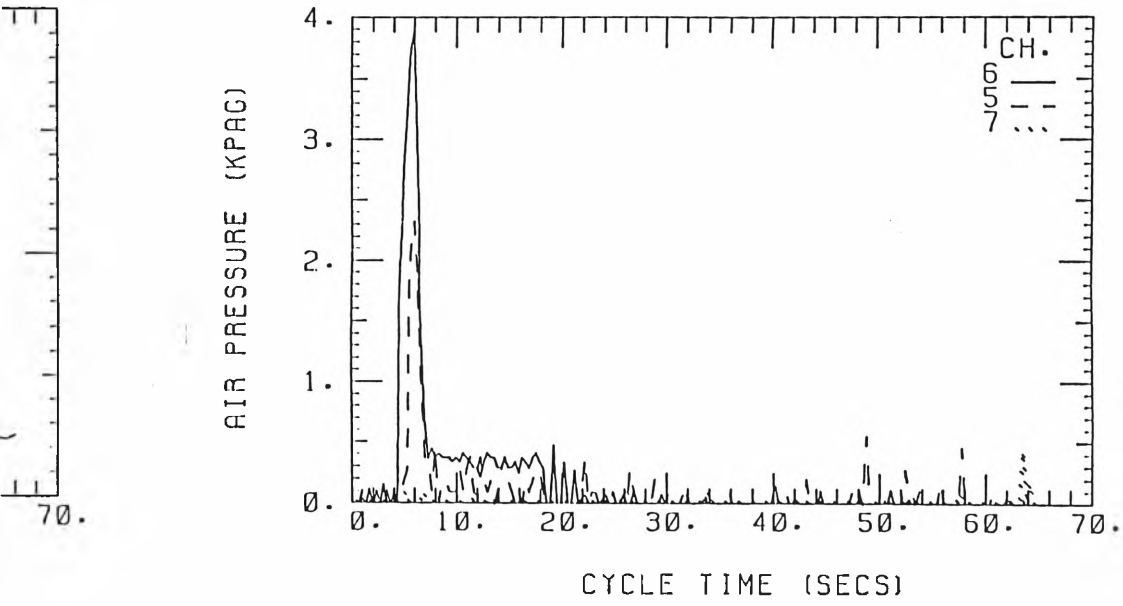

EXPERIMENT NO. 220-2
TOTAL MASS OF AIR USED (KGS) =

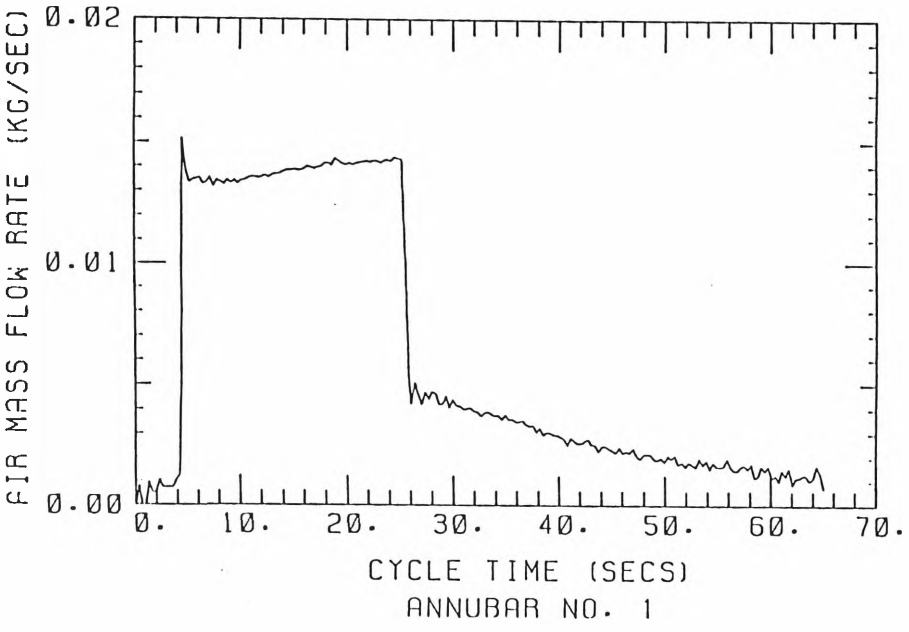

TEST DATE: 12\5\95
0.398

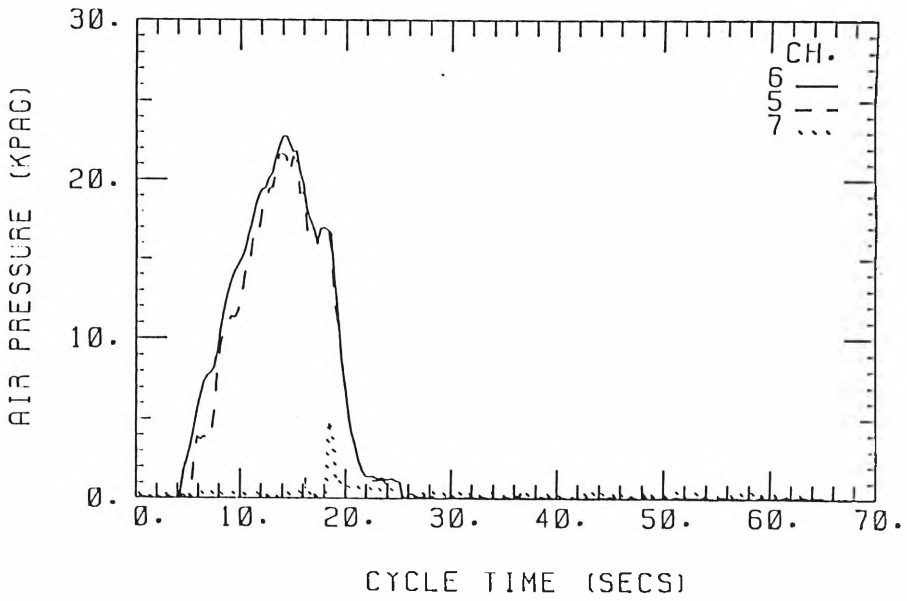

EXPERIMENT NO. 220-3

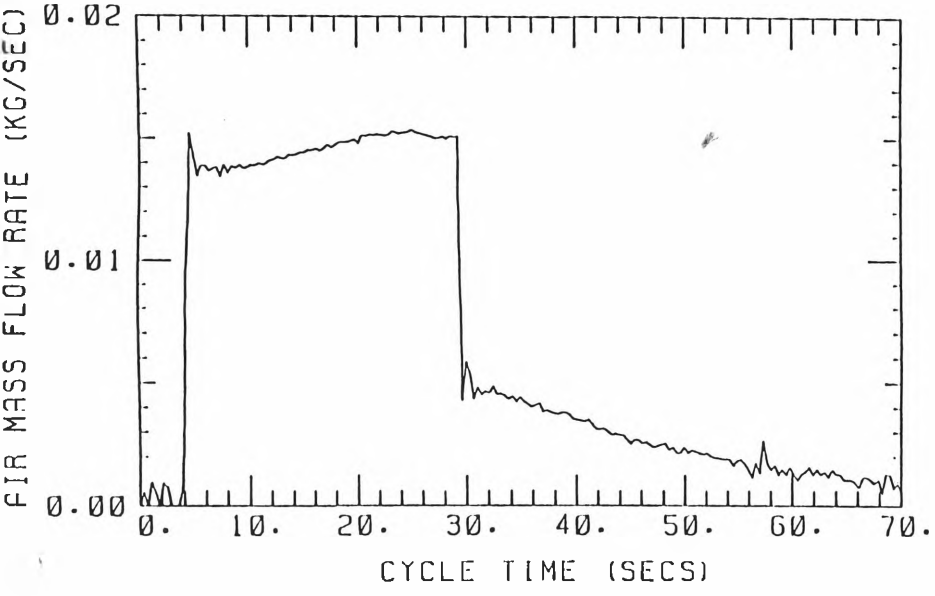

TEST DATE: 12\5\95

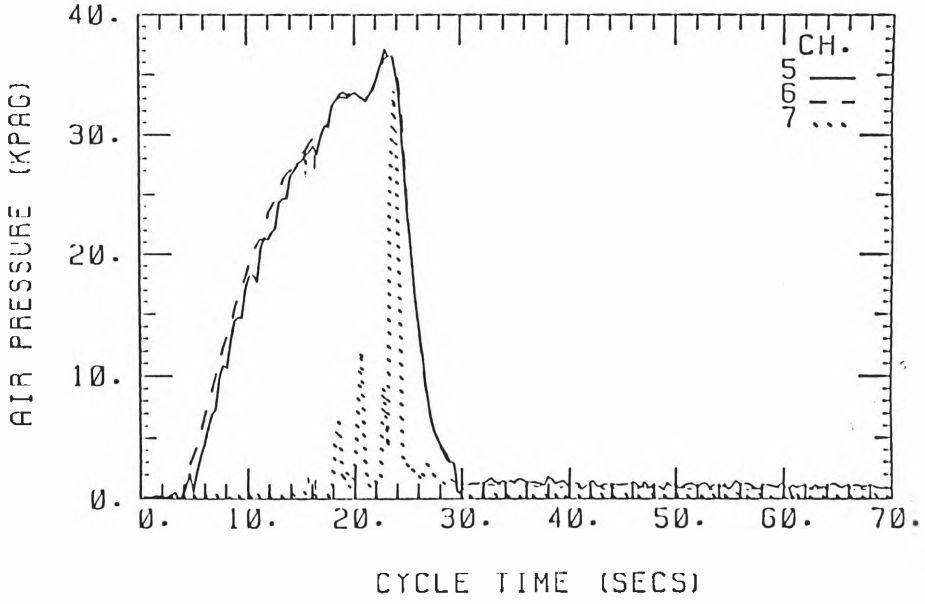

EXPERIMENT NO. 230-1
TOTAL MASS OF AIR USED (KGS) =

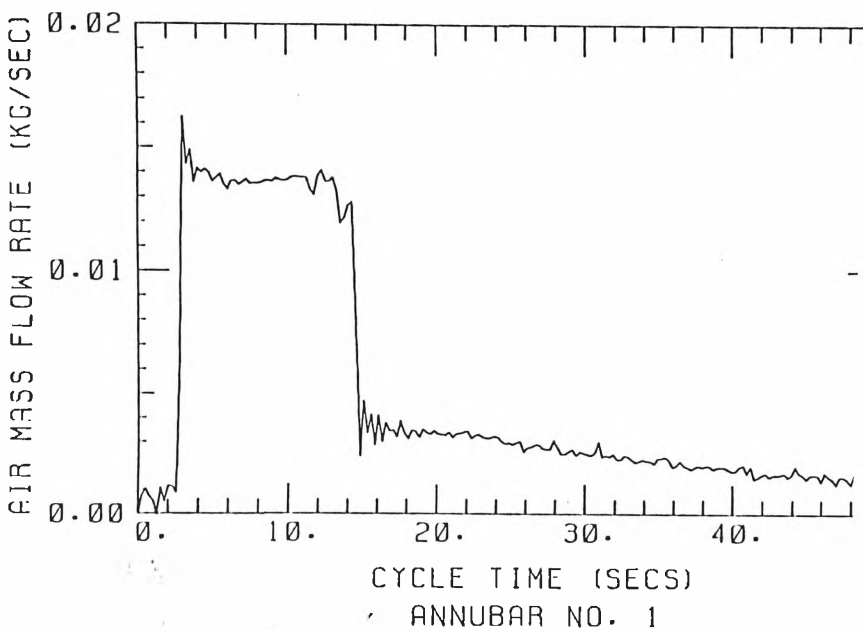

TEST DATE: 15\5\95
0.250

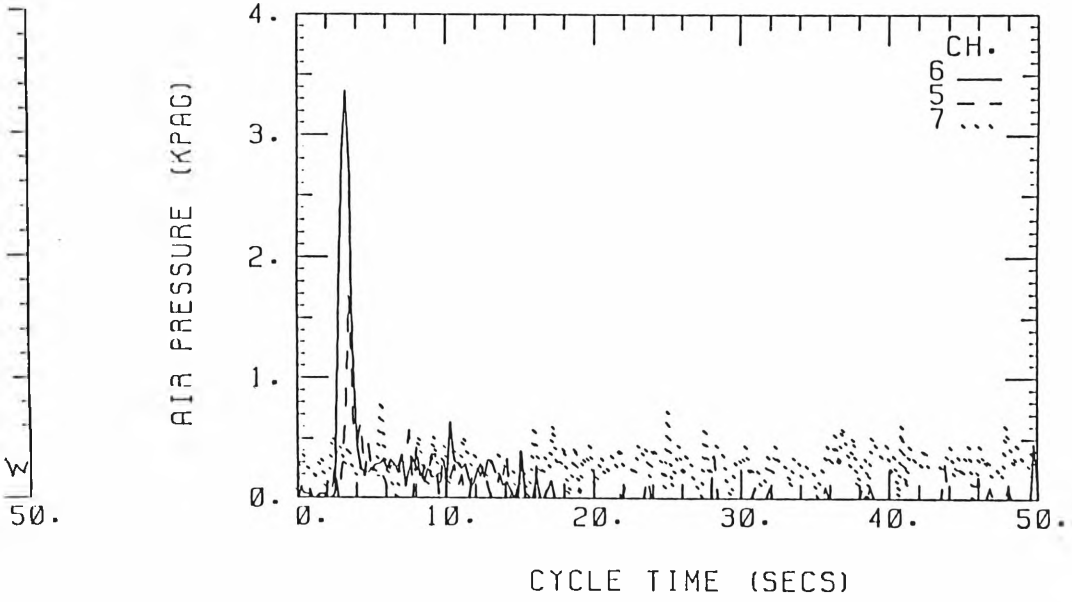

EXPERIMENT NO. 230-2
TOTAL MASS OF AIR USED (KGS) =

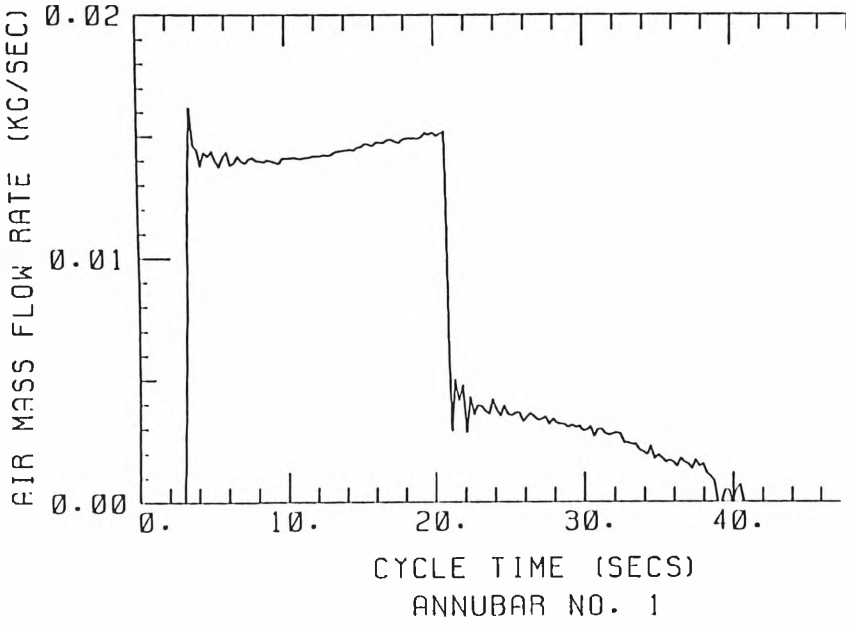

TEST DATE: 15\5\95
0.307

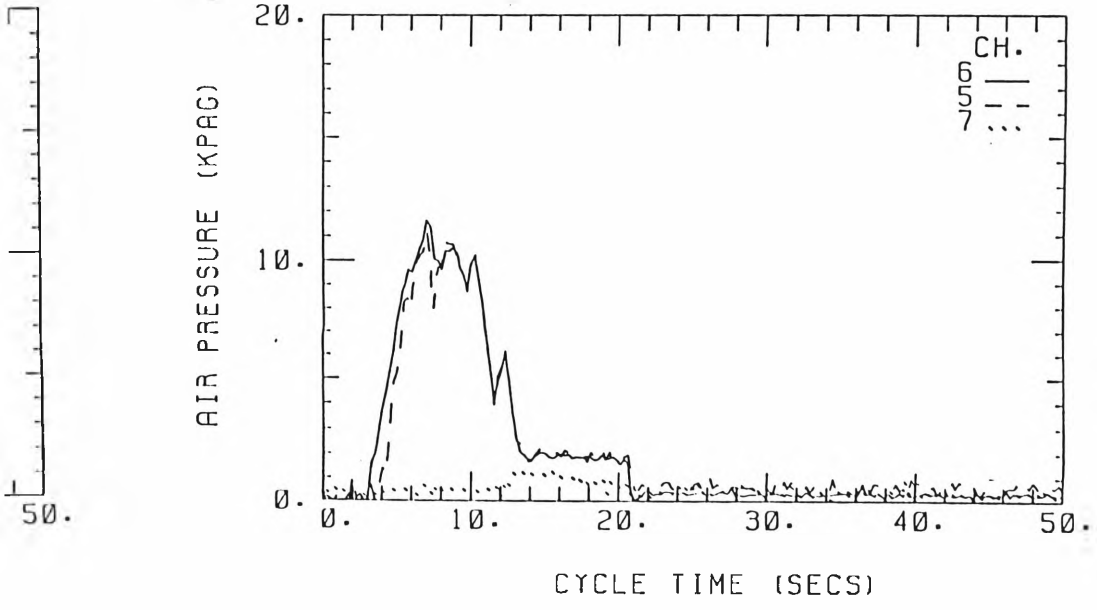

EXPERIMENT NO. 230-3
TOTAL MASS OF AIR USED (KGS) =

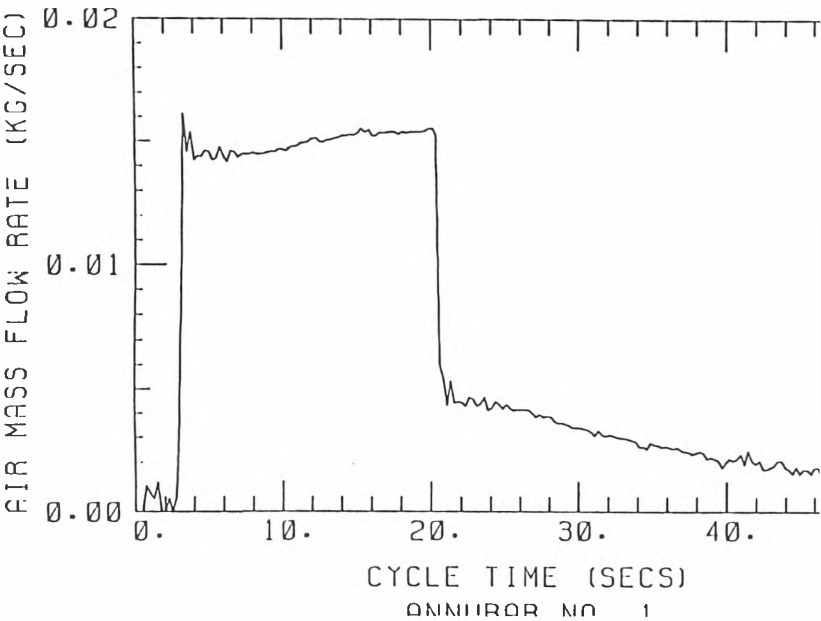

TEST DATE: 15\5\95
0.346

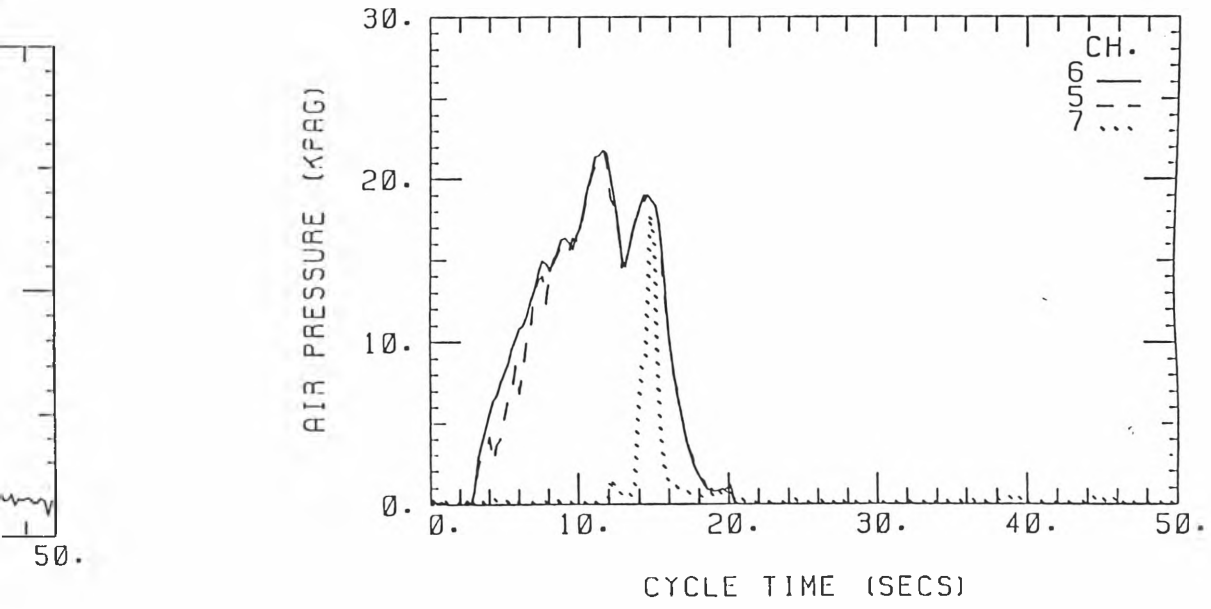

EXPERIMENT NO. 230-4
TOTAL MASS OF AIR USED (KGS) =

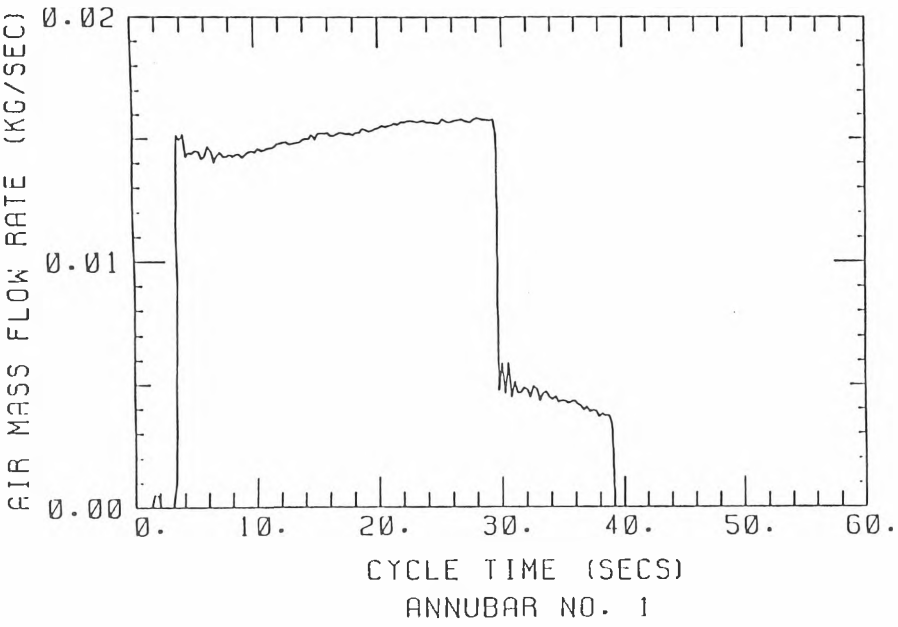

TEST DATE: 15\5\95
0.438

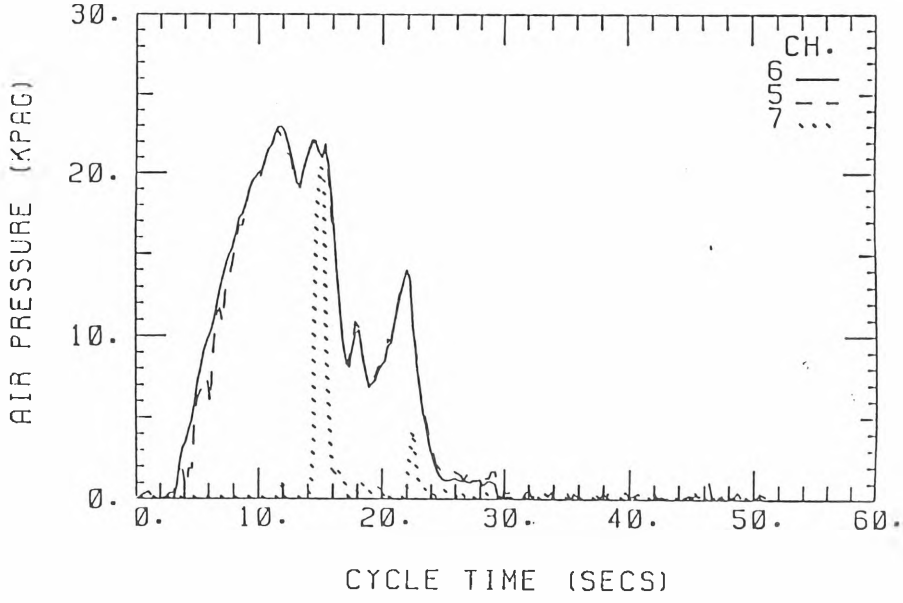

EXPERIMENT NO. 230-5 TEST DATE: 15\5\95

TOTAL MASS OF AIR USED (KGS) = 0.378

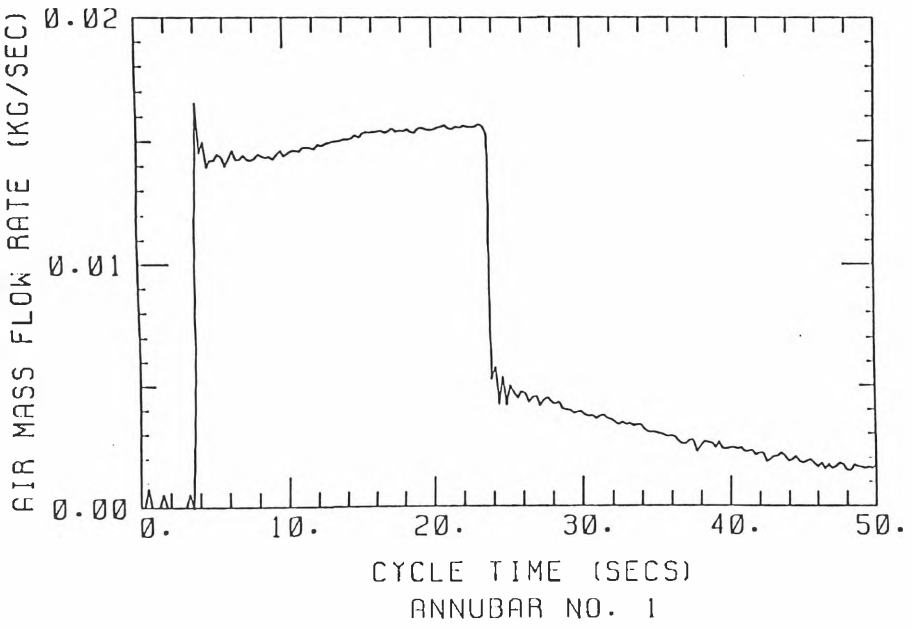

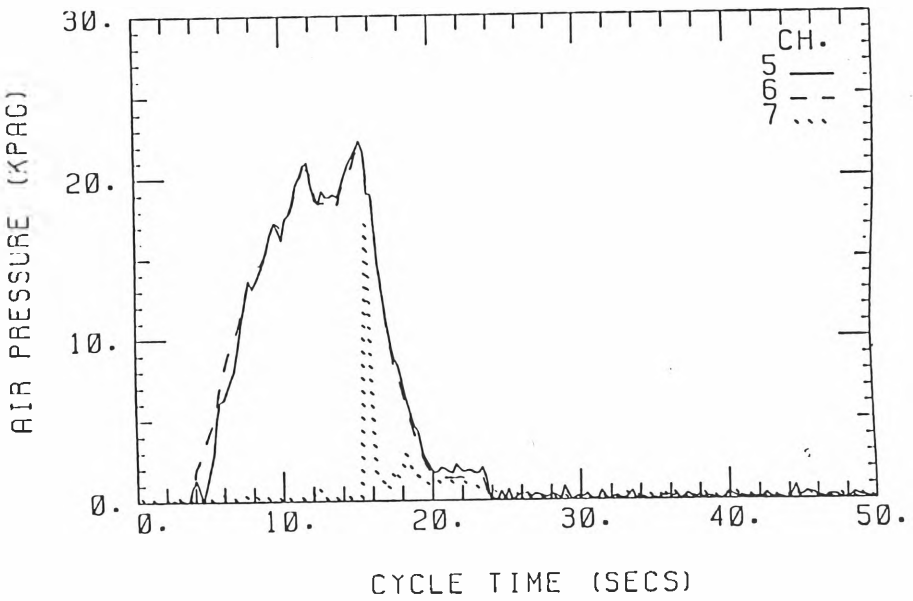

EXPERIMENT NO. 230-6
TOTAL MASS OF AIR USED (KGS)

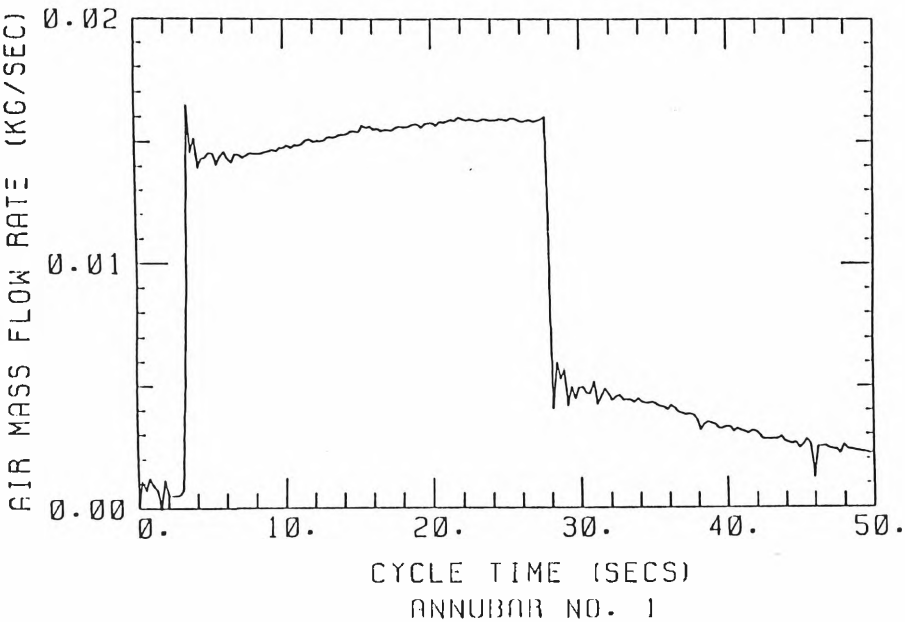

TEST DATE: 15\5\95

= 0.457

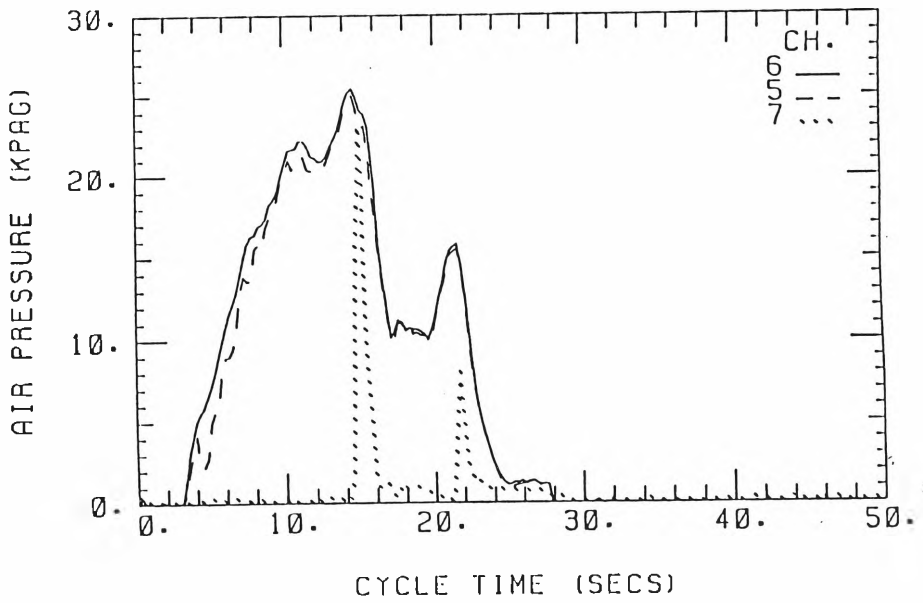

EXPERIMENT NO. 230-7
TOTAL MASS OF AIR USED (KGS) =

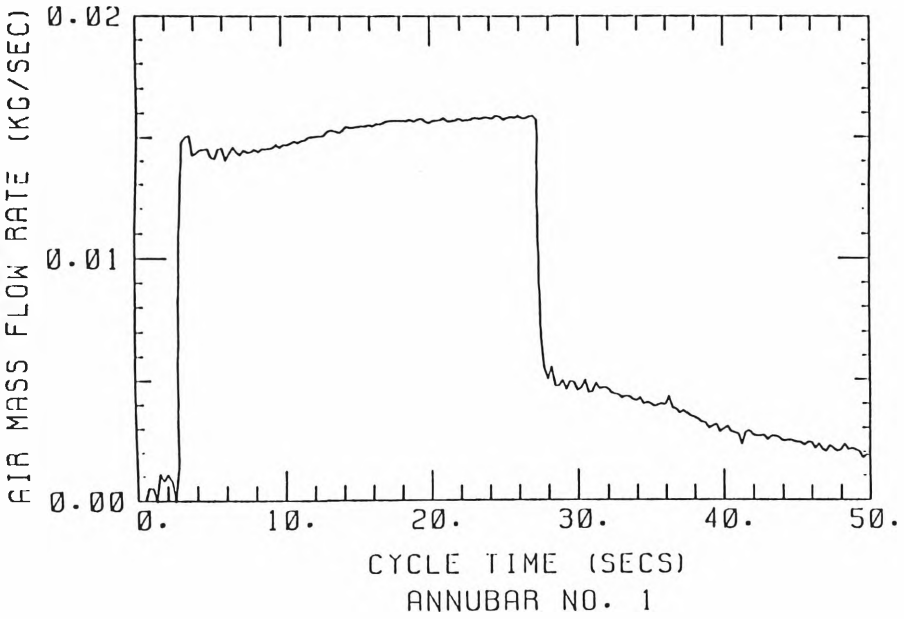

TEST DATE: 15\5\95
0.451

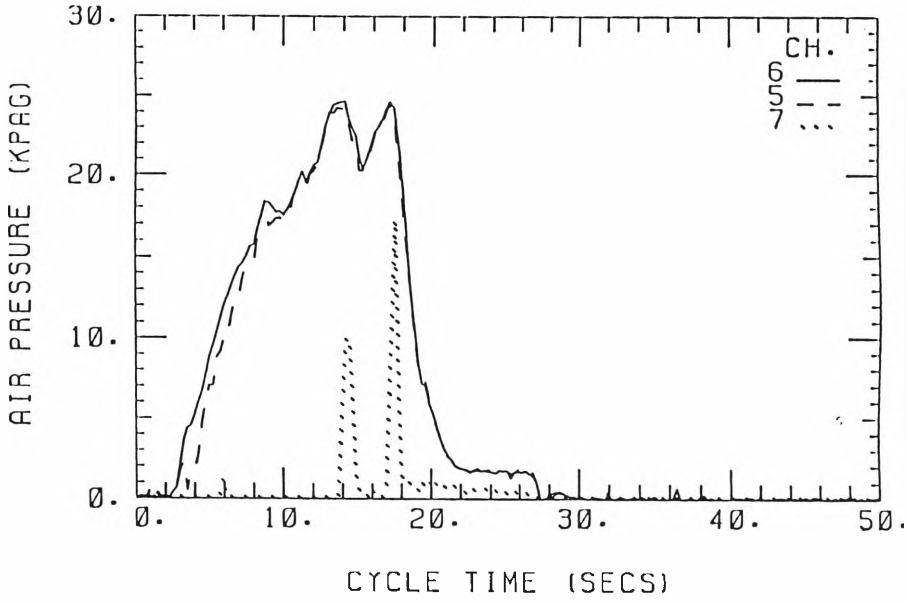

EXPERIMENT NO. 230-8
TOTAL MASS OF AIR USED (KGS) =

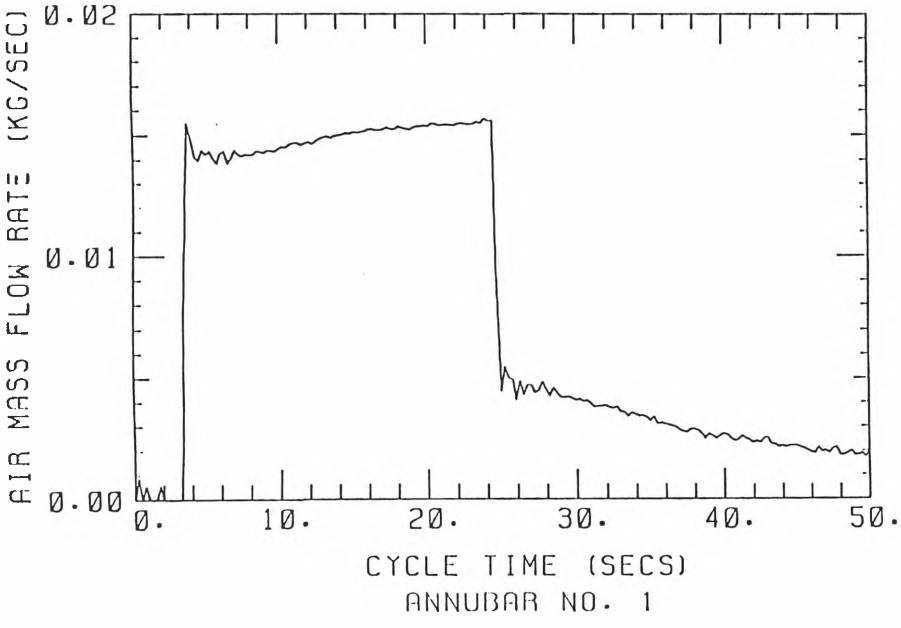

TEST DATE: 15\5\95
0.396

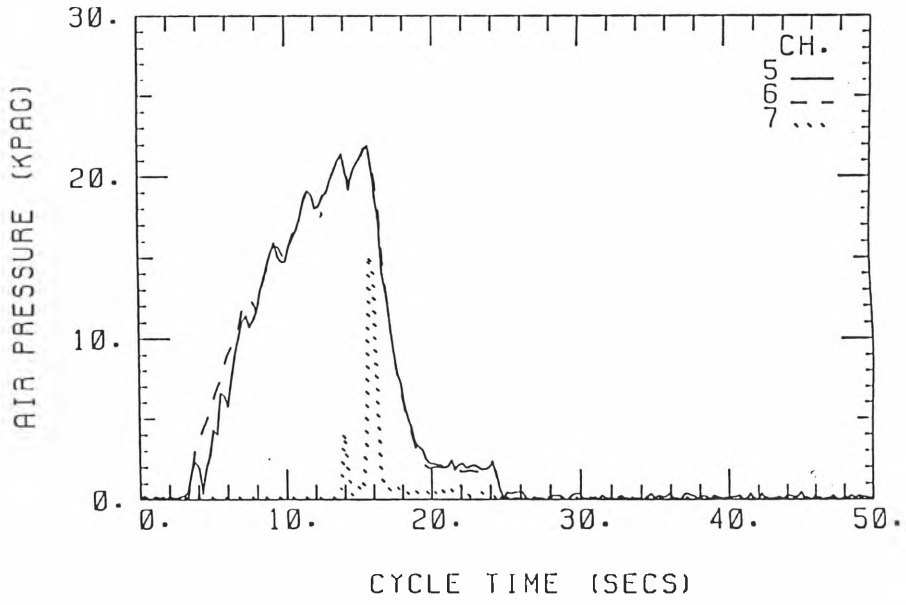

EXPERIMENT NO. 260-1 TEST DATE: 17\5\95

TOTAL MASS OF AIR USED (KGS) = 0.400

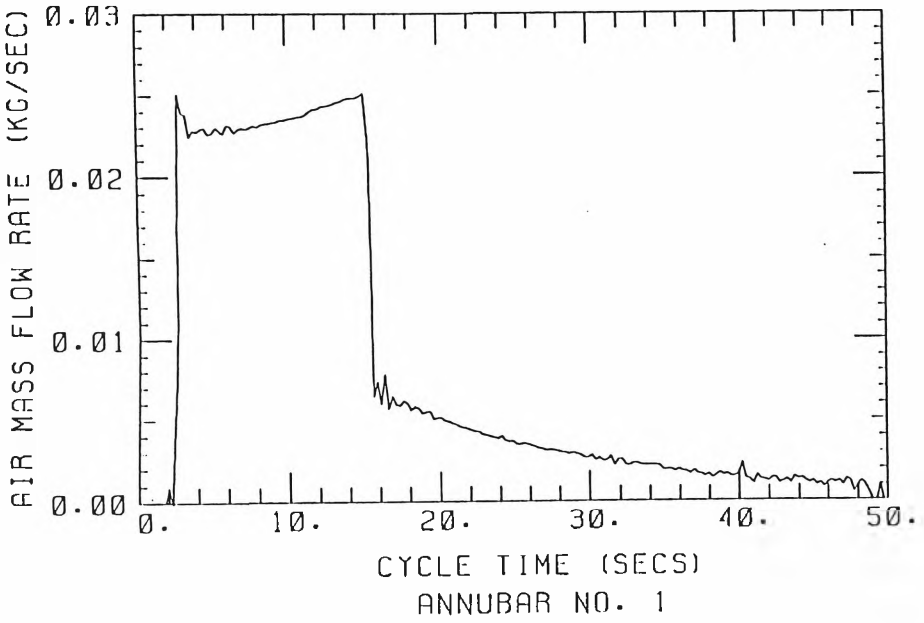

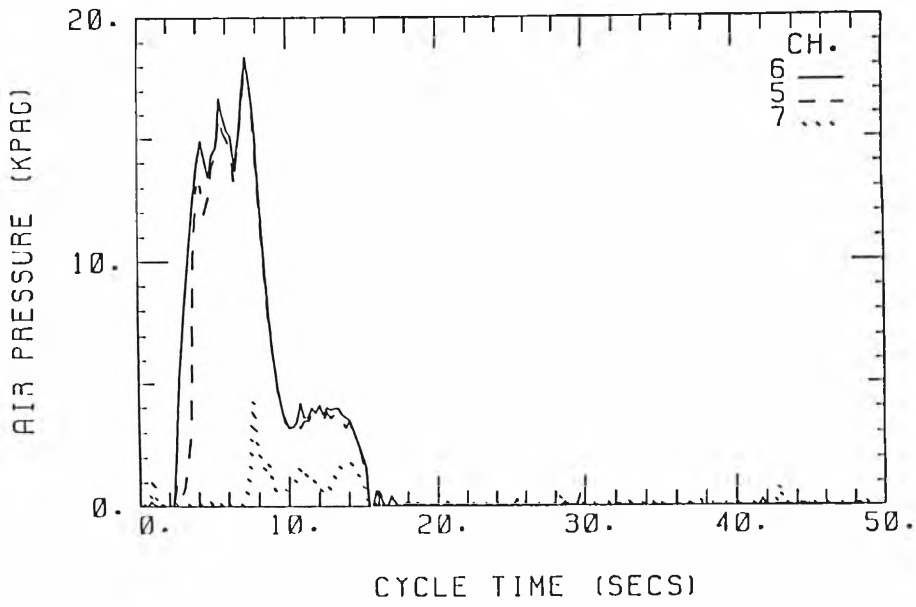

EXPERIMENT NO. 260-2
TOTAL MASS OF AIR USED (KGS) =

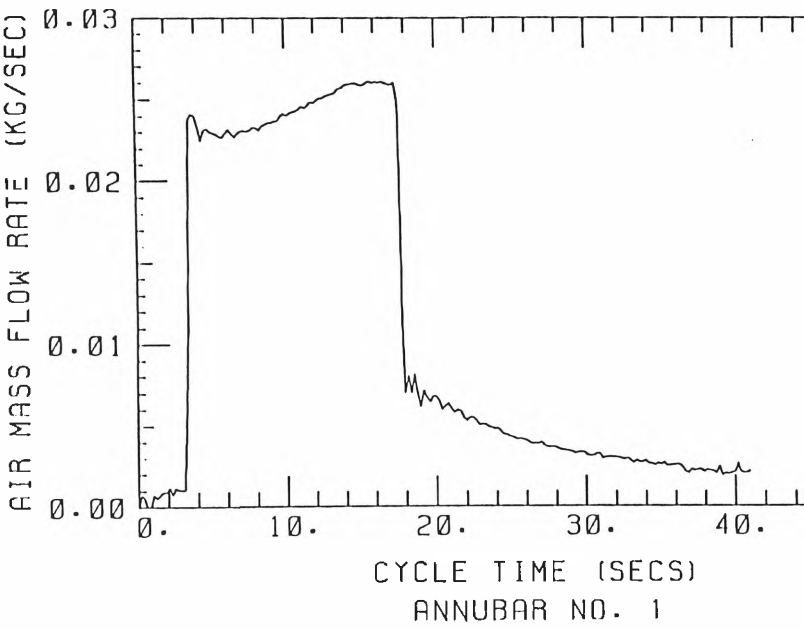

TEST DATE: 17\5\95
0.442

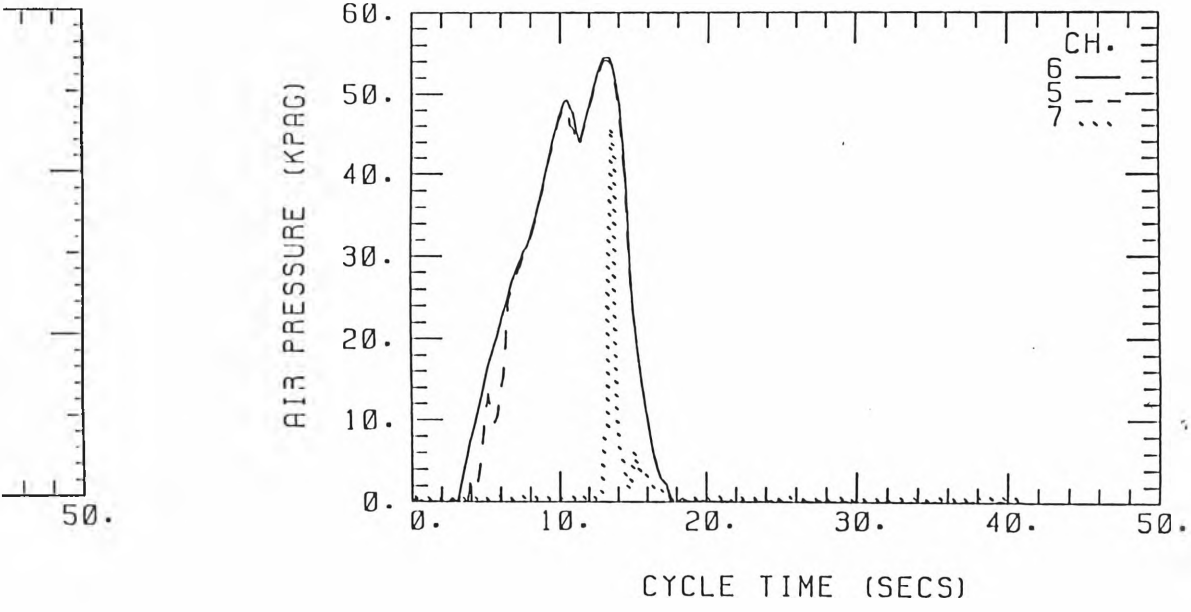

EXPERIMENT NO. 260-3 TEST DATE: 17\5\95
TOTAL MASS OF AIR USED (KGS) = 0.338

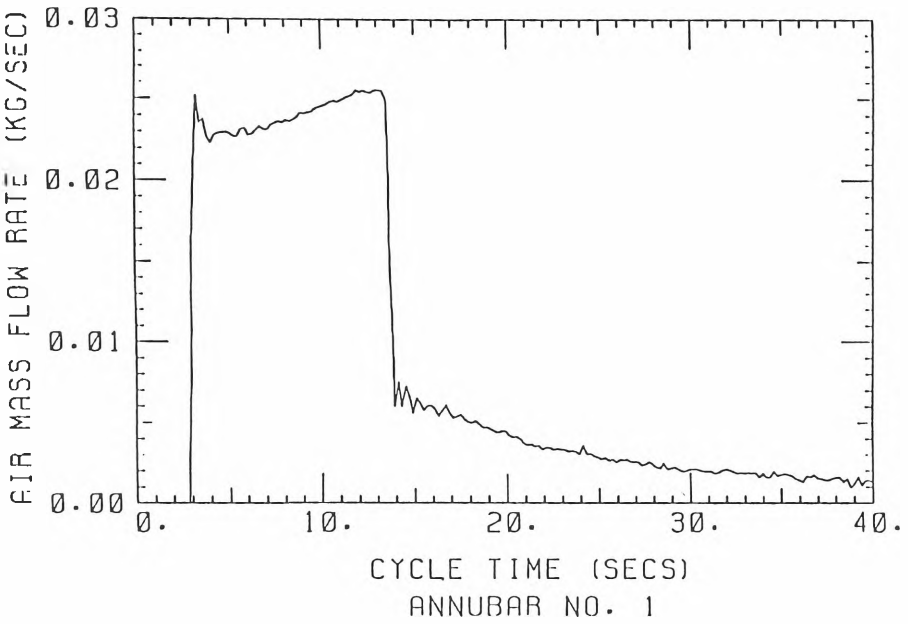

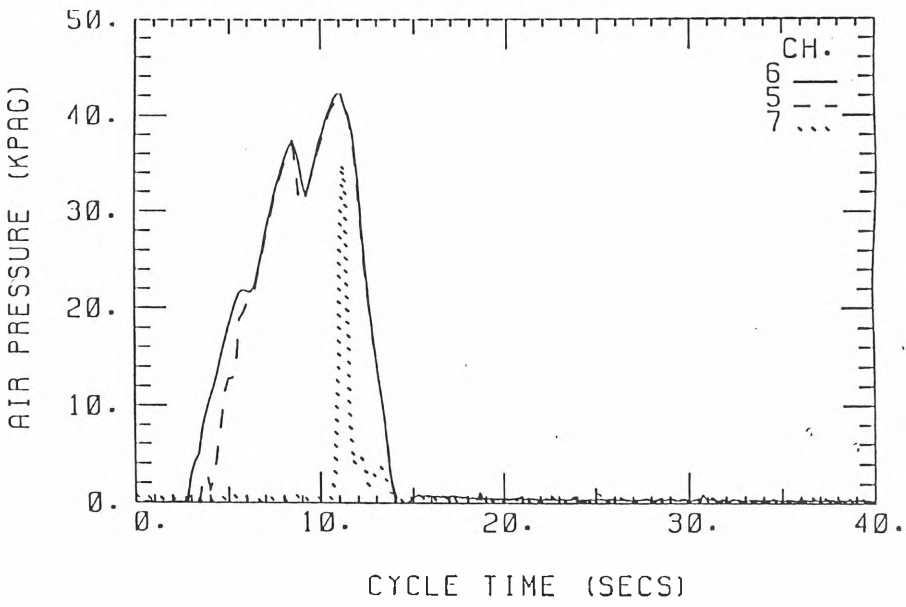

EXPERIMENT NO. 260-4
TOTAL MASS OF AIR USED (KGS) =

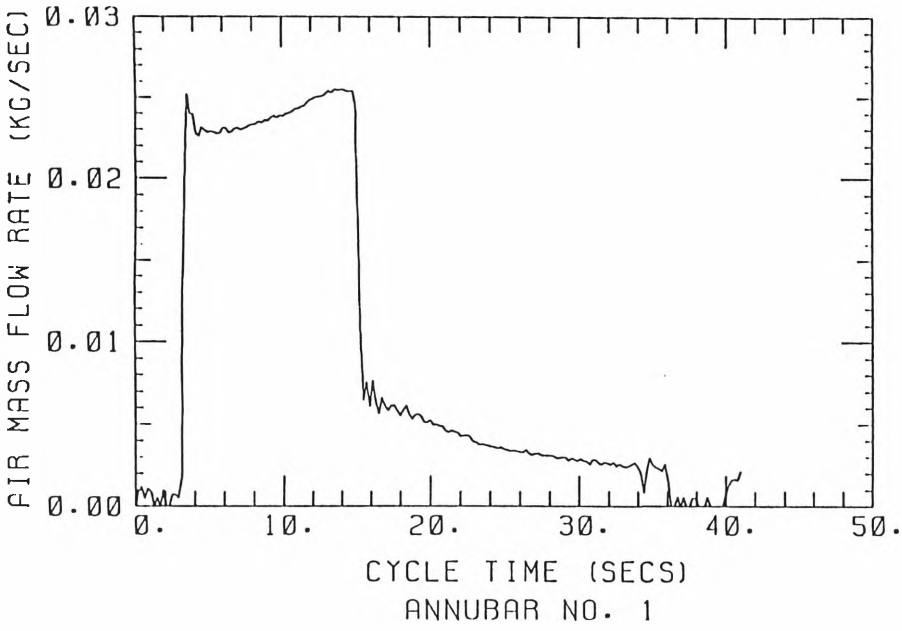

TEST DATE: 17\5\95
0.372

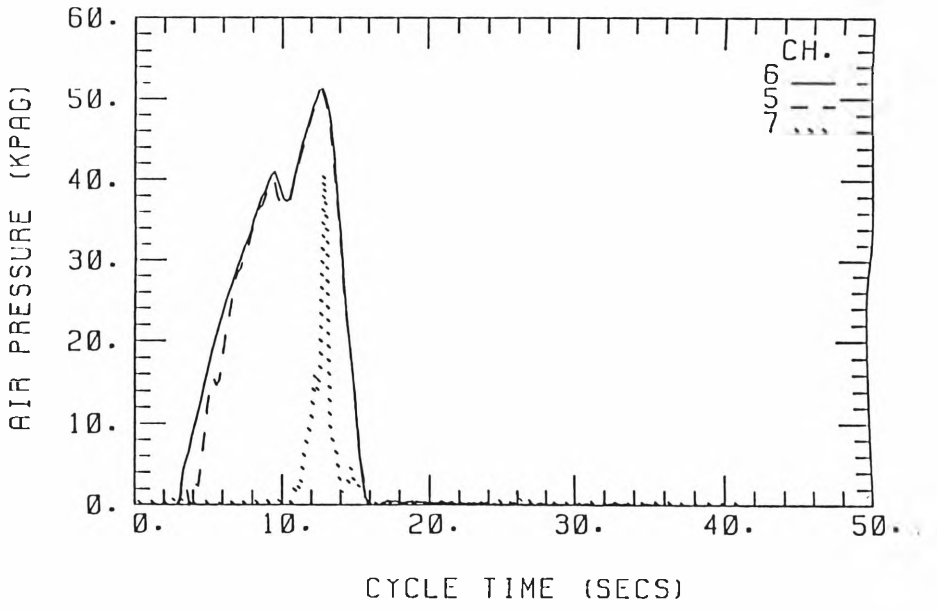

EXPERIMENT NO. 260-5
TOTAL MASS OF AIR USED (KGS) =

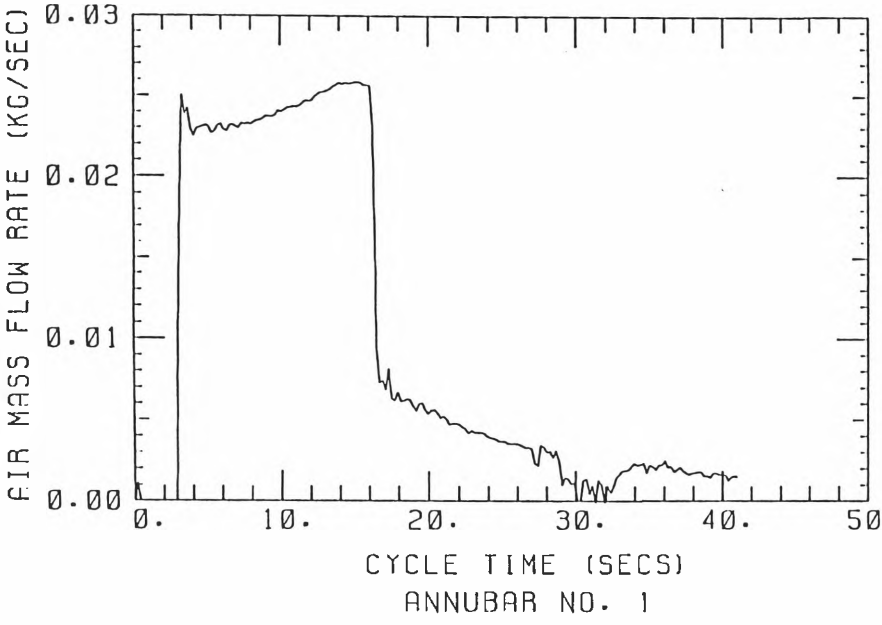

TEST DATE: 17\5\95
0.400

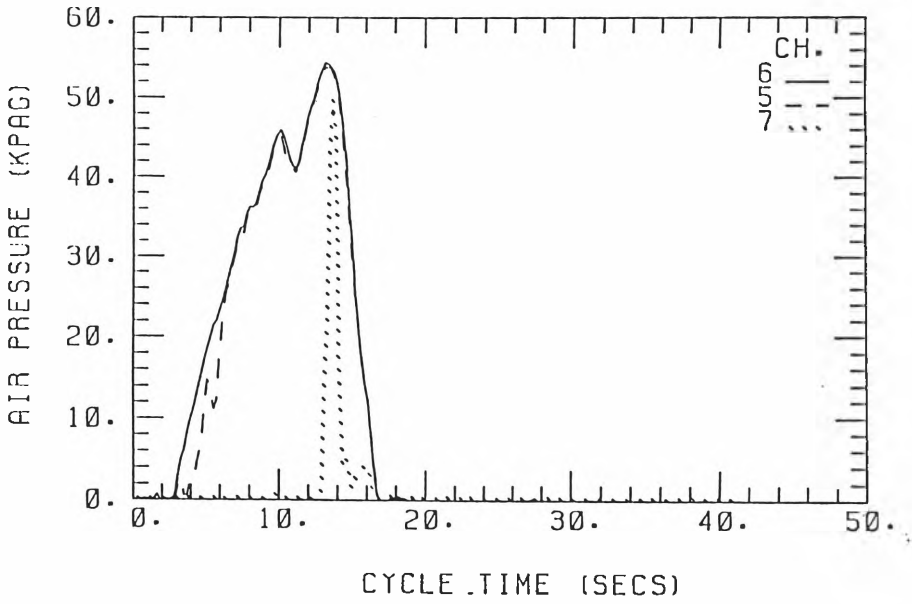

EXPERIMENT NO. 260-6 TEST DATE: 17\5\95

TOTAL MASS OF AIR USED (KGS) = 0.333

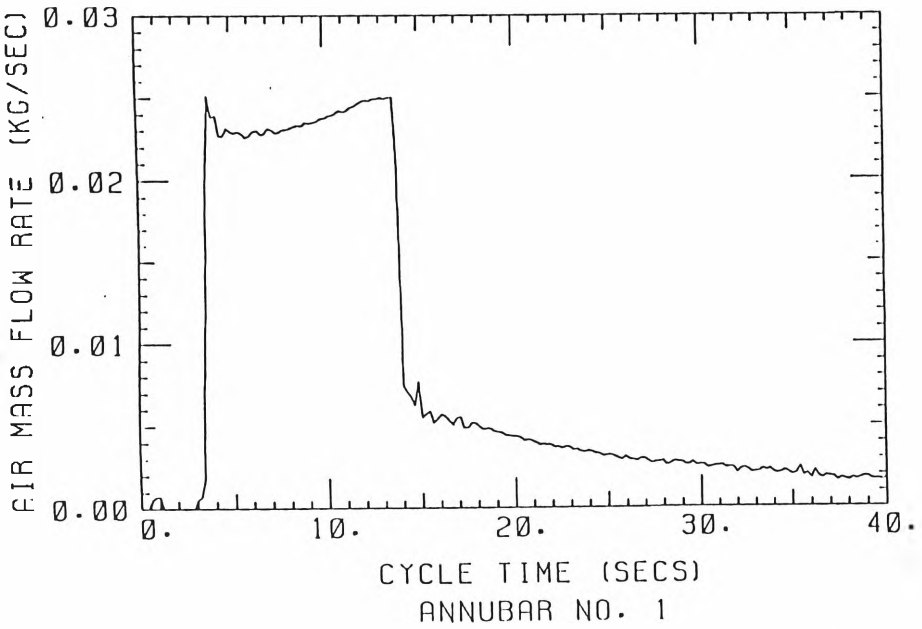

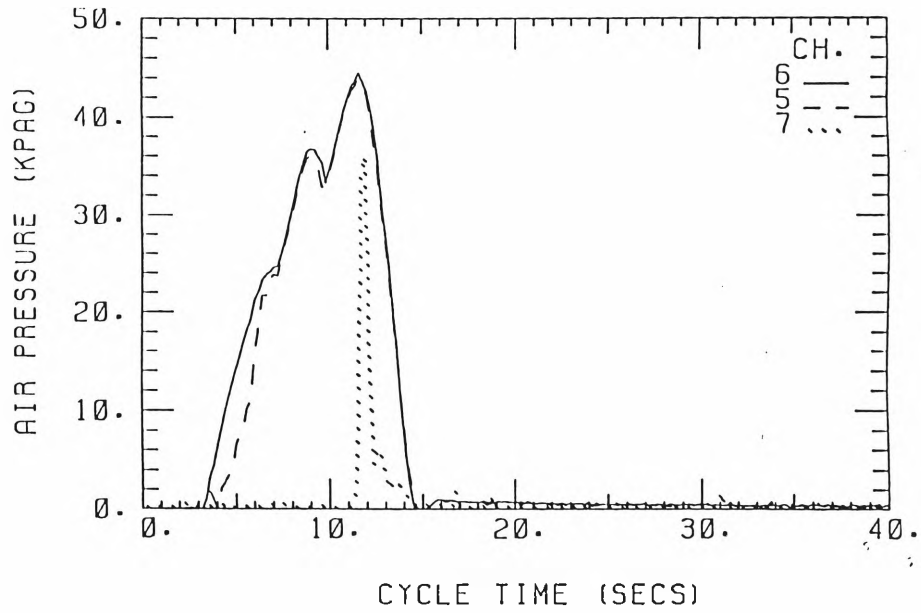

EXPERIMENT NO. 260-7
TOTAL MASS OF AIR USED (KGS) =

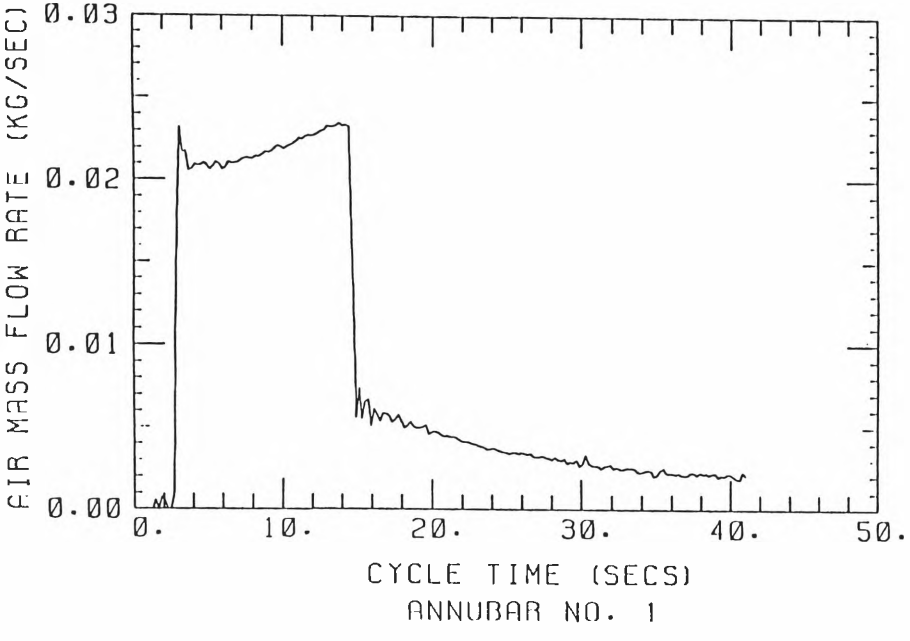

TEST DATE: 17\5\95
0.351

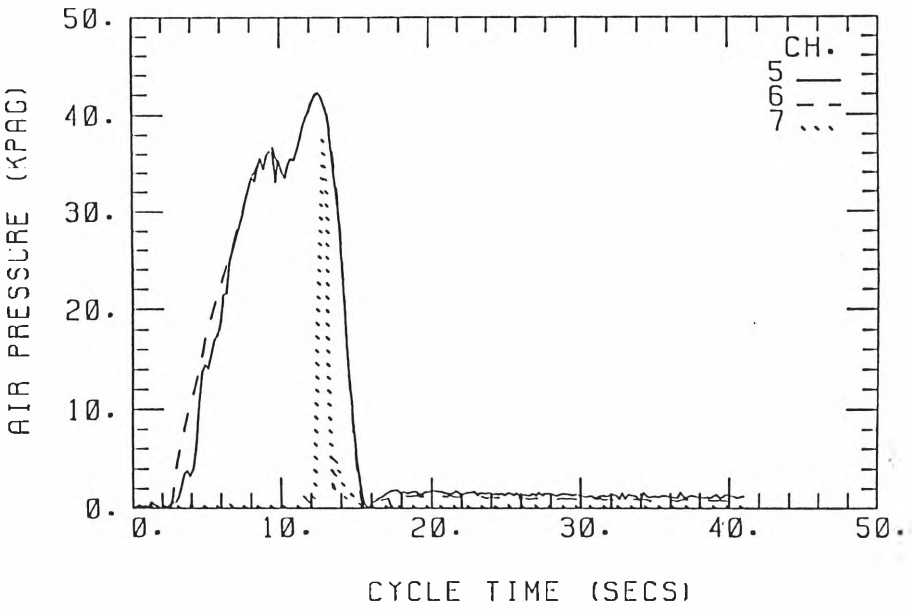

EXPERIMENT NO. 260-8
TOTAL MASS OF AIR USED (KGS) =

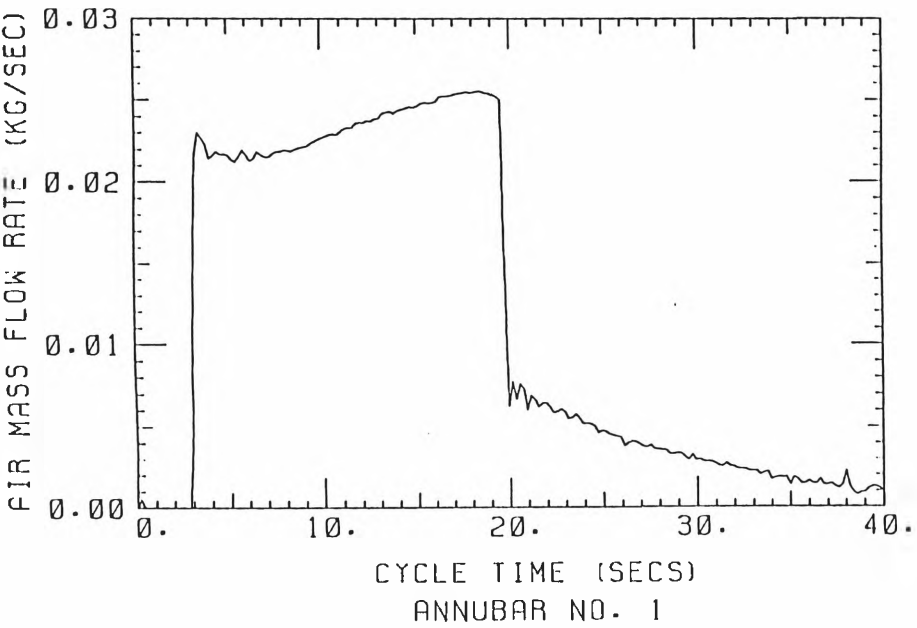

TEST DATE: 17\5\95
0.458

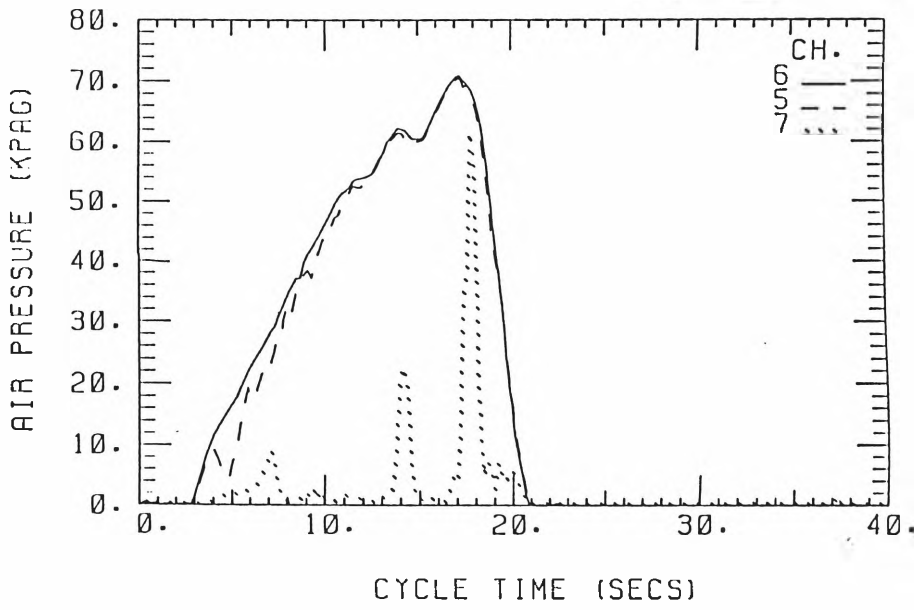

EXPERIMENT NO. 260-9 TEST DATE: 17\5\95

TOTAL MASS OF AIR USED (KGS) = 0.461

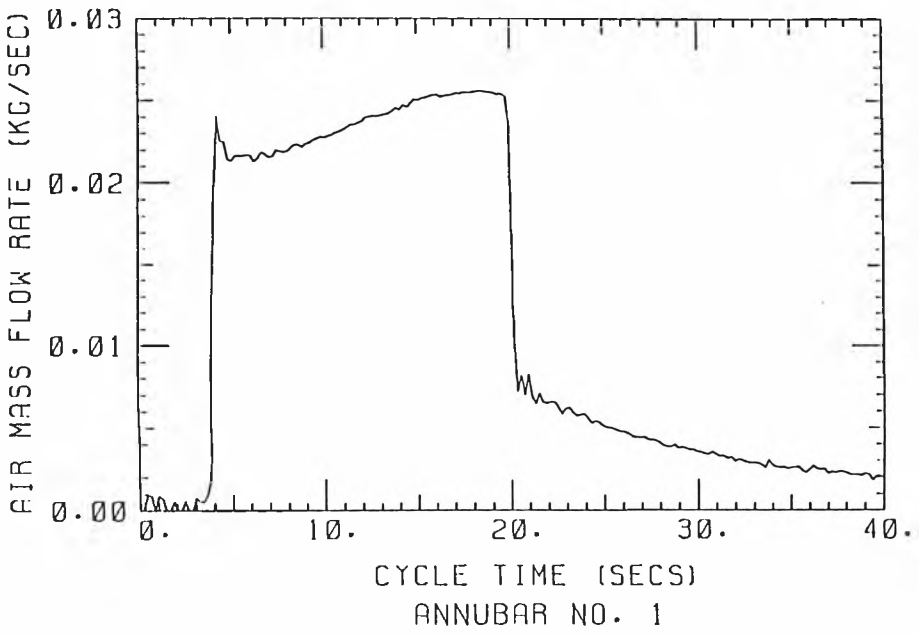

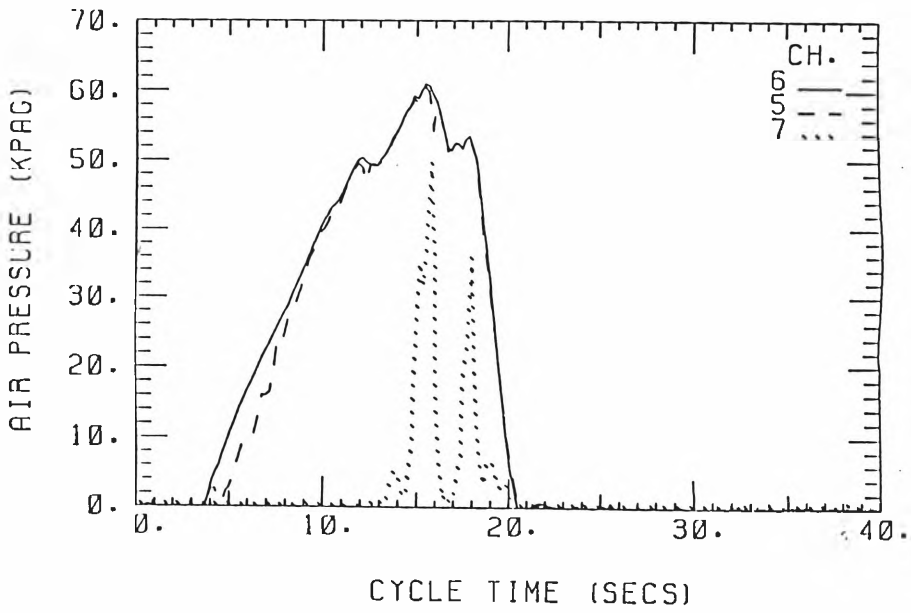

Appendix C Experimental Plots for Table 4.2

The measured data in Table 4.2 are based on the following experimental plots.

Pressure meter A is connected to channel 5, pressure meter B to channel 6, pressure meter C to channel 7, pressure meter D to channel 8 and pressure meter E to channel 9.

Table C.1 Experimental values for t_{pm} and Δp

Exp. No.	$\Delta p(kPa)$	$t_{pm}(s)$
1	100	5
2	120	5
3	110	6
4	111	6
5	112	5
6	110	5

EXPERIMENT NO. 1 TEST DATE: 22\9\95
TOTAL MASS OF AIR USED (KGS) = 1.135

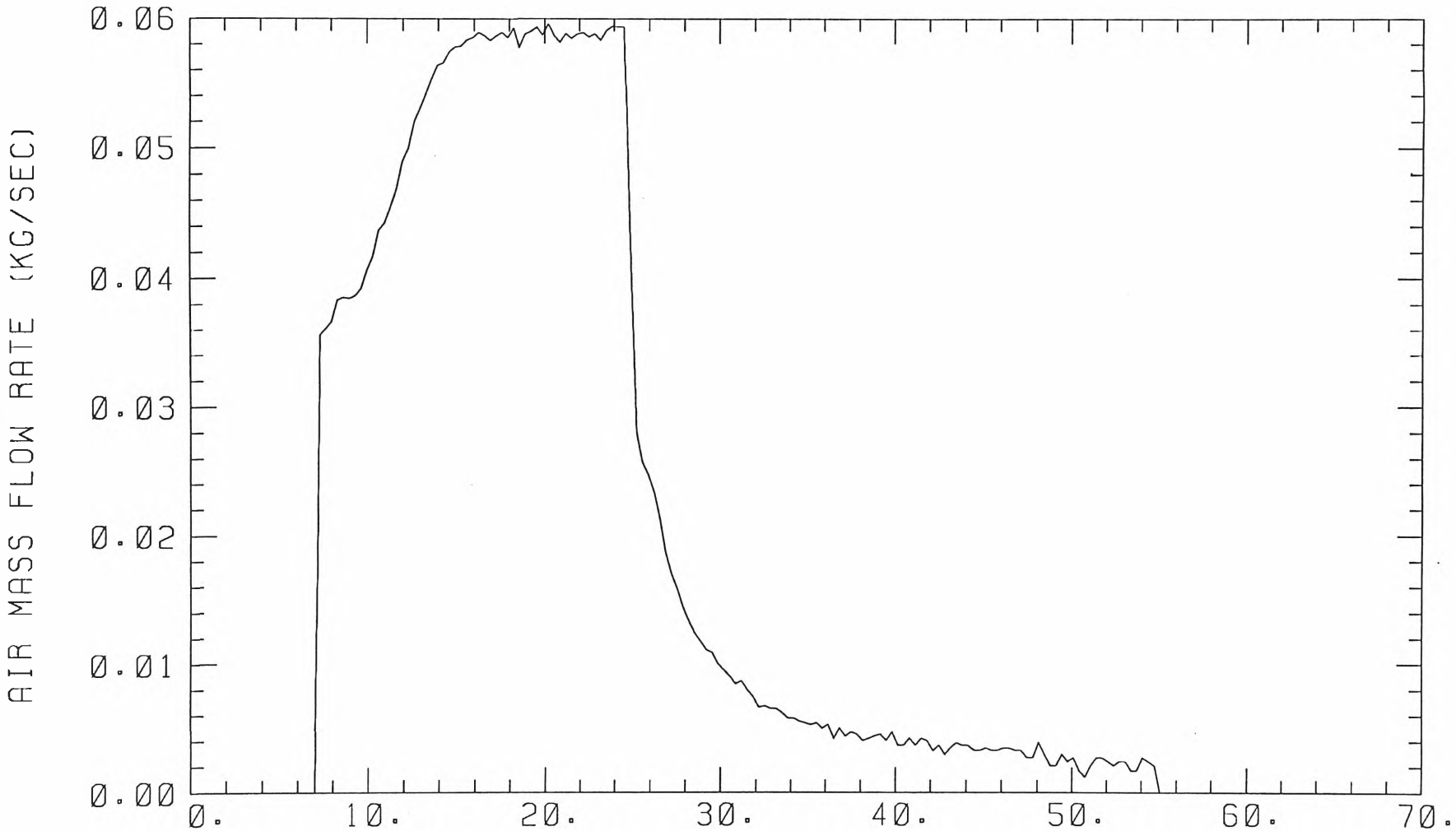

ANNUBAR NO. 3

EXPERIMENT NO. 1 TEST DATE: 22\9\95

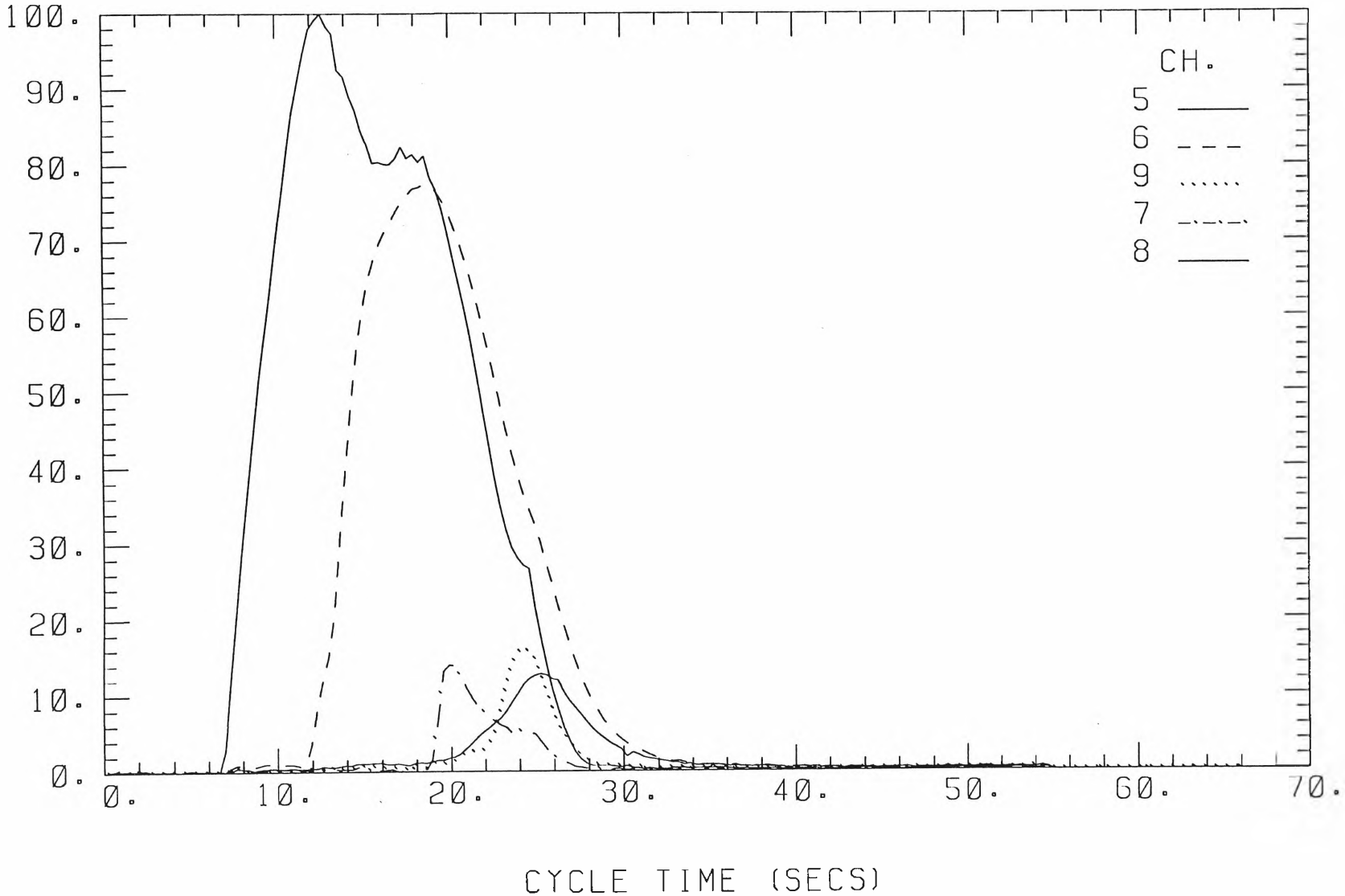

EXPERIMENT NO. 2 TEST DATE: 22\9\95

TOTAL MASS OF AIR USED (KGS) = 1.371

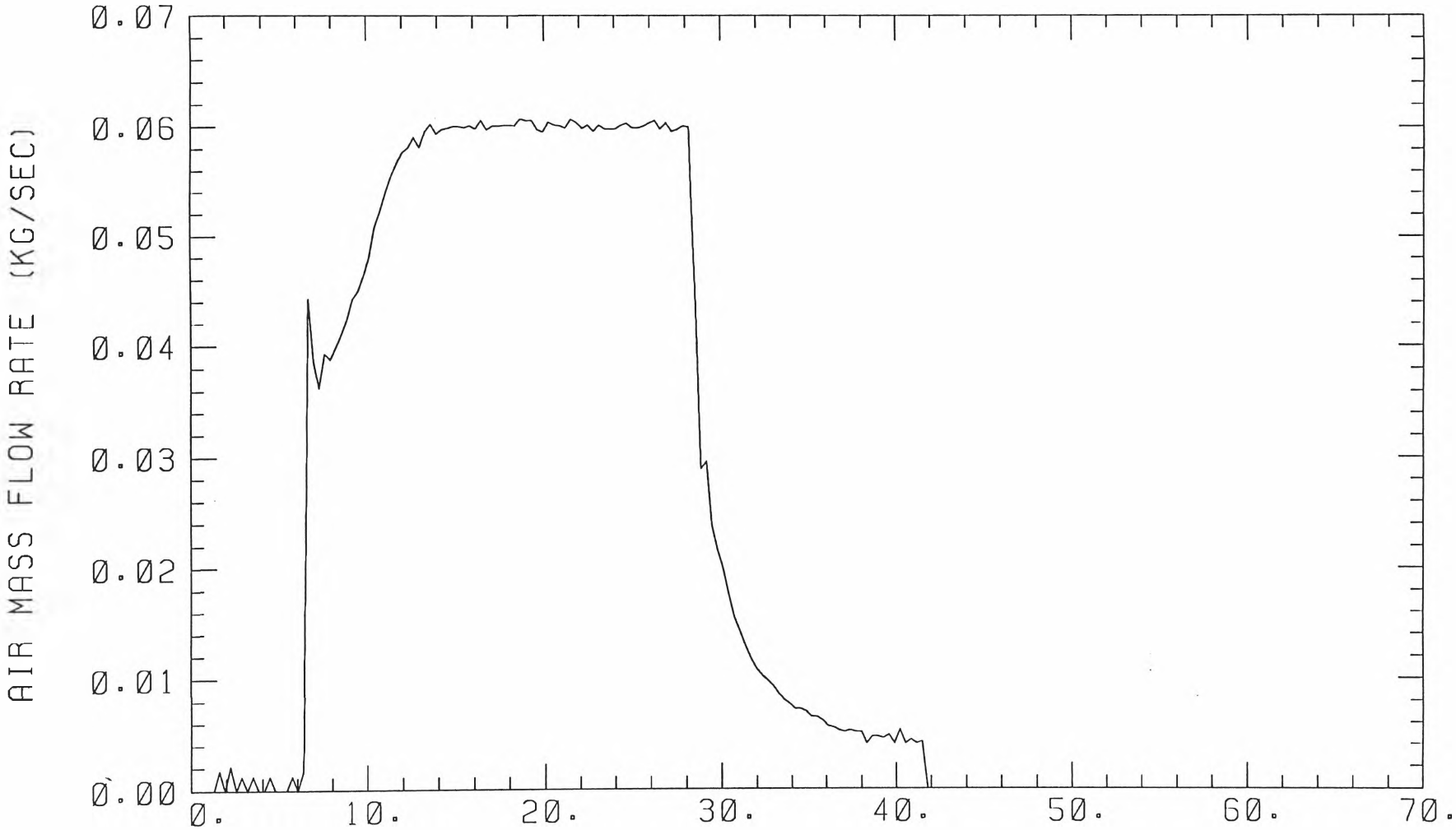

ANNUBAR NO. 3

EXPERIMENT NO. 2

TEST DATE: 22\9\95

EXPERIMENT NO. 3 TEST DATE: 22\9\95

TOTAL MASS OF AIR USED (KGS) = 1.696

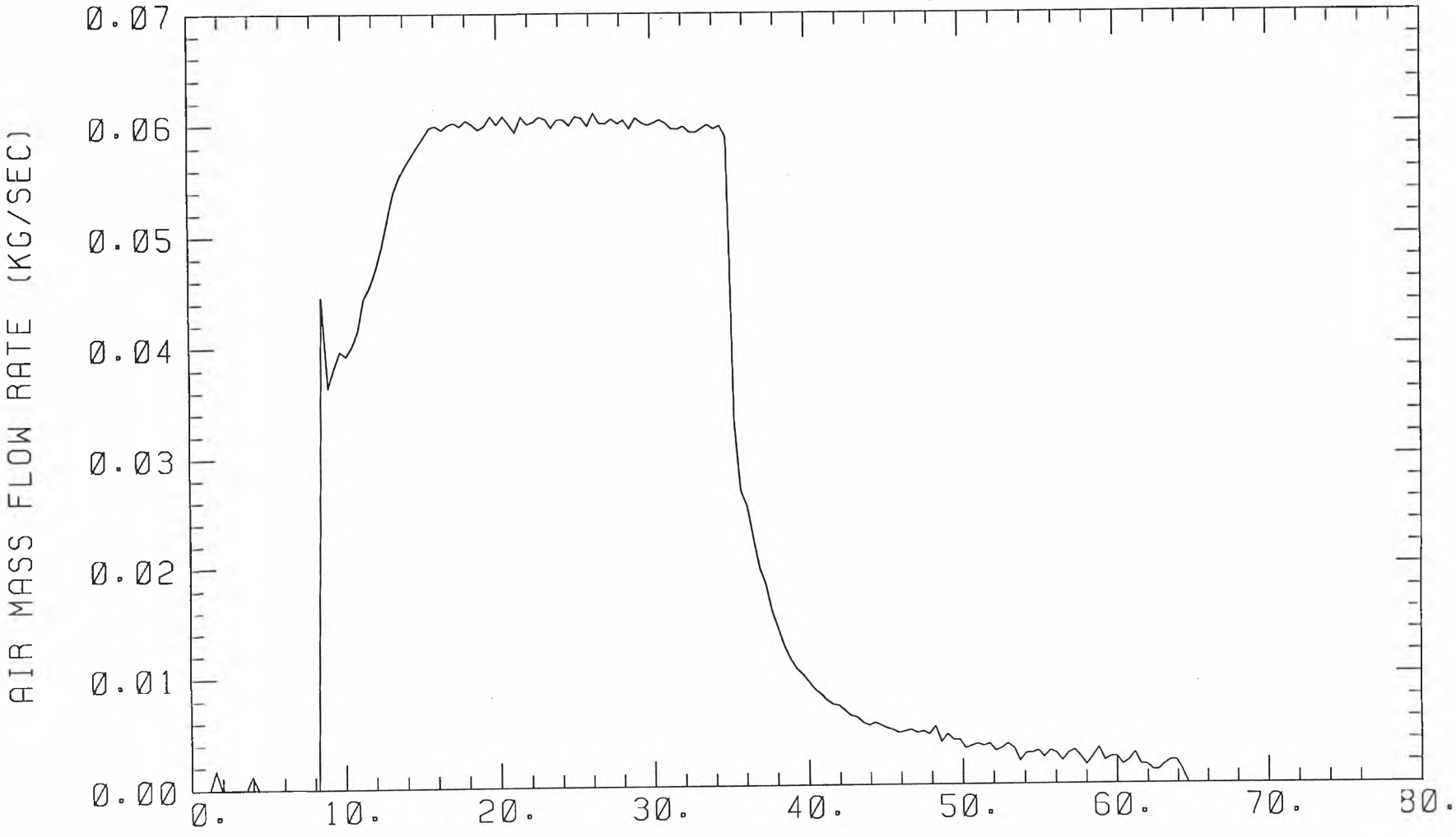

ANNUBAR NO. 3

AIR PRESSURE (KPAG)
EXPERIMENT NO. 3
TEST DATE: 22\9\95
200.
100.
0.
0.
10.
20.
30.
40.
50.
60.
70.
80.
CH.
5
6
9
8
7
CYCLE TIME (SECS)

EXPERIMENT NO. 4 TEST DATE: 22\9\95

TOTAL MASS OF AIR USED (KGS) = 1.668

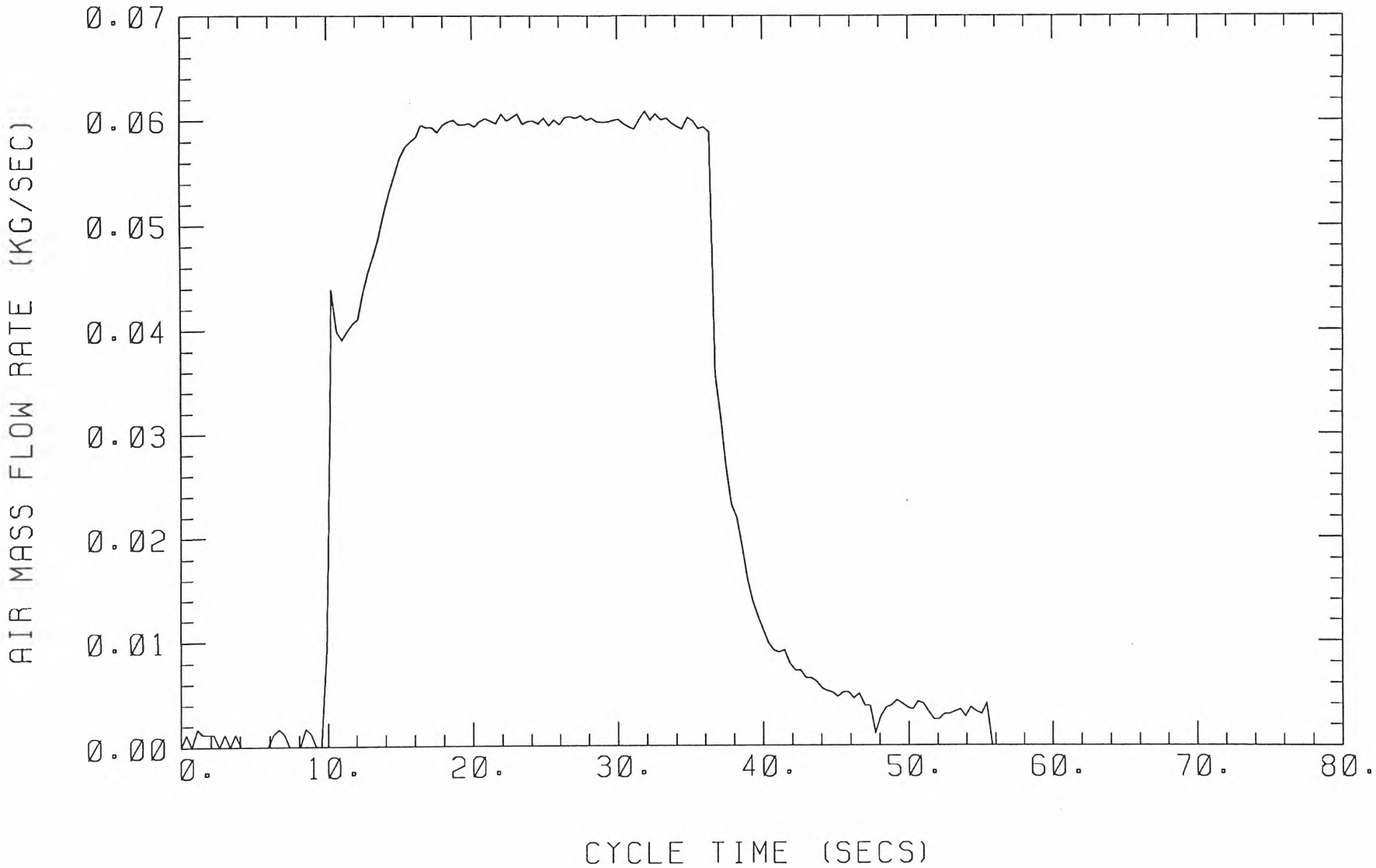

ANNUBAR NO. 3

EXPERIMENT NO. 4 TEST DATE: 22\9\95

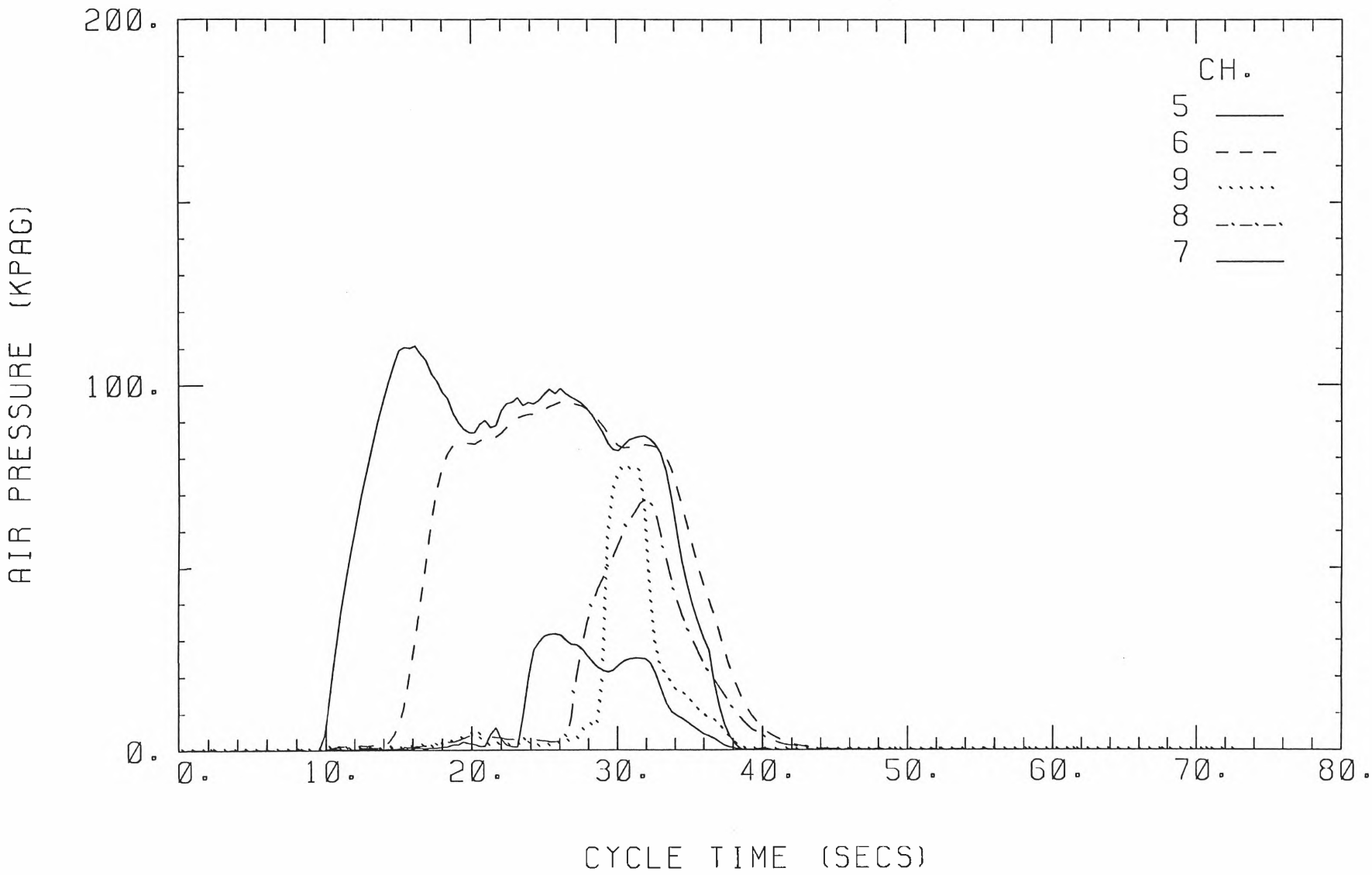

EXPERIMENT NO. 5 TEST DATE: 22\9\95
TOTAL MASS OF AIR USED (KGS) = 1.690

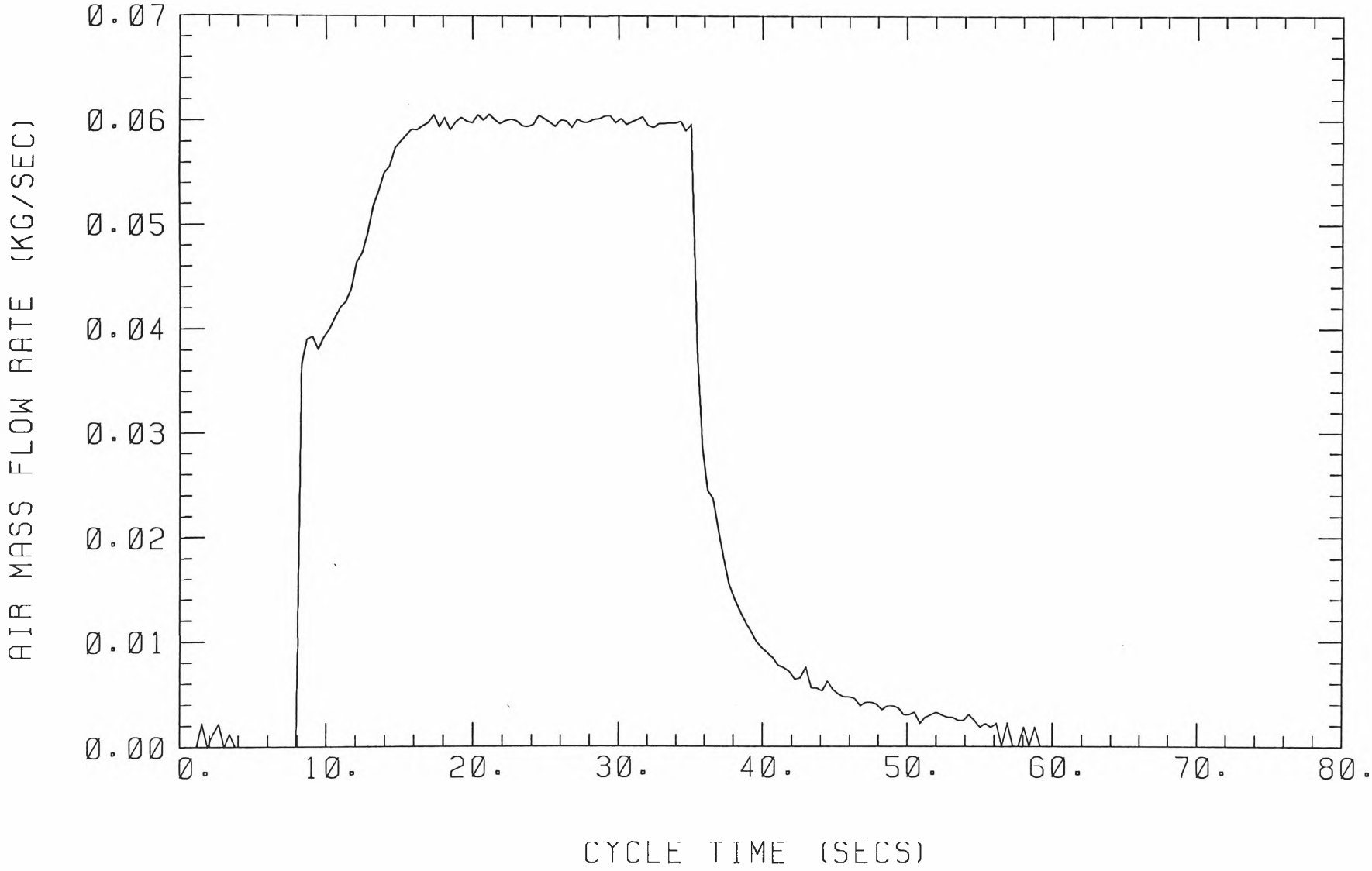

ANNUBAR NO. 3

EXPERIMENT NO. 5 TEST DATE: 22\9\95

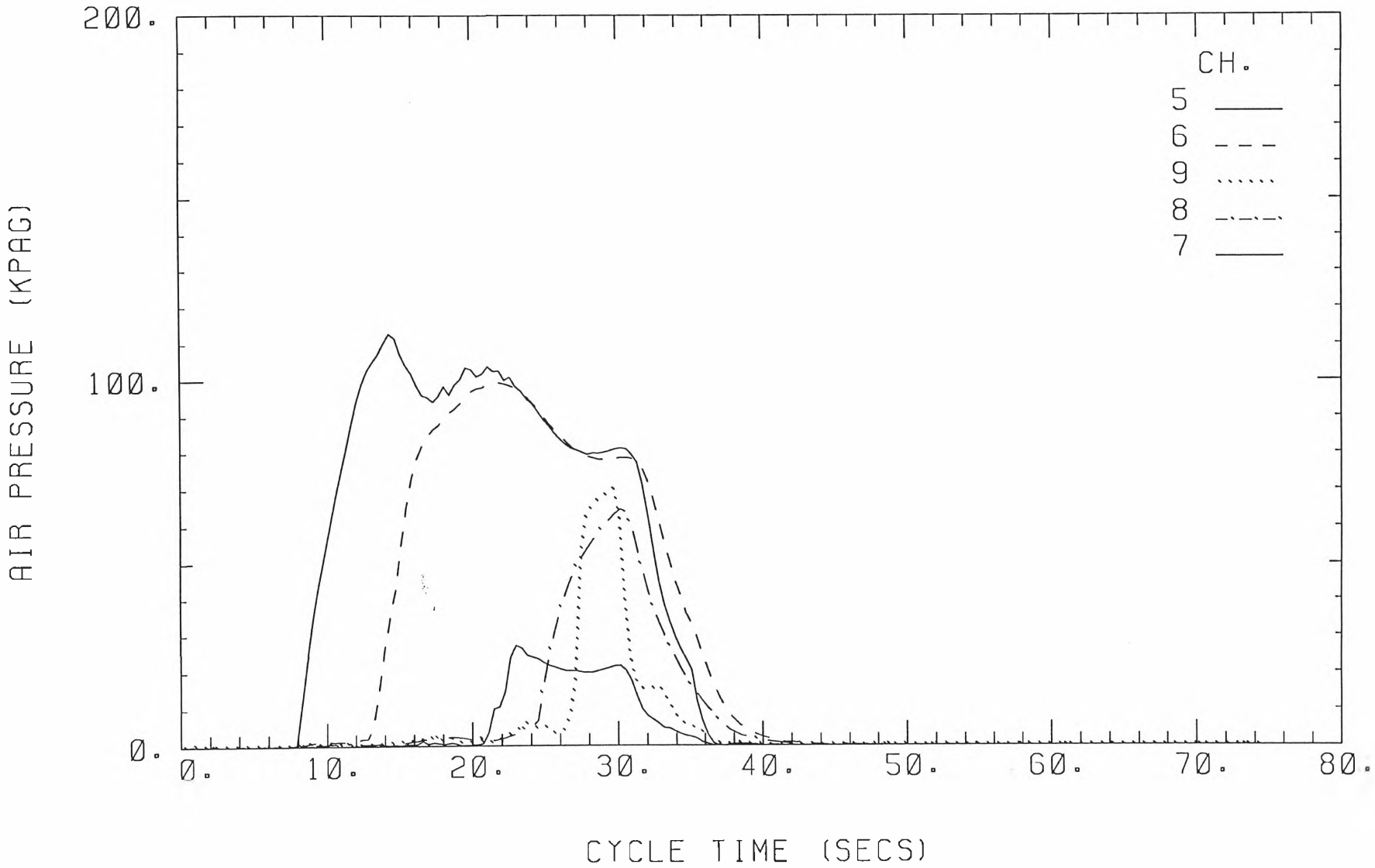

EXPERIMENT NO. 6 TEST DATE: 22\9\95

TOTAL MASS OF AIR USED (KGS) = 1.297

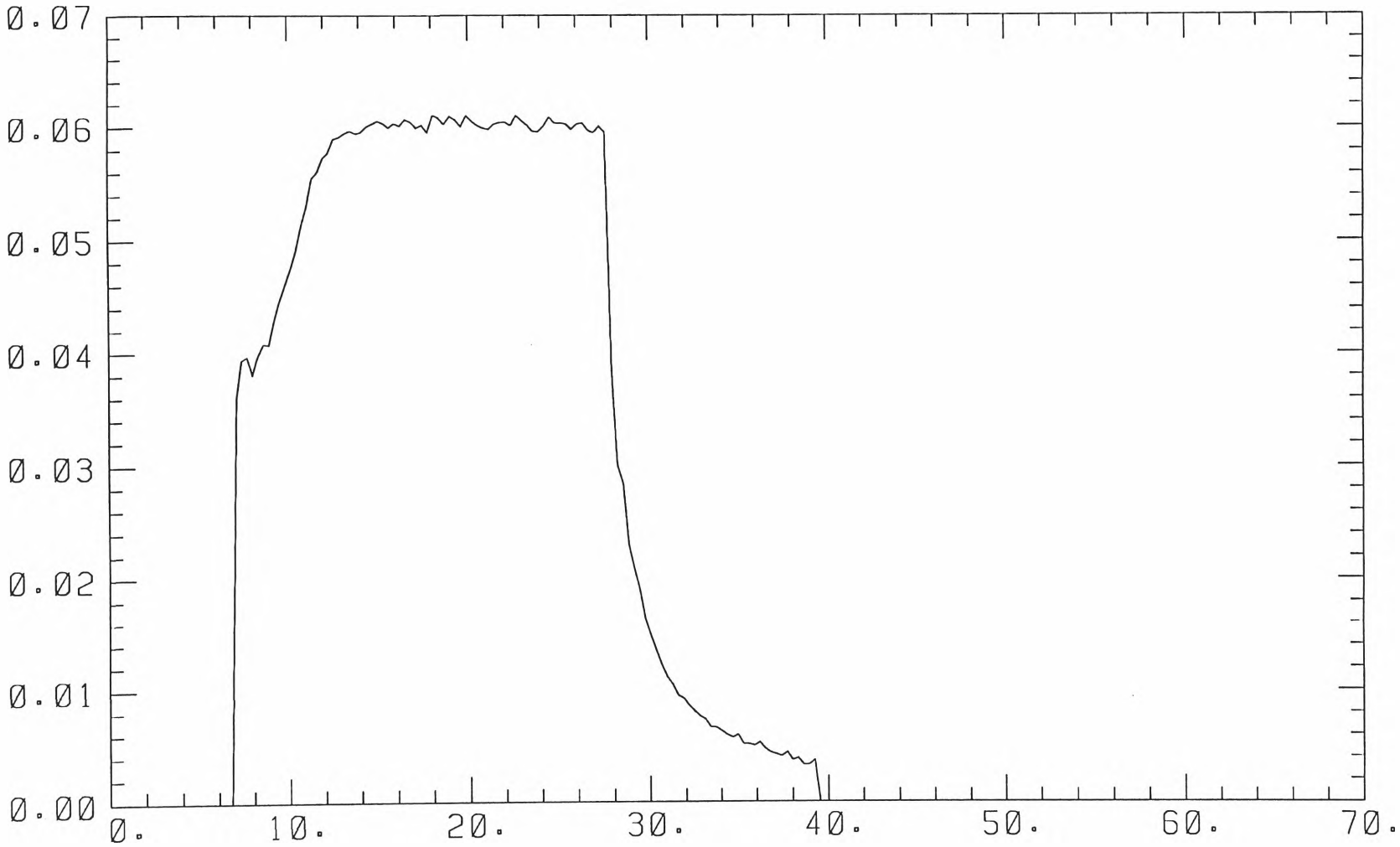

ANNUBAR NO. 3

EXPERIMENT NO. 6 TEST DATE: 22\9\95

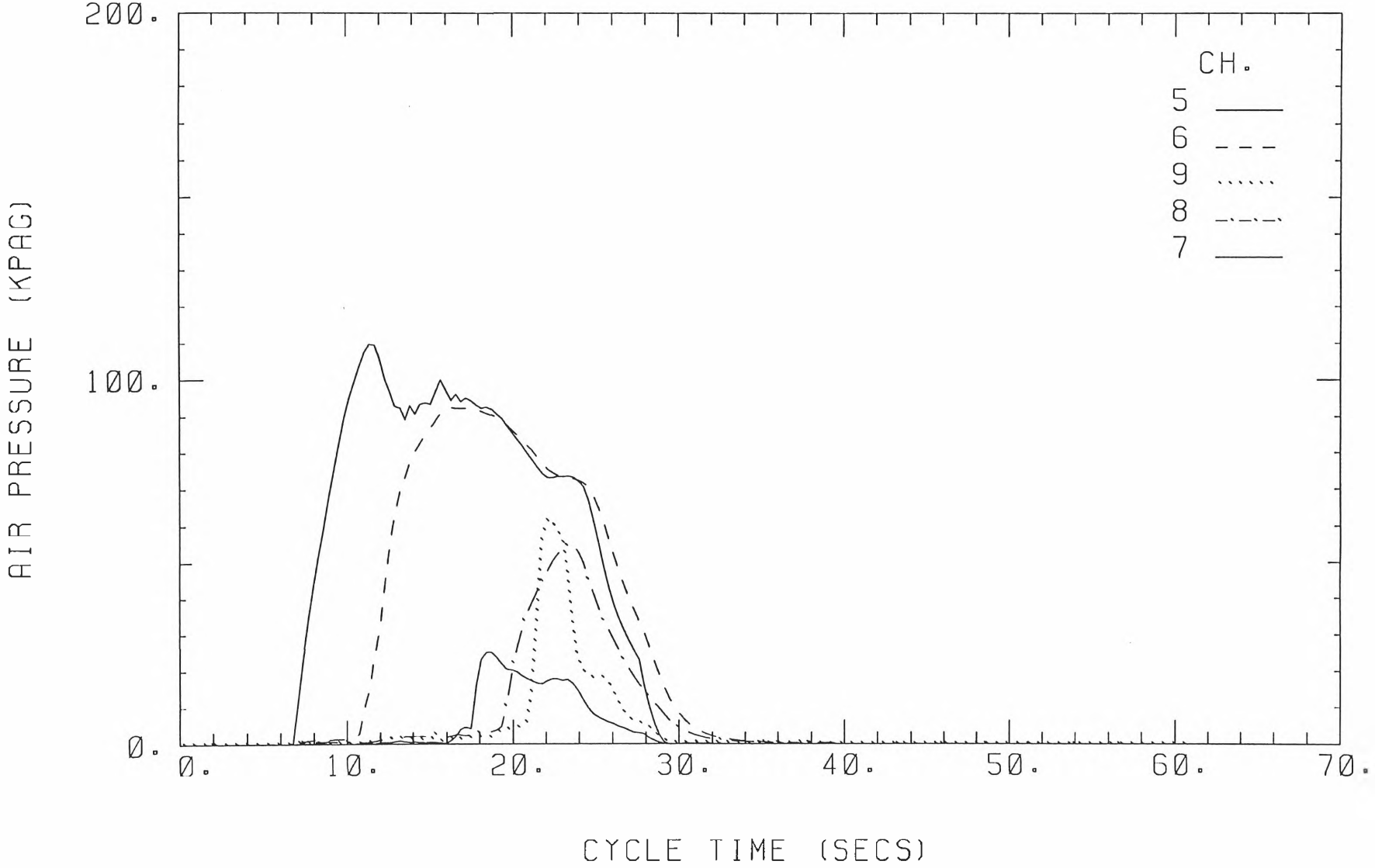

Appendix D Experimental Plots for Table 4.3

The measured data in Table 4.3 are based on the following experimental plots.

Pressure meter A is connected to channel 5, pressure meter B to channel 6, pressure meter C to channel 7, pressure meter D to channel 8 and pressure meter E to channel 9.

Table D.1 Experimental values for t_{pm} and Δp

Exp. No.	$\Delta p(kPa)$	$t_{pm}(s)$
1	110	6
2	125	6
3	120	6
4	122	6
5	115	5
6	100	5
7	115	6
8	113	6

EXPERIMENT NO. 1
TOTAL MASS OF AIR USED

TEST DATE: 22\9\95

(KGS) = 1.341

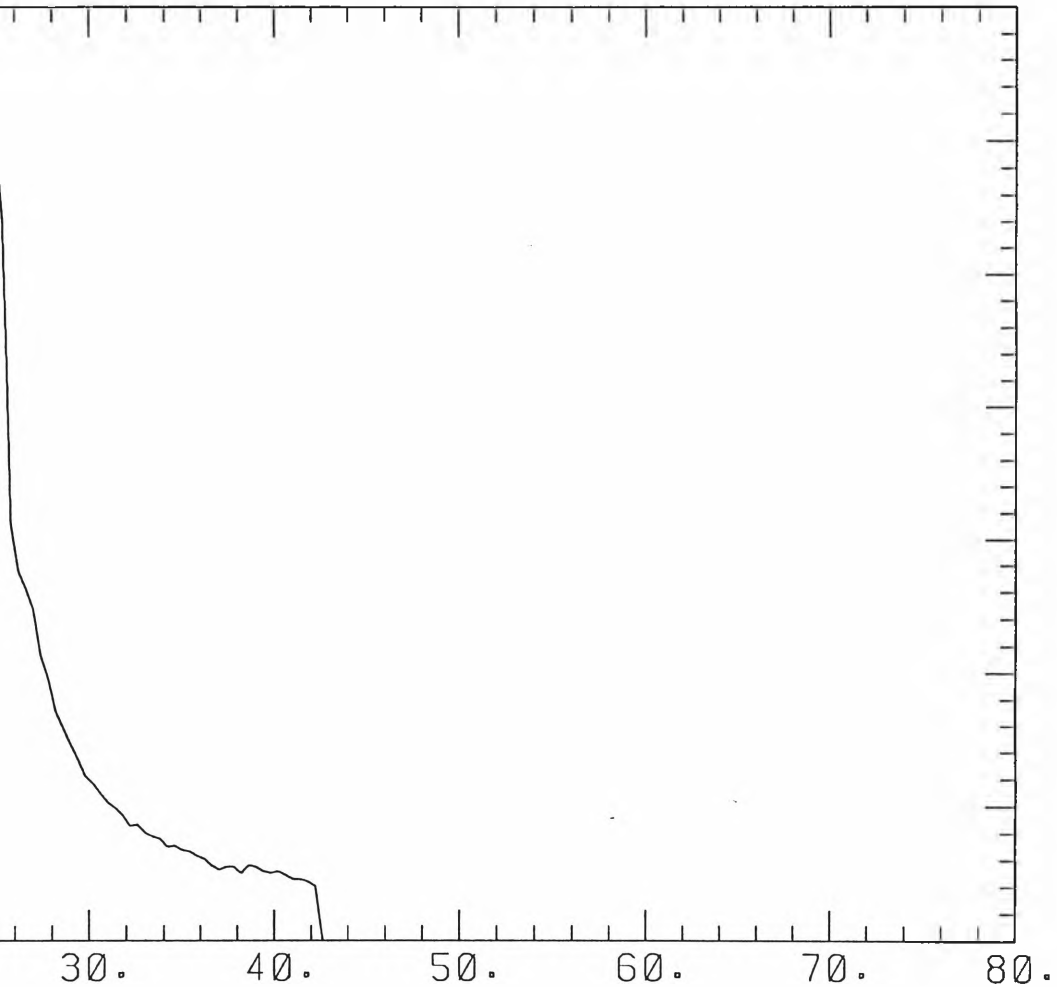

CYCLE TIME (SECS)

ANNUBAR NO. 3

EXPERIMENT NO. 1 TEST DATE: 22\9\95

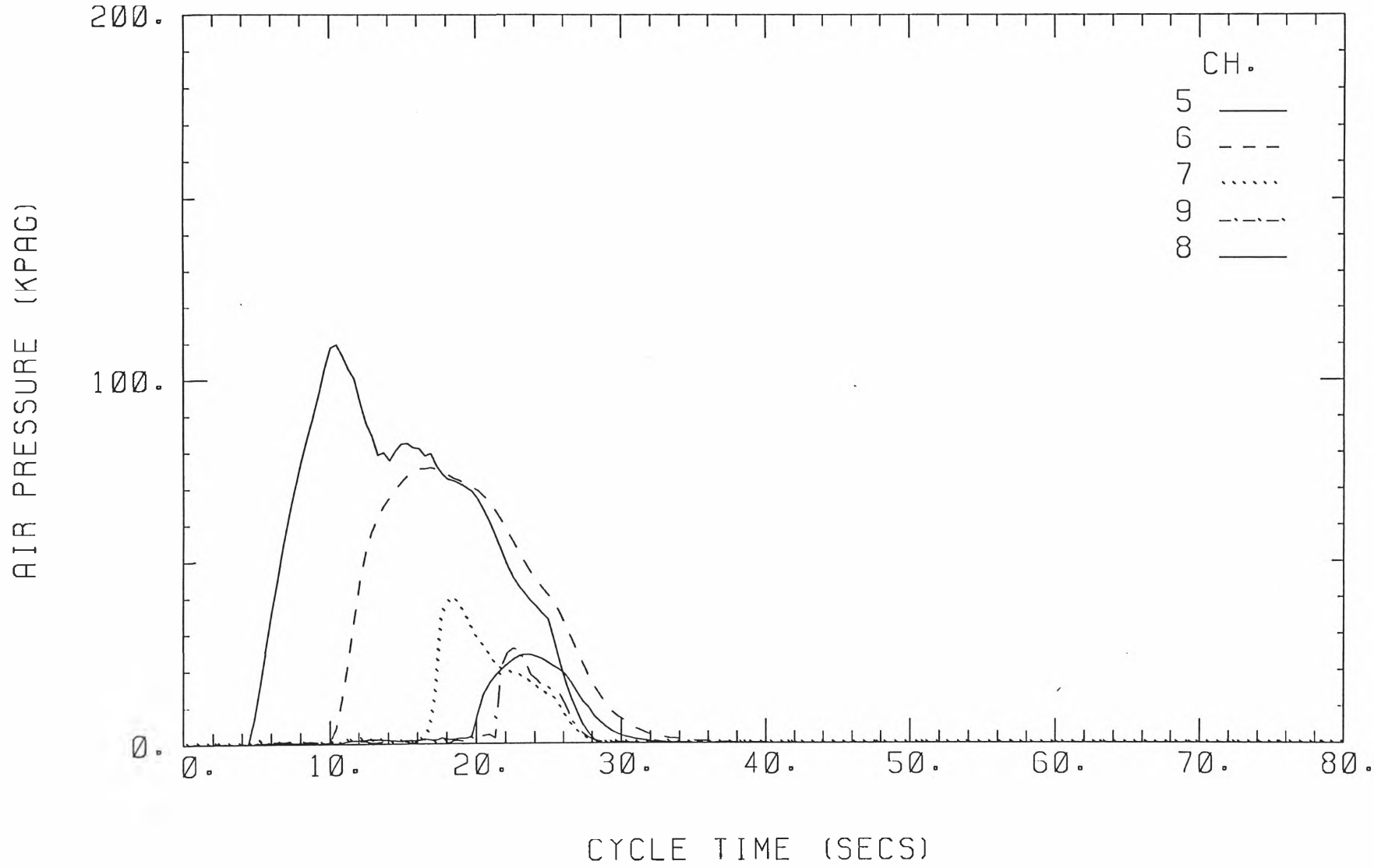

EXPERIMENT NO. 2
TOTAL MASS OF AIR USED

TEST DATE: 22\9\95

(KGS) = 1.461

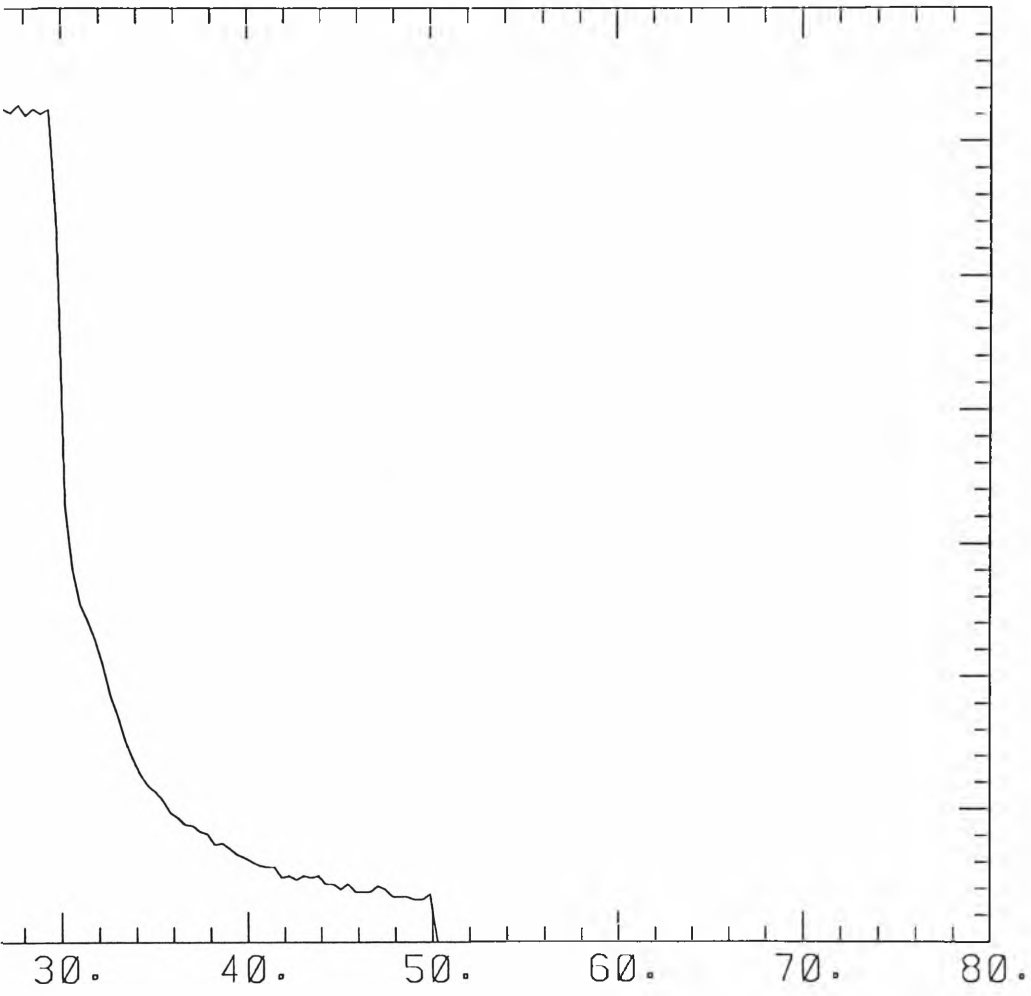

CYCLE TIME (SECS)

ANNUBAR NO. 3

EXPERIMENT NO. 2 TEST DATE: 22\9\95

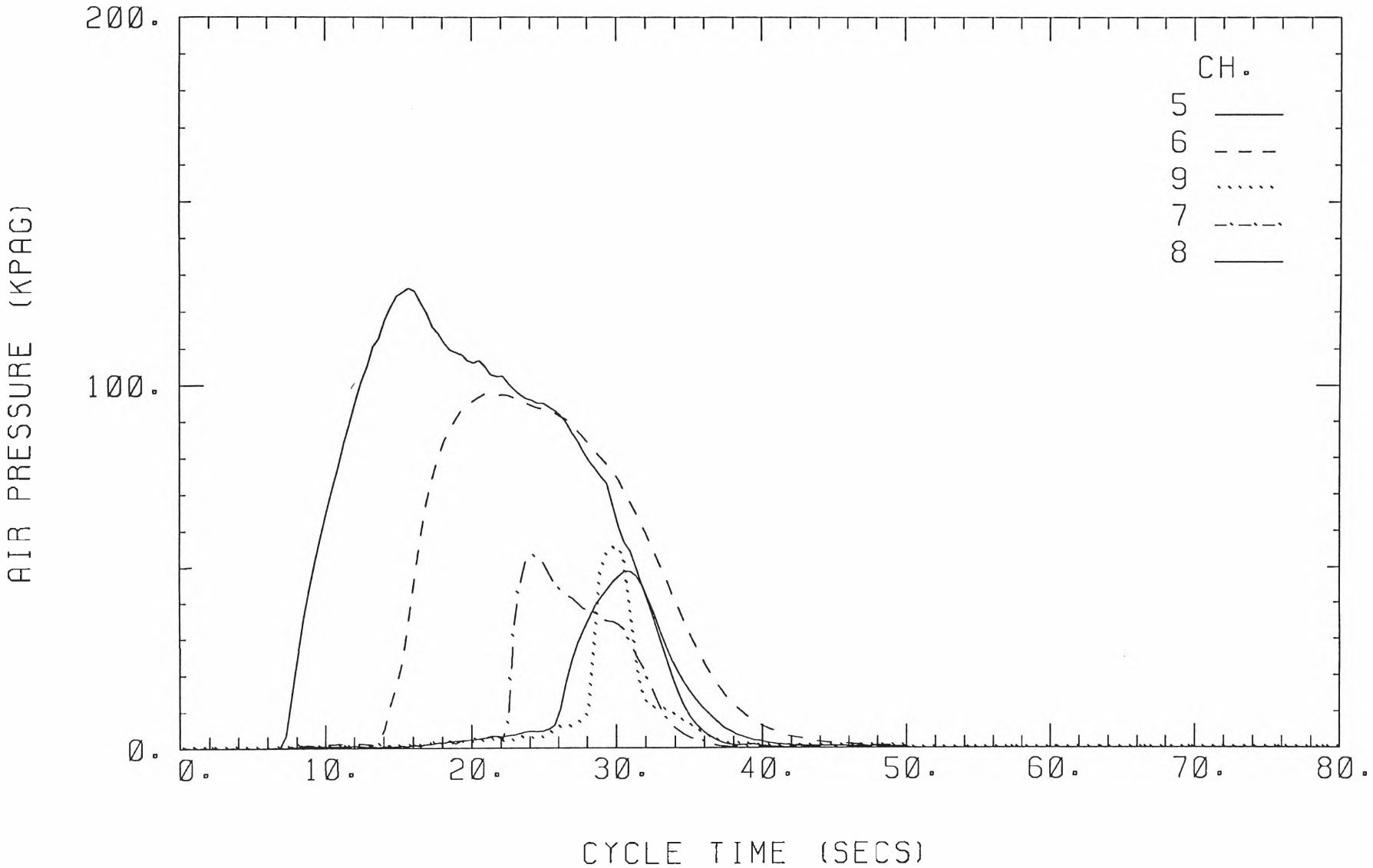

EXPERIMENT NO. 3 TEST DATE: 22\9\95
TOTAL MASS OF AIR USED (KGS) = 2.446

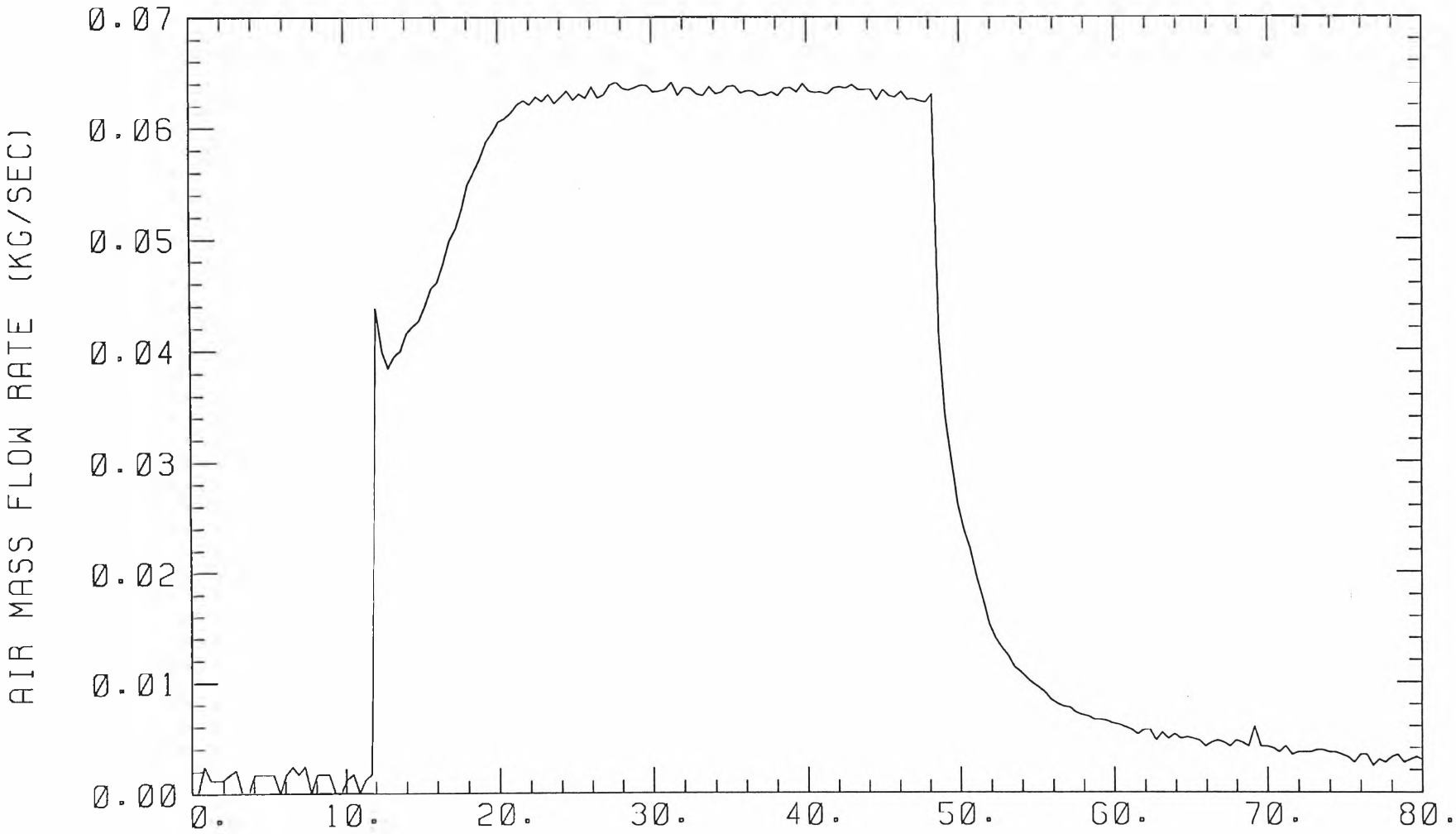

ANNUBAR NO. 3

EXPERIMENT NO. 3

TEST DATE: 22\9\95

EXPERIMENT NO. 4 TEST DATE: 22\9\95

TOTAL MASS OF AIR USED (KGS) = 2.180

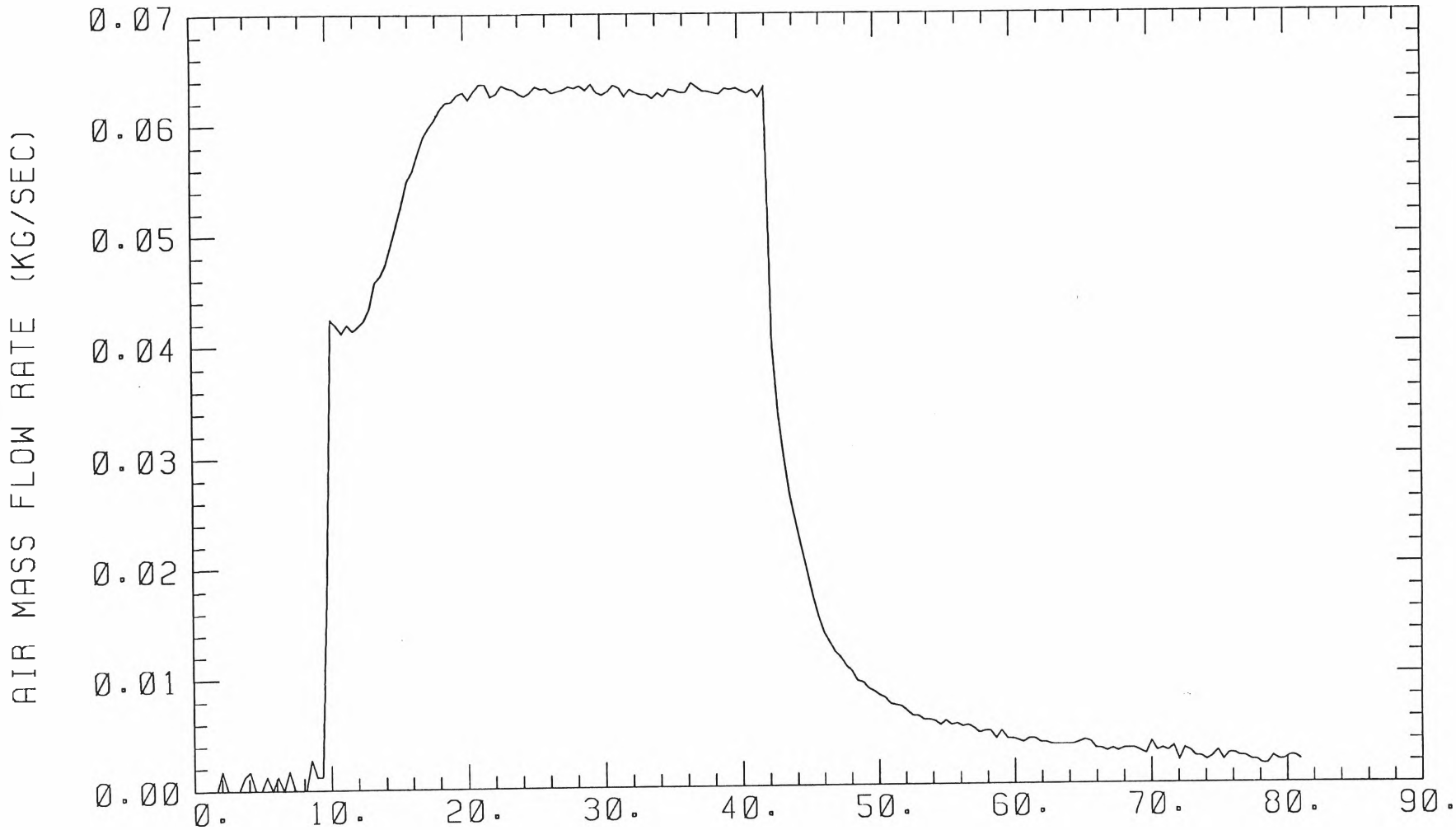

ANNUBAR NO. 3

EXPERIMENT NO. 4 TEST DATE: 22\9\95

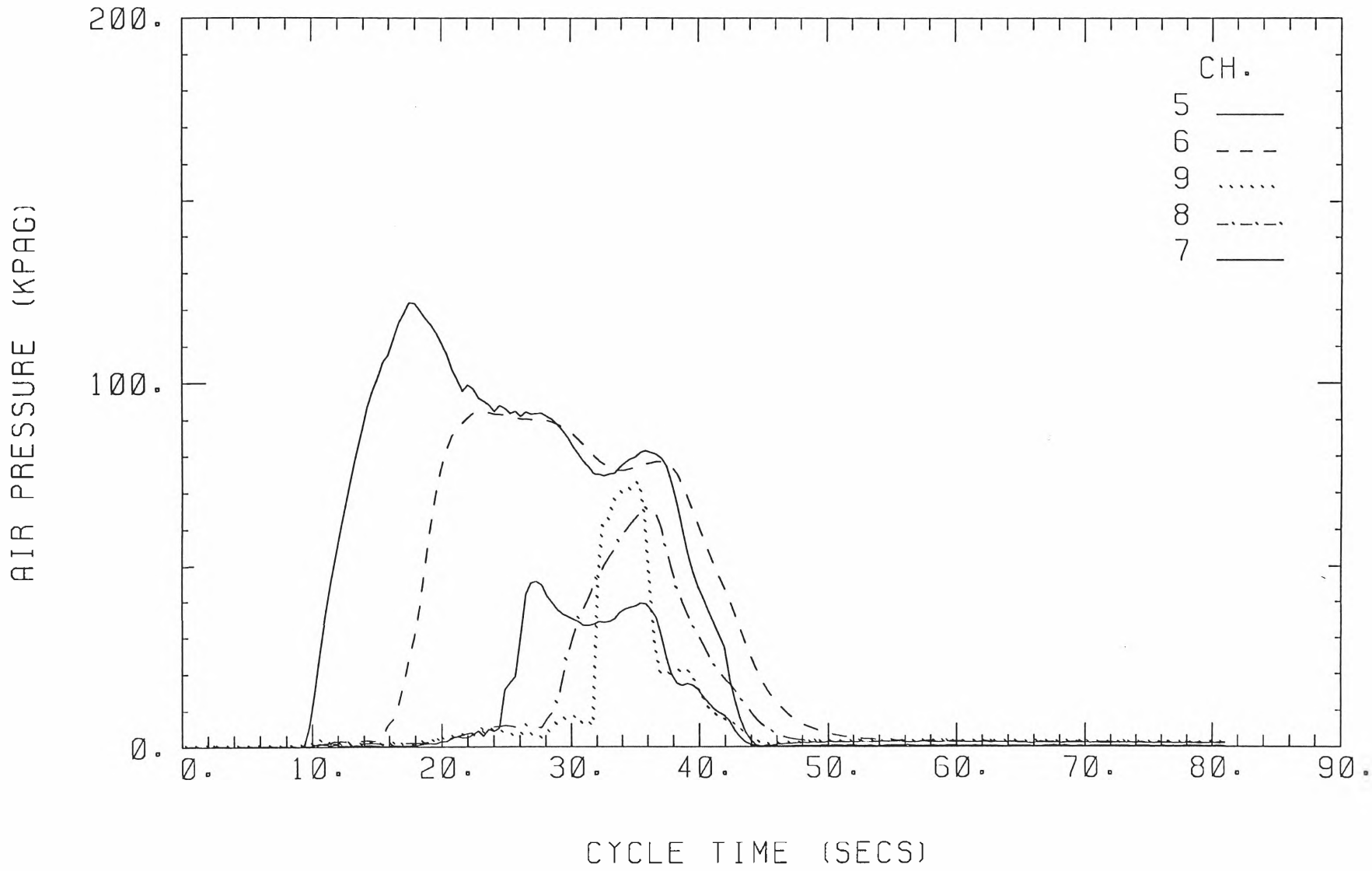

EXPERIMENT NO. 5 TEST DATE: 22\9\95
TOTAL MASS OF AIR USED (KGS) = 1.523

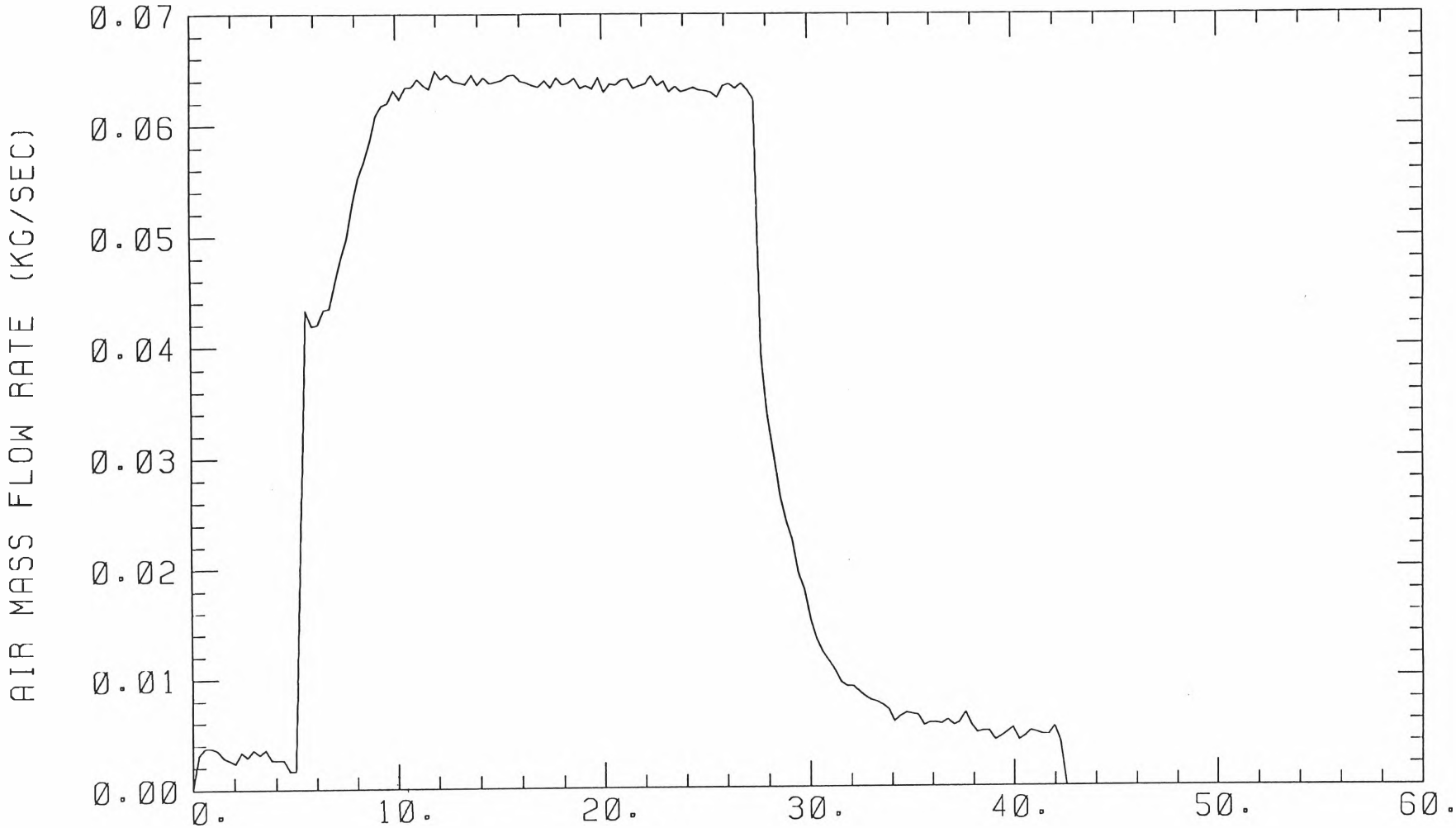

ANNUBAR NO. 3

EXPERIMENT NO. 5 TEST DATE: 22\9\95

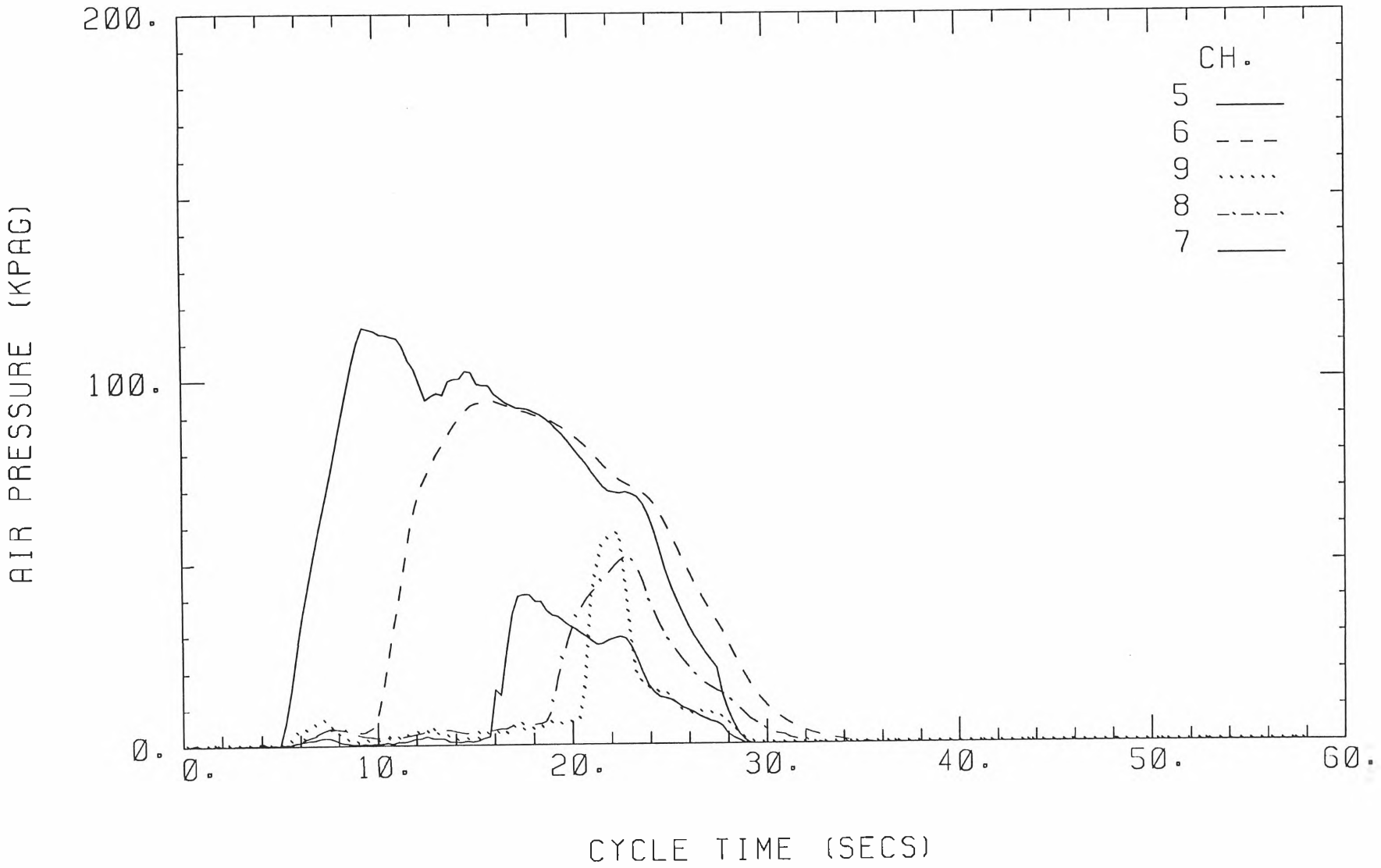

EXPERIMENT NO. 6 TEST DATE: 22\9\95
TOTAL MASS OF AIR USED (KGS) = 1.880

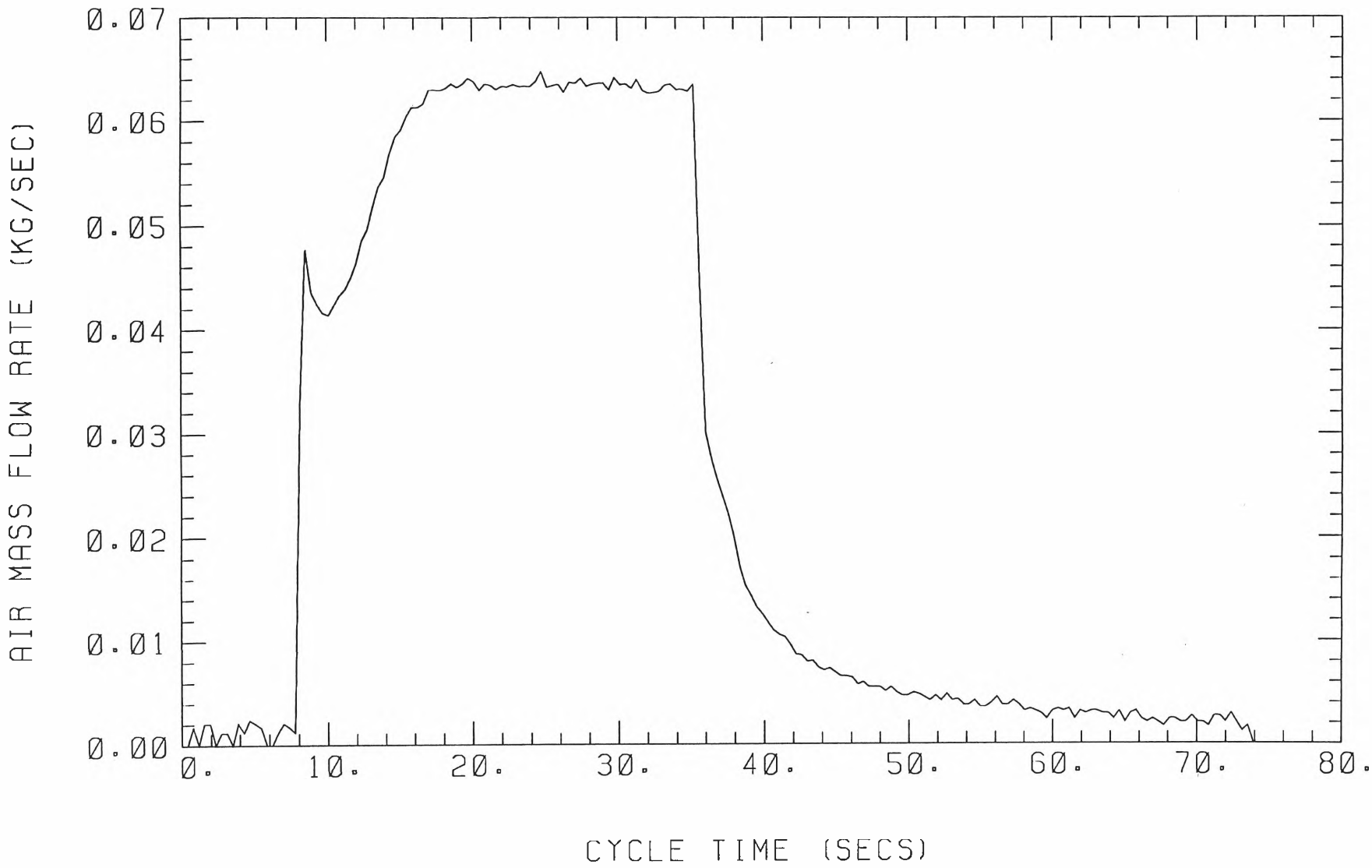

ANNUBAR NO. 3

EXPERIMENT NO. 6

TEST DATE: 22\9\95

EXPERIMENT NO. 7
TOTAL MASS OF AIR USED
AIR MASS FLOW RATE (KG/SEC)
0.07
0.06
0.05
0.04
0.03
0.02
0.01
0.00
0.
10.
20.

TEST DATE: 22\9\95

(KGS) = 2.060

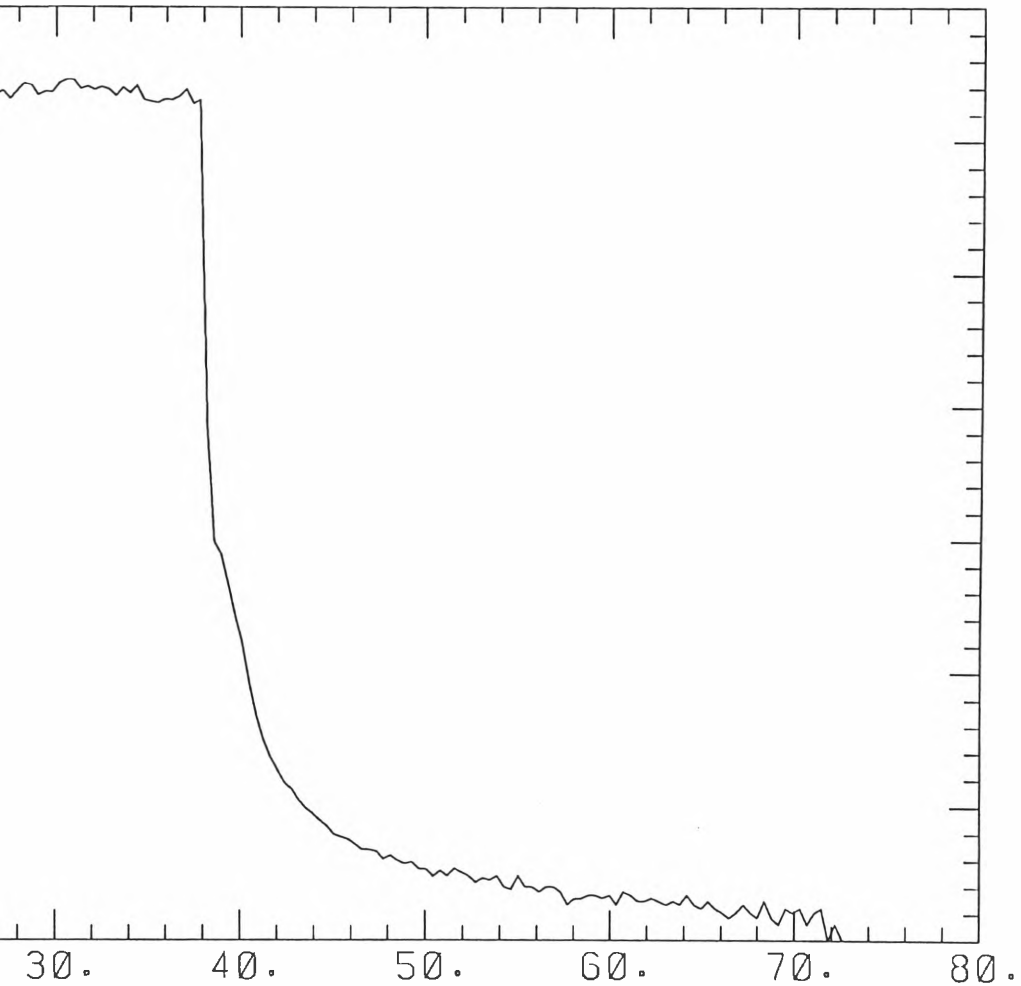

CYCLE TIME (SECS)

ANNUBAR NO. 3

EXPERIMENT NO. 7

TEST DATE: 22\9\95

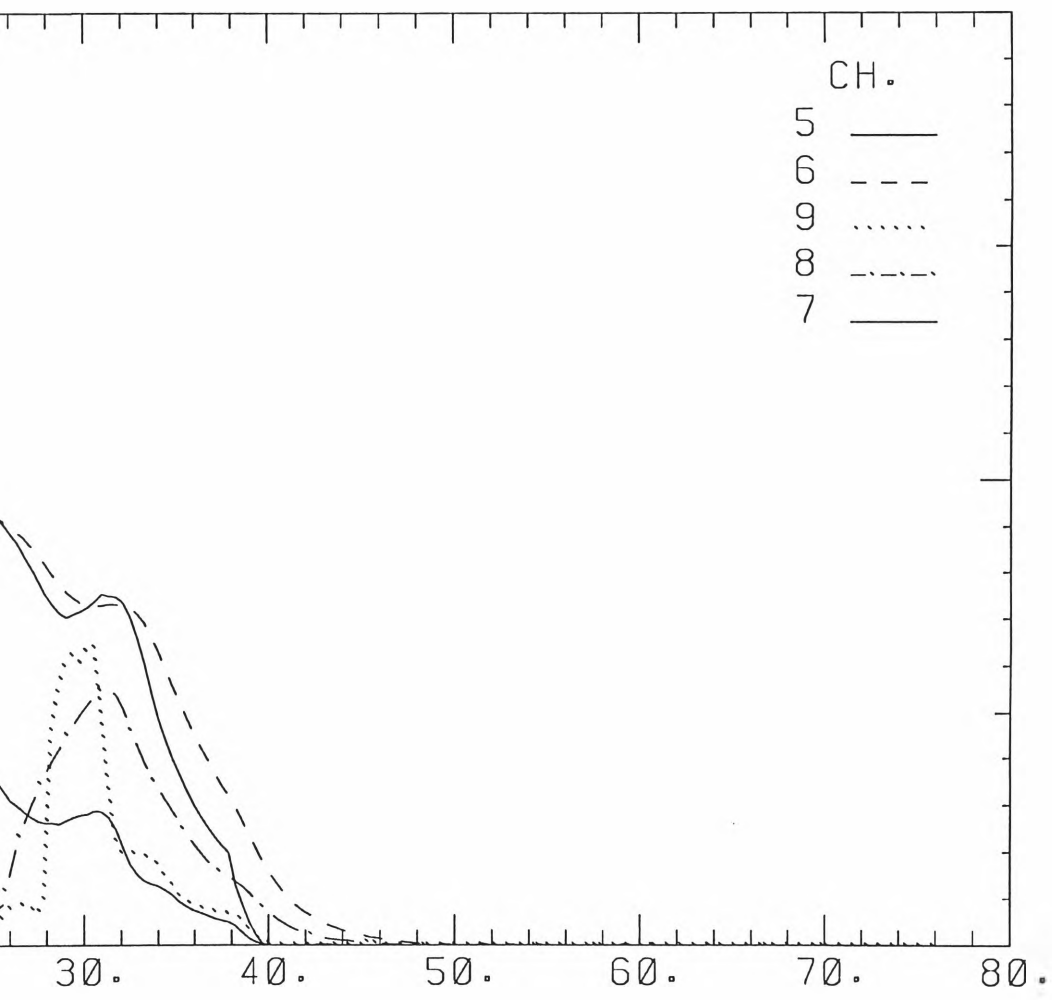

CYCLE TIME (SECS)

EXPERIMENT NO. 8
TOTAL MASS OF AIR USED

TEST DATE: 22\9\95

(KGS) = 1.810

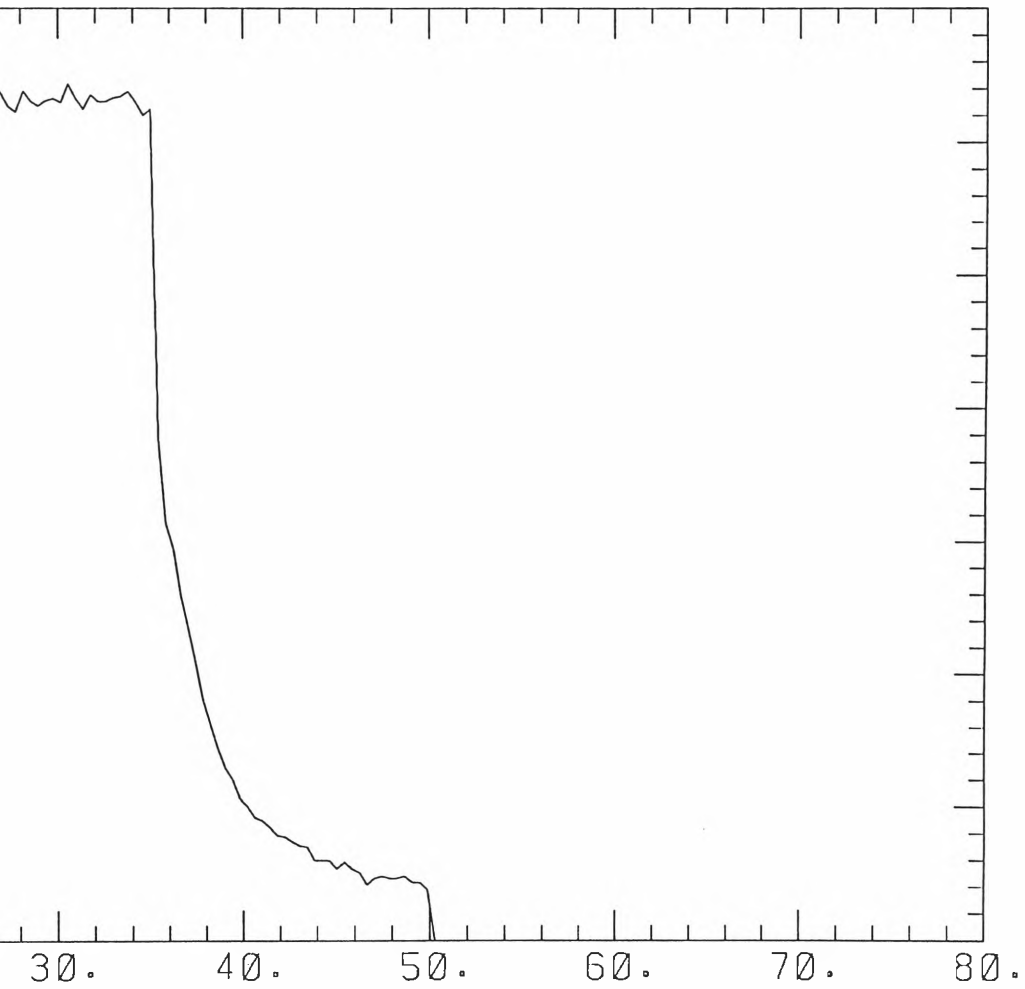

CYCLE TIME (SECS)

ANNUBAR NO. 3

EXPERIMENT NO. 8 TEST DATE: 22\9\95

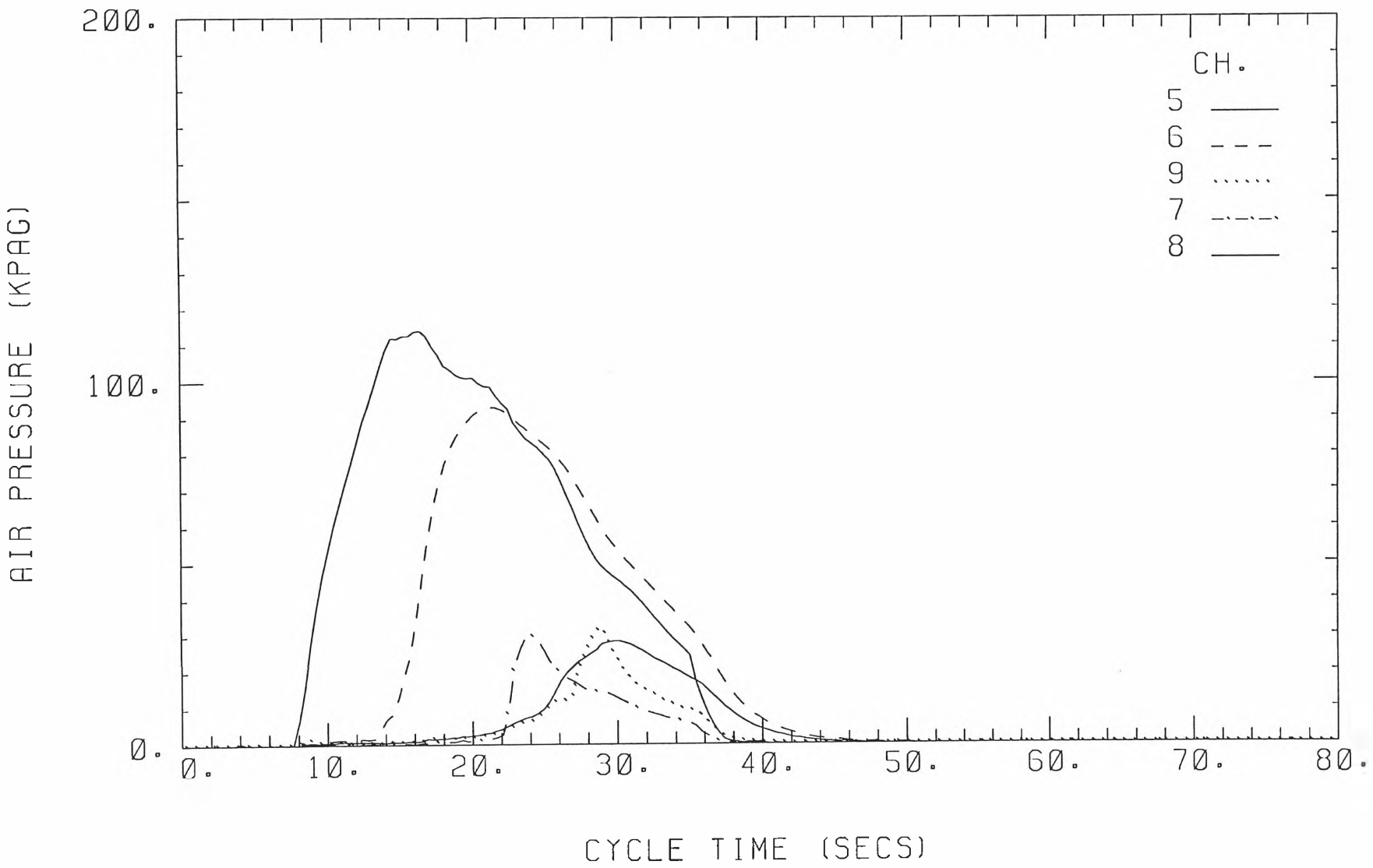

Appendix E Experimental Plots for Table 4.4

The measured data in Table 4.4 are based on the following experimental plots.

Pressure meter A is connected to channel 5, pressure meter B to channel 6, pressure meter C to channel 7, pressure meter D to channel 8 and pressure meter E to channel 9.

Table E.1 Experimental values for t_{pm} and Δp

Exp. No.	$\Delta p(kPa)$	$t_{pm}(s)$
1	160	6.5
2	155	6
3	172	6.5
4	160	7
5	162	6.5
6	155	6

EXPERIMENT NO. 1
TOTAL MASS OF AIR USED

TEST DATE: 24\10\95

(KGS) = 2.227

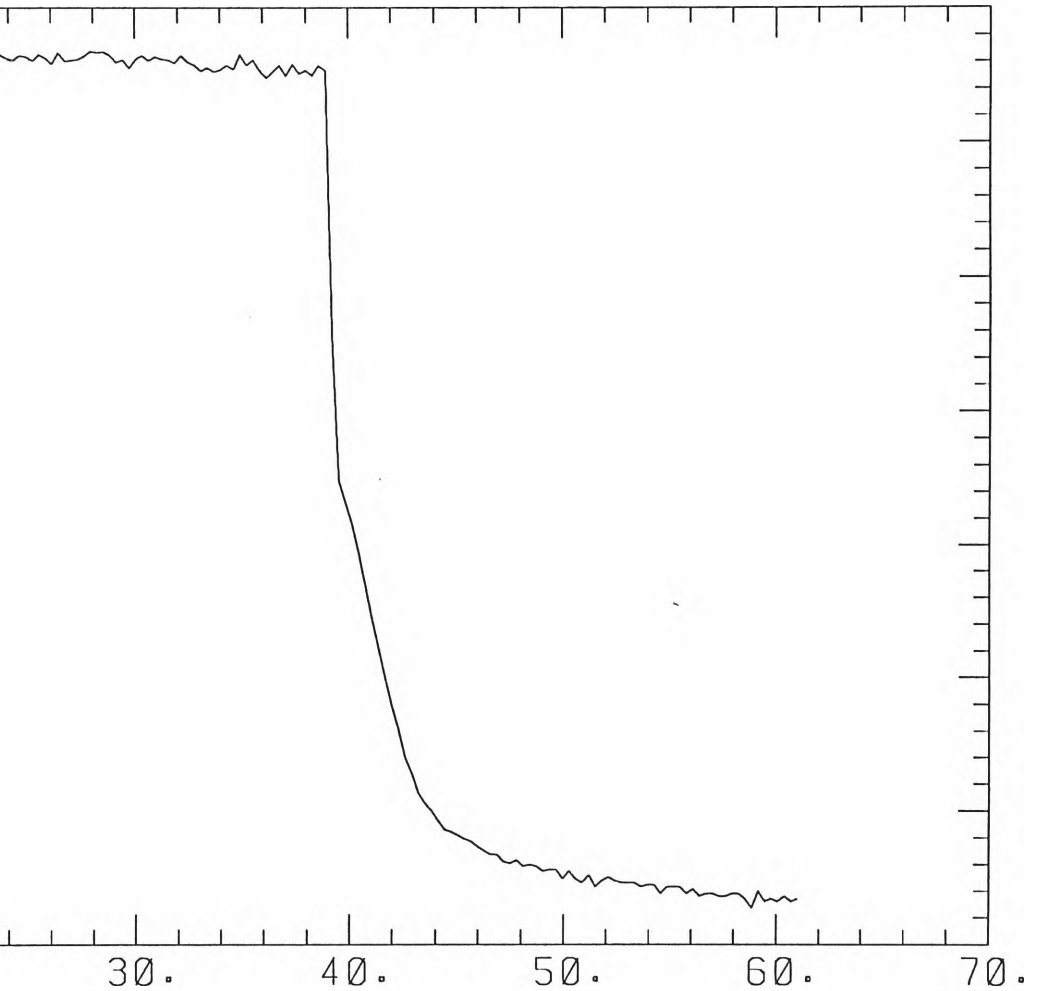

CYCLE TIME (SECS)

ANNUBAR NO. 3

EXPERIMENT NO. 1 TEST DATE: 24\10\95

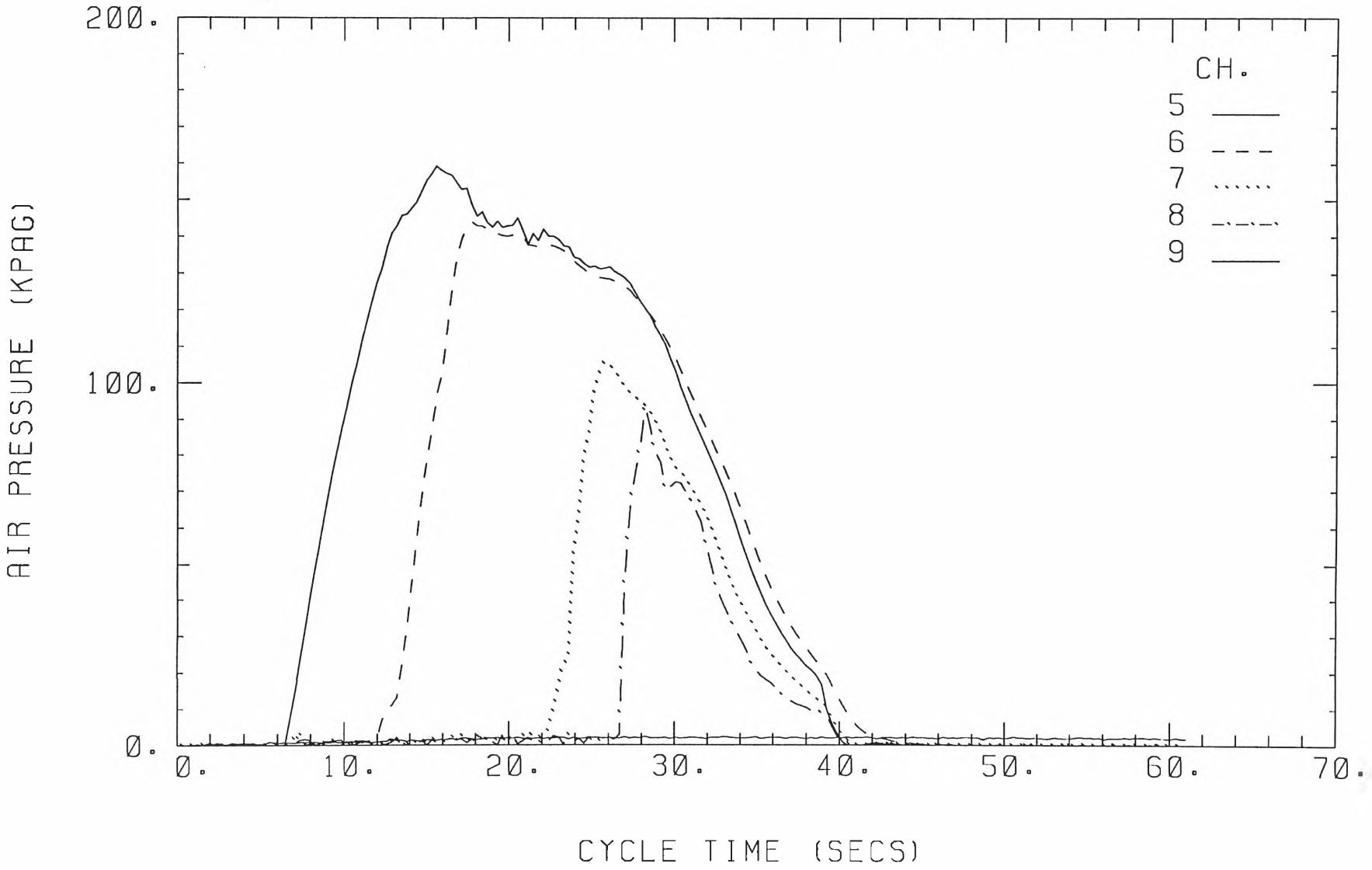

EXPERIMENT NO. 2
TOTAL MASS OF AIR USED

TEST DATE: 24\10\95

(KGS) = 2.071

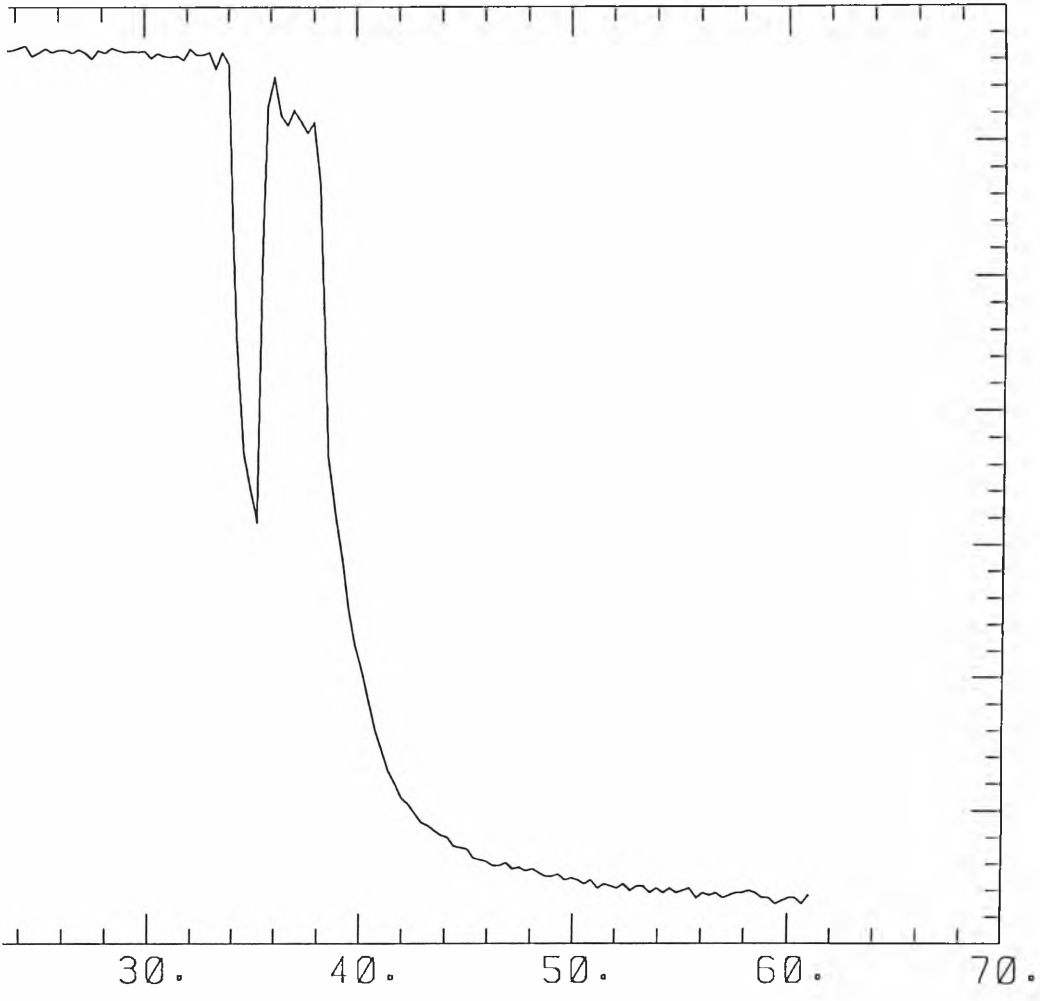

CYCLE TIME (SECS)

ANNUBAR NO. 3

EXPERIMENT NO. 2 TEST DATE: 24\10\95

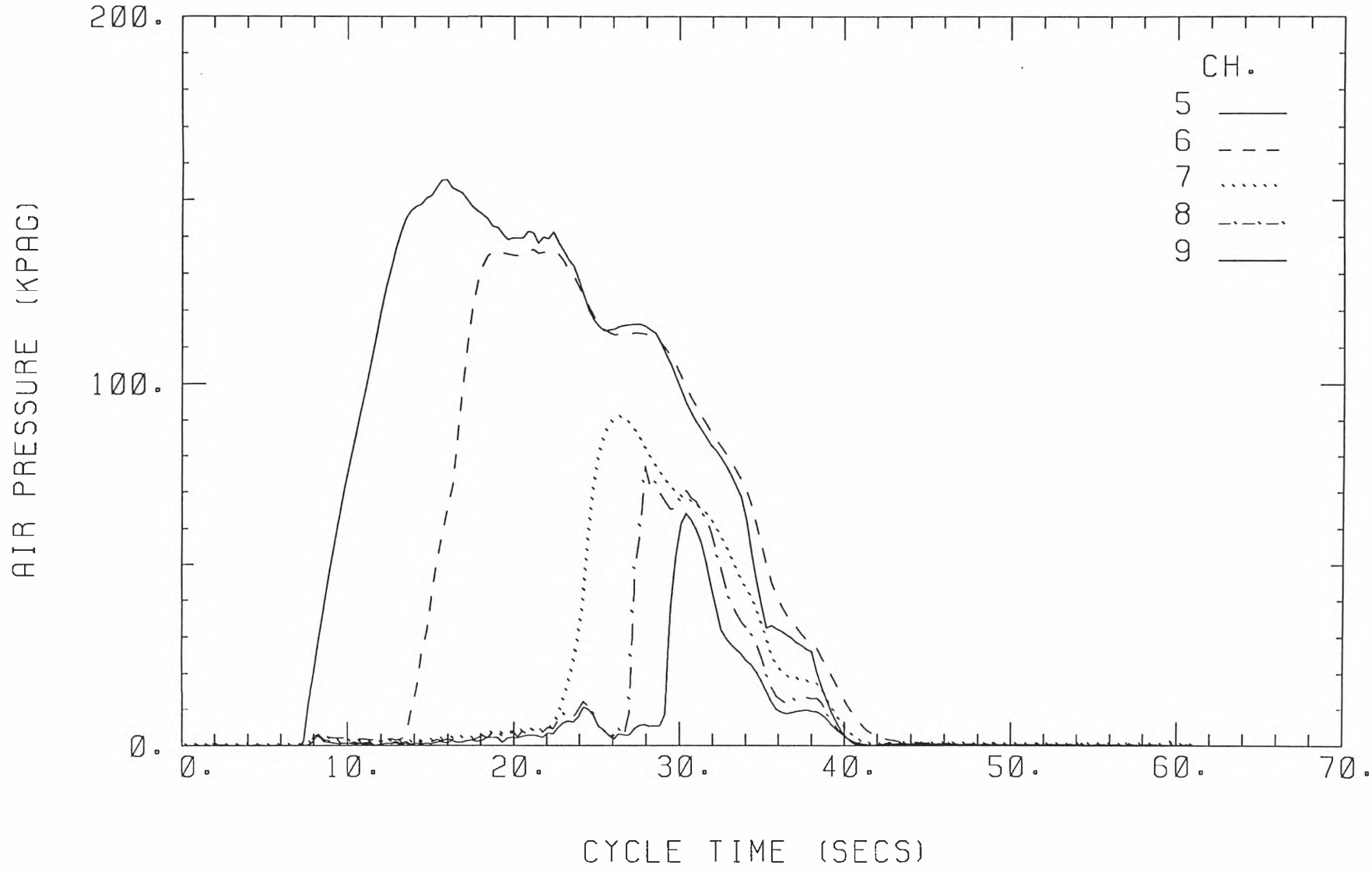

EXPERIMENT NO. 3 TEST DATE: 24\10\95

TOTAL MASS OF AIR USED (KGS) = 2.274

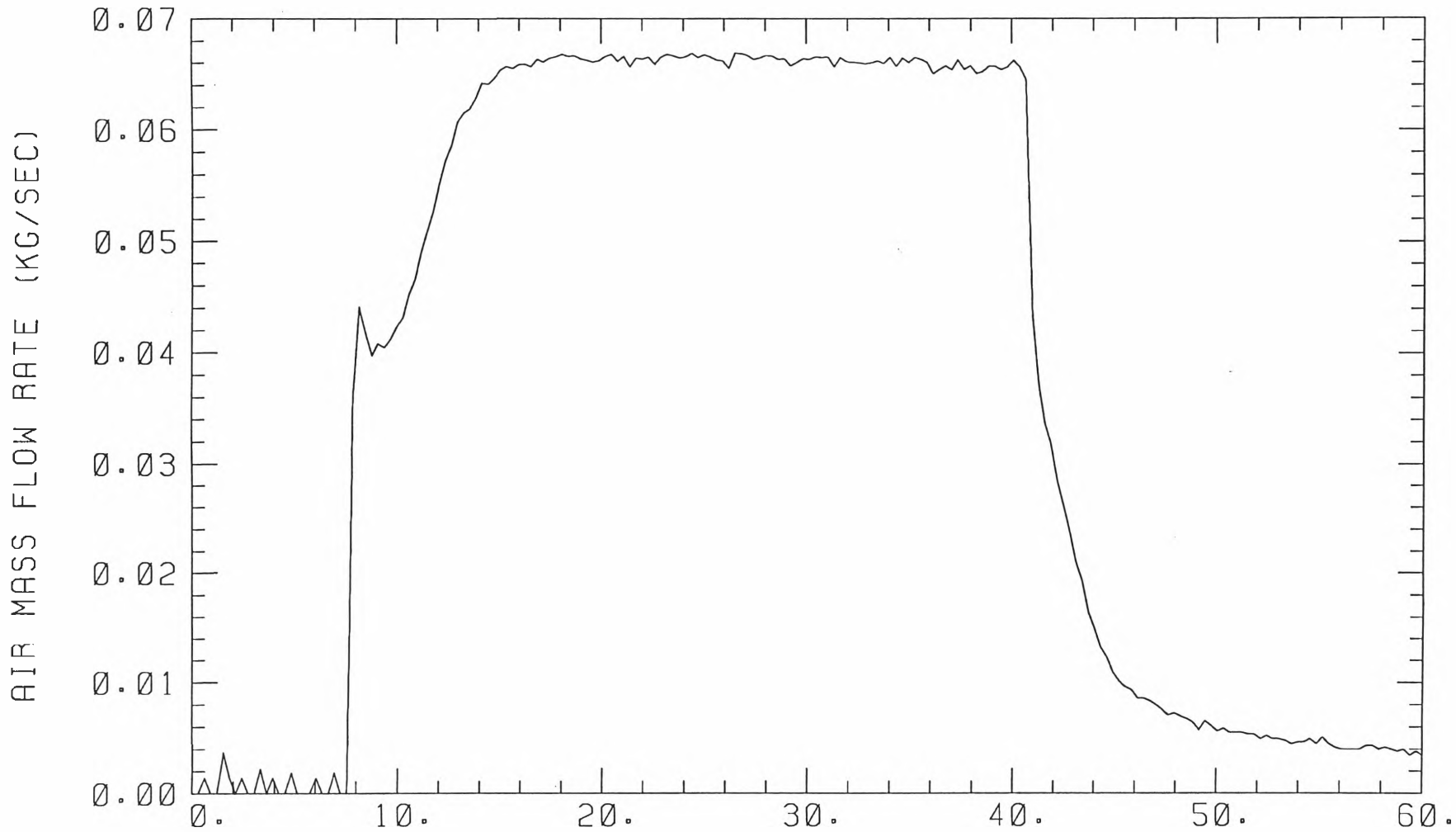

ANNUBAR NO. 3

EXPERIMENT NO. 3 TEST DATE: 24\10\95

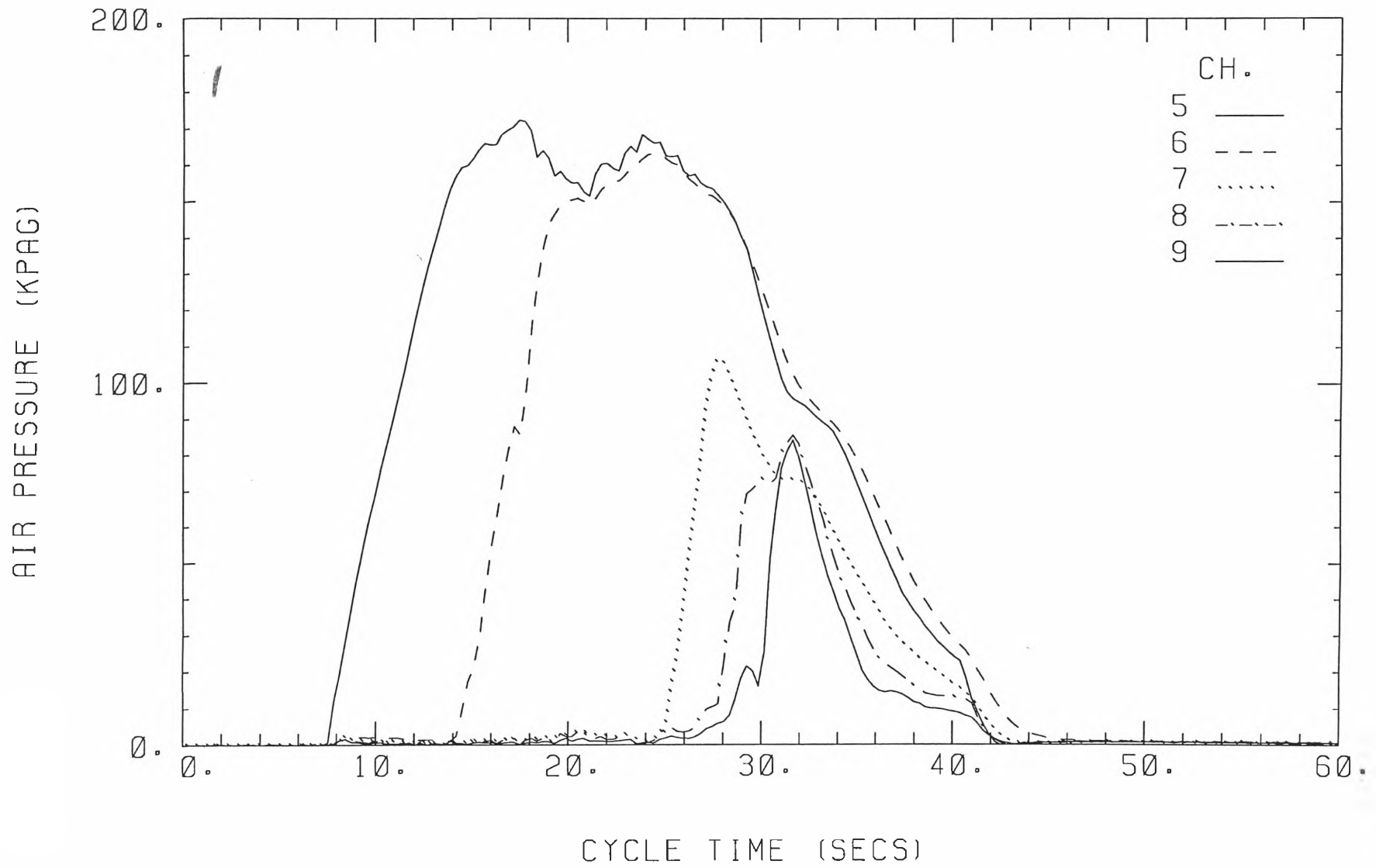

EXPERIMENT NO. 4
TOTAL MASS OF AIR USED

TEST DATE: 24\10\95

(KGS) = 2.207

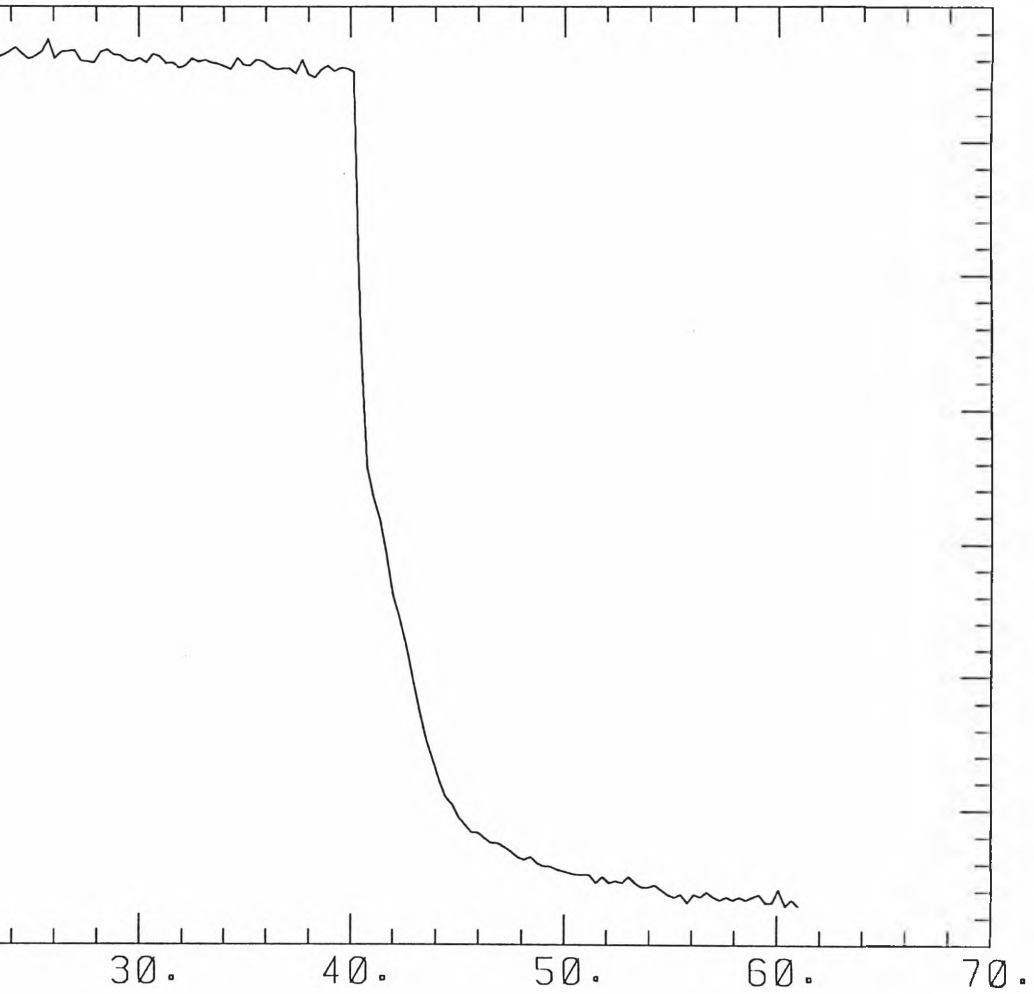

CYCLE TIME (SECS)

ANNUBAR NO. 3

EXPERIMENT NO. 4 TEST DATE: 24\10\95

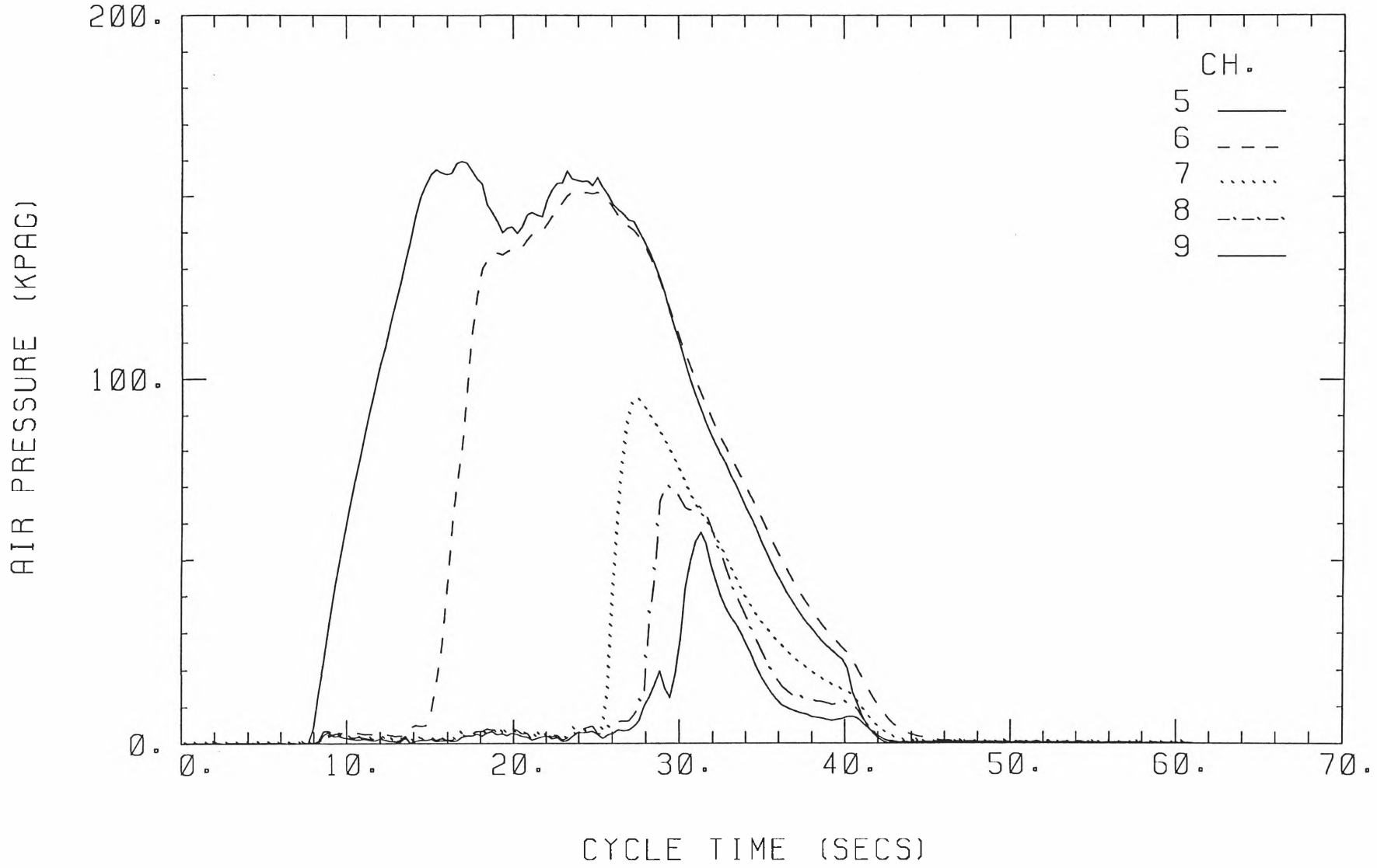

EXPERIMENT NO. 5 TEST DATE: 24\10\95
TOTAL MASS OF AIR USED (KGS) = 2.496

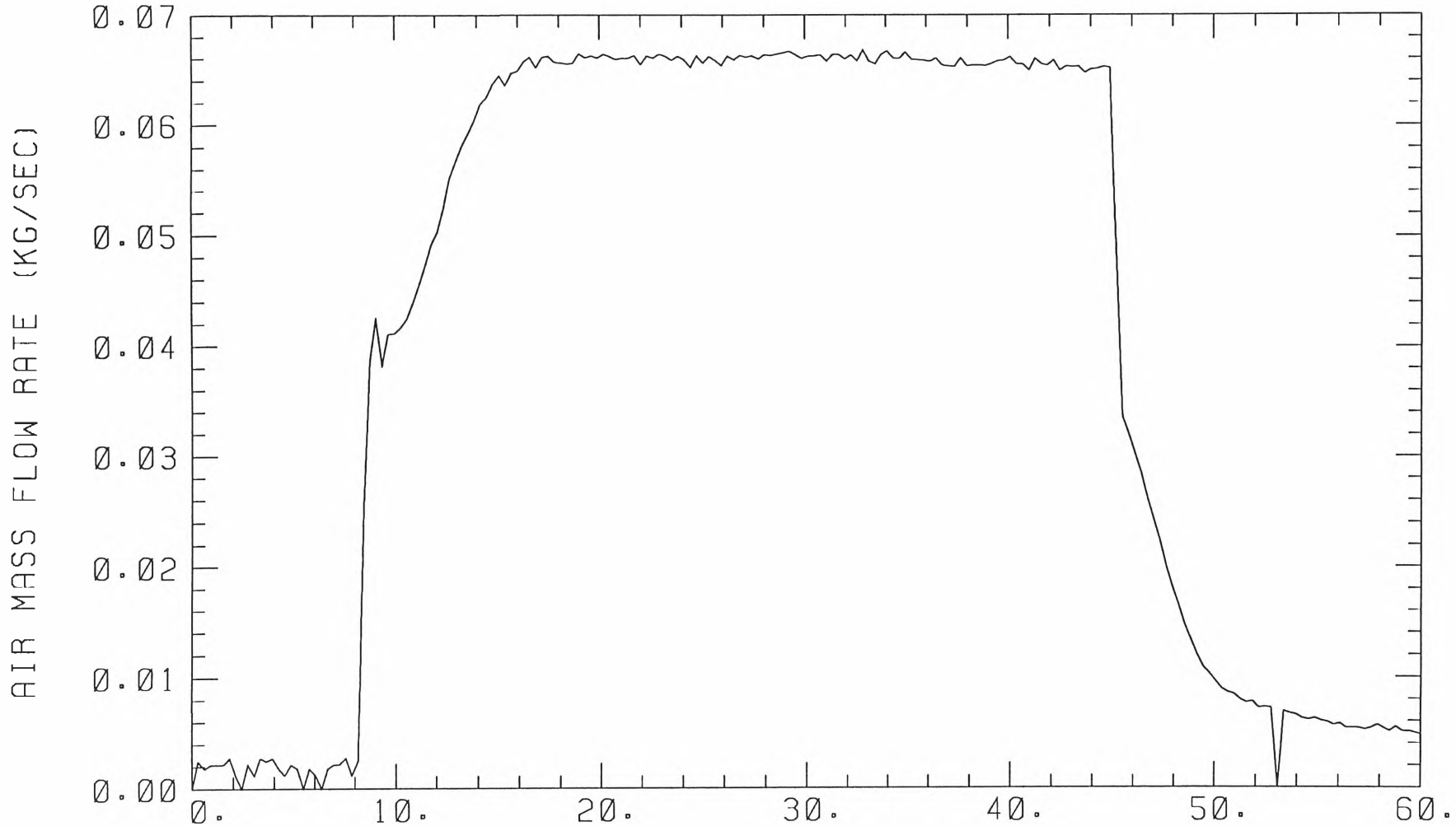

ANNUBAR NO. 3

EXPERIMENT NO. 5 TEST DATE: 24\10\95

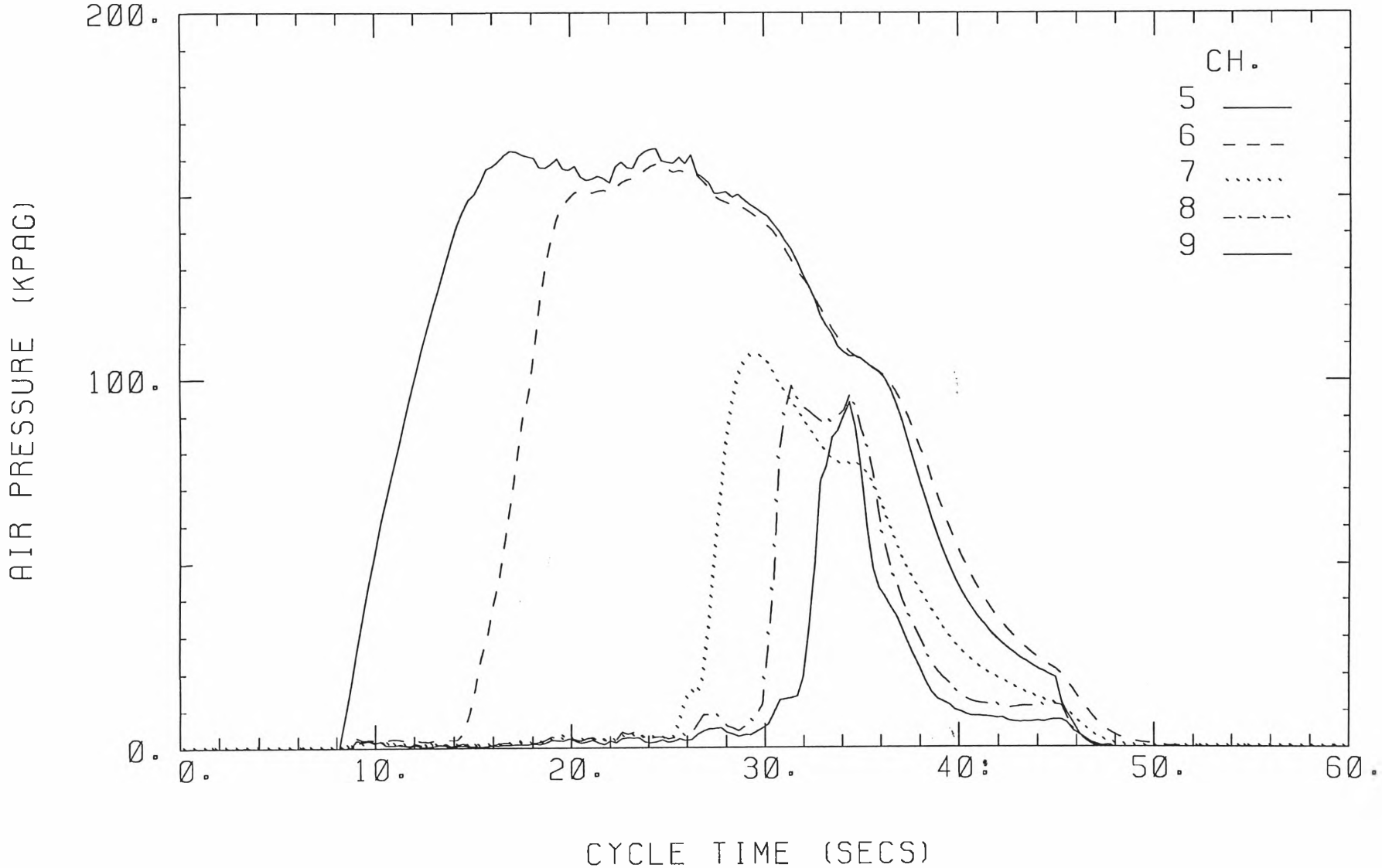

EXPERIMENT NO. 6 TEST DATE: 24\10\95
TOTAL MASS OF AIR USED (KGS) = 2.551

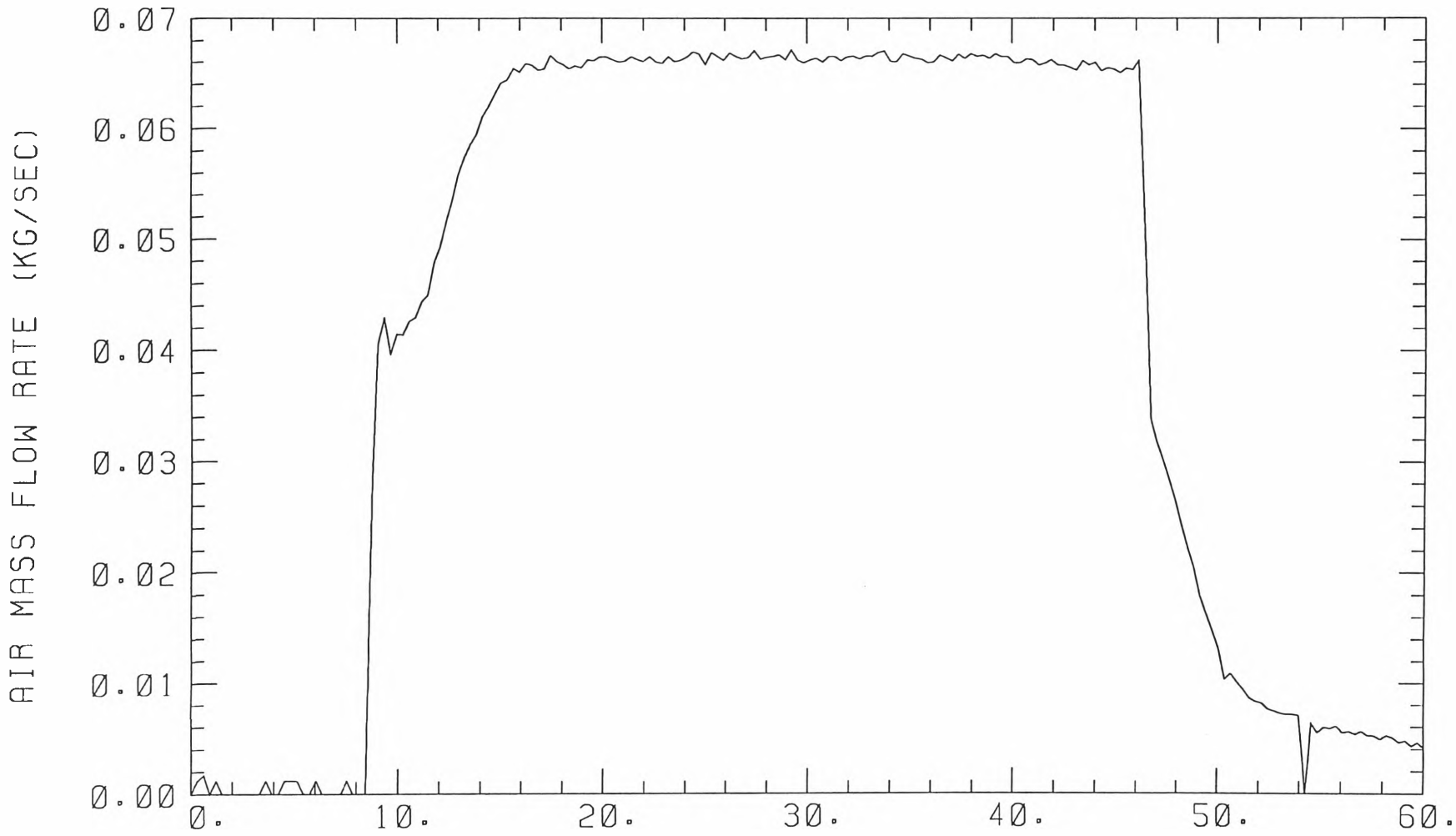

ANNUBAR NO. 3

EXPERIMENT NO. 6 TEST DATE: 24\10\95

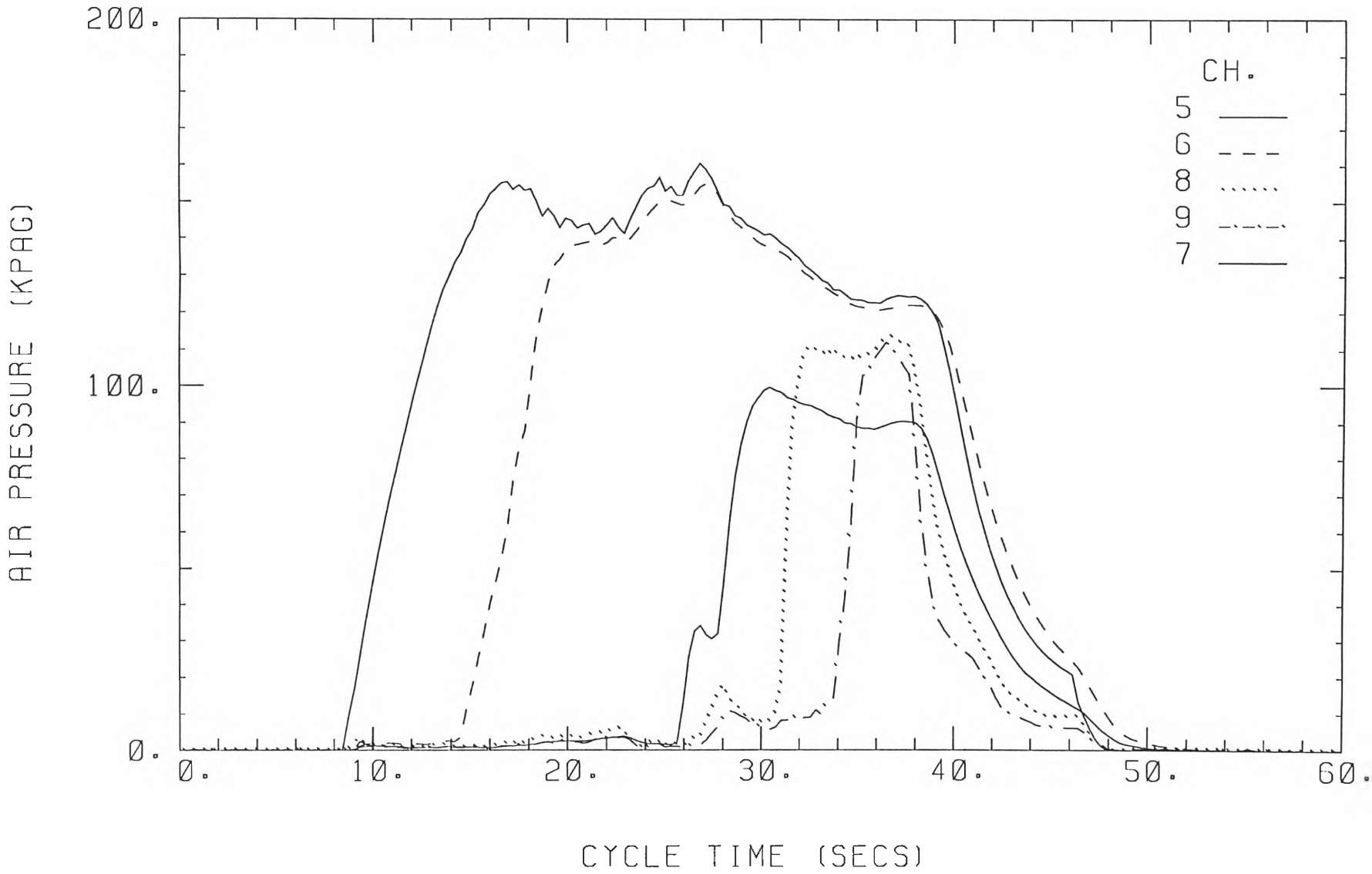

Appendix F Experimental Plots for Table 4.5

The measured data in Table 4.5 are based on the following experimental plots.

Pressure meter A is connected to channel 5, pressure meter B to channel 6, pressure meter C to channel 7, pressure meter D to channel 8 and pressure meter E to channel 9.

Table F.1 Experimental values for t_{pm} and Δp

Exp. No.	$\Delta p(kPa)$	$t_{pm}(s)$
1	108	7
2	110	6
3	120	7
4	120	7
5	110	7
6	110	7

EXPERIMENT NO. 1 TEST DATE: 26\10\95
TOTAL MASS OF AIR USED (KGS) = 1.067

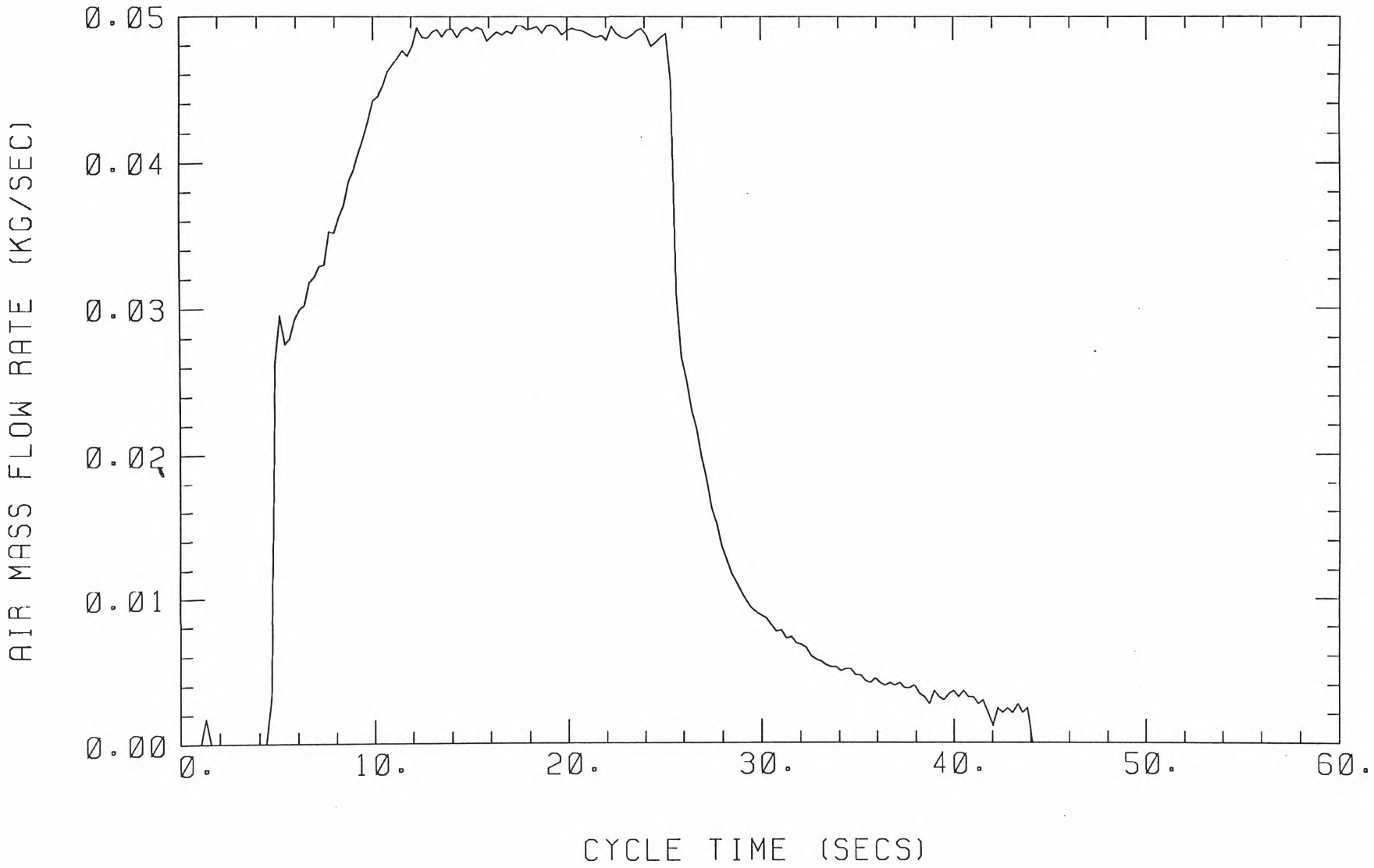

ANNUBAR NO. 3

EXPERIMENT NO. 1 TEST DATE: 26\10\95

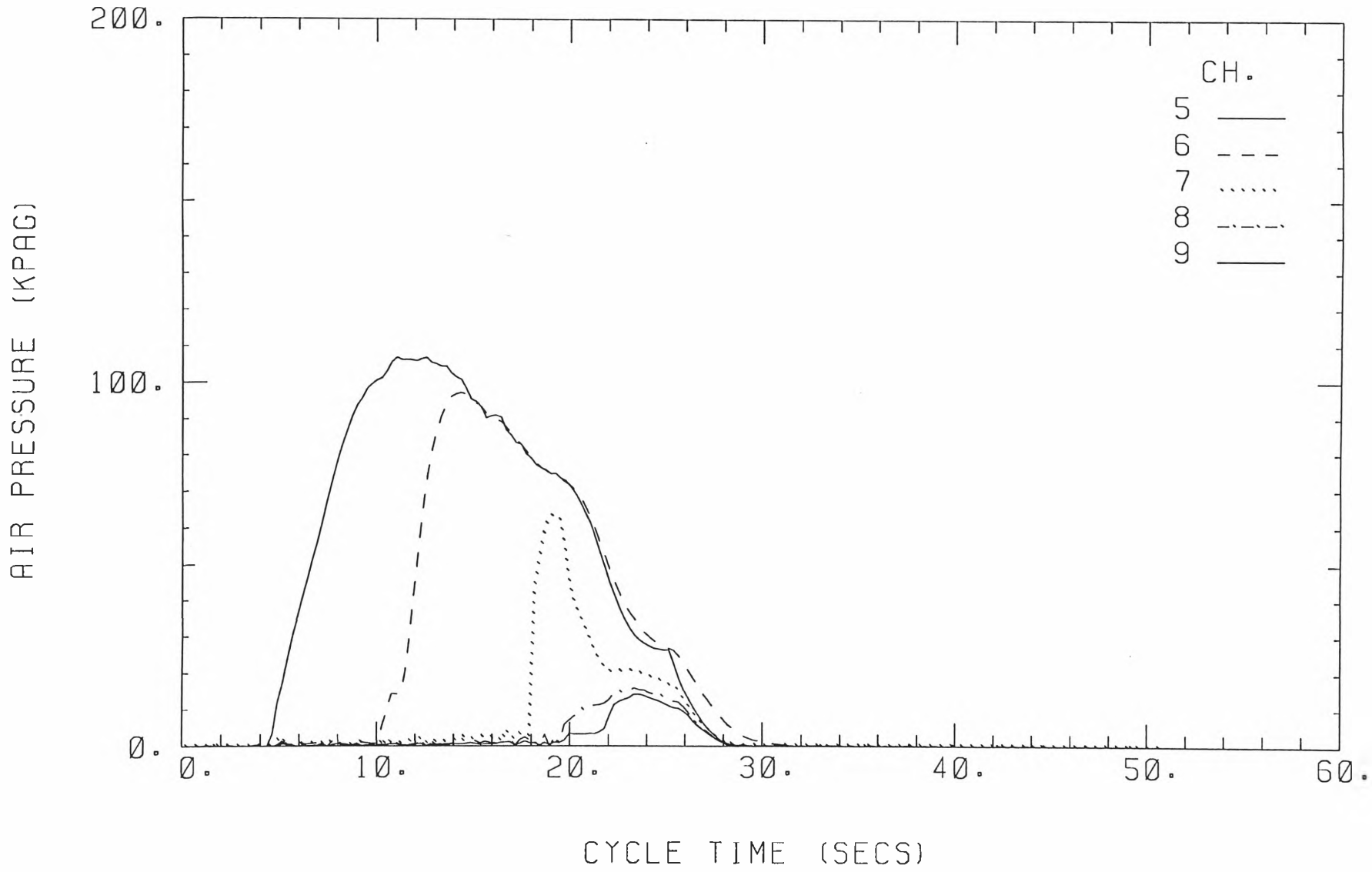

EXPERIMENT NO. 2 TEST DATE: 26\10\95
TOTAL MASS OF AIR USED (KGS) = 1.293

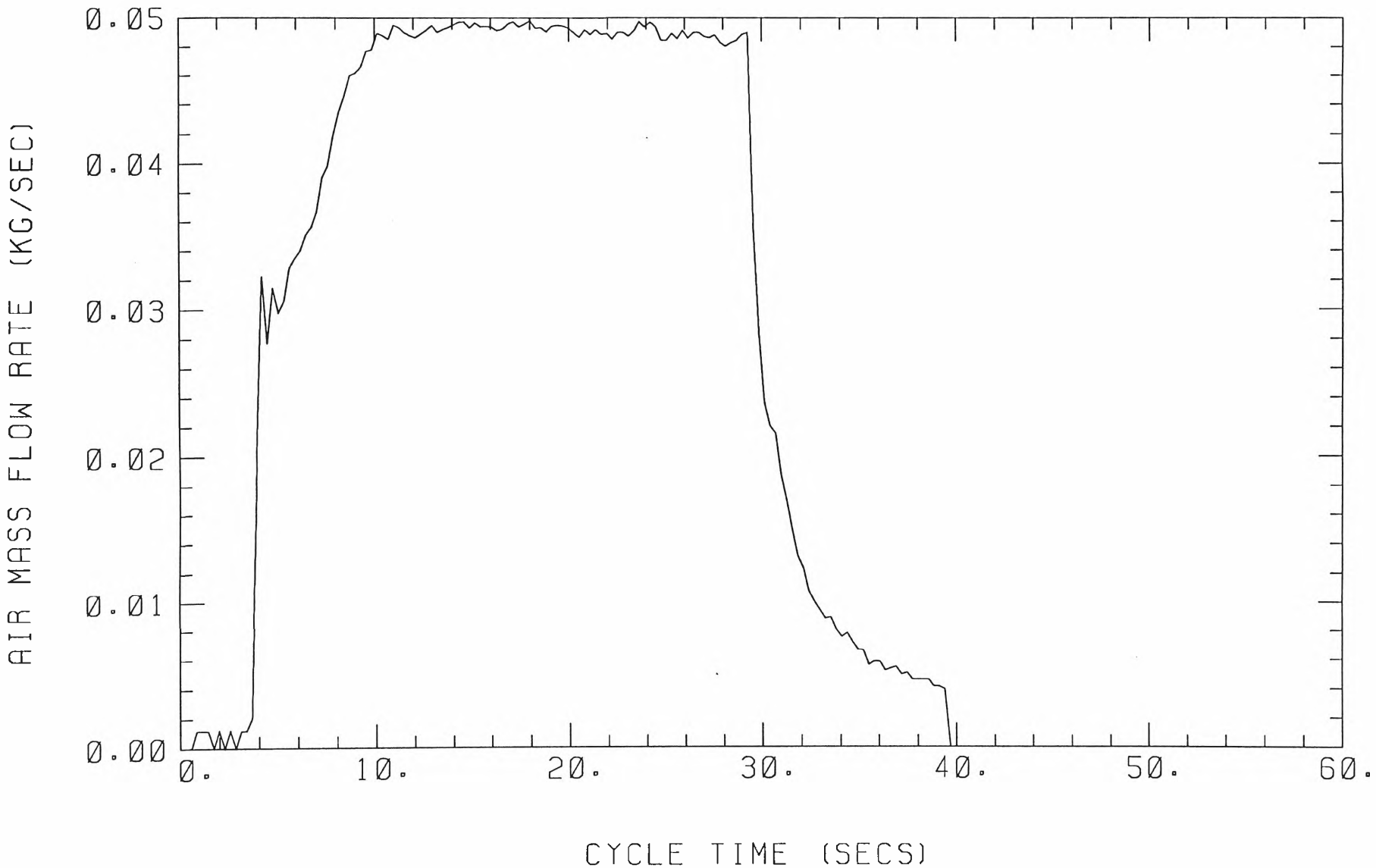

ANNUBAR NO. 3

EXPERIMENT NO. 2 TEST DATE: 26\10\95

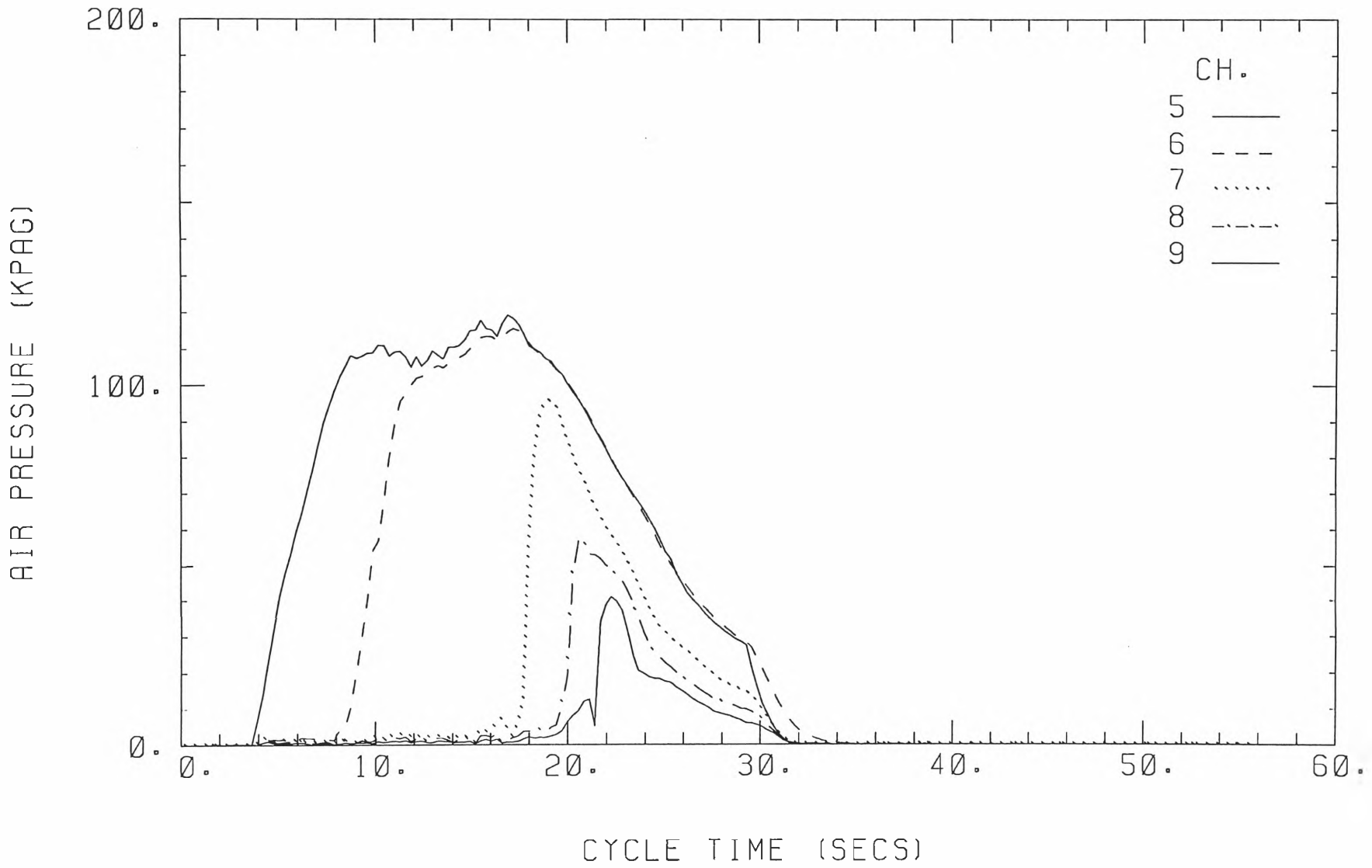

EXPERIMENT NO. 3
TOTAL MASS OF AIR USED

TEST DATE: 26\10\95

(KGS) = 1.752

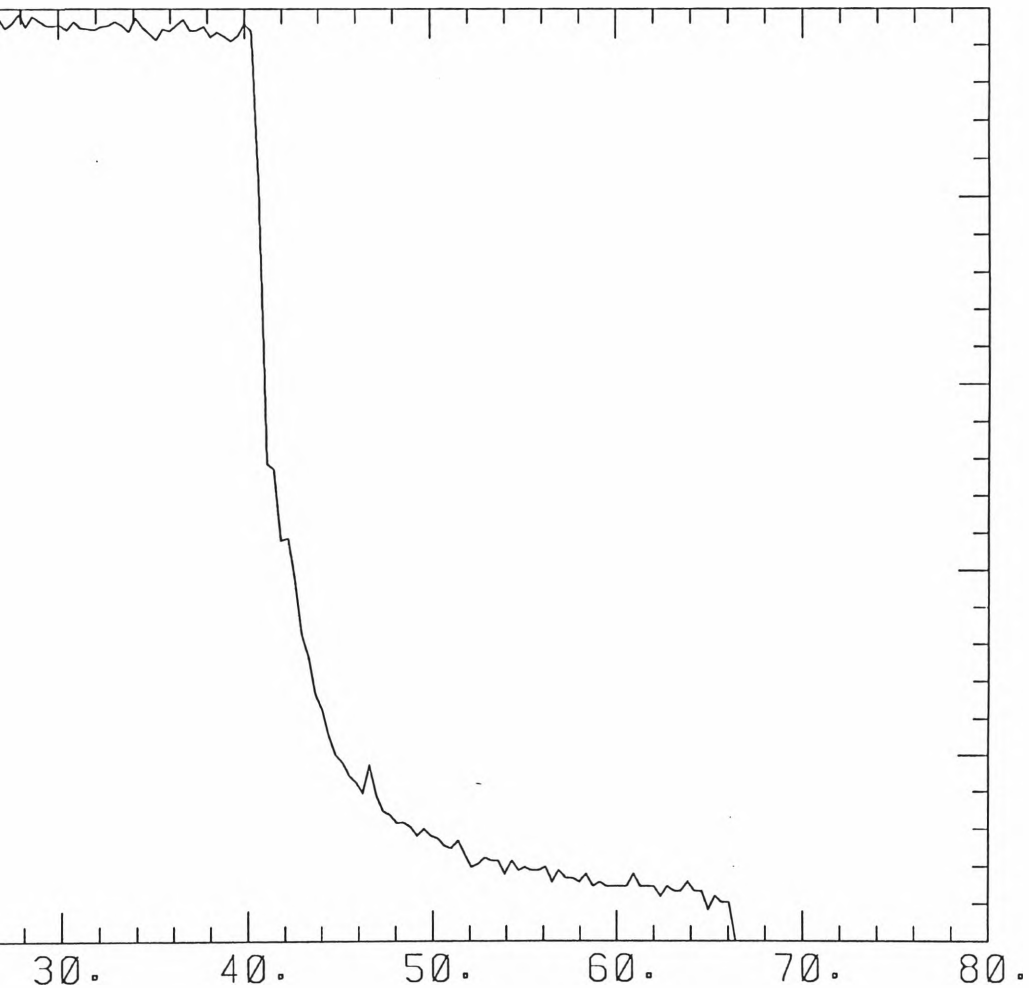

CYCLE TIME (SECS)

ANNUBAR NO. 3

EXPERIMENT NO. 3

TEST DATE: 26\10\95

AIR PRESSURE (KPAG)

200.
100.
0.

0. 10. 20. 30. 40. 50. 60. 70. 80.

CH.
5
6
7
8
9

CYCLE TIME (SECS)

EXPERIMENT NO. 4 TEST DATE: 26\10\95

TOTAL MASS OF AIR USED (KGS) = 2.294

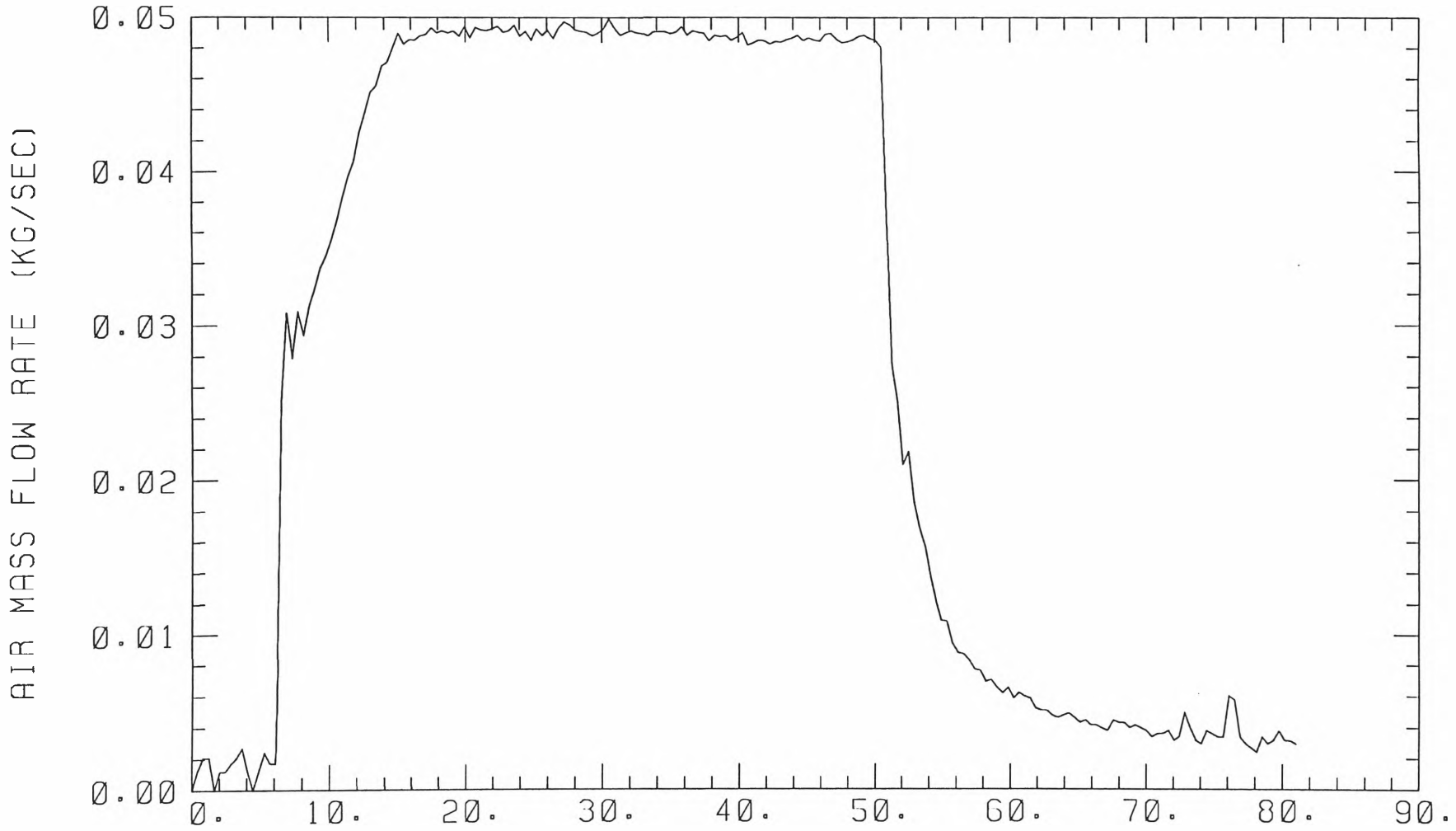

ANNUBAR NO. 3

EXPERIMENT NO. 4 TEST DATE: 26\10\95

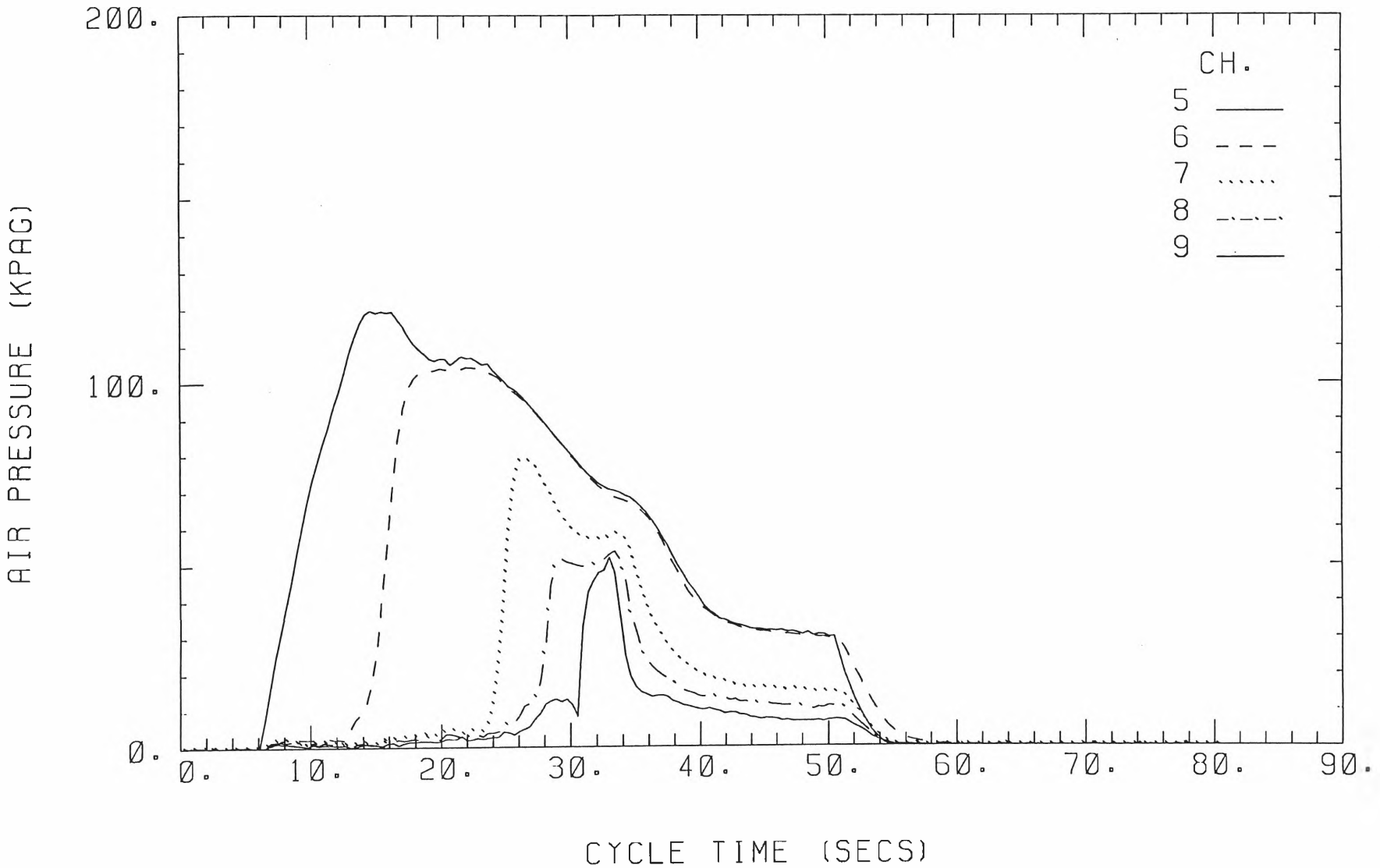

EXPERIMENT NO. 5
TOTAL MASS OF AIR USED

TEST DATE: 26\10\95

(KGS) = 2.248

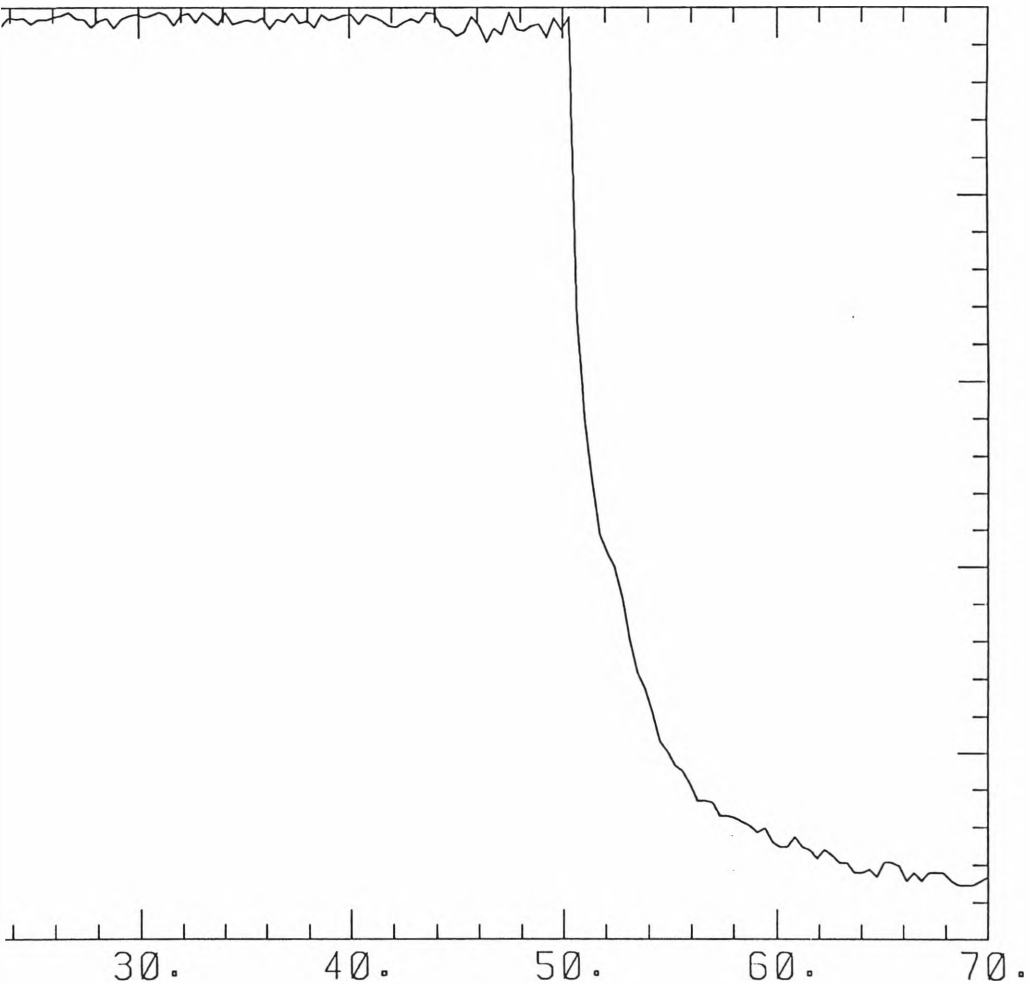

CYCLE TIME (SECS)

ANNUBAR NO. 3

EXPERIMENT NO. 5 TEST DATE: 26\10\95

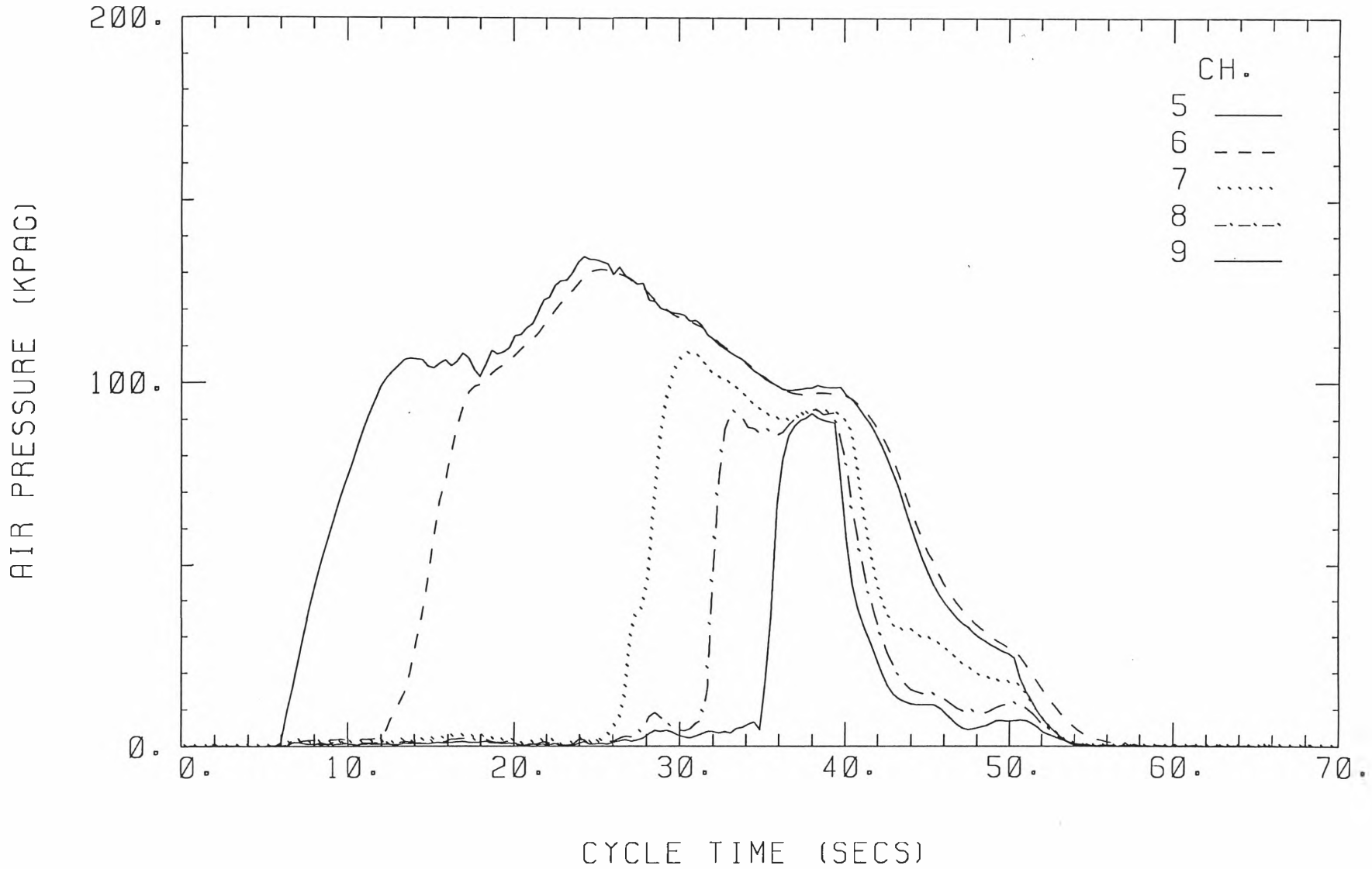

EXPERIMENT NO. 6
TOTAL MASS OF AIR USED

TEST DATE: 26\10\95

(KGS) = 2.002

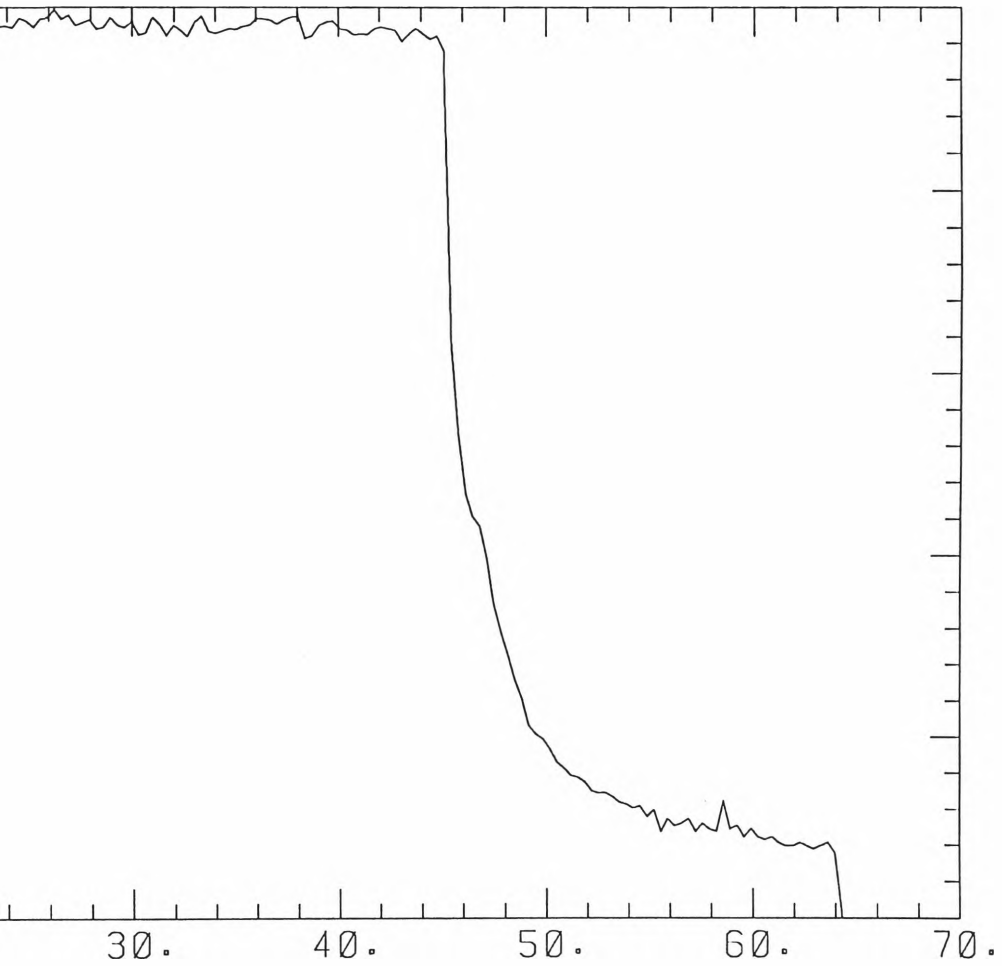

CYCLE TIME (SECS)

ANNUBAR NO. 3

EXPERIMENT NO. 6 TEST DATE: 26\10\95

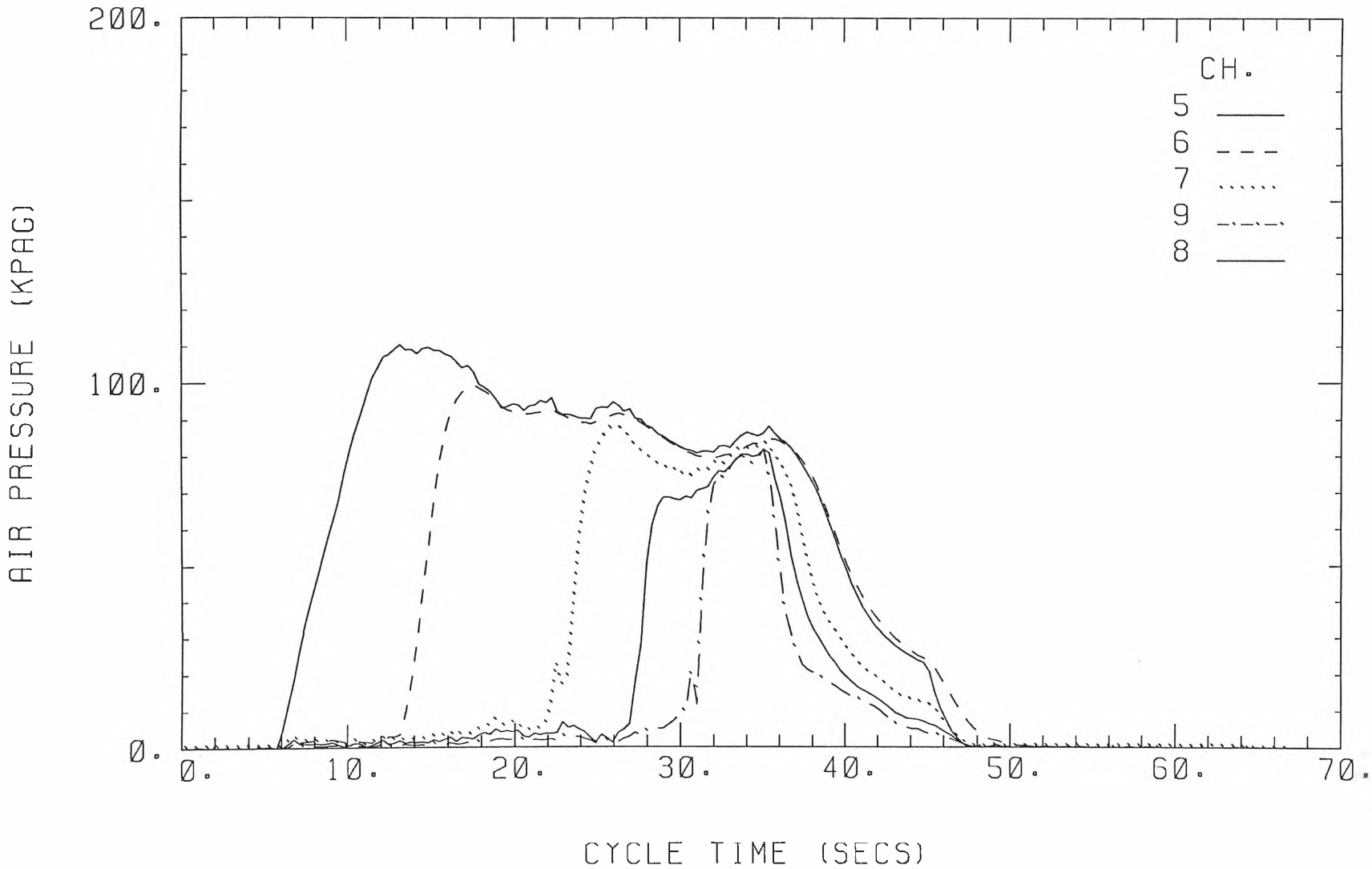

Appendix G Experimental Plots for Table 4.6

The measured data in Table 4.6 are based on the following experimental plots.

Pressure meter A is connected to channel 5, pressure meter B to channel 6, pressure meter C to channel 7, pressure meter D to channel 8 and pressure meter E to channel 9.

Table G.1 Experimental values for t_{pm} and Δp

Exp. No.	$\Delta p(kPa)$	$t_{pm}(s)$
1	108	5
2	108	5.5
3	115	5.5
4	112	5.5
5	110	5.5
6	121	5.5

EXPERIMENT NO. 1
TOTAL MASS OF AIR USED
AIR MASS FLOW RATE (KG/SEC)
0.06
0.05
0.04
0.03
0.02
0.01
0.00
0.
10.

TEST DATE: 27\10\95

(KGS) = 1.217

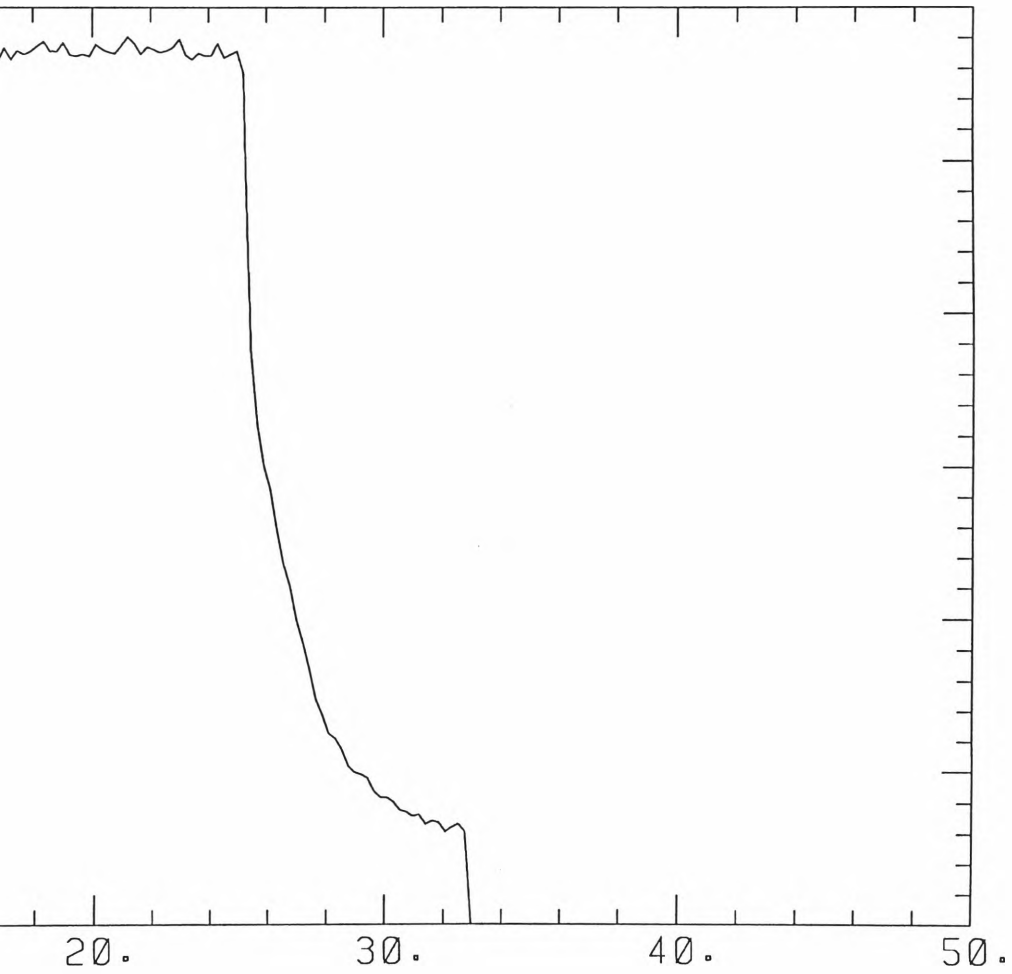

CYCLE TIME (SECS)

ANNUBAR NO. 3

EXPERIMENT NO. 1 TEST DATE: 27\10\95

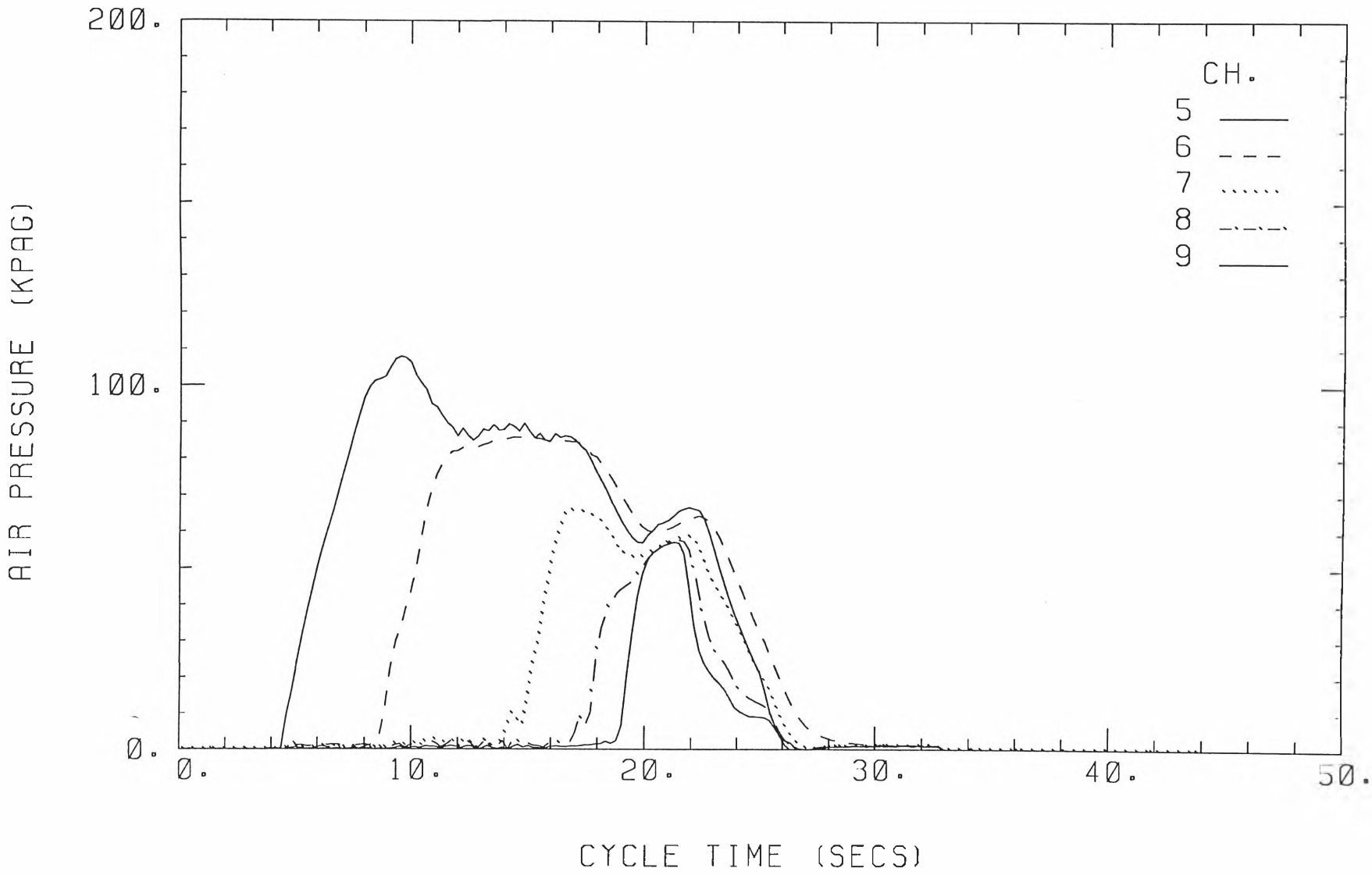

EXPERIMENT NO. 2 TEST DATE: 27\10\95

TOTAL MASS OF AIR USED (KGS) = 1.325

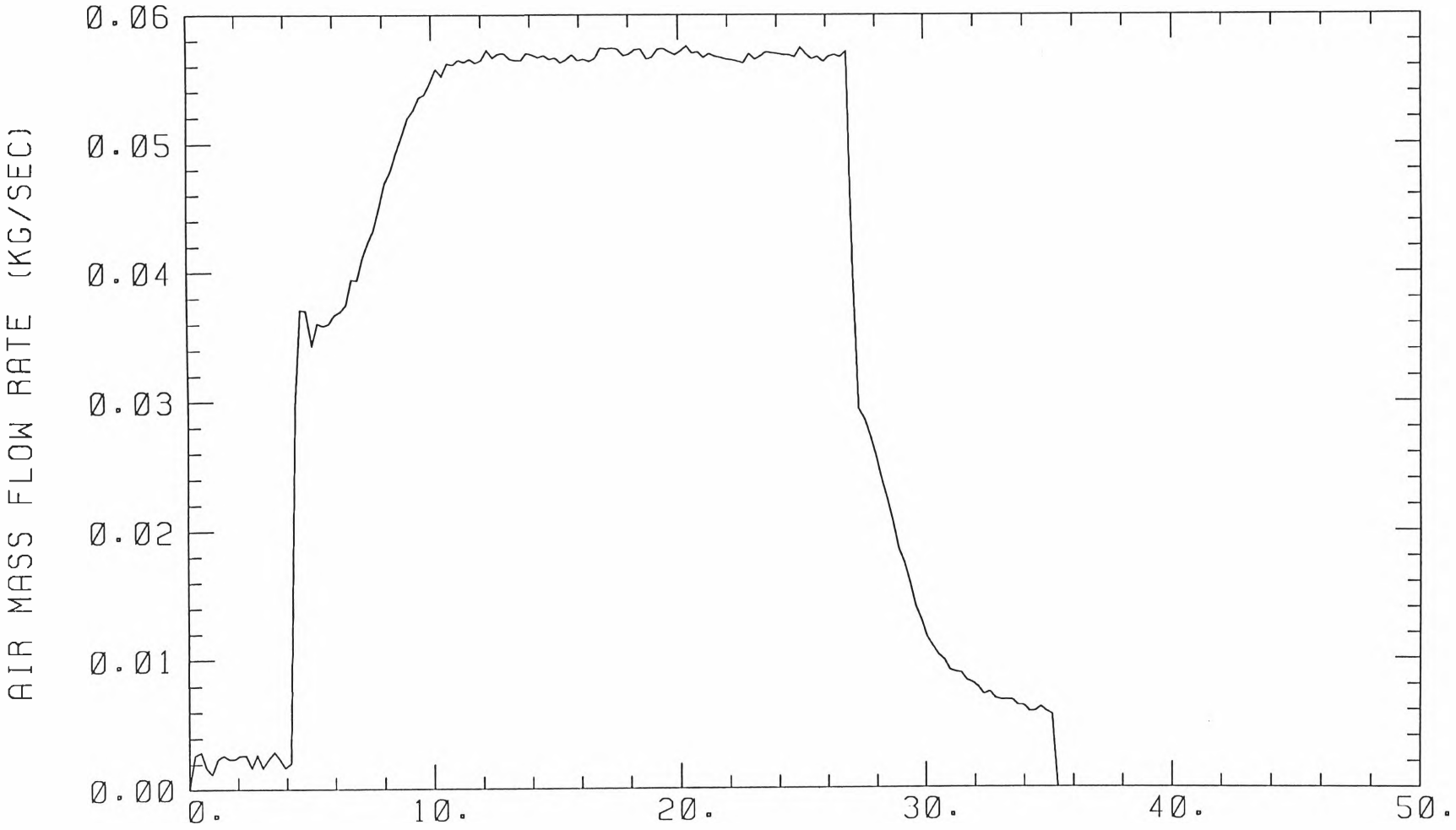

ANNUBAR NO. 3

EXPERIMENT NO. 2 TEST DATE: 27\10\95

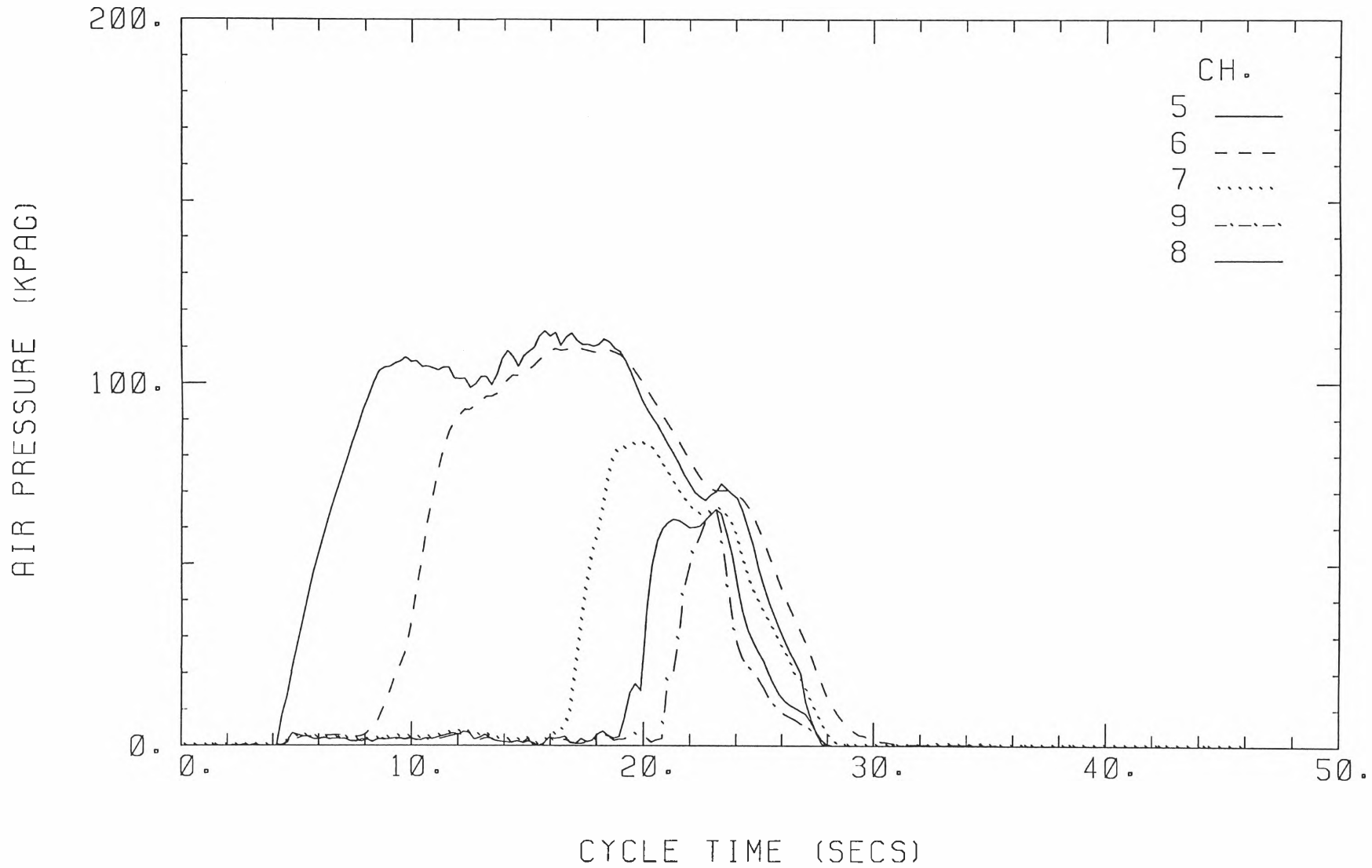

EXPERIMENT NO. 3 TEST DATE: 27\10\95

TOTAL MASS OF AIR USED (KGS) = 1.162

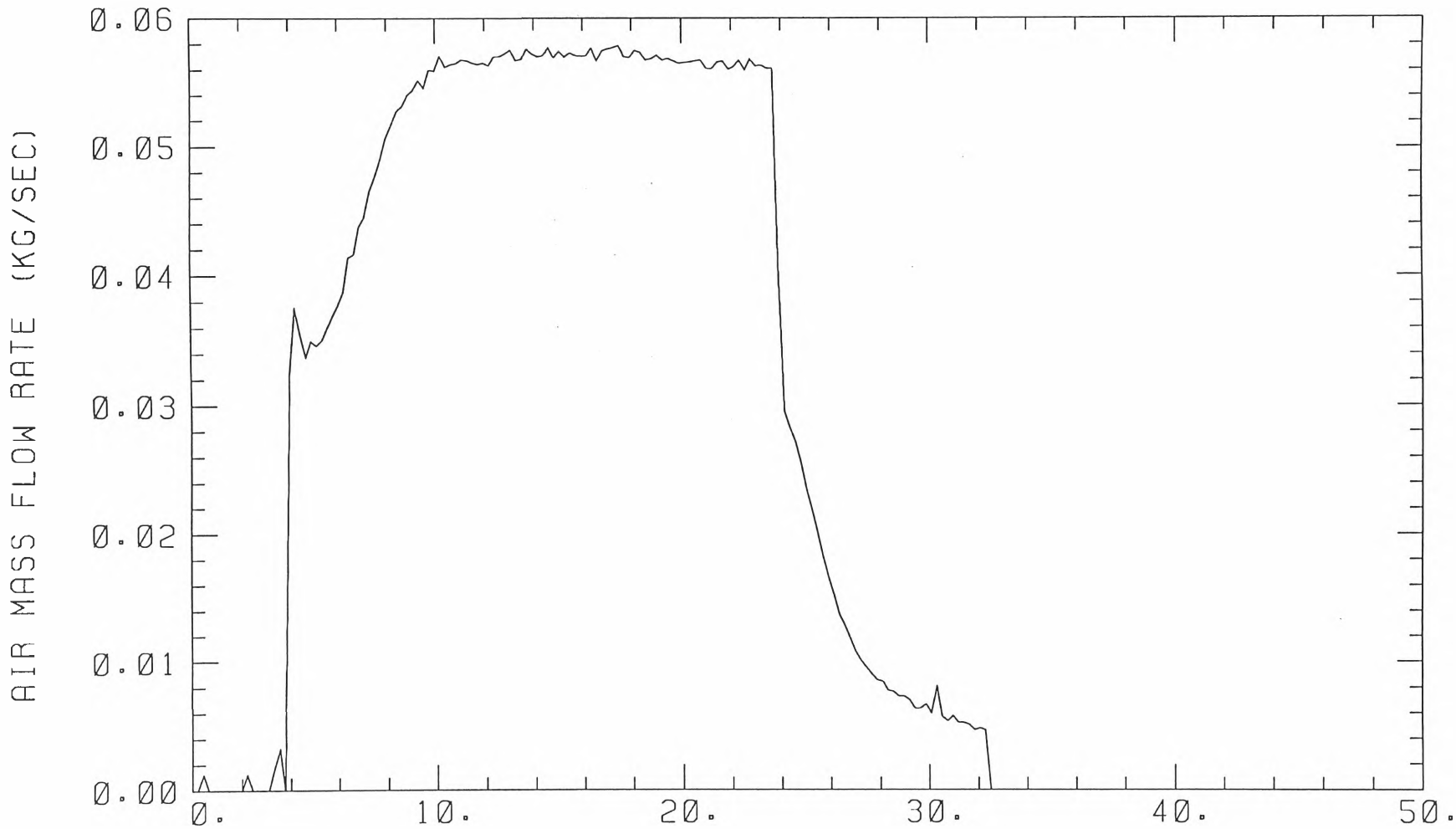

ANNUBAR NO. 3

EXPERIMENT NO. 3

TEST DATE: 27\10\95

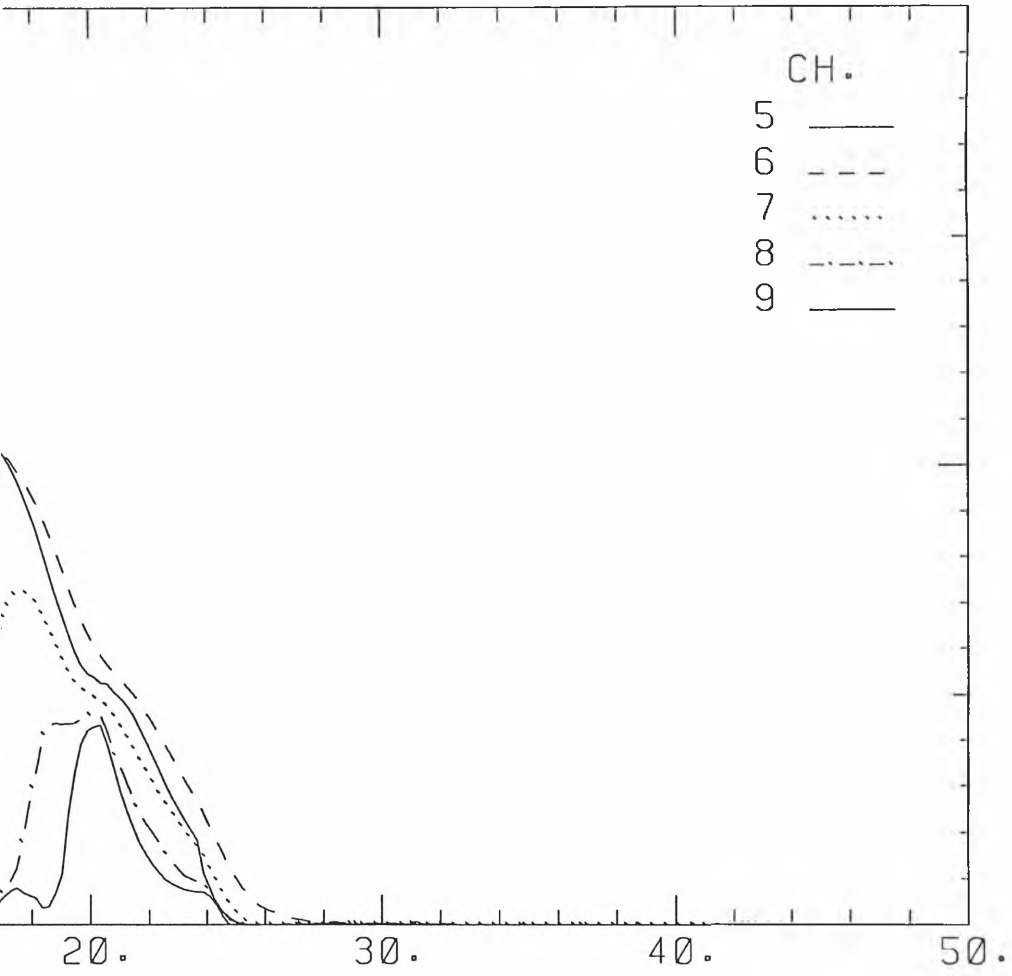

CYCLE TIME (SECS)

EXPERIMENT NO. 4 TEST DATE: 27\10\95

TOTAL MASS OF AIR USED (KGS) = 1.518

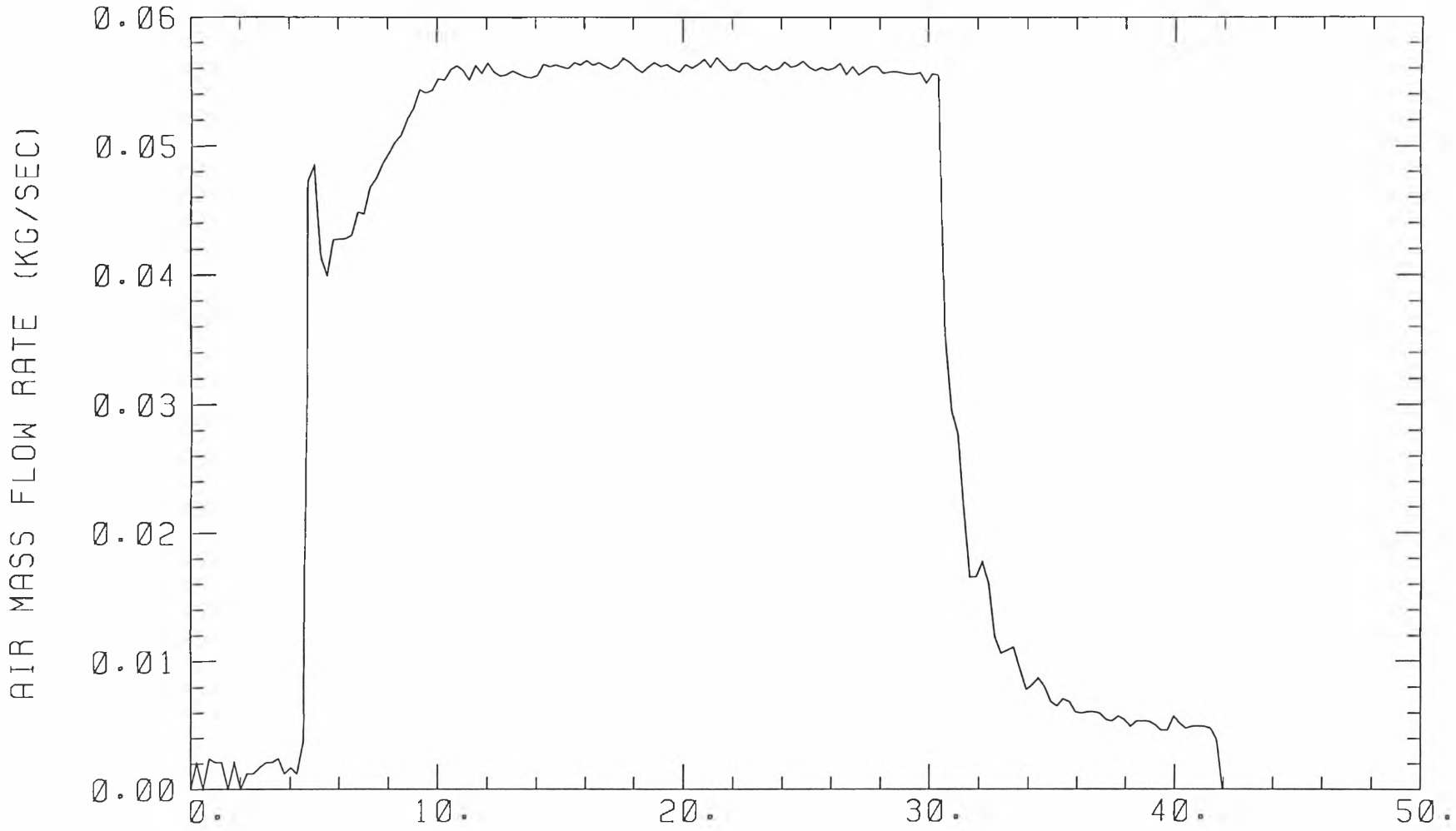

ANNUBAR NO. 3

EXPERIMENT NO. 4

TEST DATE: 27\10\95

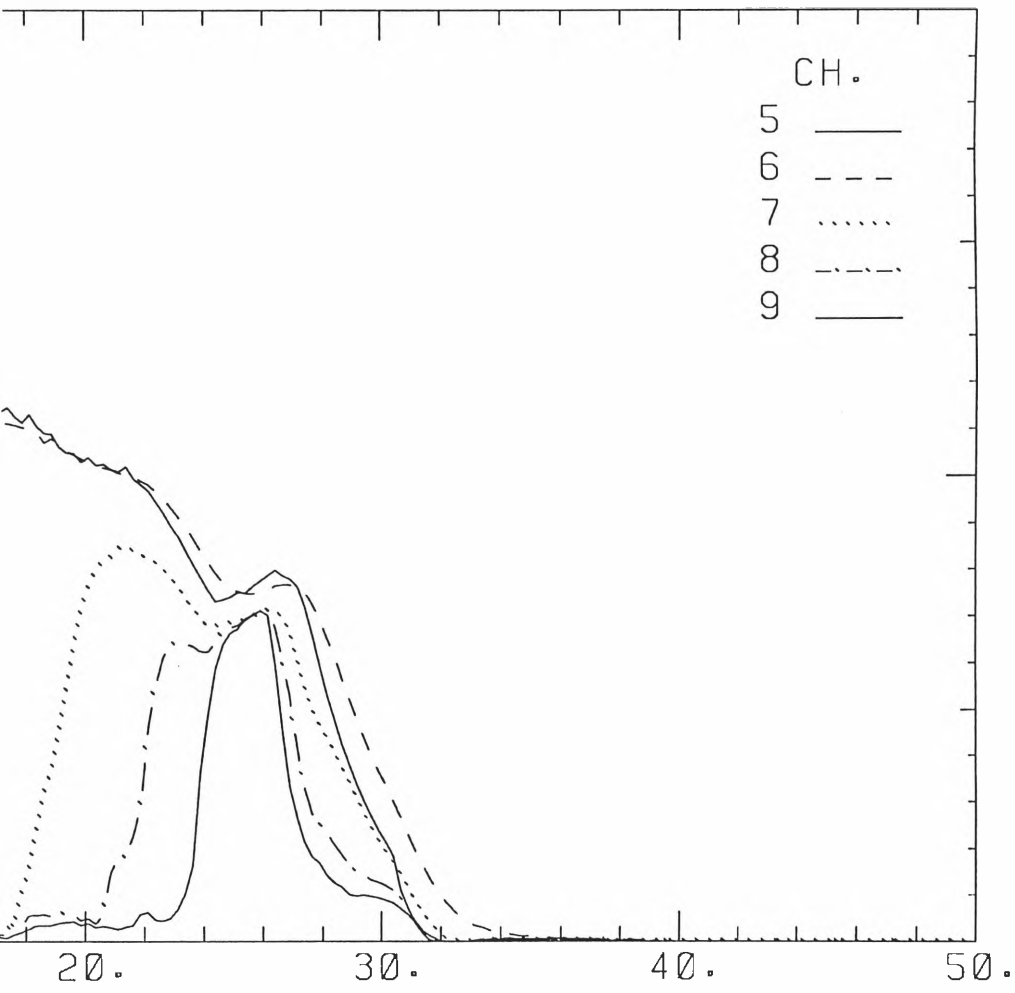

CYCLE TIME (SECS)

EXPERIMENT NO. 5
TOTAL MASS OF AIR USED

TEST DATE: 27\10\95

(KGS) = 1.721

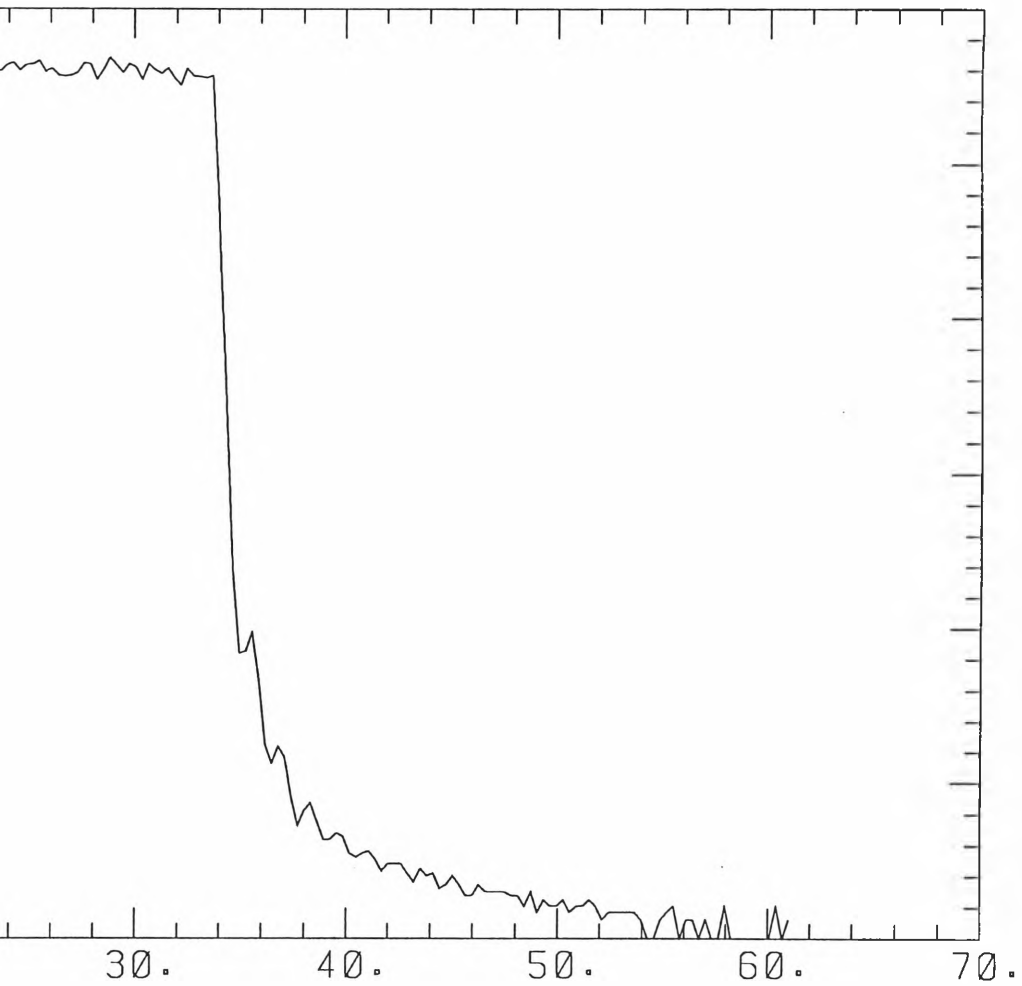

CYCLE TIME (SECS)

ANNUBAR NO. 3

EXPERIMENT NO. 5 TEST DATE: 27\10\95

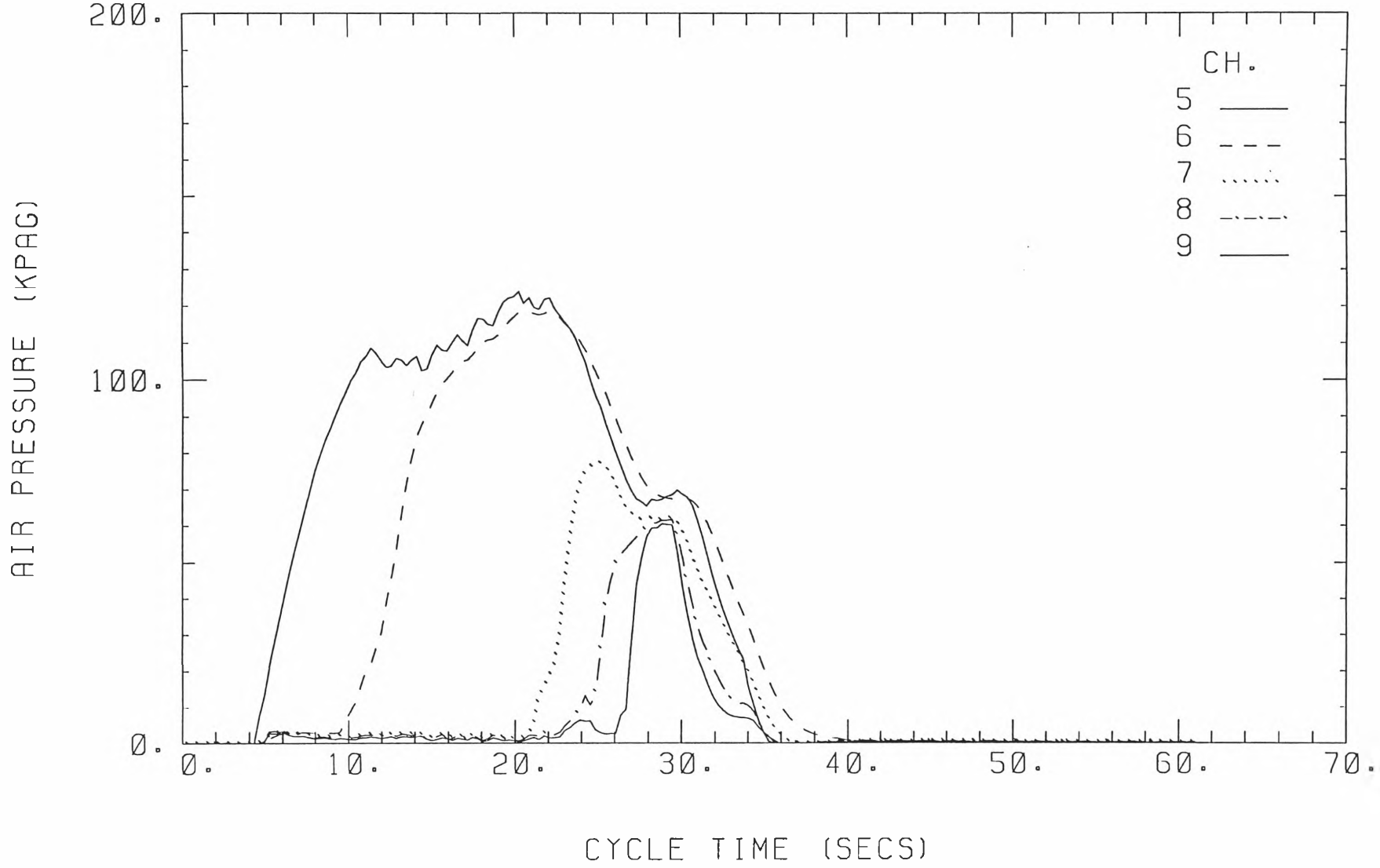

EXPERIMENT NO. 6 TEST DATE: 27\10\95

TOTAL MASS OF AIR USED (KGS) = 1.321

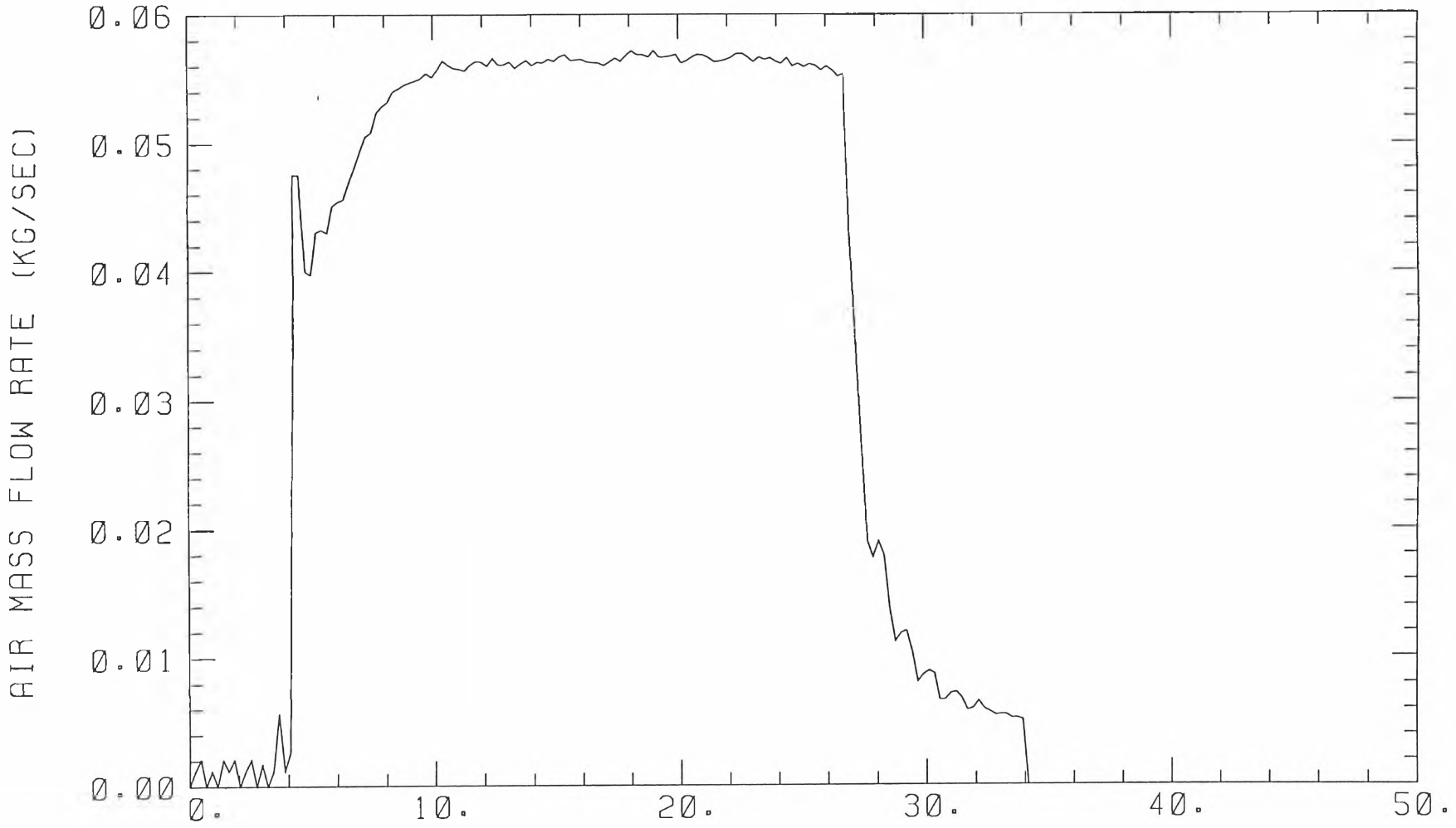

ANNUBAR NO. 3

EXPERIMENT NO. 6 TEST DATE: 27\10\95

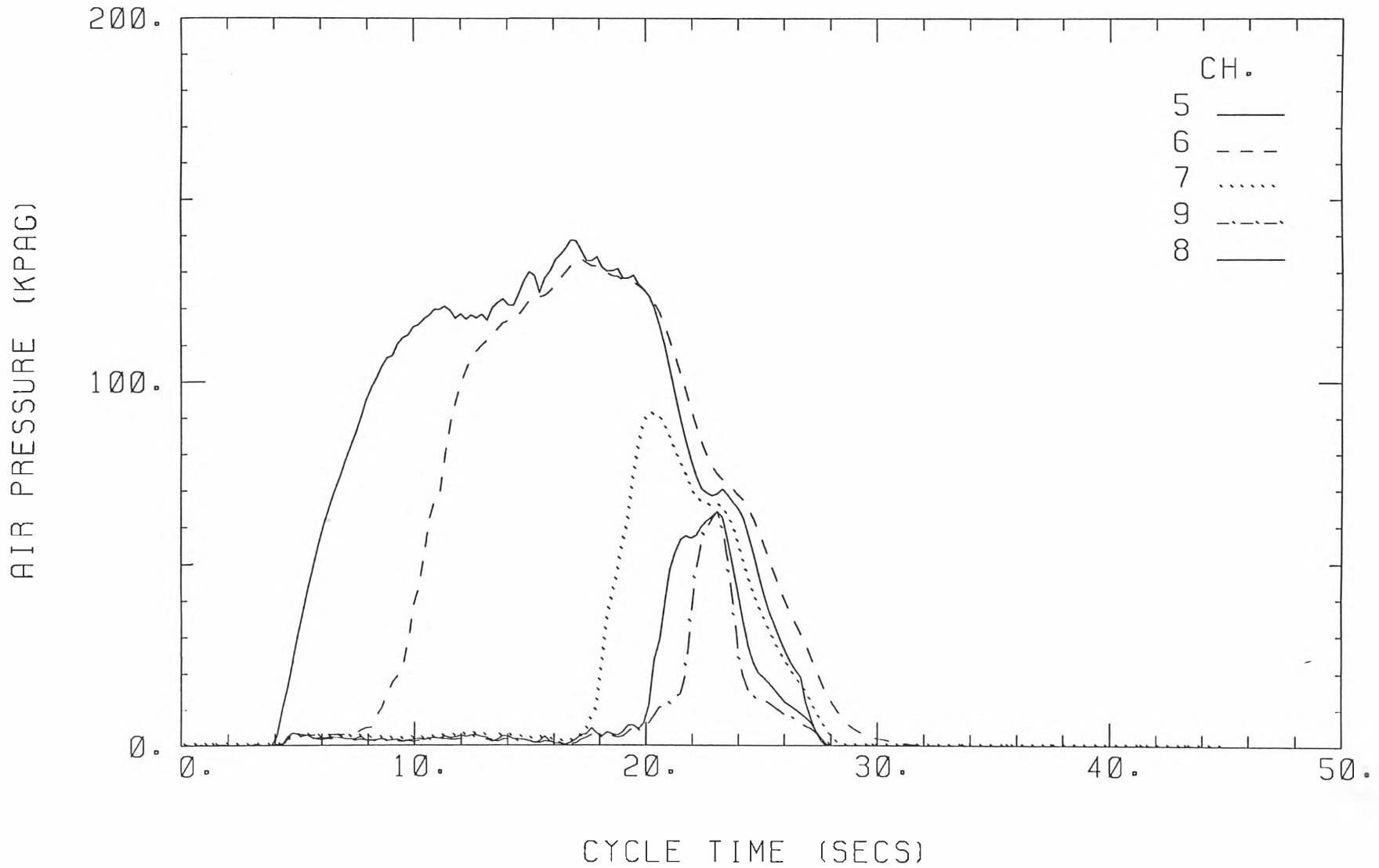

Appendix H Experimental Plots for Table 4.7

The measured data in Table 4.7 are based on the following experimental plots.

Pressure meter A is connected to channel 5, pressure meter B to channel 6, pressure meter C to channel 7, pressure meter D to channel 8 and pressure meter E to channel 9.

Table H.1 Experimental values for t_{pm} and Δp

Exp. No.	$\Delta p(kPa)$	$t_{pm}(s)$
1	86	6
2	103	6
3	105	6
4	95	5.5
5	102	6
6	90	6

EXPERIMENT NO. 1 TEST DATE: 27\10\95
TOTAL MASS OF AIR USED (KGS) = 1.213

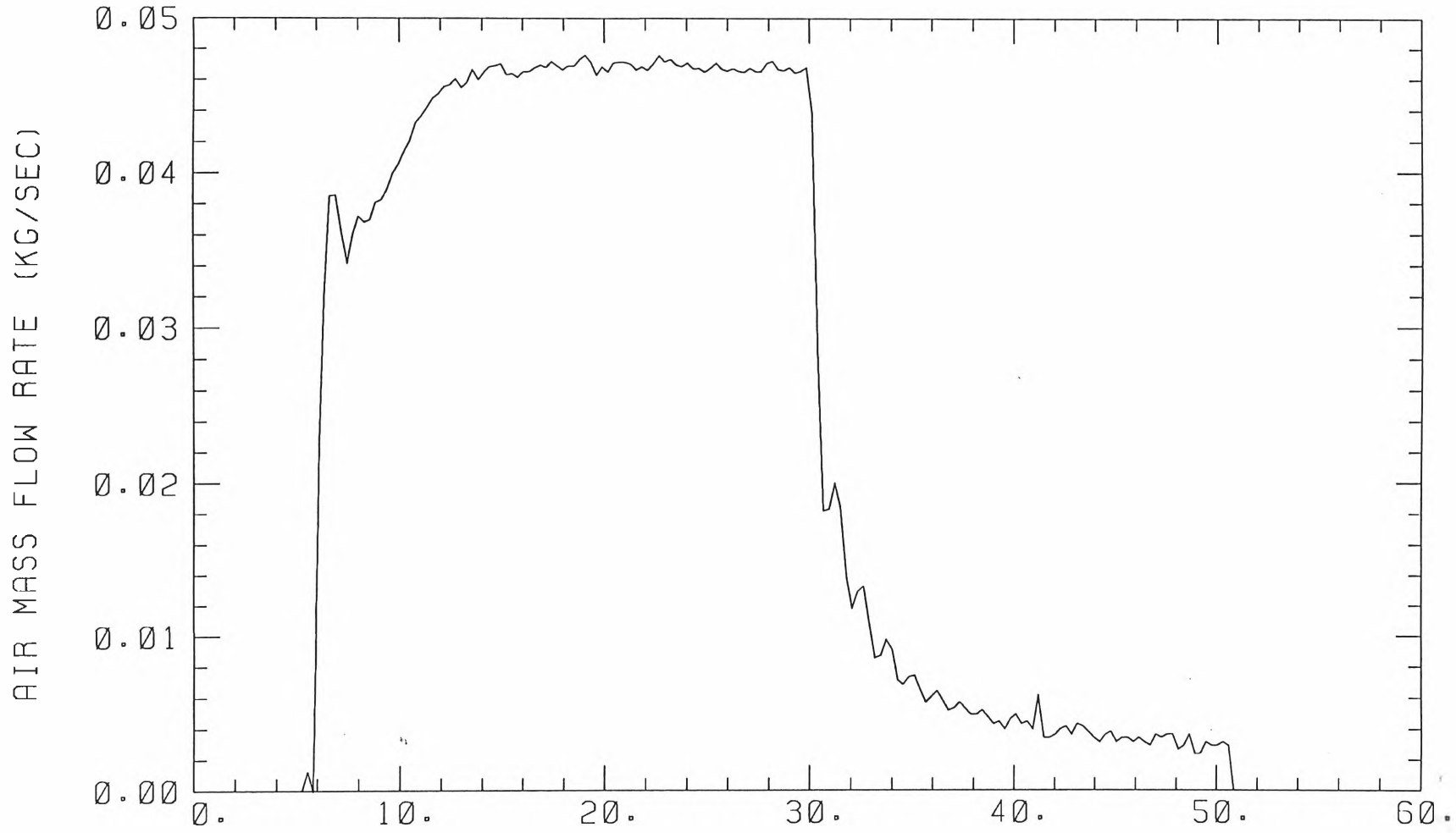

ANNUBAR NO. 3

EXPERIMENT NO. 1 TEST DATE: 27\10\95

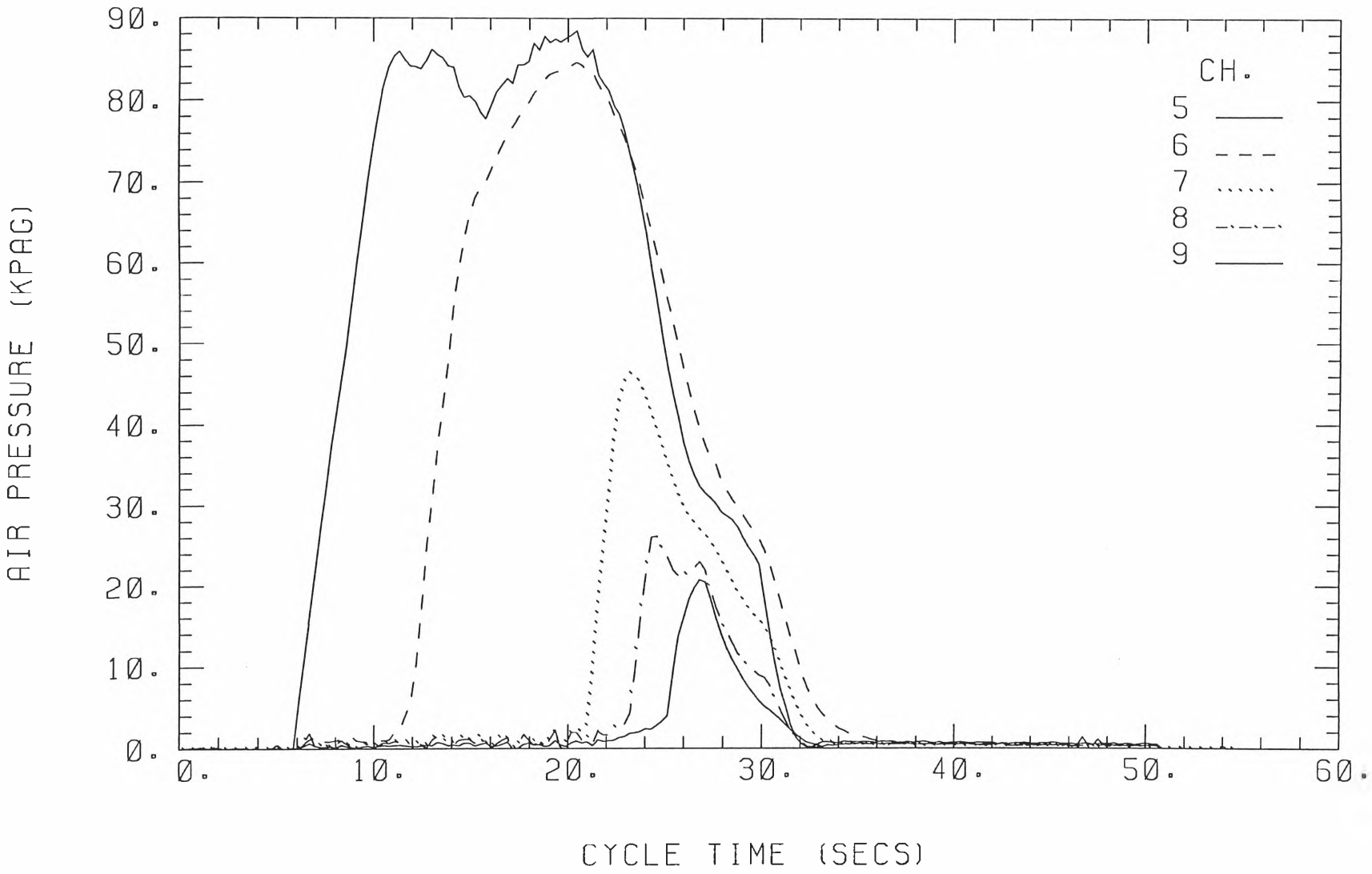

EXPERIMENT NO. 2
TOTAL MASS OF AIR USED
AIR MASS FLOW RATE (KG/SEC)
0.05
0.04
0.03
0.02
0.01
0.00
0.
10.

TEST DATE: 27\10\95

(KGS) = 1.447

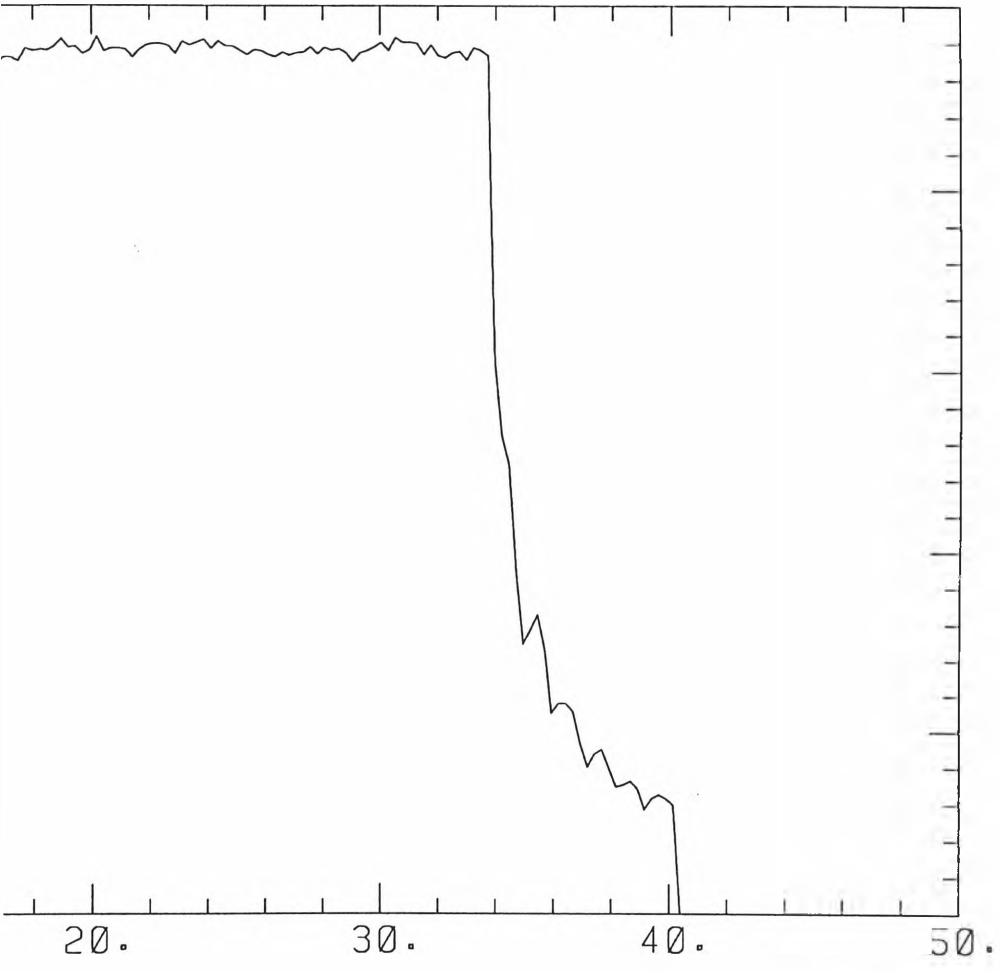

CYCLE TIME (SECS)

ANNUBAR NO. 3

EXPERIMENT NO. 2

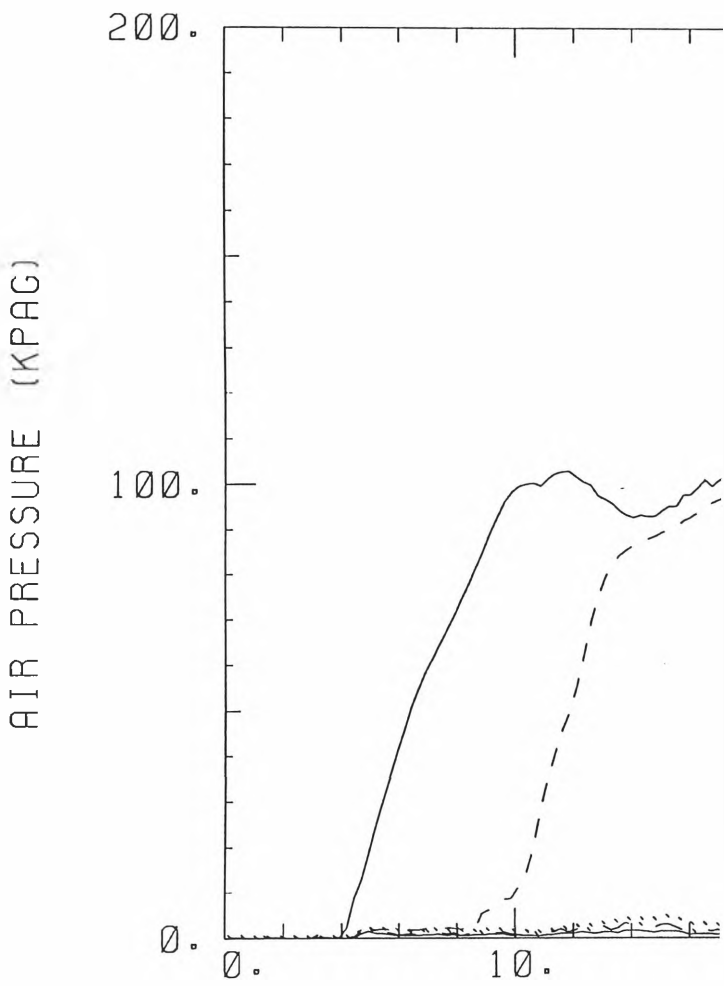

TEST DATE: 27\10\95

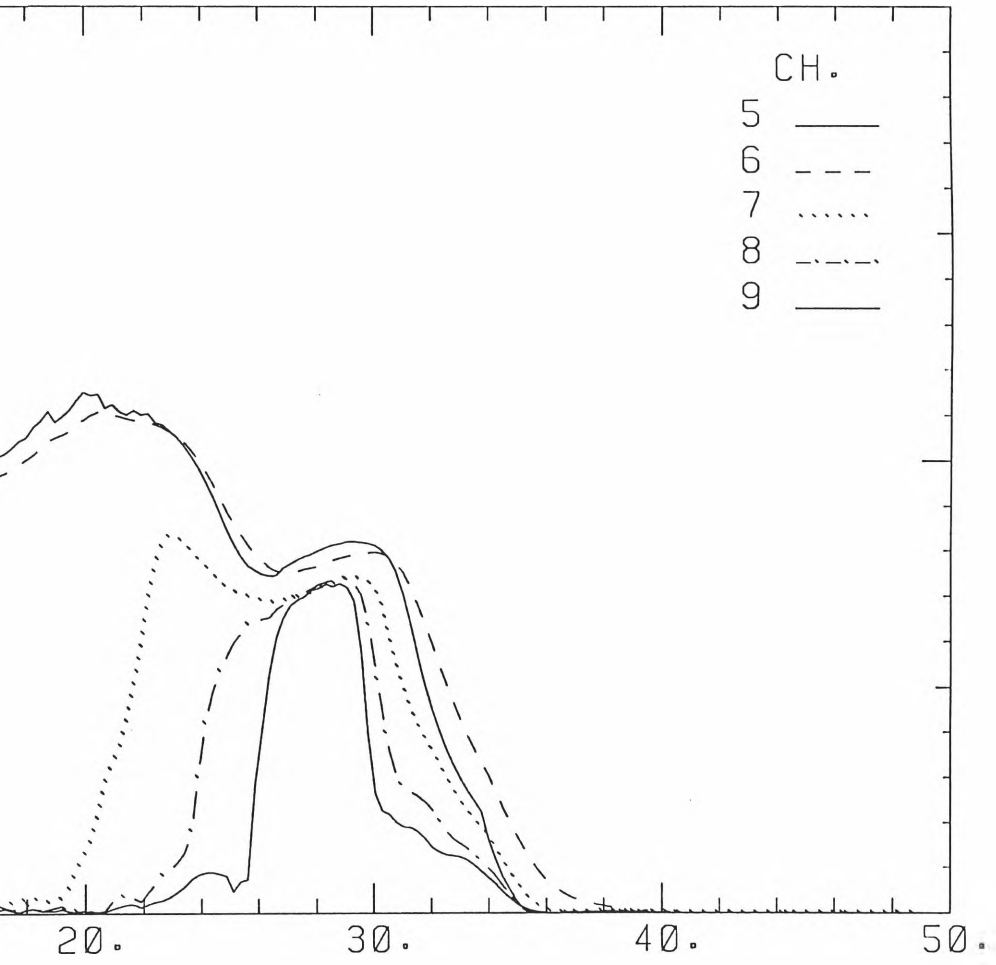

CYCLE TIME (SECS)

EXPERIMENT NO. 3 TEST DATE: 27\10\95
TOTAL MASS OF AIR USED (KGS) = 1.554

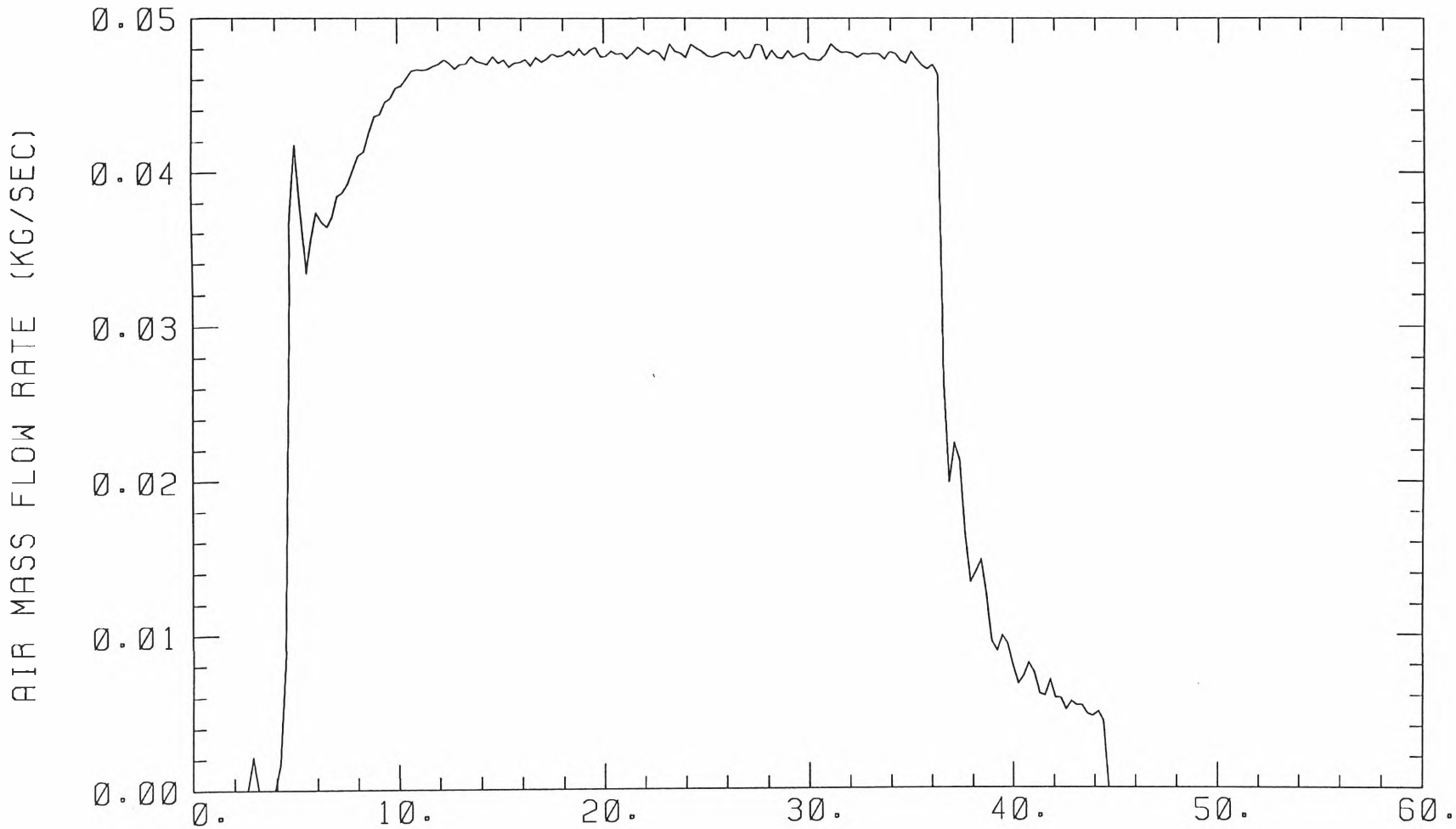

ANNUBAR NO. 3

EXPERIMENT NO. 3 TEST DATE: 27\10\95

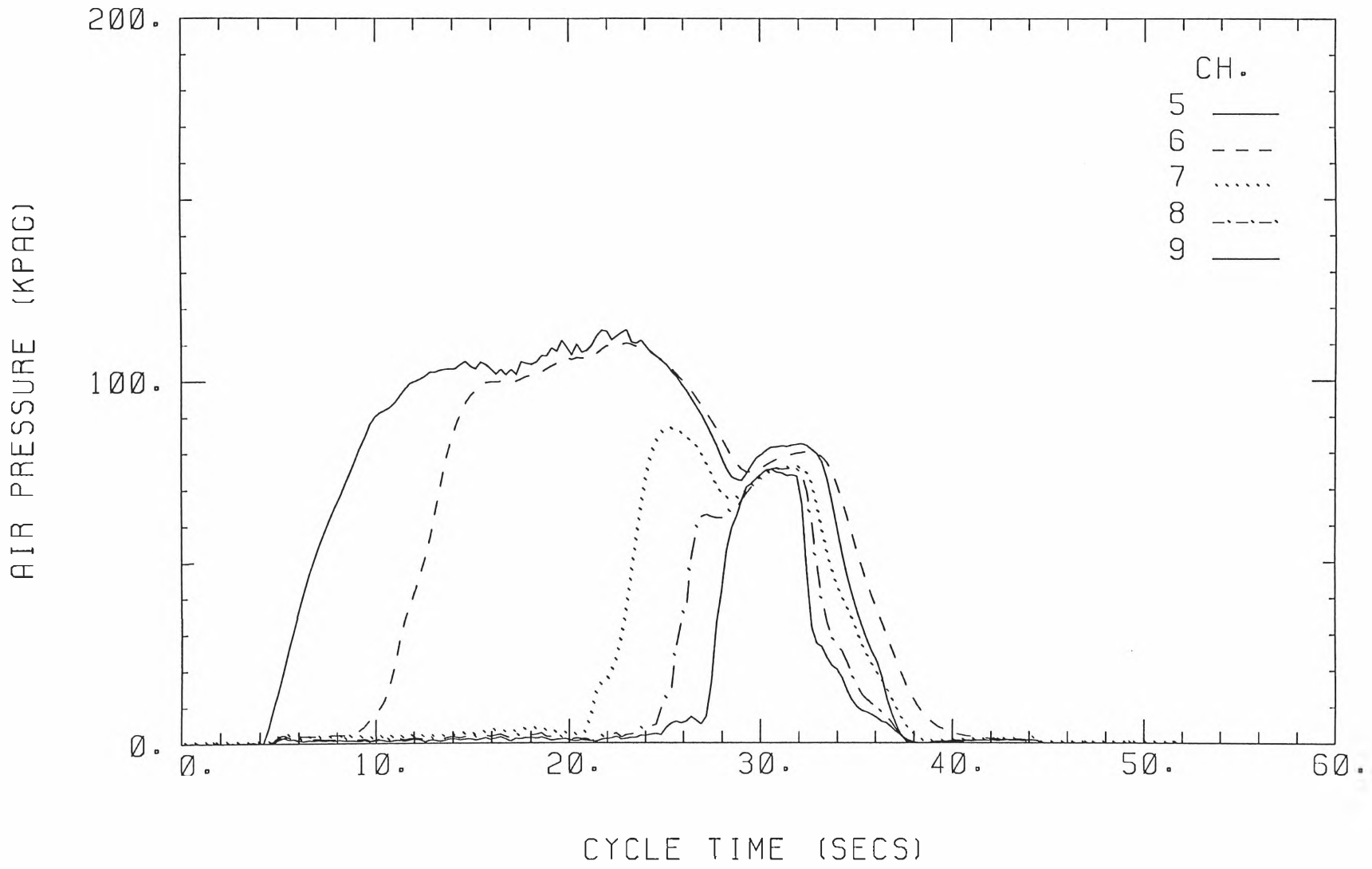

EXPERIMENT NO. 4 TEST DATE: 27\10\95
TOTAL MASS OF AIR USED (KGS) = 1.104

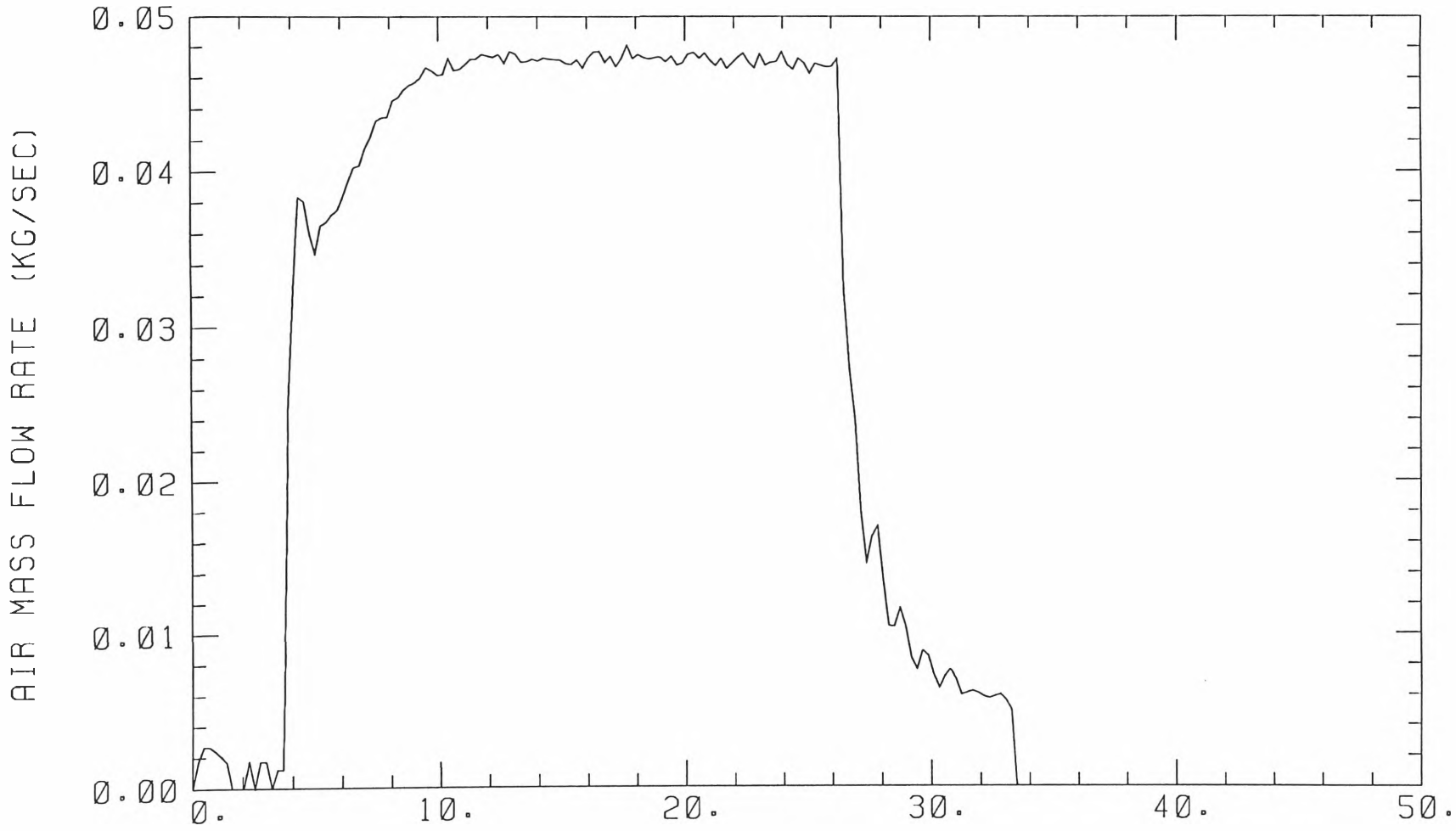

ANNUBAR NO. 3

EXPERIMENT NO. 4 TEST DATE: 27\10\95

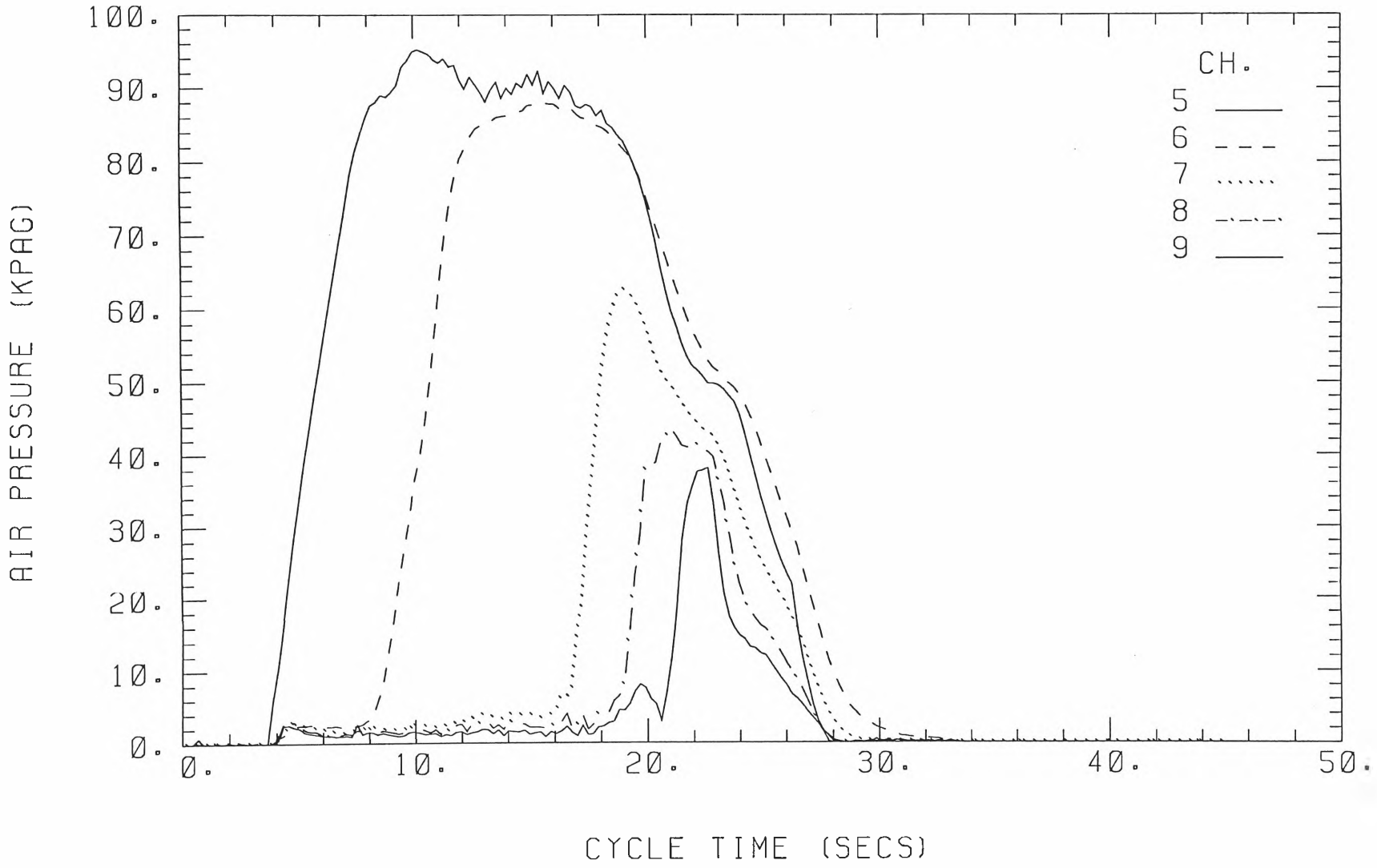

EXPERIMENT NO. 5 TEST DATE: 27\10\95
TOTAL MASS OF AIR USED (KGS) = 1.578

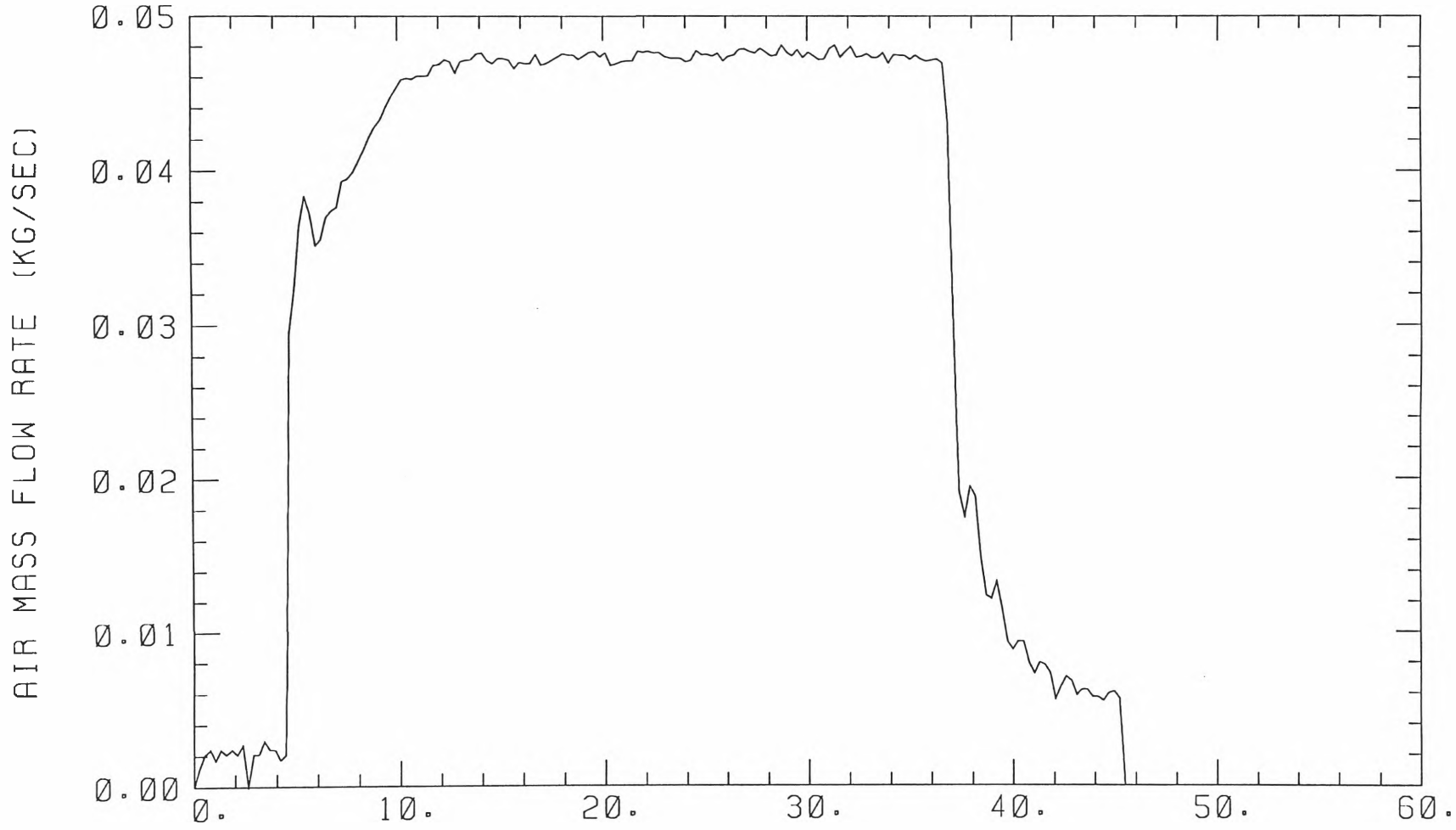

ANNUBAR NO. 3

EXPERIMENT NO. 5 TEST DATE: 27\10\95

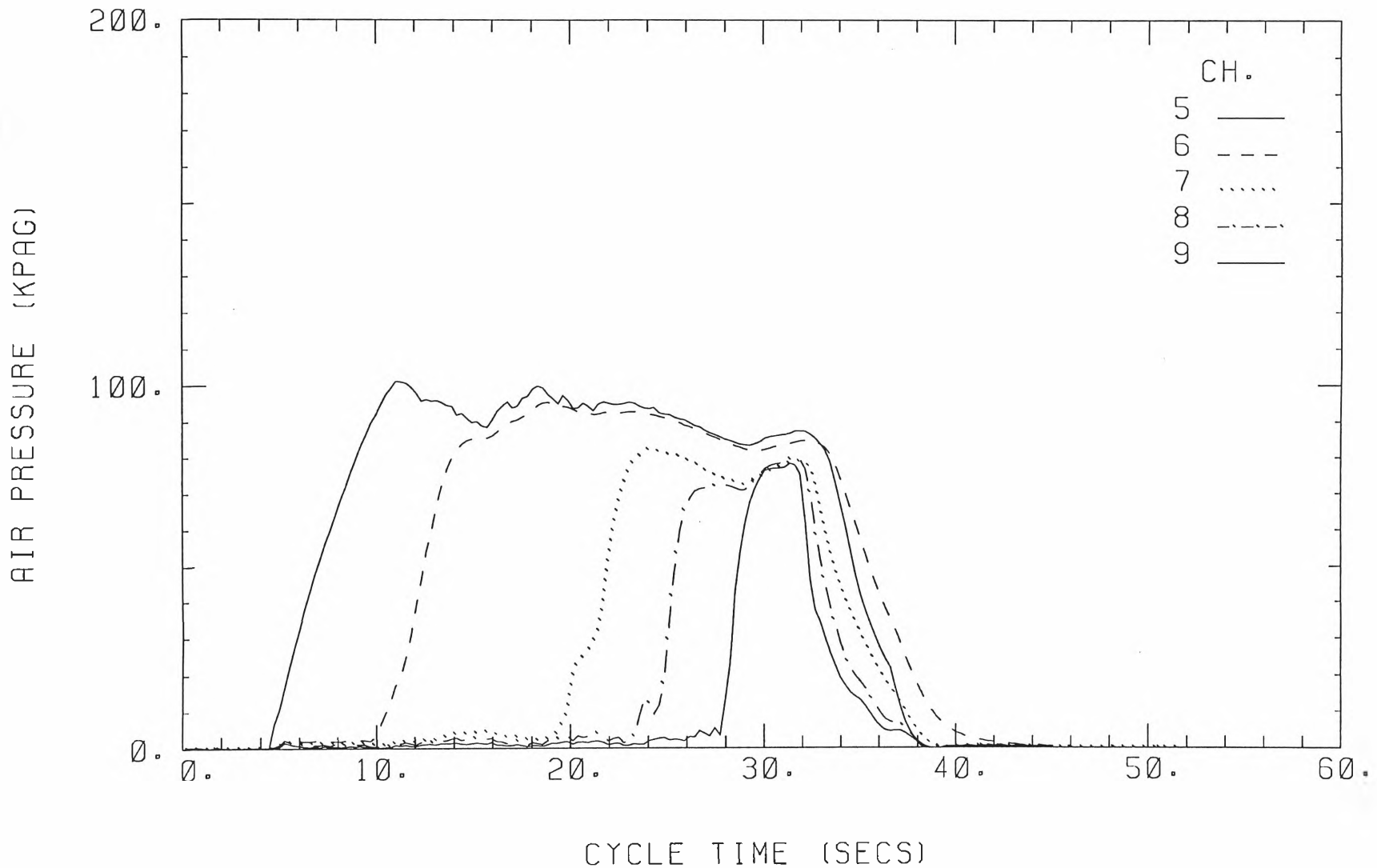

EXPERIMENT NO. 6
TOTAL MASS OF AIR USED

TEST DATE: 27\10\95

(KGS) = 1.454

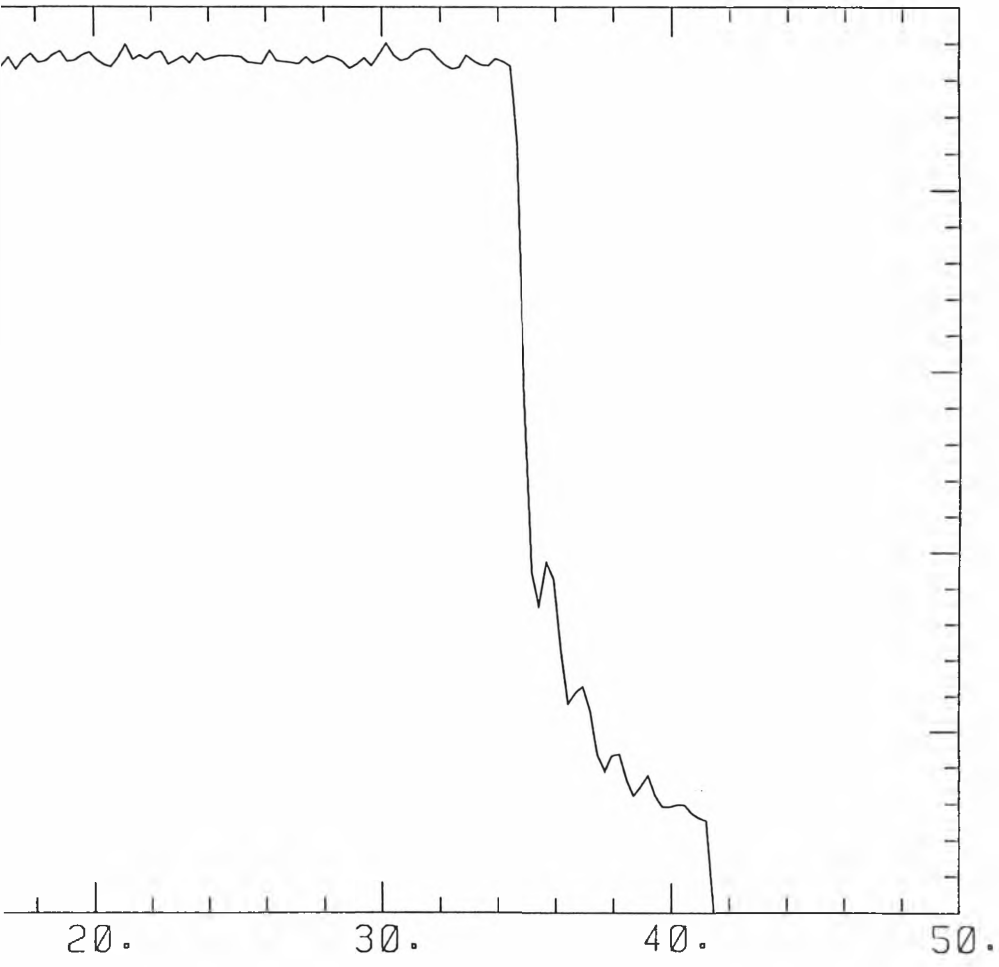

CYCLE TIME (SECS)

ANNUBAR NO. 3

EXPERIMENT NO. 6 TEST DATE: 27\10\95

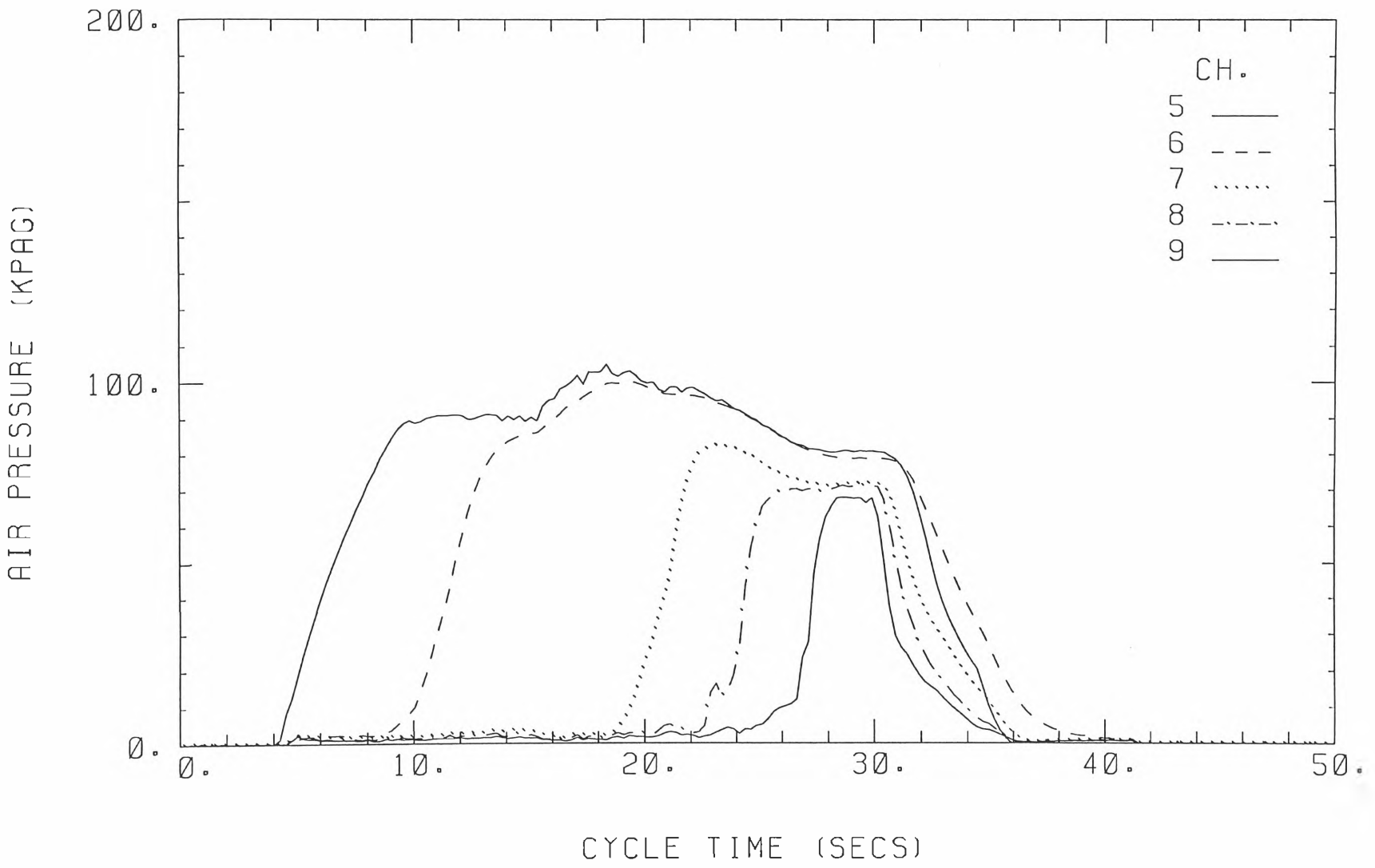

Appendix I Experimental Plots for Table 4.9

The measured data in Table 4.9 are based on the following experimental plots.

Pressure meter A is connected to channel 5, pressure meter B to channel 6, pressure meter C to channel 7, pressure meter D to channel 8 and pressure meter E to channel 9.

Table I.1 Experimental values for t_{pm} and Δp

Exp. No.	$\Delta p(kPa)$	$t_{pm}(s)$
1	110	5.8
2	120	6.0
3	125	3.3
4	90	3.7
5	85	3.0

EXPERIMENT NO. 1
TOTAL MASS OF AIR USED

TEST DATE: 2\1\96

(KGS) = 0.967

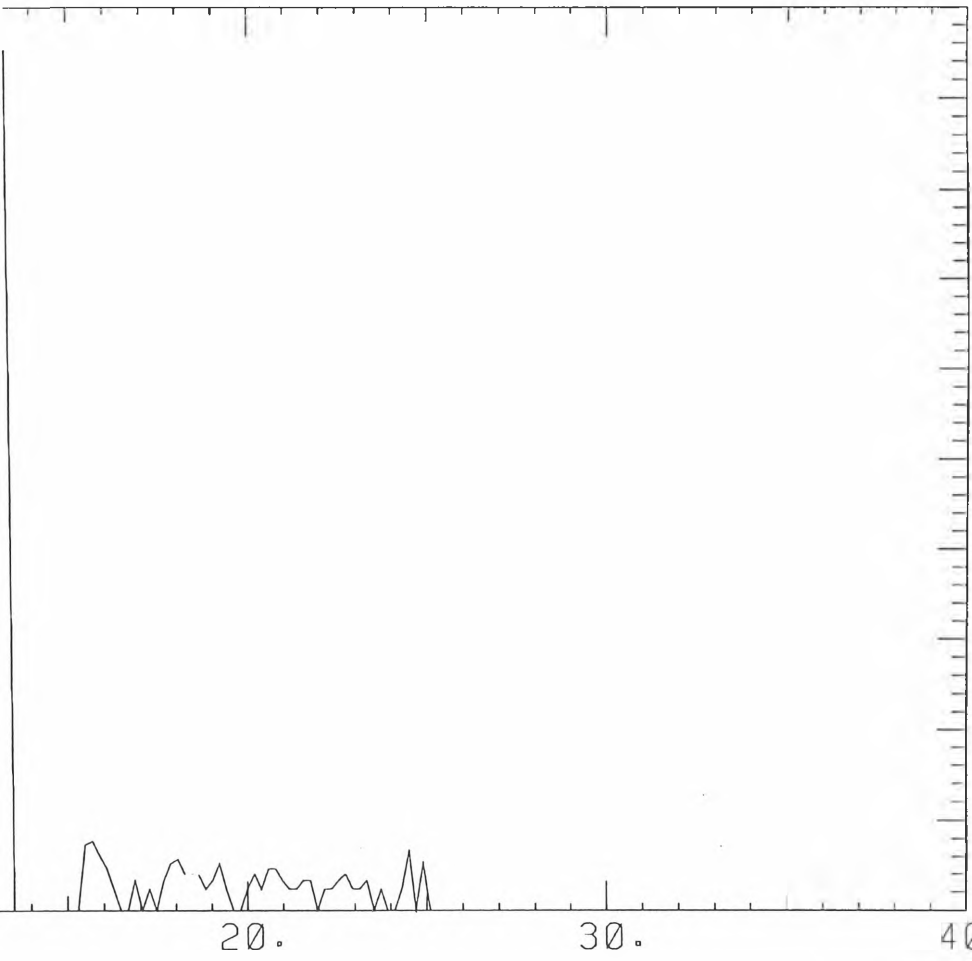

CYCLE TIME (SECS)

ANNUBAR NO. 3

EXPERIMENT NO. 1

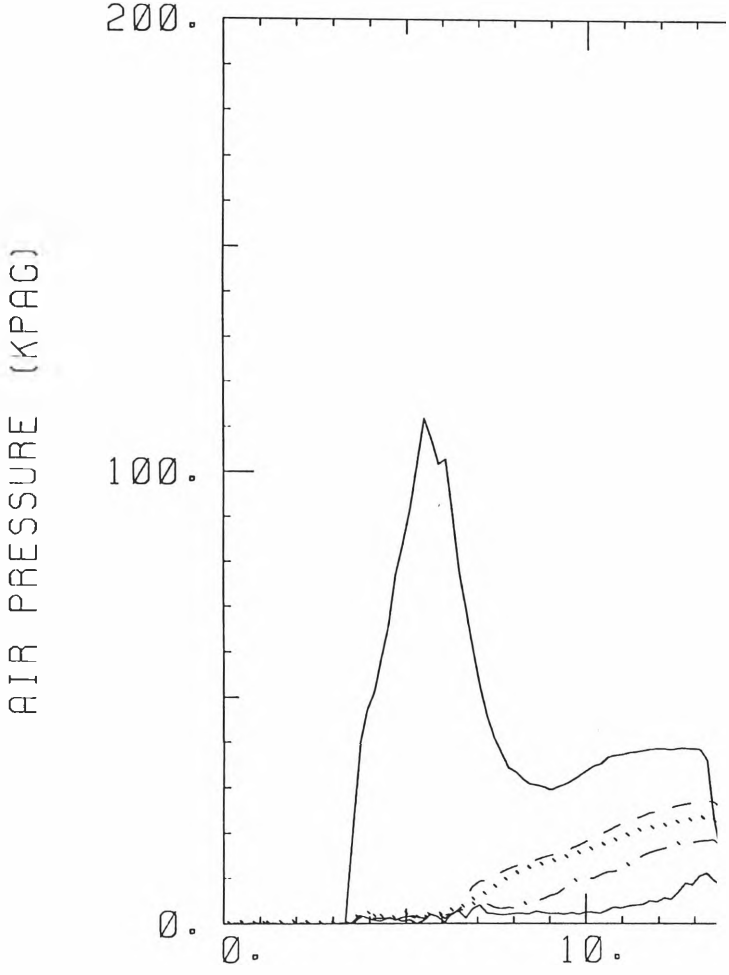

TEST DATE: 2\1\96

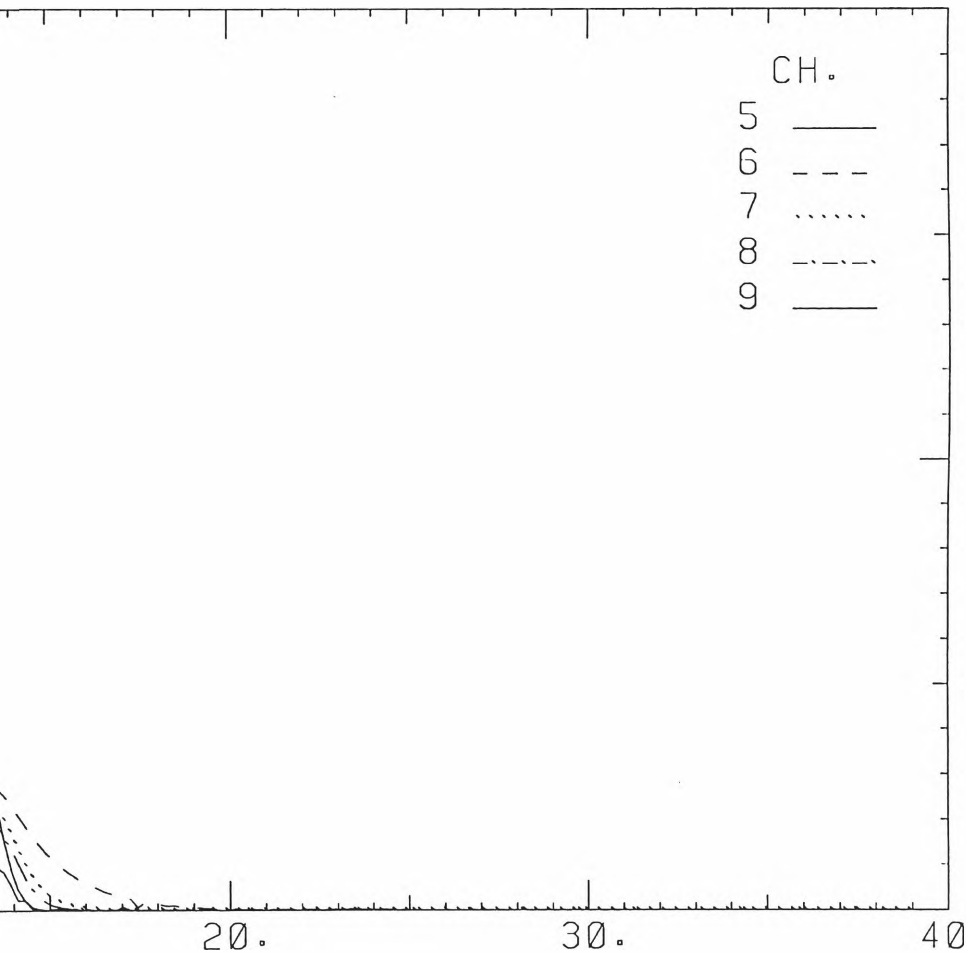

CYCLE TIME (SECS)

EXPERIMENT NO. 2
TOTAL MASS OF AIR USED
AIR MASS FLOW RATE (KG/SEC)
0.10
0.09
0.08
0.07
0.06
0.05
0.04
0.03
0.02
0.01
0.00
0.
10.
20.

TEST DATE: 2\1\96

(KGS) = 2.337

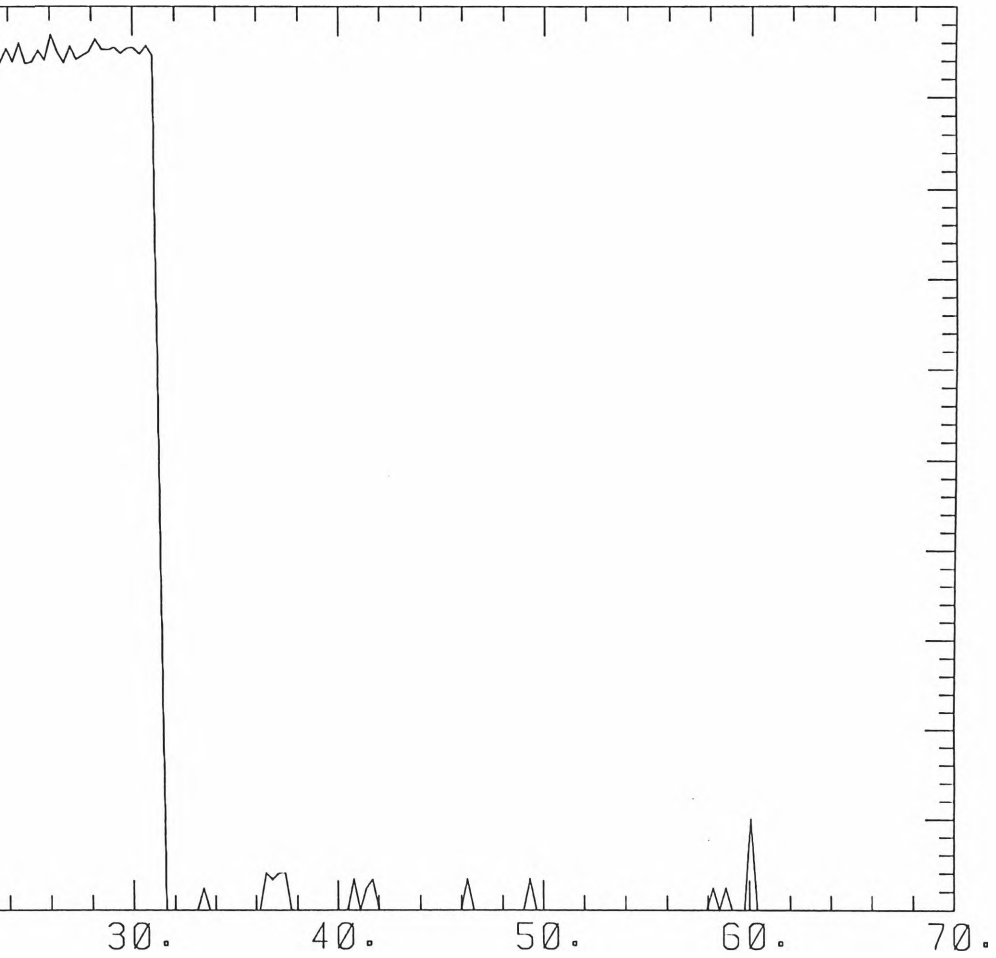

CYCLE TIME (SECS)

ANNUBAR NO. 3

EXPERIMENT NO. 2 TEST DATE: 2\1\96

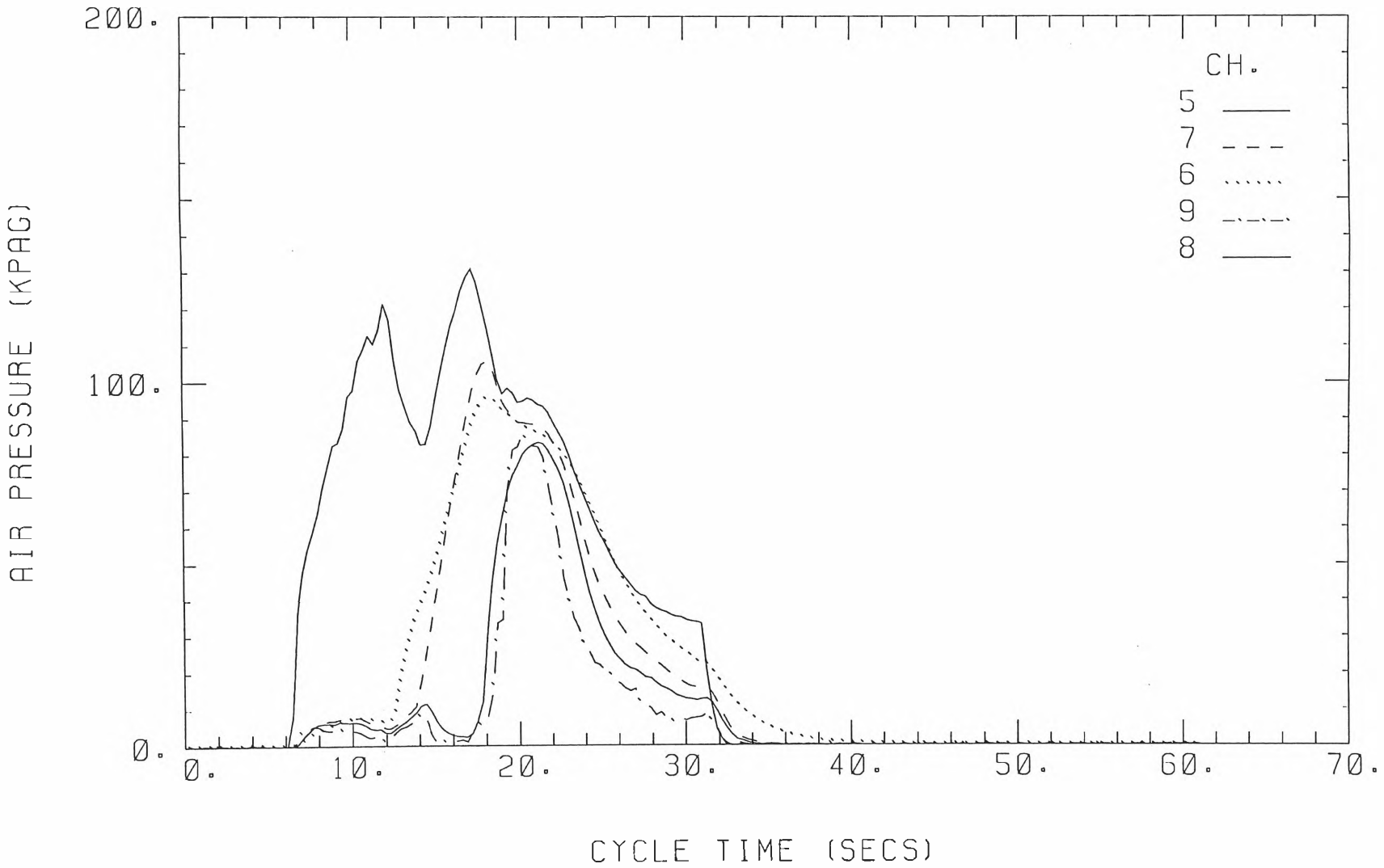

EXPERIMENT NO. 3 TEST DATE: 2\1\96

TOTAL MASS OF AIR USED (KGS) = 1.319

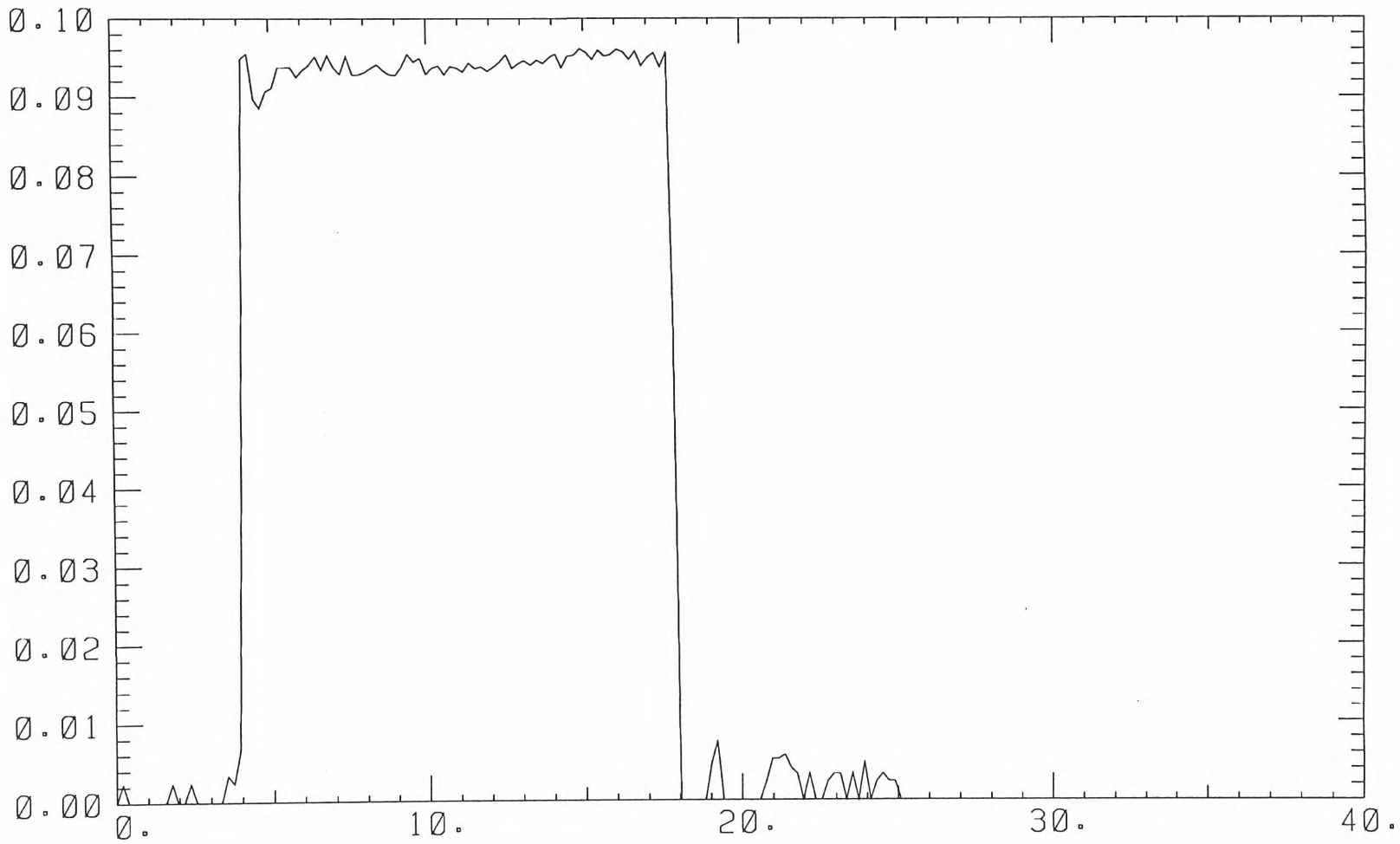

ANNUBAR NO. 3

EXPERIMENT NO. 3 TEST DATE: 2\1\96

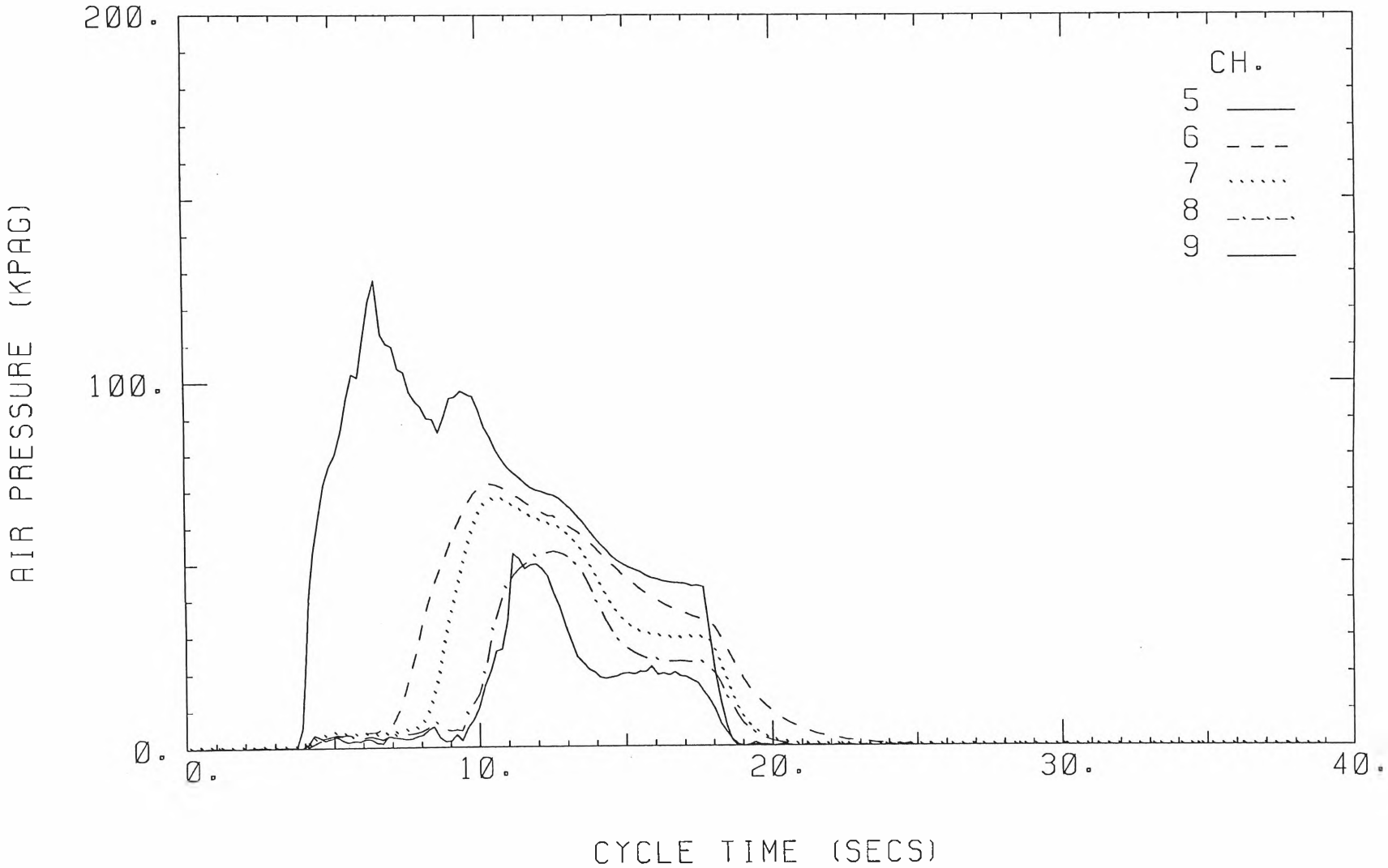

EXPERIMENT NO. 4
TOTAL MASS OF AIR USED

TEST DATE: 2\1\96

(KGS) - 1.370

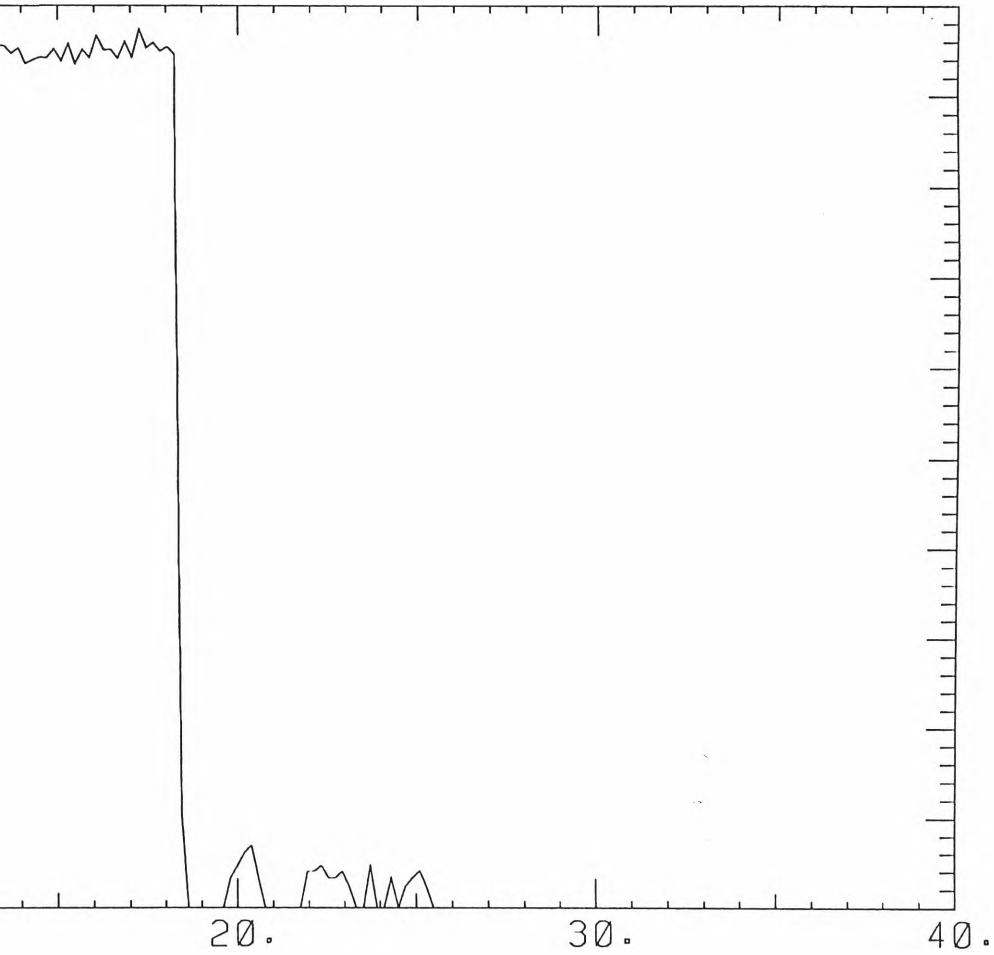

CYCLE TIME (SECS)

ANNUBAR NO. 3

EXPERIMENT NO. 4 TEST DATE: 2\1\96

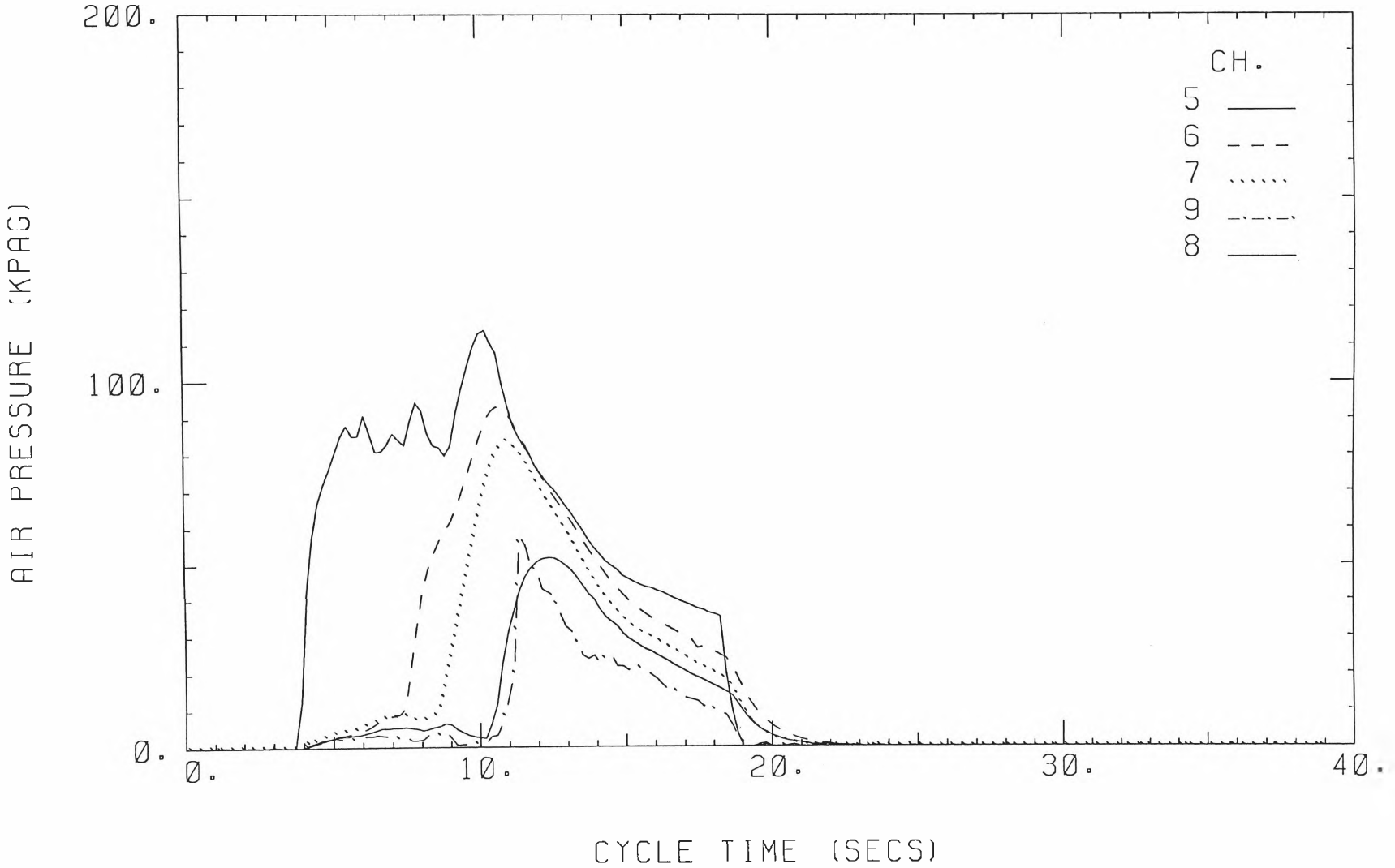

EXPERIMENT NO. 5 TEST DATE: 2\1\96
TOTAL MASS OF AIR USED (KGS) = 1.074

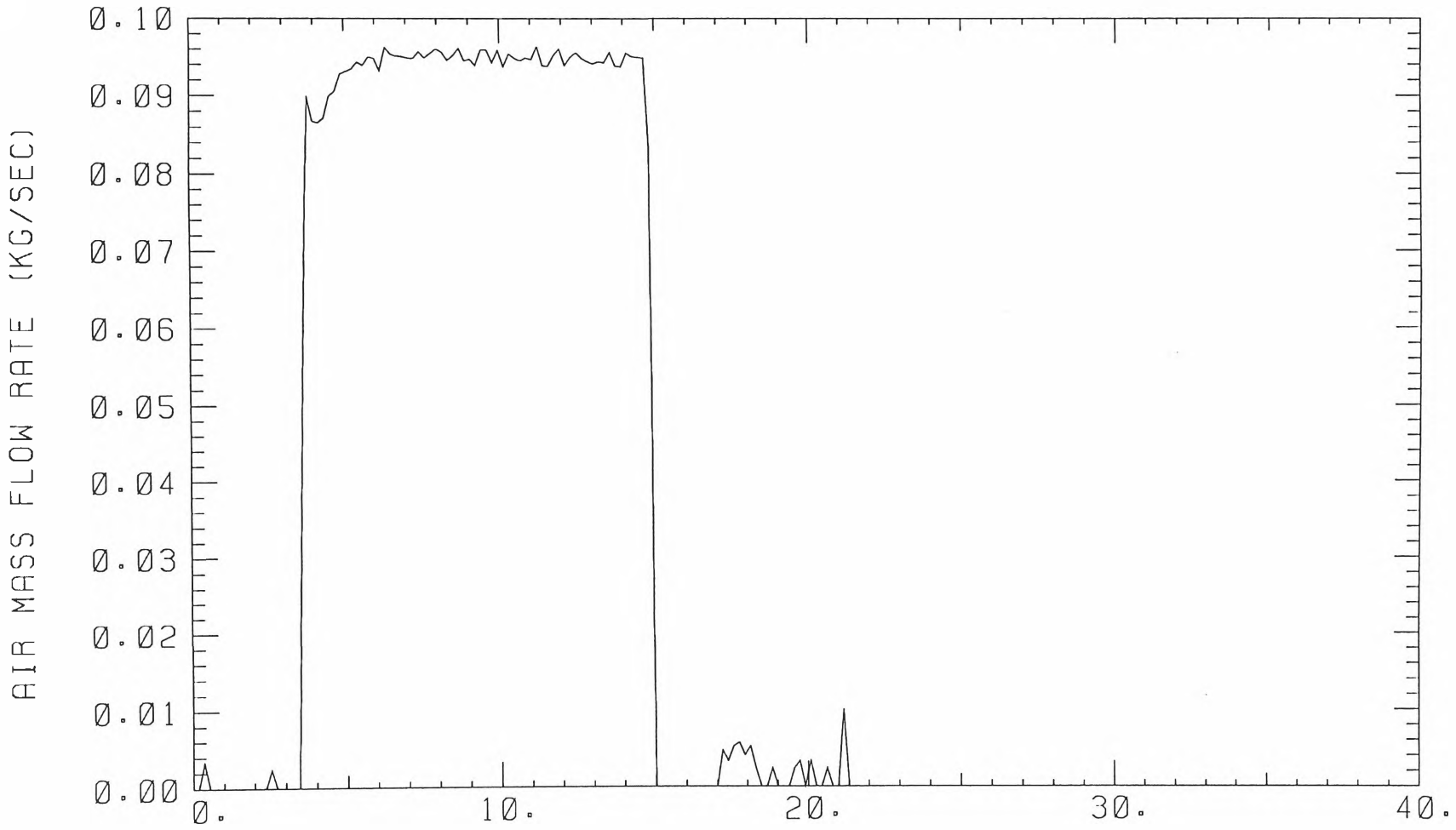

ANNUBAR NO. 3

EXPERIMENT NO. 5 TEST DATE: 2\1\96

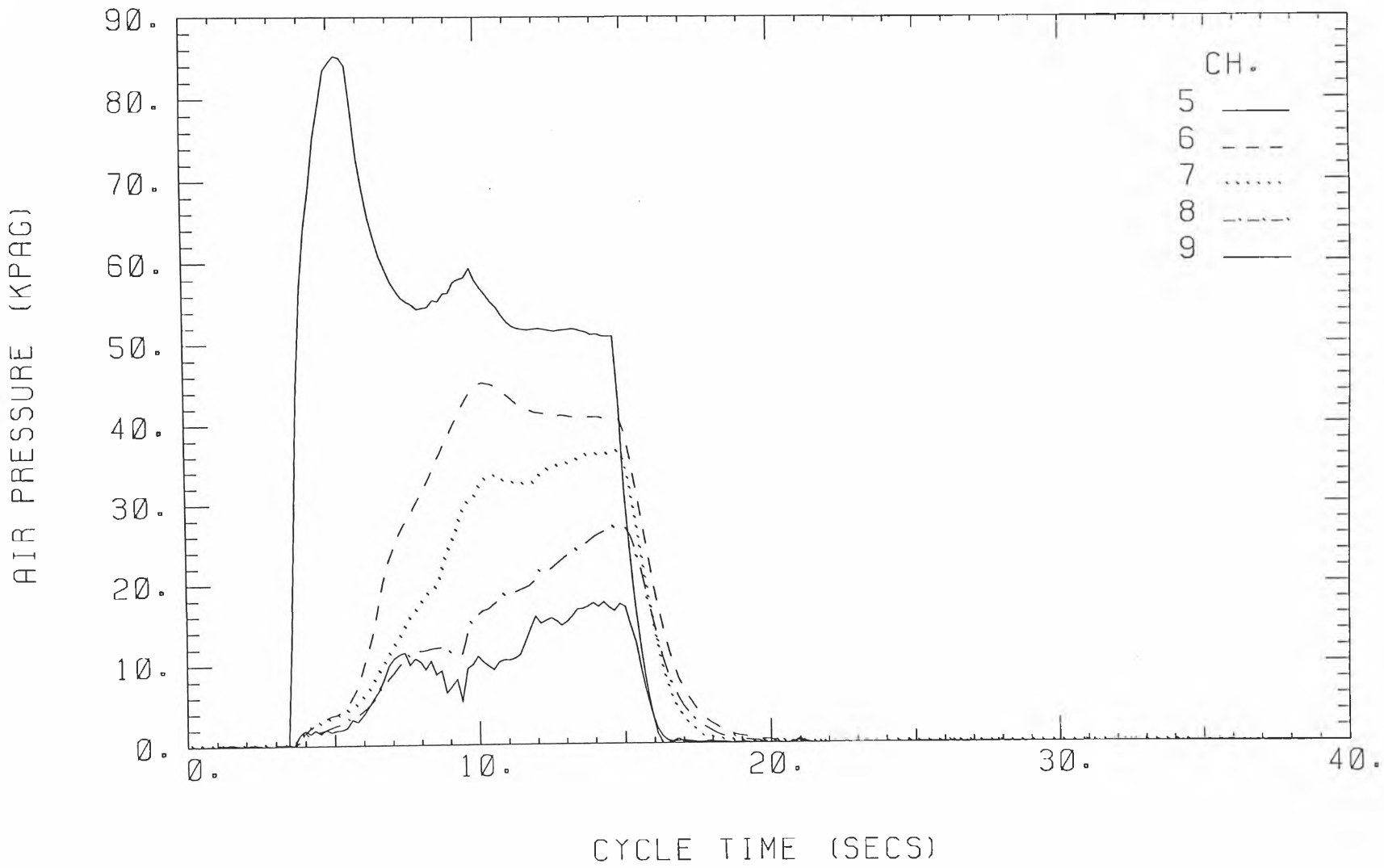

Appendix J Experimental Plots for Table 4.10

The measured data in Table 4.10 are based on the following experimental plots.

Pressure meter A is connected to channel 5, pressure meter B to channel 6, pressure meter C to channel 7, pressure meter D to channel 8 and pressure meter E to channel 9.

Table J.1 Experimental values of t_{pm} and Δp

Exp. No.	$\Delta p(kPa)$	$t_{pm}(s)$
1	85	4
2	135	6
3	180	4
4	195	4
5	155	5
6	215	5

EXPERIMENT NO. 1 TEST DATE: 2\1\96
TOTAL MASS OF AIR USED (KGS) = 1.826

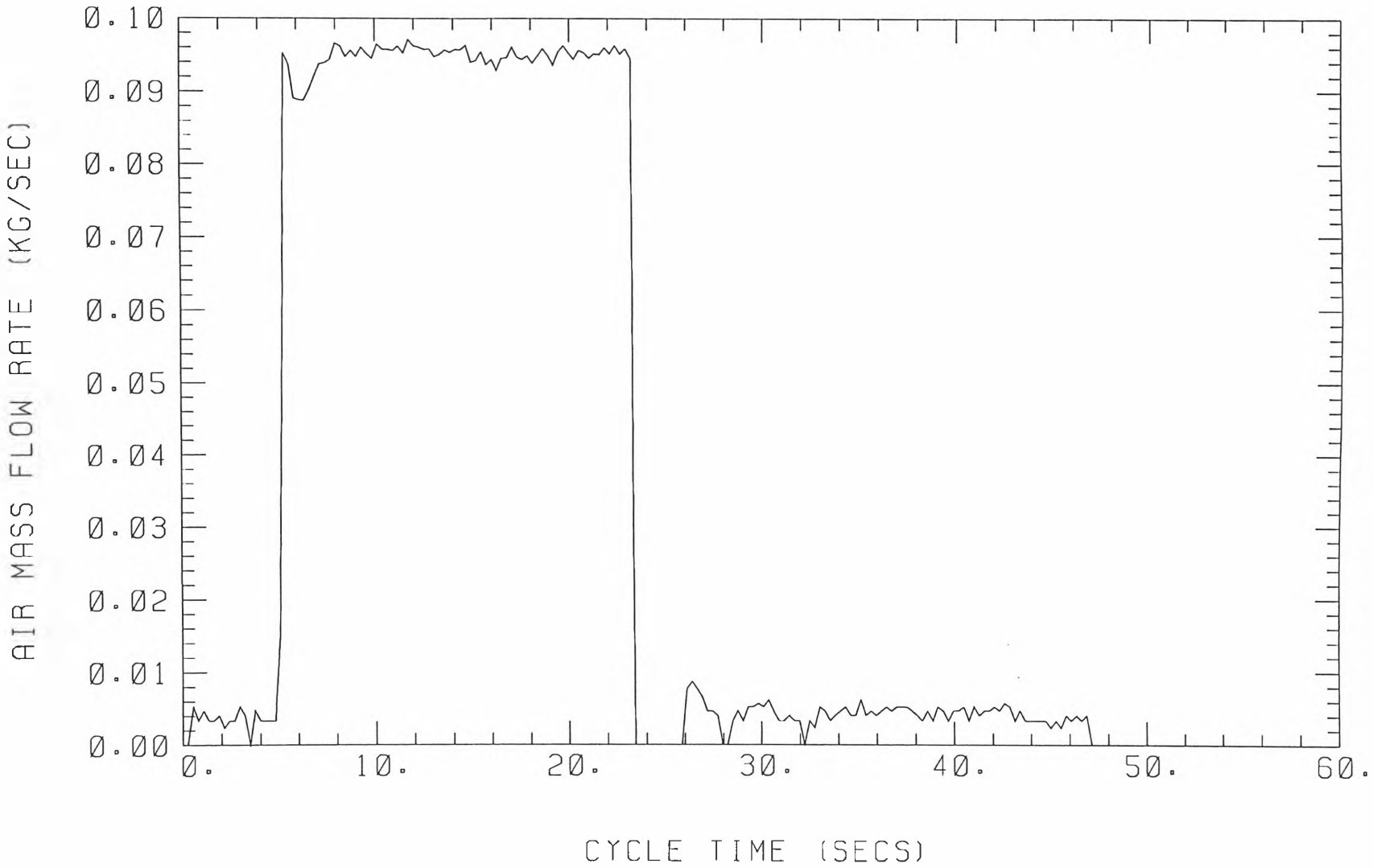

ANNUBAR NO. 3

EXPERIMENT NO. 1 TEST DATE: 2\1\96

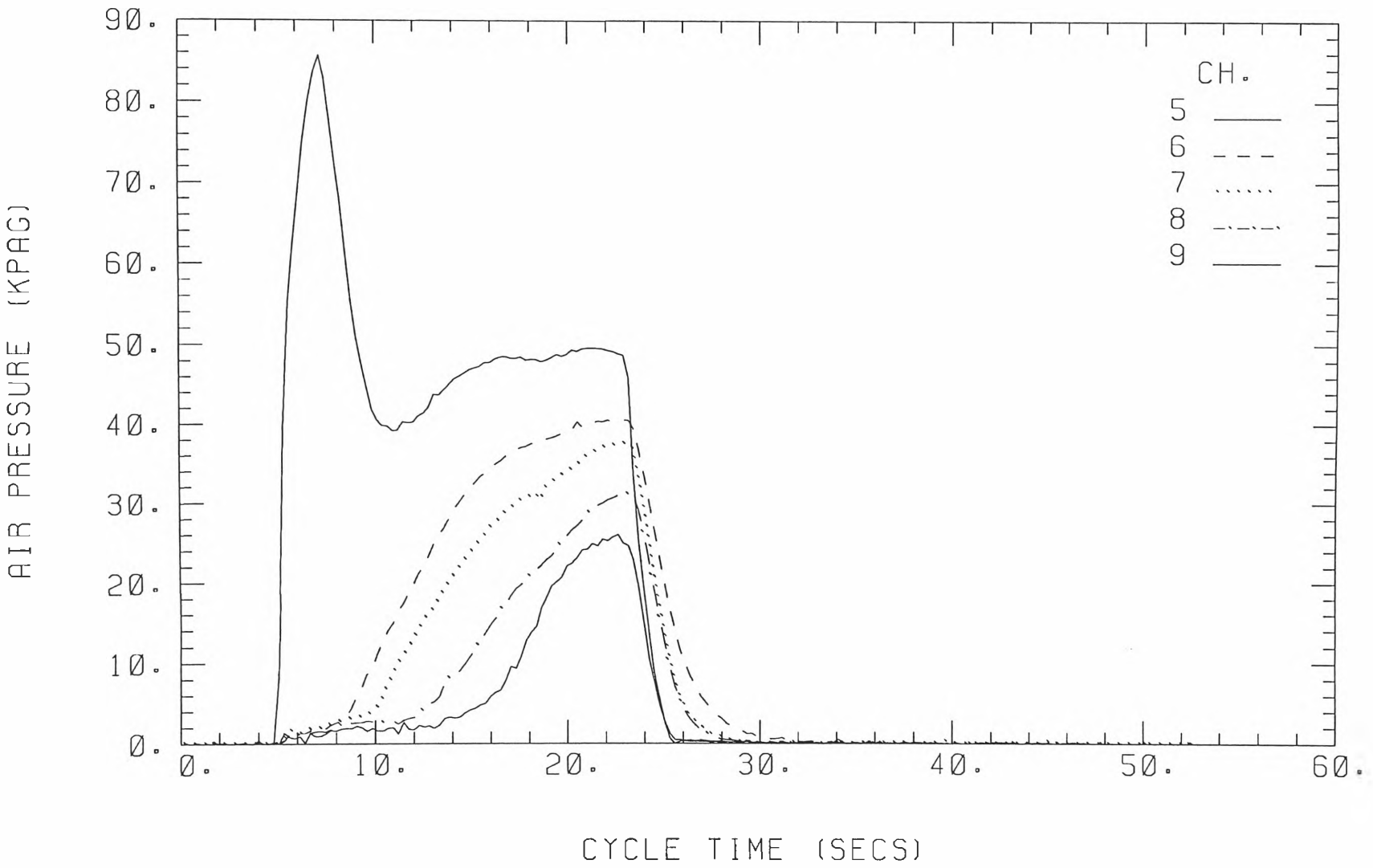

EXPERIMENT NO. 2 TEST DATE: 2\1\96

TOTAL MASS OF AIR USED (KGS) = 1.897

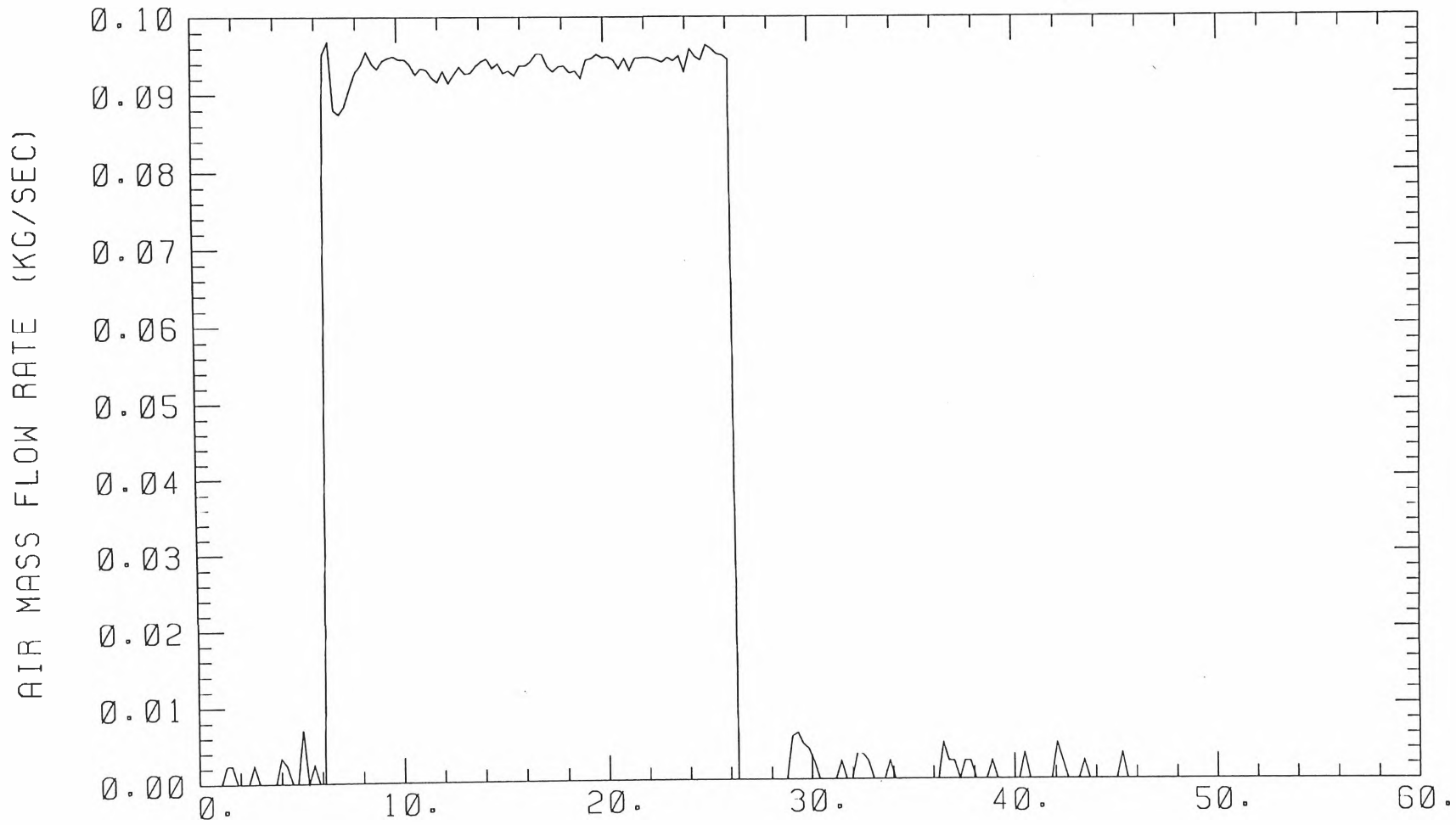

ANNUBAR NO. 3

EXPERIMENT NO. 2 TEST DATE: 2\1\96

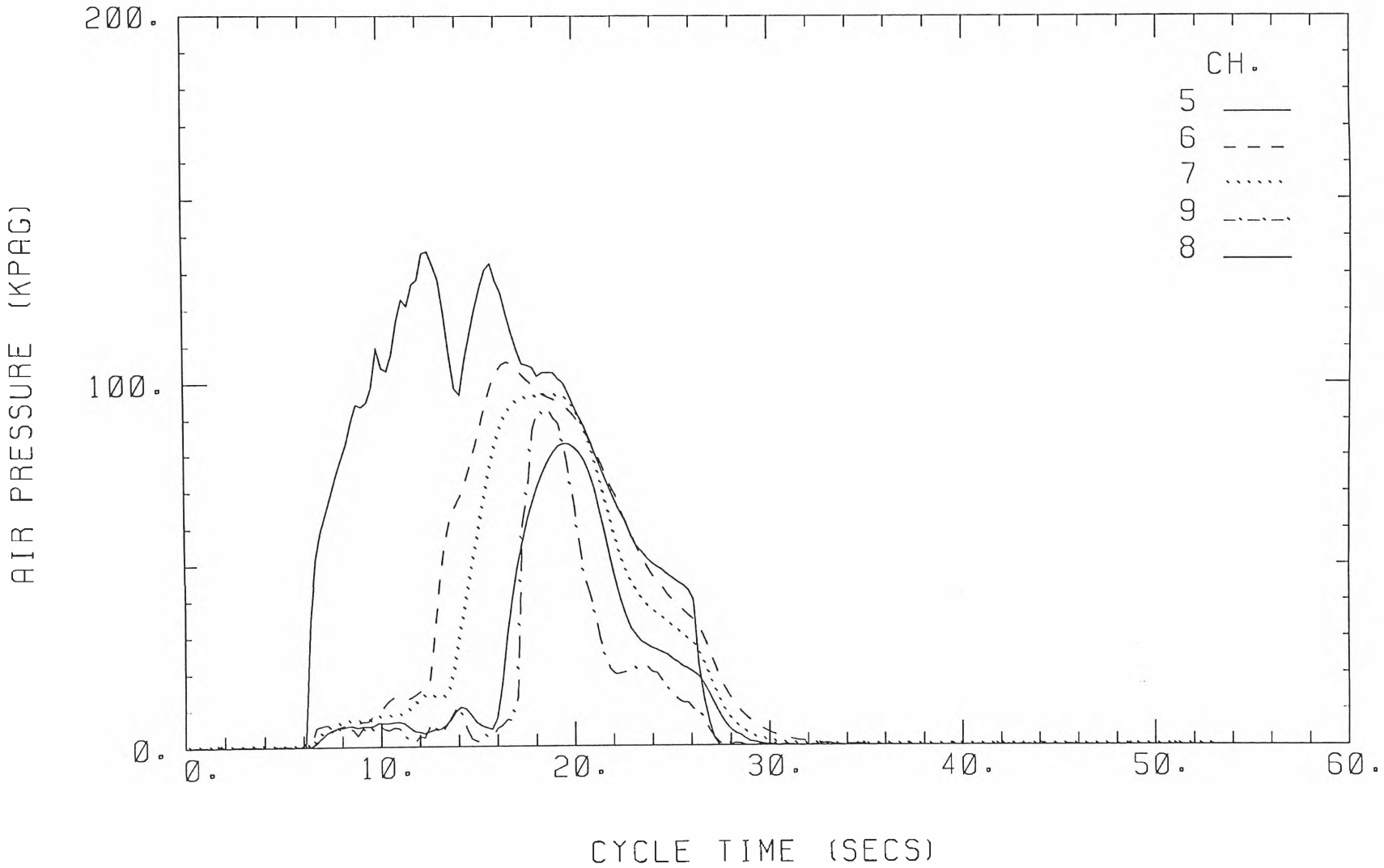

EXPERIMENT NO. 3 TEST DATE: 2\1\96

TOTAL MASS OF AIR USED (KGS) = 1.566

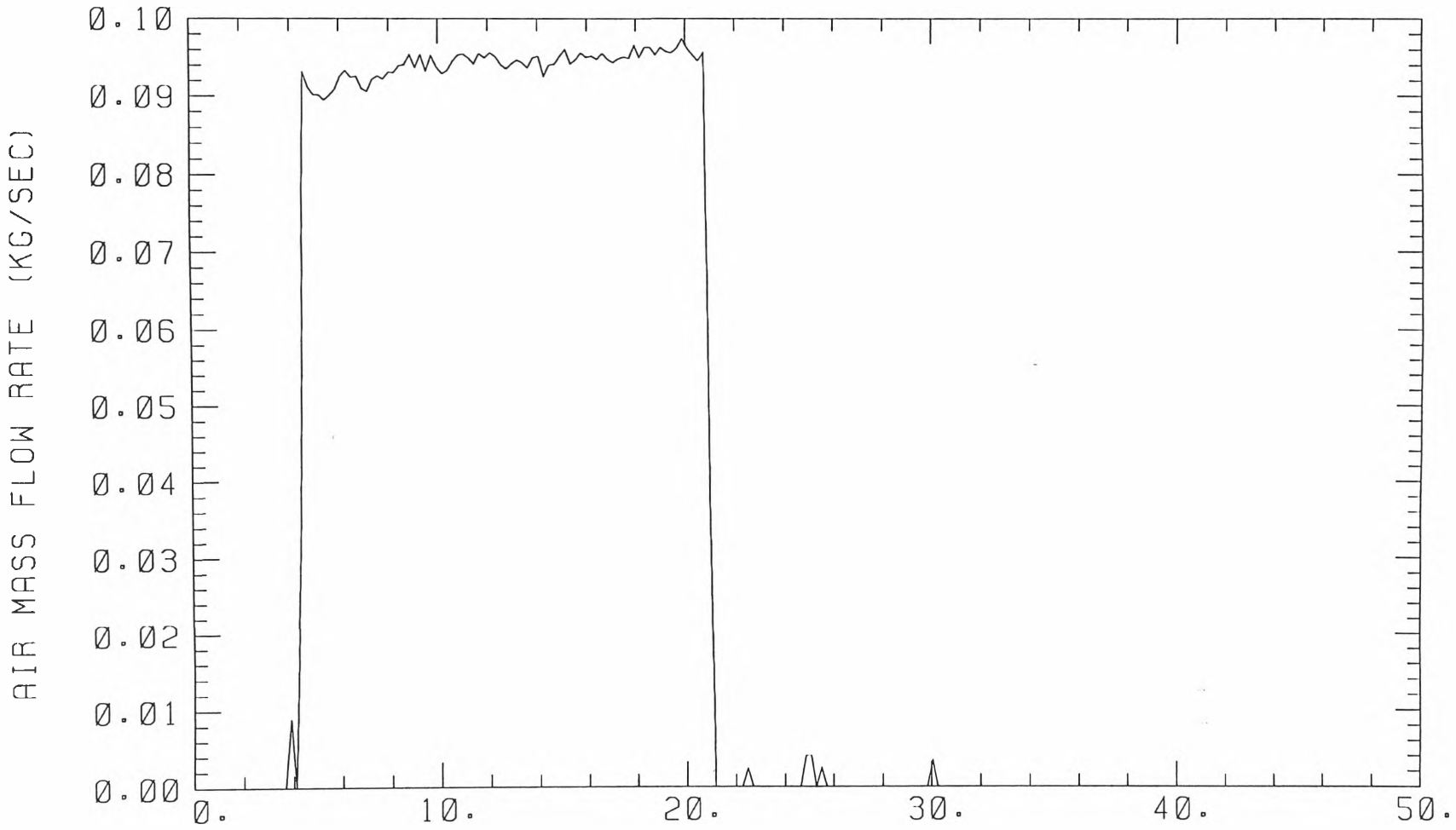

ANNUBAR NO. 3

EXPERIMENT NO. 3 TEST DATE: 2\1\96

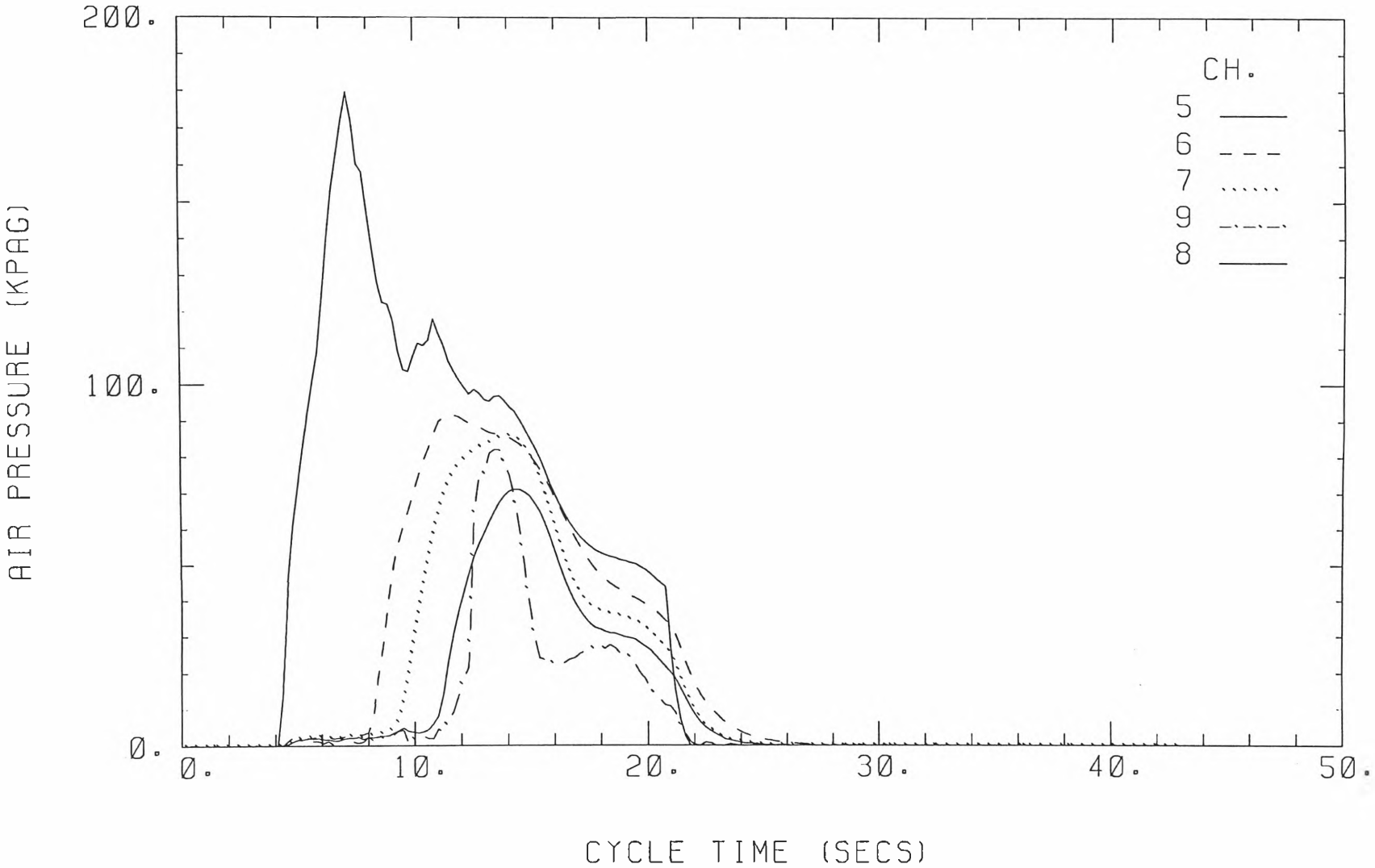

EXPERIMENT NO. 4 TEST DATE: 2\1\96

TOTAL MASS OF AIR USED (KGS) = 1.489

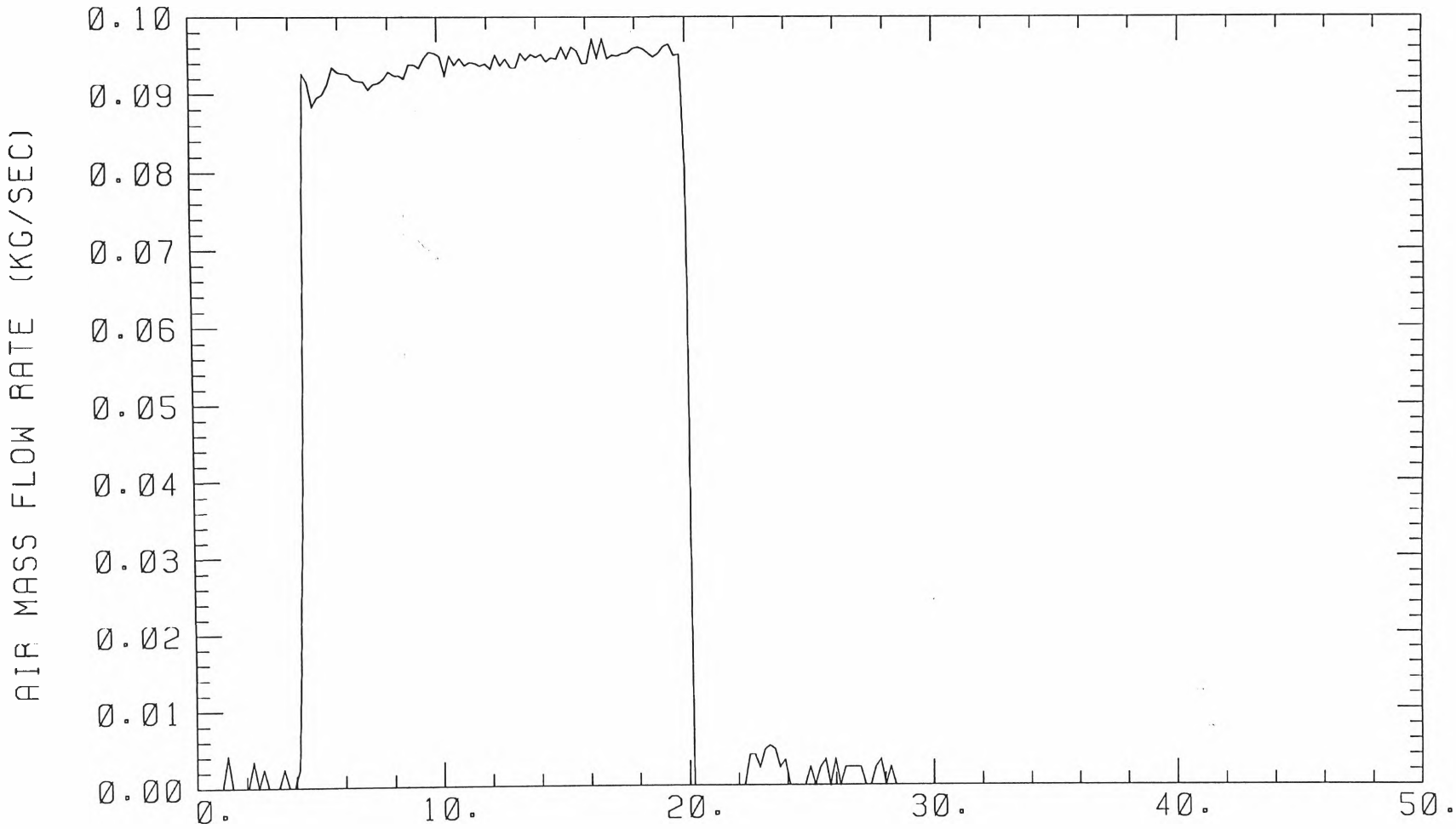

ANNUBAR NO. 3

EXPERIMENT NO. 4

TEST DATE: 2\1\96

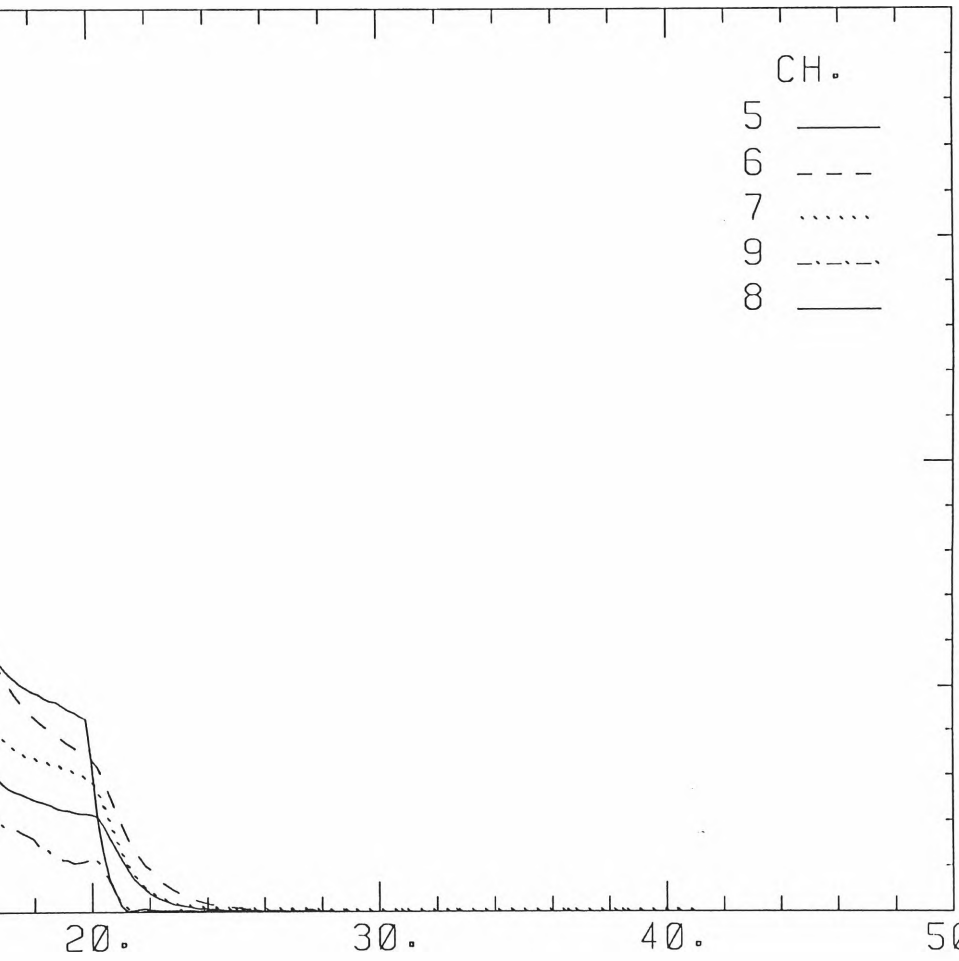

CYCLE TIME (SECS)

EXPERIMENT NO. 5
TOTAL MASS OF AIR USED

TEST DATE: 2\1\96

(KGS) = 1.735

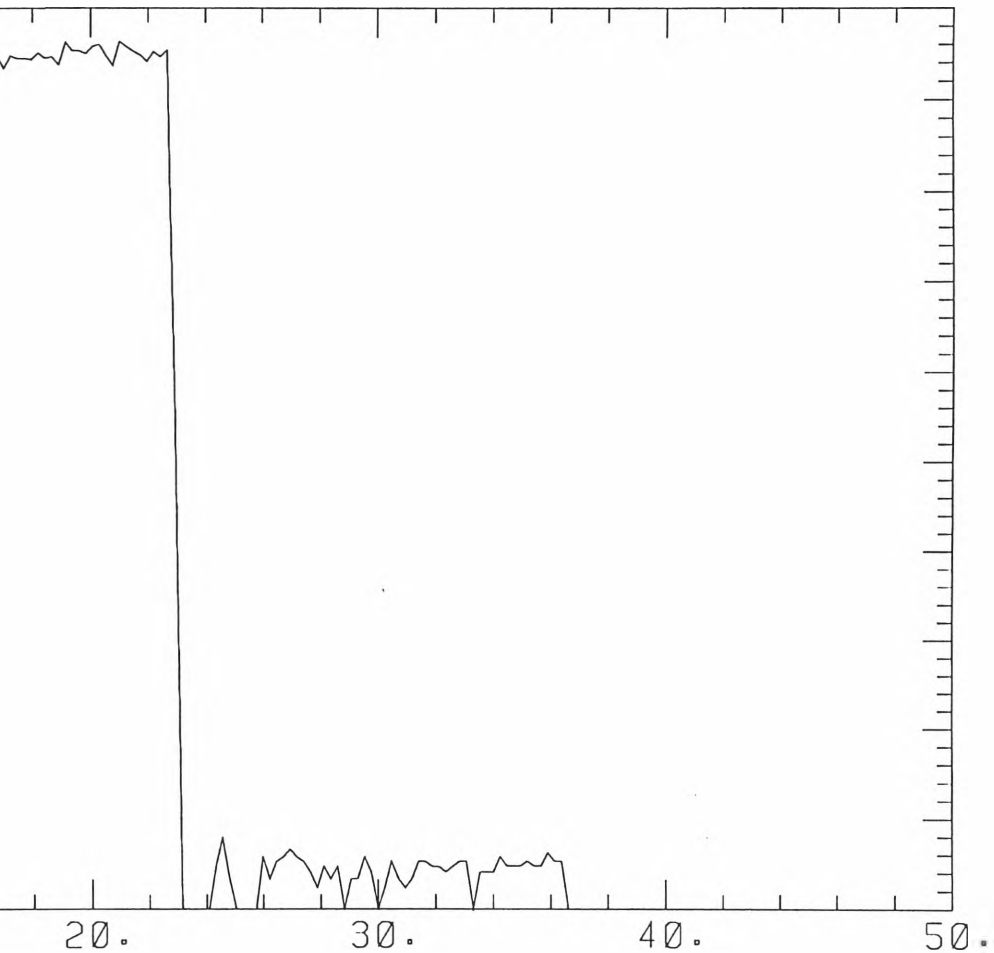

CYCLE TIME (SECS)

ANNUBAR NO. 3

EXPERIMENT NO. 5 TEST DATE: 2\1\96

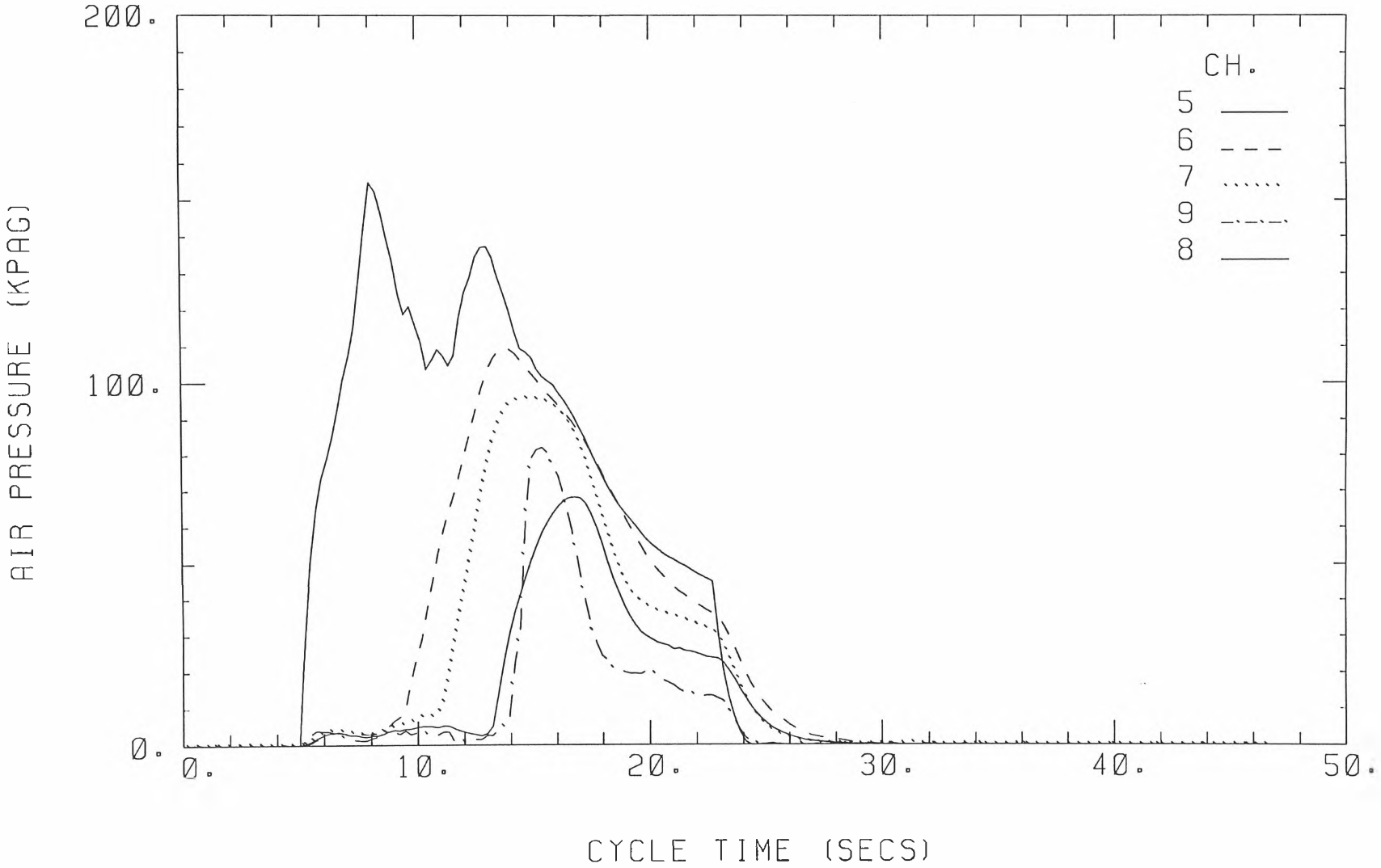

EXPERIMENT NO. 6
TOTAL MASS OF AIR USED

TEST DATE: 2\1\96

(KGS) = 1.902

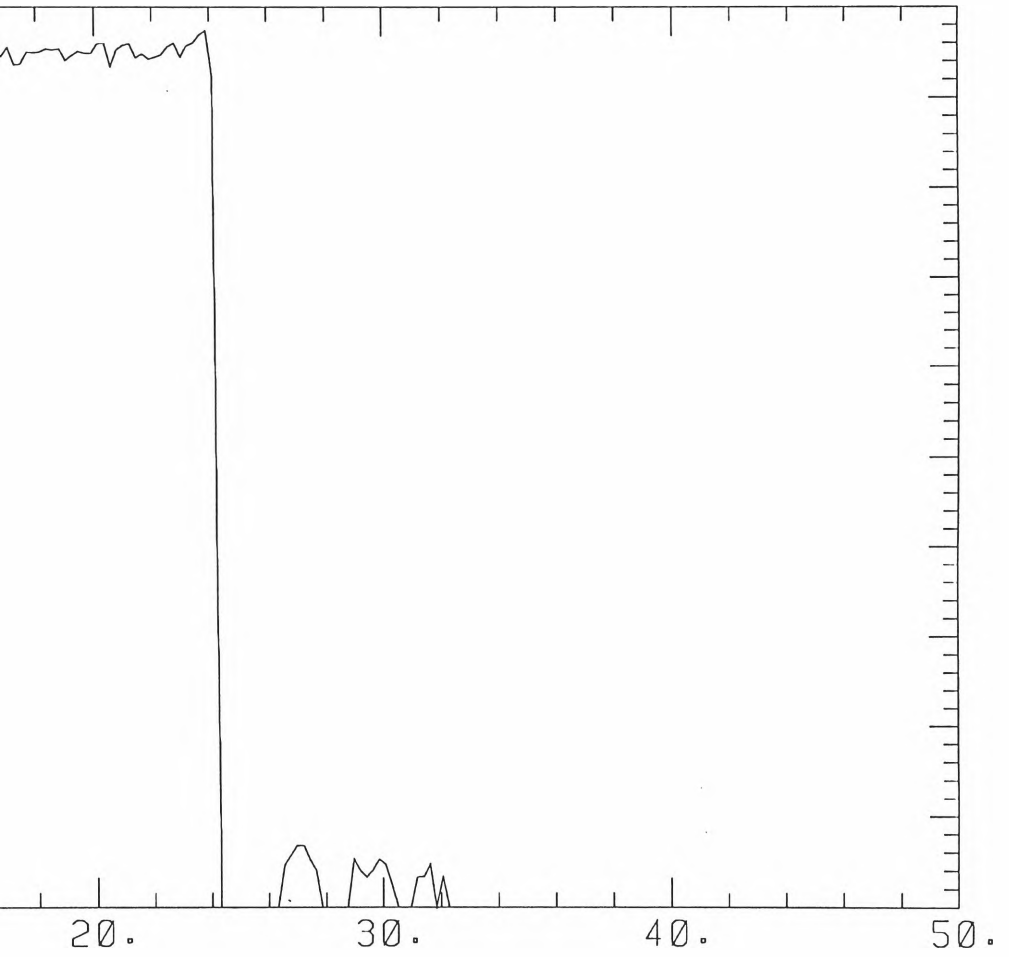

CYCLE TIME (SECS)

ANNUBAR NO. 3

EXPERIMENT NO. 6 TEST DATE: 2\1\96